PROPAGATION OF AIRGUN PULSES IN BAFFIN BAY 2012

Scientific Report from DCE – Danish Centre for Environment and Energy No. 109 2014

AARHUS UNIVERSITY
DCE – DANISH CENTRE FOR ENVIRONMENT AND ENERGY

[Blank page]

PROPAGATION OF AIRGUN PULSES IN BAFFIN BAY 2012

Scientific Report from DCE – Danish Centre for Environment and Energy No. 109 2014

Danuta M. Wisniewska[1]
Line A. Kyhn[1]
Jakob Tougaard[1]
Malene Simon[2]
Ying-Tsong Lin[3]
Arthur Newhall[3]
Kristian Beedholm[4]
James Lynch[3]
Peter T. Madsen[1]

[1] Aarhus University, Department of Bioscience
[2] Greenland Institute of Natural Resources
[3] Woods Hole Oceanographic Institution

AARHUS
UNIVERSITY
DCE – DANISH CENTRE FOR ENVIRONMENT AND ENERGY

Data sheet

Series title and no.: Scientific Report from DCE – Danish Centre for Environment and Energy No. 109

Title: Propagation of airgun pulses in Baffin Bay 2012

Authors: Danuta M. Wisniewska[1], Line A. Kyhn[1], Jakob Tougaard[1], Malene Simon[2], Ying-Tsong Lin[3], Arthur Newhall[3], Kristian Beedholm[1], James Lynch[3] & Peter T. Madsen[1]

Institutions: [1)]Aarhus University, Department of Bioscience, [2)]Greenland Institute of Natural Resources & [3)]Woods Hole Oceanographic Institution

Publisher: Aarhus University, DCE – Danish Centre for Environment and Energy ©

URL: http://dce.au.dk/en

Year of publication: August 2014

Editing completed: August 2014

Referee: Intern revision by Anders Mosbech

Quality assurance, DCE: Vibeke Vestergaard Nielsen

Financial support: The project was sponsored by the Bureau of Minerals and Petroleum, Greenland, through financial contributions from Shell Kanumas A/S, Maersk Oil Kalaallit Nunaat A/S and ConocoPhillips Global NVE Greenland LTD.

Please cite as: Wisniewska, D.M., Kyhn, L.A., Tougaard, J., Simon, M., Lin, Y.-T., Newhall, A., Beedholm, K., Lynch, J. & Madsen, P.T. 2014. Propagation of airgun pulses in Baffin Bay 2012. Aarhus University, DCE – Danish Centre for Environment and Energy, 150 pp. Scientific Report from DCE – Danish Centre for Environment and Energy No. 109 http://dce2.au.dk/pub/SR109.pdf

Abstract: In 2012 one 2D and three 3D seismic surveys were simultaneously conducted in Baffin Bay, West Greenland. The surveys were monitored using 21 acoustic dataloggers deployed in and around the seismic sites and CTD data were collected throughout the seismic season. These environmental data together with bathymetry measurements collected by the seismic vessels were fed into an advanced 3D sound propagation model to investigate the propagation of airgun pulses in Arctic Waters. Results of the model were verified using the acoustic recordings. They showed that the propagation conditions in Baffin Bay were highly complex with areas of lower than expected transmission loss resulting in higher than anticipated noise levels. The airgun pulses contained energy up to at least 48 kHz. The noise level in between seismic pulses did not fade to background levels before arrival of the next pulse and new pulses are emitted every ten seconds for each survey, which resulted in very few and short breaks without airgun blasts. On a minute by minute basis the background noise level increased on average 20 dB, but at times up to 70 dB above pre-exposure level. The implications of these findings for marine mammals in the Baffin area are discussed.

Keywords: Hydrocarbon exploration, seismic surveys, noise, propagation of seismic noise, modeling of airgun noise, airgun recordings, marine mammals, EIA modeling, test of predictive modeling.

Layout: Graphic Group, AU Silkeborg

Front page photo: Line A. Kyhn

ISBN: 978-87-7156-084-8

ISSN (electronic): 2245-0203

Number of pages: 150

Internet version: The report is available in electronic format (pdf) at http://dce2.au.dk/pub/SR109.pdf

Contents

Preface

This study is the result of collaboration between Aarhus University, Greenland Institute of Natural Resources and Woods Hole Oceanographic Institution. It was sponsored by the Bureau of Minerals and Petroleum through financial contributions from Shell Kanumas A/S, Maersk Oil Kalaallit Nunaat A/S and ConocoPhillips Global NVE Greenland LTD. The study was brought about by the Environmental Impact Assessment process of the Bureau of Minerals and Petroleum, Greenland, where a general lack of knowledge on the effects of noise from seismic airguns on marine organisms led to a number of projects during the 2012 seismic season in Baffin Bay. The overall purpose of all projects was to improve the knowledge on impacts of seismic airguns on marine life. This project, however, specifically addressed propagation of airgun pulses in an Arctic ocean: While there is now almost a century of background on underwater acoustics, the fact remains that our ability to estimate transmission loss in many areas of the world's oceans remains imperfect, hence impeding reliable impact assessment. This study therefore focused primarily on evaluating the transmission loss of airgun pulses propagating away from seismic vessels, with the secondary goal of verifying the predictive modeling made for the Environmental Impact Assessment Process.

The study was carried out in close collaboration with the crew of the seismic vessels operating in Baffin Bay, during the summer and autumn of 2012.

A draft of this report was submitted to Shell, Maersk and ConocoPhillips in December 2013, and the results were presented at a meeting with the same companies on 27th February 2014.

1 Executive summary

In 2012, four simultaneous seismic surveys and twelve shallow core drillings were planned to be carried out in Baffin Bay, northwest Greenland. In Greenland, guidelines for Environmental Impact Assessments (EIA) of seismic activities require that each participating company models its own expected noise emission, as well as the cumulative noise levels resulting from all concurrent activities in a given area. This is required in order to evaluate the potential effects of hydrocarbon exploration on marine life under the assumption that all planned activities are carried out. Model precision is very important as it is used to predict received noise levels at various ranges from the source. Since these received levels are used to predict potential effects on marine life and ultimately to evaluate whether a given project may be carried out, it is essential to be able to trust the results of predictive modeling. However, one of the important unknown factors in predictive noise modeling is the propagation of airgun pulses. On top of this, the environmental factors influencing propagation, including bottom substrate, bathymetry, salinity and temperature profiles, were poorly known for Baffin Bay. It was therefore decided that a large scale acoustic monitoring study should document the noise levels from the four planned seismic surveys. The measurements were also to be used to 1) verify the validity of the sound propagation modeling studies commissioned by the hydrocarbon companies for the purpose of the EIA, and to 2) obtain environmental data to feed into, and acoustic data to validate, an advanced sound propagation model developed by collaborators at Woods Hole Oceanographic Institution (WHOI). Furthermore, this study substituted the requirement for the companies to document their noise emission during their seismic activities.

The study was carried out by deploying 21 acoustic dataloggers at seven moored stations, each with dataloggers distributed at three different depths. Additionally, each mooring was equipped with a number of sensors, which recorded depth and temperature over the course of the deployment period. CTD measurements were taken at each station at deployment and retrieval to obtain valid environmental data for the post-season modeling. In addition to the moored stations, close-up recordings of one of the seismic airgun arrays were conducted at ranges of 0.5, 1, 2, 4 and 8 nautical miles to characterize the signature of the array at short ranges. Data from this study were supplemented with data collected by JASCO for Shell before and during the seismic program. Shell's data comprised acoustic recordings collected with moored dataloggers, and CTD data obtained at a number of locations around Baffin Bay throughout the seismic season.

19 acoustic dataloggers were successfully retrieved from Baffin Bay following the 2012 seismic season. The most apparent contribution of the seismic activities to the noise budget in Baffin Bay and Melville Bay were stepwise increases in noise levels, at the onsets of the four seismic surveys. On a minute by minute basis, on several occasions the sound exposure levels (SEL calculated over 1 minute) increased by more than 60 dB in relation to the pre-exposure background noise SEL of about 120 dB re 1 μPa^2 s. The SEL was on average approximately 20 dB higher than the pre-exposure level. Cumulative SEL (cSEL) over 24 hours increased from about 153 dB re 1 $\mu Pa^2 s$ to around 170-180 dB re 1 $\mu Pa^2 s$ and at times up to 189 dB re 1 $\mu Pa^2 s$.

During a seismic survey, the background noise level was constantly elevated, as one airgun pulse would not fade out before the arrival of the next pulse. Furthermore, with several concurrent seismic surveys undertaken in the same area, multiple pulses were constantly apparent at various levels. This general rise in background noise may cause the airgun sounds to mask other sounds in the frequency range of 1-10 kHz, including sounds of importance to marine animals, especially at close ranges to the airgun array.

The airgun signals in the close-up recordings contained significant energy above ambient noise up to, and possibly beyond, 50 kHz at close ranges. This result stresses the importance of including higher frequencies in assessments of potential effects of seismic surveys on marine organisms, especially when considering Odontocetes, which have exceptionally good high-frequency hearing.

The vertical extent of the typical of Arctic waters near-surface low-sound-speed channel was greater than expected. Accordingly, in most recordings, the highest sound levels were consistently recorded on the top dataloggers. These are also the depths at which marine mammals spend a significant amount of time to breathe and socialize. There were exceptions where the highest sound levels were recorded on the middle or bottom datalogger, which may have been caused by shadow and/or convergence zones. This is important to keep in mind when considering zones of impact in relation to mitigation of effects on marine mammals for EIAs.

The measured received sound levels were within the ranges predicted by JASCO in their pre-season modeling included in the EIAs. There were, however some exceptions were the noise levels were higher than predicted: For example the advanced model by WHOI documented a channel of low sound speed running along the slope of a north-south facing deep water area. The low transmission loss herein resulted in higher than expected sound levels to the north of the channel which was confirmed by the acoustic recordings. This channel was not picked up by the predictive modeling, most likely due to the quality of the environmental input data, which generally were inadequate for this region, and the limited number of source locations considered by the model.

Overall, the results of this study however lend weight to the utility of predictive modeling for the purpose of EIAs, and suggest that it is possible, even in some cases with less than ideal input data, to predict noise exposure from multiple seismic surveys with sufficient accuracy to provide a reasonable basis for assessing the potential impact on animals.

The fully 3D transmission loss modeling performed by WHOI demonstrated that the acoustic environment of the north-eastern Baffin Bay and Melville Bay is highly complex. In particular, the near surface low–sound-speed ducting, the bottom geoacoustic properties, and the detailed bathymetry in shallow and high gradient regions, could produce large effects on the transmission loss. Wave and ice conditions were not factored into the models, partly due to lack of good input data, but also because these effects are not yet well represented in parabolic equation models. This stresses the need for collection and dissemination of high-quality data on hydrography, bathymetry and sediment properties as well as statistics for ice coverage and surface roughness (waves) prior to impact assessment procedures.

2 Sammenfatning

Grønland åbnede for olieefterforskning af Baffinbugten i 2006 og siden har der været en stribe seismiske undersøgelser for at kortlægge undergrundens olie- og gasforekomster. I sommeren 2012 var der planlagt fire samtidige seismiske undersøgelsestogter og tolv shallow core prøveboringer i Baffinbugten i nordvest Grønland. I grønlandske farvande er det et krav, at der laves en vurdering af virkninger på miljøet (en såkaldt VVM-redegørelse), inden der gives tilladelse til udførelse af seismiske undersøgelsestogter, da de anvendte airguns støjer kraftigt. Heri er det påkrævet, at firmaet modellerer den forventede støjpåvirkning til havmiljøet, samt at alle firmaer i samme område (her Baffinbugten) modellerer den samlede kumulative støjpåvirkning af alle samtidige aktiviteter og præsenterer resultaterne i deres VVM-redegørelse. Dette er påkrævet for at kunne vurdere potentielle effekter på dyreliv i havet, inden der gives tilladelse til de ansøgte projekter. Pålideligheden af de anvendte modeller er uhyre vigtig, da de bruges til at forudsige støjniveauerne på forskellige afstande af et seismisk survey, og til at forudsige effekter på marine organismer. En seismisk undersøgelse i vand foregår ved, at der sendes trykbølger af lyd mod havbunden fra en luftkanon (en såkaldt airgun). Støjniveauet kan derfor ultimativt være afgørende for om et projekt anses for sikkert at gennemføre. Imidlertid er en af de vigtige faktorer i denne type modellering netop den akustiske udbredelse af airgunstøj og denne faktor er dårligt kendt.

På denne baggrund blev dette projekt til som et storskala akustisk moniteringsstudie med henblik på at kvantificere lydudbredelsen fra de fire planlagte seismiske undersøgelsestogter. Endvidere skulle de akustiske målinger bruges til at undersøge om de i VVM'erne anvendte modeller var præcise nok. De indsamlede miljødata som salinitet, temperatur og dybde skulle desuden anvendes i en avanceret lydudbredelsesmodel udviklet af Woods Hole Oceanographic Institution (WHOI) for at øge dennes præcision, og de indsamlede akustiske data skulle bruges til at validere de i modellen fundne lydniveauer.

Moniteringen blev udført ved at udsætte 21 akustiske dataloggere på syv målestationer i Baffinbugten fordelt med tre dybder pr. station. På hver målestation var der endvidere temperatur- og salinitetsdataloggere fordelt over dybden, og der blev lavet CTD-målinger (konduktivitet, temperatur, dybde) i forbindelse med udsætning og optagning af stationerne for at indsamle aktuelle miljødata til modelleringen. Herudover blev der lavet akustiske optagelser tæt på et af de seismiske airgunarrays på afstande af 0,5, 1, 2, 4 og 8 sømil for at dokumentere den akustiske signatur tættere på skibet. Data fra dette studie blev suppleret med data indsamlet af JASCO Applied Sciences for Shell før, under og efter det seismiske undersøgelsesprogram. Disse data består af akustiske data indsamlet med udsatte dataloggere og CTD data indsamlet på en stribe positioner i Baffinbugten. Begge datatyper blev også brugt til at forfine og validere den avancerede model fra WHOI.

Projektet lykkedes, og i alt nitten af de enogtyve dataloggere kunne indsamles efter det seismiske program i 2012. CTD målinger blev lavet på alle stationer to gange i løbet af sæsonen. Det mest direkte støjbidrag fra de seismiske undersøgelser til Baffin- og Melvillebugten var en serie abrupte forøgelser af baggrundsstøjen, med de enkelte trin svarende til påbegyndelsen af hvert af de fire seismiske undersøgelsestogter. På minutbasis steg lydeksponeringsniveauet (fra engelsk forkortet SEL) nogle gange så meget som 70 dB i forhold til baggrundsstøjsniveauet på ca. 120 dB re. 1 μPa^2s før det seismiske undersøgelsestogt, og generelt var lydeksponeringsniveauet mindst 20 dB højere end det baggrundsstøjsniveau, der kunne måles før togterne. Det kumulative lydeksponeringsniveau over et døgn (cSEL) steg fra ca. 153 dB re μPa^2s til omkring 170-180 dB re μPa^2s og nogen gange op til 189 dB re μPa^2s.

Det var endvidere tydeligt, at baggrundsstøjsniveauet under et seismisk undersøgelsestogt er konstant forhøjet, idet påvirkningen fra en enkelt airgunpuls ikke når at aftage helt til baggrundsstøjsniveauet inden den næste puls ankommer. Med flere samtidige seismiske undersøgelser i samme område betyder det, at adskillige airgunpulser konstant er synlige/hørbare med forskellig styrke. Denne generelle forøgelse af baggrundsstøjen betyder, at airgunstøjen kan maskere andre lyde med frekvensindhold mellem 1 og 10 kHz, vigtigst af alt lyde, der kan have betydning for dyr i området, særligt tæt på airgunarrayet.

Karakteristikken af det ene airgunarray viste, at de optagede airgunpulser havde et energiniveau signifikant over baggrundsstøjsniveauet, muligvis helt op til 50 kHz på korte afstande. Dette resultat understreger nødvendigheden af at inkludere højere frekvenser (>10 kHz) i konsekvensberegninger af effekter af airgunstøj på havpattedyr, tandhvaler i særdeleshed.

Den vertikale udbredelse af den almindeligt forekommende lydkanal med lave lydhastigheder, der findes nær overfladen i arktiske farvande, var større end forudset. De lavere lydhastigheder skyldes, at koldt overfladevand med relativ lav saltholdighed giver en afbøjning af lyden mod overfladen, og der bliver derfor en koncentration af lyden nær overfladen. Derfor blev de højeste støjniveauer også i langt de fleste tilfælde optaget på de øverste dataloggere, som lå tættest på lav-lydhastighedskanalen. Dette er også den dybde, havpattedyr bruger meget tid i til at trække vejret og socialisere. Der var enkelte undtagelser, hvor det højeste støjniveau blev optaget på en af de dybere dataloggere, hvilket kan skyldes såkaldte konvergenszoner, hvor reflekterede kopier af en lyd overlapper og dermed kan forårsage højere lydtryk end den direkte ankomne lyd alene. Denne effekt er vigtig at inkludere i konsekvensberegninger og beregner påvirkningszoner i forhold til havpattedyr i forbindelse med VVM-redegørelser.

De målte støjniveauer faldt inden for de støjniveauer JASCO havde modelleret sig frem til i industriens VVM-redegørelser. Der var dog undtagelser. For eksempel forårsagede den af WHOI modellen beskrevne nord-syd løbende lydkanal med lave lydhastigheder forhøjede støjniveauer nord for kanalen, som blev bekræftet af vores målinger, men ikke påvist i VVM-modelleringen. Kanalen blev ikke påvist af VVM-modelleringen, sandsynligvis på grund af kvaliteten af de miljødata der var tilgængelige for modellen, og som generelt er mangelfulde for området, og på grund af det begrænsede antal stationer der blev medtaget i modellen.

Resultaterne fra dette studie ser dog ud til at understøtte validiteten af forhåndsmodellering til VVM'er. Endvidere viser studiet, at det kan være muligt, selv med mindre end ideelle inputdata, at forudsige støjniveauer fra flere samtidige seismiske undersøgelser med tilstrækkelig nøjagtighed til at vurdere potentielle effekter på havpattedyr.

Den lydudbredelsesmodel, WHOI udførte og forfinede med data fra denne undersøgelse, viser, at det akustiske miljø i Baffinbugten er særdeles komplekst. Modelleringen viste som sagt, at der findes en lavlydhastighedskanal i en nord-sydlig retning langs kanten af et dybt havområde. Eksistensen af denne kanal blev endvidere bekræftet af de data, som de involverede olieselskaber indsamlede under de seismiske undersøgelser. De komplekse lydudbredelsesbetingelser tæt på kysten med varierende dybder, smeltende isbjerge og smeltevand fra land resulterede i lavere støjniveauer end i den åbne del af Baffinbugten. Nøjagtigheden af den akustiske modellering var derfor stærkt påvirket af de miljømæssige inputdata til modellen, som kom fra dette studie, sammen med korrekt valg af modelgeometri. Dette understreger behovet for indsamling og offentliggørelse af højkvalitetsdata om hydrografi, dybde og sedimentegenskaber, såvel som statistik for havisudbredelse og bølgehøjder (sea state) før VVM-redegørelsesprocessen for seismiske undersøgelser begynder et givent sted.

3 Imaqarniliap kalaallisuunngortinnera

Baffinbugtenimi uuliamik ujaasineq kalaallinit 2006-imi ammarneqarpoq, taamanikkumiillu sumiiffimmi uuliaqarnersoq gasseqarnersorlu qulaajaaffiginiarlugu immap naqqanik sajuppillatitsisarluni misissuisoqalerpoq. Kalaallit Nunaata avannaani Baffinbugtenimi umiarsuarmik immap naqqanik sajuppillatsitsiartortarluni sisamariarluni angalanissaq aqqaneq-marloriarlunilu misiliilluni qillerisoqarnissaa 2012-imi aasakkut pilersaarutaasimavoq. Kalaallit Nunaata imartaani immap naqqanik sajuppillatsitsisarluni misissuinissat akuerineqannginneranni avatangiisinut sunniutaasinnaasunik nalilersuineq (VVM-imik naliliinermik taaneqartartoq) pillugu nassuiaasiortoqartassasoq piumasaqaataavoq, tassami qamutillit nipimik aallartitsisartut atorneqartut nipitoorujussuummata. Tassani immami avatangiisinut nipiliornissatut naatsorsuutigineqartut pillugit ingerlatseqatigiiffimmit qarasaasiaq atorlugu qanoq issinnaaneranik takussutissiornissaq piumasaqaataavoq aamma ingerlatseqatigiiffiit Baffinbugtenimiittut tamarmik VVM-imik naliliinerminni sulianit tamanit nipiliornerit ataatsimut katillugit piffissaq kingusinnerusumut allaat sunniutigisinnaasaanik qarasaasiatigoortumik missingiussaminnik takussutissiortussaatitaapput . Tamanna suliniutit qinnuteqaatigineqartut akuersissutitassaannik tunniussinnginnermi immami uumasunut sunniutaasinnaasunik nalilersuisoqarniassammat taamatut piumasaqaateqartoqarpoq. Missingersuiniarluni periutsini eqqoqqissaartumik pinissaq pingaaruteqartorujussuuvoq, tassami tamakku sajuppillatsitsisarluni misissuinernit nipit assigiinngitsunik ungasissulinninngaanniit ungasissusillit nipitussusiannik missingiussiniarnernut atorneqartarmata. Taamatulli periuseqarnerni nipip qamutilimmit aallartinneqarnermini imarmi siammartarneranik pissutsit ilisimaneqanngitsut ilagaat. Suliniut manna umiarsuarnik sisamariarluni nipi atorlugu immap naqqanik sajuppillatsitsisarluni misissuiartornissanit sisamaasussatut pilersaarutigineqartunit nipit siammartarnerisa uppernarsarneqarnissaat tunngavigalugu nipimik suliniutitut angisuutut pilersinneqarpoq. Aammattaaq nipi atorlugu uuttortaanerit EIA-ni periutsit atorneqartut eqqortuunersut misissorniarlugit atorneqartarput. Nipinik uuttortaanerit, immap tarajoqassusia, kiassusia itissusialu pillugit paasissutissanik katersukkat eqqortumik pinissaq tamanna suli eqqornerusunngortinniarlugu nipimik siammartiterissummi Woods Hole Oceanographic Institutionimi (WHOI) ineriartortinneqarsimasumi aamma atorneqartussaapput.

Baffinibugtenimi nipimik uuttortaassutit paasissutissanik katersissutit 21-t immami uuttortaaveqarfinni immikkoortuni arfineq-marluusuni itissutsinilu pingasuni inissinneqarsimasuni siaruaanikkut misissuisoqarpoq. Uuttortaavinni tamani aamma itissutsini assigiinngitsuni kissamik aamma immap tarajoqassusianik paasissutissanik katersissutit agguataarneqarsimapput aamma paasissutissanik katersuivinnik tamakkuninngalu qaqitseriarluni periutsimi avatangiisit pillugit paasissutissanik katersilluni CTD-nik uuttortaasoqarpoq. Tamatuma saniatigut nipimik aallartitsissut qamutilik ilisarnaaserniarlugu nipimik qamutillip qanigisaani nipinik immiussissutit atorlugit immiussisoqarpoq. Misissuinermit tassannga paasissutissat Shell nipi atorlugu sajuppillatsitsisarluni misissuilinnginnerani, sajuppillatsitsisarnerata nalaani kingornalu paasissutissanik ilaneqarput. Paasissutissat tamakku uuttortaavinnit paasissutissanik katersaneersuullutillu aamma CTD-mik paasissutissaammata Baffinbugtenimi sumiiffinni assigiinngitsuneersuupput. Tamatuma kingorna paasissutissat assigiinngitsut marlunnut immikkoortitat taakku WHOI-mit periusissiami nutaaliaaqisumi atorneqarput.

Suliniut iluatsippoq aamma paasissutissanik katersuiviit katillugit 21-iusut ilaat 19-it 2012-imi nipi atorlugu immap naqqanik sajuppillatsitsisarluni misissuisoqareermat qaqeqqinneqarsinnaasimapput. CTD-mik uuttortaanerit piffissap misissuiffiusup nalaani marloriarluni uuttortaavinni tamani uuttortaasoqartarpoq. Baffinbugtenimi Qimusseriarsuarmilu nipi atorlugu immap naqqanik sajuppillatsitsisarluni misissuinerit iluaqutaanerpaat tassaanerupput tunua´tungaani nipiliornerit sisamariarluni umiarsuarmik nipi atorlugu sajuppillatsitsisarluni misissuiartortarnerni aallaqqaammut nipiusartut assigaat. Minutsimiit minutsimut nipi (tuluttut SEL-imik naalisagaq) nipimut tunuliaqutaasumut umiarsuit atorlugit nipimik sajuppillatsitsisarluni misissuiartortoqannginneranit issariarnermut 120 dB re 1 µPa² s mut sanilliullugu nipi 70 dB-mut nipittortarpoq, nalinginnaasumik nipi tunuliaqutaasoq siusinnerusukkut 20 dB-nik nipitunerugaluarpoq. Ullup unnuallu ataatsip ingerlanerani nipi nipittoriartuuaartoq (cSEL) issariarnermut 153 dB re 1 µPa² s -niit issariarnermut 189 dB re 1 µPa² s - nut nipittorpoq.

Umiarsuarmik nipi atorlugu immap naqqanik sajuppillatsitsisarluni misissuiartornerni nipi tunuliaqutaasoq nipittoriartuinnartartoq aamma ersarippoq, tassami nipimik qamutilimmit nipi aallartitaq nipip tulliuttup aallartinneqannginnerani nipaarunneq ajormat tunuliaqutitulluunniit nipinngortarmat. Sumiiffimmi ataatsimi nipi atorlugu arlalinnik sajuppillatsitsisaraanni nipimik qamutilimmit nipit arlallit assigiinngitsumik sakkortussuseqartut tusaaneqarsinnaasarput. Nipip tunuliaqutaasup nalinginnaasumik nipittoriartortarnera pissutigalugu nipimik qamutilimmit nipip nipit allat 1 aamma 10 kHz-it akornanniittut tusarsaajunnaarsissinnaavai, pingaarnerpaamik nipit sumiiffimmi uumassuseqartunut pingaaruteqarsinnaasut, ingammik nipimik qamutillup eqqaaniittut.

Nipimik qamutillip aappaanik 0,5, 1, 2, 4 aamma 8 sømilinit ungasitsigisumiit nipiliortitsisoqarpoq. Nipimik qamutilimmit nipit immiunneqartut nipimit tunuliaqutaasumit nipitunerujussuupput immaqalu 50 kHz tikillugu nipitussuseqarsinnaasarlutik. Angusap tamatuma nipimik qamutillup immami uumasunut miluumasunut sunniutigisinnaasaasa, ingammik arfernut kigutilinnut, kingunerisinnaasaanik naatsorsuinermi ilanngussisoqartariaqarnera takutippaa.

Nipip qatituup nipillu aqqutaata Issittup imartaata immap qaavata killinnguaniittumi siammarsimanera naatsorsuutigisamit siammarluarsinnaaneruvoq. Taamaattumik nipit nipitunerpaat uuttortaatinit immap qaavanut qaninnerusuniittunit uuttortarneqarput. Itissuseq tamanna uumasut imarmiut miluumasut anersaartorfigisarpaat uumasoqatiminnillu ingiaqateqarfigisarlugu. Nipit nipitunerpaaffii aamma uuttortaatinit immap qaavaniit atsissumiittunit immiunneqarput, tamakku tassaapput nipinik assigiinnik taaneqartartut, tamatumani nipit imminnut qaleriittarput nipimillu nipitunermik pilersitsisarlutik. Sunniutip tamatuma

VVM-imik naliliinermi uumasunut imarmiunut miluumasunut tunngatillugu kingunissanik naatsorsuusiornerni sunniutilinilu eqqaamaneqartariaqarpoq.

WHOI-mi nipip siammartarneranik misissuinerup, suliniummit matuminnga paasissutissanit katersorneqartunit pitsaanerulersinneqartup, paasinarsisippaa Baffinbugtip imartaani nipit siammartarnerat ima-iliallaannaq paasisassaanngitsoq. Periutsip takutippaa immap naqqata imavissuarmut itiseriarnera sinerlugu avannamut-kujammut nipi qatitooq ingerlaartartoq. Nipip ingerlaarfia tamanna uuliasiorfiutileqatigiiffiit nipi atorlugu immap naqqanik sajuppillatsitsisarlutik paasissutissaataannit katersorneqartunit aamma uppernarsarneqarpoq. Sinerissap qanittuani itissutsini assigiinngitsuni, aattunik iluliaqarfiusuni aamma nunamit apummik aattumik imilimmi nipit siammartarneri ima-iliallaannaq paasisassaanngikkaluartut, tamaattoq Baffinbugtenimi immamit ammaannartumit tamatuma nipiliorfiunnginnerunera paasineqarpoq. Nipip immami siaruartarneranik qarasaasiaq atorlugu periusissiaq piviusorsiornerpaajutinniaraanni misissuinermit matuminnga paasissutissat katersorneqartut immami avatangiisinut tunngassuteqartut assorujussuaq sunniuteqarput, taamatut aamma immap ilaata tarajukinneruffiinut tarajoqarneruffiinullu kiisalu immap naqqata sannaanut tunngassutillit periusissiamut ilanngutissallugit pingaaruteqarpoq, paasissutissallu tamakku sapinngisamik eqqornerpaajunissaat pingaaruteqarpoq.Tamatuma sumiiffimmi aalajangersimasumi VVM-imik nalilersuisoqannginnerani immap kissassusianut/nillissusianut tarajoqassusianut qanoq issusianullu aamma immap naqqata qanoq issusianik tamatumalu qaleriissiternerata sannaanik ilisimasanik aamma immap sikuata siammarsimaneranik mallillu portussusiinik (sea state) paasissutissanik katersisariaqarneq tamanullu nalunaarutiginninnissap pisariaqartinneqarnera erseqqippoq.

Uuliasioqatigiiffiit VVM-imik nalilersuineranni nipitussutsit Jasco-mit (suliffeqarfik qarasaasiakkut periusissiamik suliaqartoq) qarasaasiakkut missingiunneqartut iluinniittutut nipit uuttortarneqartut inissipput. Taamaattumik misissuinermit tassannga angusat VVM-mik naliliinermi siumoortumik missingiussiniartarnerni atorneqarsinnaarpasipput. Aammattaaq misissuinerit takutippaat, paasissutissanik pitsavissuunngikkaluartunik, nipit immap naqqanik sajuppillatsitsisarluni misissuinernit arlalinneersut ataatsikkoortut nipittoriartortullu uumasunut imarmiunut miluumasunut sivisuumik sunniutaasinnaasunik nalilersuutitut naammattumik nipitussuseqartut.

4 Introduction

4.1 Background for the study

Since the first round of licensing for hydrocarbon exploration in Greenland, in 2006, there have been hydrocarbon-related offshore activities in western Greenland every summer. Baffin Bay was opened to hydrocarbon exploration in 2010 when five licenses were awarded for blocks: Qamut (ConocoPhillips), Anu (Shell), Pitu (Cairn), Napu (Shell) and Tooq (Maersk) (**Figure 1**). The first large-scale activities took place in autumn 2011, when Cairn conducted a 2D seismic survey in the Pitu block (Perry et al. 2011; Annon. 2012). This was followed by a very large program in the summer-autumn 2012, where seismic surveys were conducted simultaneously in the four remaining blocks (LGL & Grontmij ; InuplanA/S & GolderAssociates 2012; NunaOil & Associates 2012).

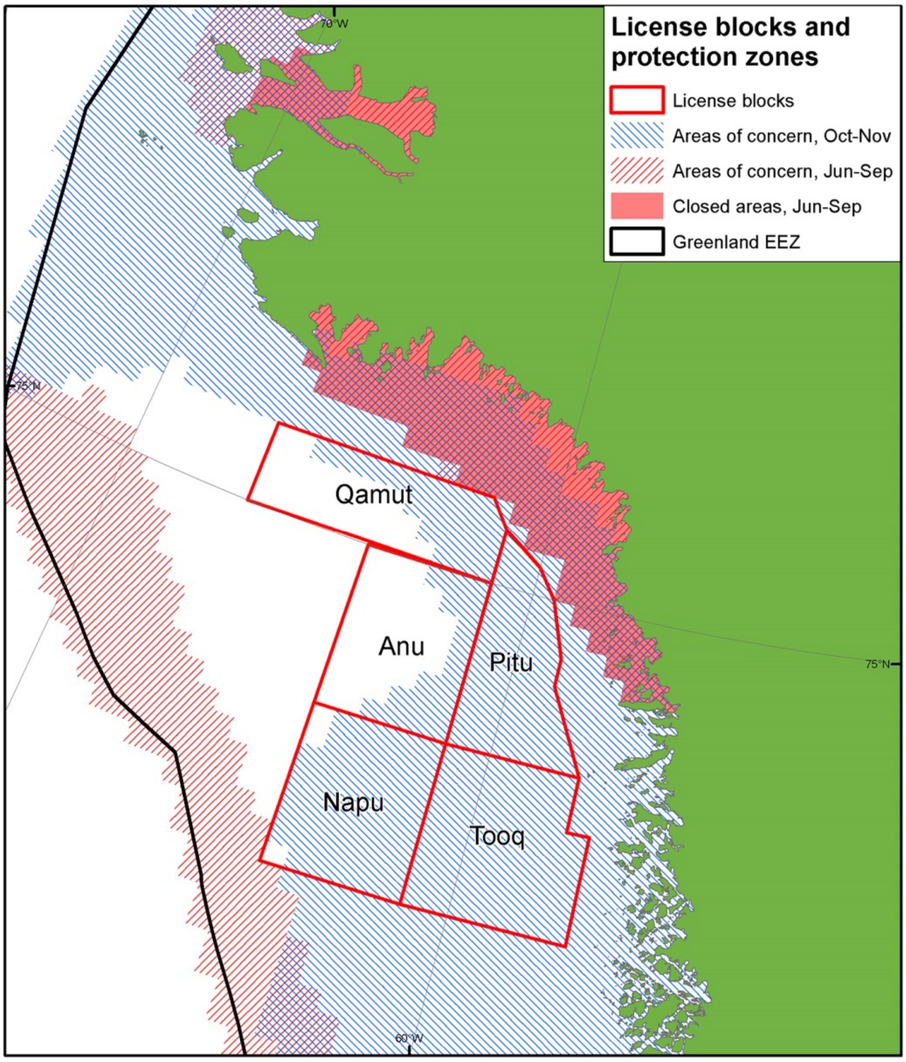

Figure 1. Location of the five exploration license blocks in the Baffin Bay with respect to protection zones: Jun-Sep for narwhals and bowhead whales (red dashed area), Oct-Nov for narwhals and belugas (blue dashed area), and the narwhal reserve (solid red area). Datum: WGS84; projection: Mercator.

Melville Bay, which forms the northernmost part of Baffin Bay, is a very important summering area for West Greenland narwhals, which are protected by a reserve inside Melville Bay (**Figure 1**). As narwhals reside in the Melville Bay Reserve during late summer and early autumn, at the same time as ice conditions permit seismic surveys to be conducted in Baffin Bay, concerns have continuously been raised over the possible impacts of seismic surveys on these animals (Tougaard et al. 2012).

Several major gaps exist in our knowledge of animals in the Baffin Bay/Melville Bay and their responses to powerful underwater noise. Consequently, in 2011, when the first seismic surveys were conducted by Cairn Energy in the Pitu block, a need to establish an adequate monitoring program to assess and quantify the effects of hydrocarbon exploration on marine mammals in the area, and narwhals in particular, was acknowledged (Kyhn & Boertmann 2011). One of the unknown factors in impact assessment is propagation of airgun pulses. It was therefore decided that a large scale acoustic monitoring study should be conducted to document the sound propagation from the four seismic surveys planned for 2012.

Although some information is available on narwhals, such as population estimates (Heide-Jørgensen et al. 2010b) and information on migration in and out of Melville Bay from satellite-tracked animals (Dietz & Heide-Jørgensen 1995; Heide-Jørgensen et al. 2013b), very little is known about the effects of seismic surveys on this species. Such information has yet to be obtained from West Greenland and the lack of knowledge on the noise levels to which the animals are exposed during seismic activities, would make it difficult to unequivocally relate any observed effects on narwhals to the seismic noise. Thus, the need for new information on the impacting noise was deemed the most important knowledge gap to fill.

The aim of the present study was therefore, to characterize both output from large 2D- and 3D seismic arrays and the propagation of these signals by means of in situ sound measurements during actual hydrocarbon exploration surveys (**Figure 2**). The measurements were also used to 1) verify the validity of the predictive sound propagation modeling commissioned by the hydrocarbon companies as part of the Environmental Impact Assessment process, and to 2) obtain environmental data to feed into, and acoustic data to validate, an advanced sound propagation model developed by collaborators at Woods Hole Oceanographic Institution (WHOI). Model precision is crucial as modeling is often used in EIAs to predict noise level changes with range from the source in relation to potential effects on marine life.

Figure 2. One of the seismic vessels used in Baffin Bay in 2012: *Polarcus Asima*. Photo: sea-hawk.com/arctic-achievements.

4.2 Baffin Bay and Melville Bay

Baffin Bay extends from West Greenland to the High Arctic Canadian Archipelago. It is limited northwards by the Nares Strait and southward by the 70° latitude in Davis Strait. Melville Bay (Qimusseriarsuaq in Greenlandic) constitutes the coastal area of the Northeast Baffin Bay, from the Upernavik archipelago to Kap York. Both Baffin Bay and Melville Bay are within the high Arctic zone. Icebergs from the glaciers in Melville Bay and sea ice dominate the physical marine environment.

4.2.1 Bathymetry

Shallow sills, both to the north and south of Baffin Bay, create a relatively isolated body of cool, deep, polar water, unique among the Arctic Seas. The shelf (depths less than 200 m) (**Figure 1**) is generally rather narrow, usually extending less than 50 km from the coast. Outside of the shelf, depths reach more than 2.000 m in the central parts of the bay where sediments are mainly silt.

The shoreline of Melville Bay is an archipelago dominated by bedrock. Multiple glaciers cover long stretches of the coastline. The depth within the Melville Bay archipelago is largely uncharted. Outside of the archipelago, the depth of Melville Bay is approximately 300-500 m. Kap York Iceberg Bank is located centrally in the Bay with depths of only 100-200 m. In the southern part of the bay, a deep trench extends northwest into the bay with depths of about 600-700 m and a deep basin of 1100-1200 m (**Figure 1**).

4.2.2 Hydrography

The water in Baffin Bay has two sources; The Arctic Ocean and the Atlantic Ocean (Muench 1971). The polar water inflow from the Arctic Ocean, through the Nares Strait, to Baffin Bay is strongest during spring and early summer (May-July), whereas the inflow of Atlantic water is strongest during autumn and winter.

Three water masses can be identified in Baffin Bay; Arctic water in the upper 100-200 m depth, West Greenland Intermediate Water in the intermediate 200-800 m depth and Deep Baffin Bay water at all depths deeper than 1200 m (Tang et al. 2004)). The Deep Baffin Bay water is characterized by relatively high temperatures (1°C-4°C) and high salinity (34-35 ppt), the West Greenland Intermediate Water by low temperatures (-0,5°C-1°C) and high salinity (34,5 ppt) and finally, the Arctic water is characterized by low temperatures (-1°C-1°C) and relatively lower salinity (32-34 ppt) (Tang et al. 2004). As a result, the highest density water masses in Baffin Bay are located at 50-150m depth.

Strong winds occur in Baffin Bay, prevailing North-West, and storms are especially strong and frequent during winter. Although wind stress mixes the upper water masses, at depths below 300 m, there is limited annual variability in salinity and temperature.

4.2.3 Ice conditions

Melville Bay and Baffin Bay are dominated by two types of ice; icebergs originating from the glaciers and sea ice, forming when temperatures drop in winter.

4.2.3.1 Icebergs

About 19 large glaciers are located within Melville Bay, releasing thousands of icebergs each year into the Baffin and Melville Bays, which subsequently release freshwater into the surrounding sea when melted. Some of the glaciers can produce icebergs with diameters of 1 km, and annually an estimated volume of 60 km^3 of icebergs is produced in Melville Bay. In addition to Melville Bay, the more southern glaciers in Uummannaq Fjord and Disko Bay also produce a substantial output of icebergs, the majority of which are carried northwards to Baffin and Melville Bay (**Figure 3**). From here, the majority of icebergs will drift southward in the western Davis Strait, joining the Labrador Current further south (**Figure 3**).

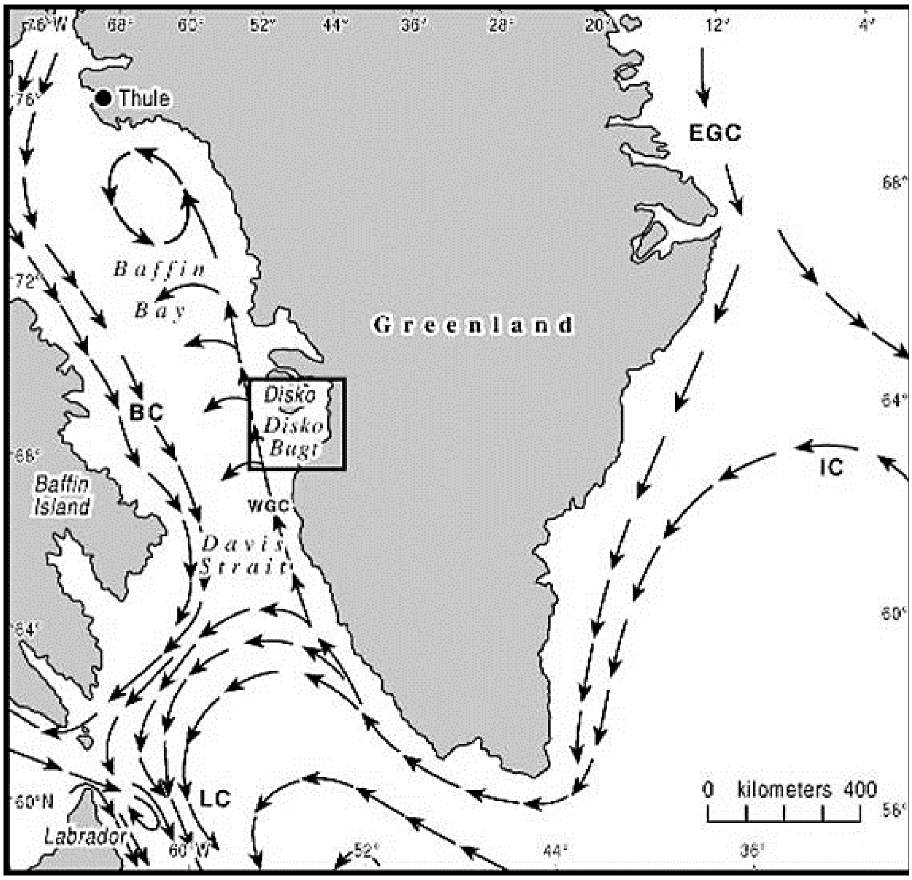

Figure 3. Surface sea currents in Baffin Bay and Davis Strait. Source: Tübingen University.

4.2.3.2 Sea ice

Two types of sea ice can occur in the Baffin Bay and Melville Bay: multi-year sea ice and first-year sea ice. Multi-year ice normally enters from the polar sea as drift ice through the Nares Strait and stays on the Canadian side of the Baffin Bay allowing first-year sea ice to dominate Melville Bay and the Greenland side of Baffin Bay.

In Melville Bay, the sea ice is land fast and forms inside the fjords independently of the ice conditions in Baffin Bay. The sea ice formation in Melville Bay begins in late September, early October, and reaches more than 130-180 cm thickness at its peak in March (Valeur et al. 1996). In Baffin Bay, the sea ice gradually builds up in October from the west and meets the land fast ice along the Greenland coast in January. The sea ice in Baffin Bay also peaks in March where it can reach up to 120-150 cm in thickness (Valeur et al. 1996). By late July, Baffin Bay and Melville Bay are usually completely ice-free, although fields of drift ice may remain in the area throughout summer until late September when the process of ice formation starts over (Taylor et al. 2001).

4.3 Marine mammals in Baffin Bay

Baffin Bay and Melville Bay have a large diversity of marine mammals with four species of seals, walrus, polar bear and at least eleven species of cetaceans (Boertmann & Mosbech 2011). Even though the focus of this study is on propagation of airgun pulses, a brief description of the marine mammals of the area is provided to help the reader appreciate the importance of the noise monitoring program. Here we will briefly outline distribution, migratory routes and sensitivity to disturbances of the most common species and those most likely to be affected by seismic activities in the area.

4.3.1 Narwhal (*Monodon monoceros*, Linnaeus, 1756)

Narwhals are common and endemic to the Arctic. In Greenland narwhals move between summering and wintering grounds and they show strong site fidelity to these grounds and migratory routes (Dietz et al. 2001; Heide-Jørgensen et al. 2002; Heide-Jørgensen et al. 2003a; Dietz et al. 2008). The identification of the many Canadian and Greenlandic stocks is based on the summering grounds, while several stocks can meet on the same wintering ground (Heide-Jørgensen et al. 2003a). Baffin Bay and Melville Bay are important habitats to narwhals and the animals occur throughout the year in different areas of Baffin Bay. Protection zones have been assigned for protection of narwhals in relation to seismic surveys (**Figure 4**) (Kyhn et al. 2011).

In Baffin Bay there are two main summering grounds: Inglefield Bredning and Melville Bay, with summer abundance estimates of 8,368 (95 % CI 5,209-13,442, year 2007) and 2,800 (95 % CI 1,354 – 5,827, year 2012), respectively (Heide-Jørgensen et al. 2010a; Heide-Jørgensen et al. 2013b). The narwhals arrive to the summering grounds when the sea ice opens in June-July. In the autumn, upon the formation of fast ice, narwhals are forced to move east and south out of these regions and spend the winter in areas covered by dense offshore pack ice (Dietz & Heide-Jørgensen 1995; Dietz et al. 2001; Heide-Jørgensen et al. 2002; Heide-Jørgensen et al. 2003a; Dietz et al. 2008). When leaving the summering grounds they follow similar routes to the wintering grounds as during the spring migration. Whales from different stocks have similar timing for abandoning their wintering grounds and initiating spring migration. Narwhals tracked from Melville Bay during the autumns of 1993-94 (n=2) and 2006 -07 (n=7) began their migration in October and reached the wintering grounds in November, following a migration corridor that extended from coastal waters to the 1000 m depth contour (Dietz & Heide-Jørgensen 1995; Heide-Jørgensen & Dietz 1995). They remain in their wintering grounds from late November through March. One whale was tracked for 13 months and it returned to Melville Bay the year after it was tagged. During winter months, narwhals are widely dispersed in Baffin Bay and Davis Strait with high concentrations between 55°-64°W and 68°-71° N and off Disko Bay (Heide-Jørgensen et al. 1993; Koski & Davis 1994; Dietz et al. 2001; Heide-Jørgensen & Acquarone 2002; Heide-Jørgensen et al. 2002; Dietz et al. 2008; Laidre & Heide-Jørgensen 2011). During spring, concentrations of narwhals are seen along ice edges on the east coast of Baffin Island, at the entrances of Lancaster and Jones Sound, and in Smith Sound (e.g. (Bradstreet 1982; Koski & Davis 1994). Narwhals are also known to move along the ice edges off West Greenland and to concentrate in the North Water Polynya in spring before entering Inglefield Bredning (Born et al. 1994; Heide-Jørgensen 2004; Heide-Jørgensen et al. 2013b).

In the late 1800's and until late 1900's narwhals were hunted in large numbers. In the period of 1993-2003 an average of 519 narwhals were hunted annually in West Greenland (GNIR). The unregulated hunt decreased the population and in 2004 annual hunting quotas were established. The annual quota in West Greenland for 2013-2015 is 310 narwhals per year. The Quota for Melville Bay (Savissivik & Upernavik) 2012 was 81 narwhals. In Melville Bay narwhals are usually caught from October through May, when they migrate through the area in October and May-June. The population in West Greenland is red-listed as 'Critically Endangered', while the global population is listed as 'Data Deficient' (DD).

Narwhals produce a number of different sounds for echolocation and communication. Echolocation clicks are broadband with peak energy around 48 kHz, while communication clicks have peak energy around 38 kHz (Miller et al. 1995). Buzzes and whistles have the main energy in the range between 300 Hz and 18 kHz (Miller et al. 1995). The hearing of narwhals has not been measured, but that of a closely related species, the beluga, has (Awbrey et al. 1988). The results show very sensitive high-frequency hearing (see below 4.3.2).

Narwhals are sensitive to anthropogenic noise (see below 4.5.3.2). As a consequence, three protection zones for narwhals have been designated in relation to seismic activities (Mosbech et al. 2000; Boertmann et al. 2010).

Figure 4. Narwhal protection zones and closed areas in Melville Bay.

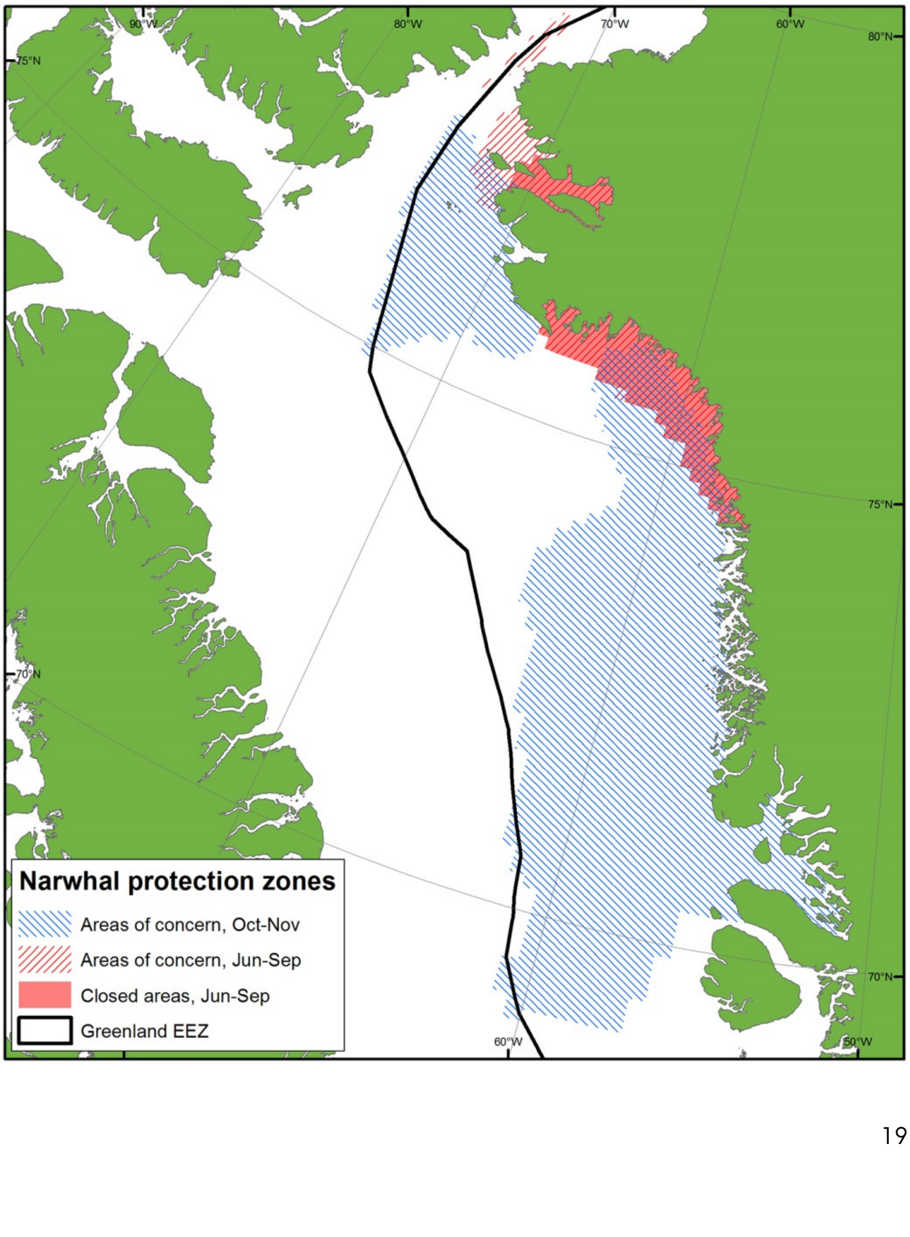

Narwhal zone I is the summer habitat, where narwhals are present when the sea ice melts in the summer until the fall migration (1 June to 15 Oct). White whales (beluga whales) also occur in this area from 1 October. The boundary is defined by a straight line (Long./Lat. projection) between Cape York and Wilcox Head on Holm Island. In zone I seismic activities shall be limited as much as possible and best avoided. Narwhal zone II is the fall migration habitat where the narwhals (and belugas) are present from 15 October at least until 1 Dec. Seismic activities in narwhal zone II shall be confined to a minimum in the protection period. Narwhal zone III is the winter habitat (15 Nov. to 30 March).

4.3.2 Beluga (*Delphinapterus leucas*, Pallas, 1776)

Belugas are common to the ArcticThe belugas seasonally inhabiting Baffin Bay migrate from the Canadian Arctic archipelago, through Baffin Bay in October-November on their way to the wintering grounds around Store Hellefiskebanke south of Baffin Bay (**Figure 5.** Protection zones for beluga in East Greenland.). While on the wintering grounds they consume the majority of their annual food intake. In April-June the belugas travel back northeast through Baffin Bay to their summering grounds in the Canadian Arctic archipelago (**Figure 5**). This migratory pattern has only been confirmed by two satellite tagged belugas (GINR unpublished data) and generally the knowledge on beluga migrations is limited.

Regular aerial surveys have been carried out to estimate the abundance of belugas in West Greenland. Between 1981 and 1999 there was a significant decline in the population due to the high hunting pressure (Heide-Jørgensen & Reeves 1996; Heide-Jørgensen & Acquarone 2002). The annual catch in 1993-2003 was on average 550 whales. The population seems to be increasing again after the introduction of catch quotas in 2005. An aerial survey in 2006 revealed an estimated abundance of 10,595 (95 % CI 4,904-24,650) individuals in the west Greenland population. Since 2009 the quota has been 350 belugas. According to official numbers, this quota has never been caught completely (Piniarneq, Greenland Government). Due to past catch history and population trends belugas using Baffin Bay have an unfavourable conservation status, listed as 'Critically Endangered' on the Greenland Red List and as 'Near Threatened' on the Global Red List (IUCN 2010).

Belugas produce a variety of sounds for echolocation and communication. Communication sounds have the main energy from 100 Hz to 12 kHz (O'Corry-Crowe 2002) and echolocation clicks have the main energy between 40 and 120 kHz depending on target and background noise (Au et al. 1985; Turl et al. 1991). The beluga whale has its best hearing around 38-58 kHz and hears well at low frequencies as well (Awbrey et al. 1988; Klishin et al. 2000).

Figure 5. Protection zones for beluga in East Greenland.

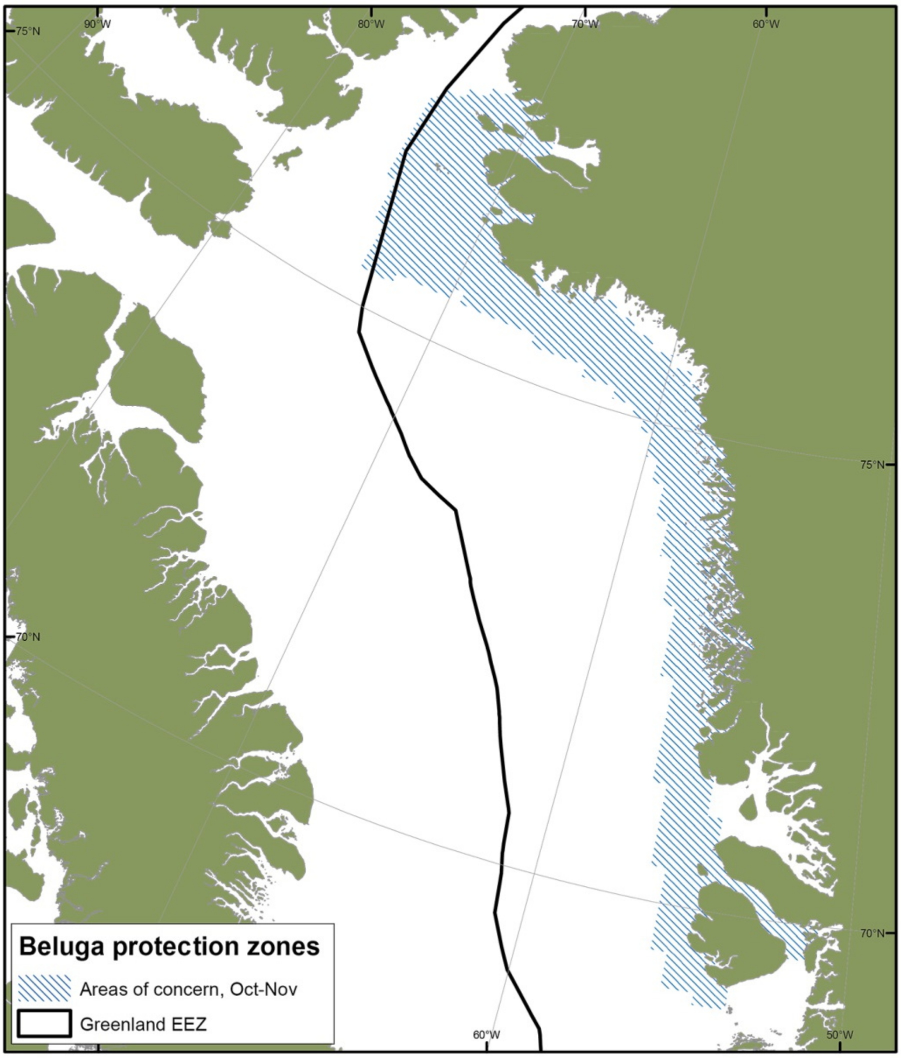

4.3.3 Bowhead whale (*Balaena mysticetus*, Linnaeus, 1758)

The primary area for bowhead whales in West Greenland is Disko Bay south of Baffin Bay, but they are found along the coast from Nordre Strømfjord to Qaanaaq (**Figure 6**). Bowheads migrate from Canada to West Greenland in December-January, where they come to feed on the abundant zooplankton, mainly copepods. Mating is believed to take place in March, and in May-June the whales migrate northeast through Baffin Bay which is still partly ice covered at that time. Bowhead whales are adapted to live in sea ice and possibly travel through leads and cracks in the pack ice (Heide-Jørgensen et al. 2003b; Heide-Jørgensen et al. 2006). From Baffin Bay bowheads migrate to the Canadian Arctic Archipelago where they spend the summer and fall before migrating through Davis Strait back to Disko Bay.

The bowhead whales in West Greenland are part of a population covering the Canadian High Arctic Archipelago and part of West Greenland (IWC 2012). In 2006, the abundance estimate for bowhead whales in the high density area of Disko Bay was estimated to 1,229 animals (95 % CI: 495-2,939) (Heide-Jørgensen et al. 2007). However, the overall population size is much larger as the abundance on the Canadian side was estimated to 6,344 animals (95 % confidence limits 3,119-12,906) (IWC 2008). During the commercial whaling period the bowhead whale was hunted to near extinction, and although it has recently shown signs of recovery (Heide-Jørgensen & Laidre

2010) the population size is still much smaller than the assumed pre-whaling population size (Allen & Keay 2006). Canada hunts a few bowhead whales per year whilst Greenland has a quota, through the IWC, of two individuals per year. However, in recent years no animals have been taken in Greenland. Due to the recent increase in population size, the bowhead whale population migrating through Baffin Bay is now listed as 'Near Threatened' (NT) on the Greenland Red List and as 'Least Concern' (LC) on the international Red List (IUCN 2010).

Bowhead whales produce a number of different calls for communication. The different calls have the primary energy between 20 Hz and 2 kHz (Tervo et al. 2009). The hearing of bowhead whales has, not surprisingly, never been measured, but given their vocalizations, there is reason to believe that they have good low frequency hearing.

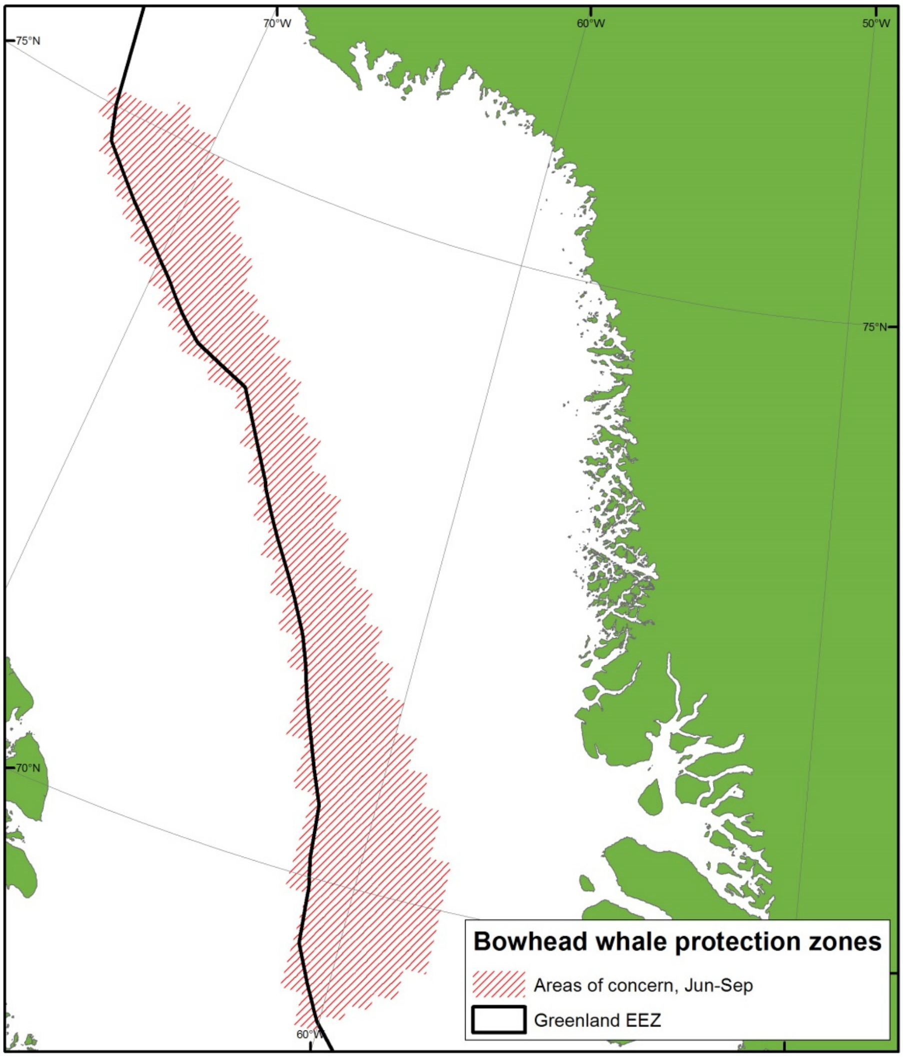

Figure 6. Protection zones for Bowhead whales in East Greenland.

4.3.4 Seals

Four species of seals are known to inhabit Baffin Bay and Melville Bay; bearded seal (*Erignathus barbatus*), ringed seal (*Pusa hispida*), hooded seal (*Cystophora cristata*) and harp seal (*Pagophilus groenlandica*). Although some species seasonally migrate out of Baffin Bay, all four are present in the area during the open water season when seismic and other explorative activities occur.

4.3.4.1 Bearded seal

Bearded seals in Baffin and Melville Bay are part of a large and widespread population present in the area all year; however, no abundance estimates of bearded seals are currently available. Due to the lack of knowledge on population boundaries and numbers they are listed as 'Data Deficient' on the Greenland Red List. During mating and whelping (March-June), the distribution is linked to the extent of the sea ice (Gjertz et al. 2000), and in winter, to the areas with thin sea ice, leaks and polyneas, which are required to make and maintain breathing holes. The hunt is considered sustainable and on a global scale bearded seals are listed as 'Least Concern' (IUCN 2010).

Bearded seal males produce calls to attract females. The calls are frequency-modulated down sweeps. The frequency content varies geographically, but the main energy is typically between 100 Hz to 3 kHz (Risch et al. 2007). The hearing of bearded seals has not been tested.

4.3.4.2 Ringed seal

High numbers of ringed seals are present in Baffin and Melville Bay throughout the year. Their distribution is linked to the sea ice on which they are completely dependent during whelping (March-April), weaning (March-May) and moulting (June). During winter they are spread out in Baffin and Melville Bay, breathing through holes made and maintained in the fast or new ice. The catch in Baffin and Melville Bay, of about 40,000 ringed seals per year, has been stable for many years and is considered sustainable with the population listed as of 'Least Concern' (LC) on the Greenland Red List.

Ringed seal males use underwater calls to attract females. The calls have the main energy between around 500 Hz to 4 kHz (Stirling 1973). Ringed seals have their best hearing around 16 kHz, but can hear down to at least 1 kHz and have not been tested lower. Equally, they can hear up to at least 90 kHz (Terhune & Ronald 1975).

4.3.4.3 Hooded seals

The hooded seals in Baffin Bay are part of the large West Atlantic population in the Baffin Bay/Davis Strait region, however, no abundance estimates of this species in Baffin Bay are available. After whelping (March-April) in Newfoundland and Davis Strait, and moulting (June-July) on drift ice in SE Greenland, the majority of the adult population migrates to feed in Baffin Bay from September to November (Stenson et al. 1996; Andersen et al. 2009). The annual catch of about 500 individuals is considered sustainable (ICES 2006) and hooded seals are listed as of 'Least Concern' (LC) on the Greenland Red List.

Hooded seal males produce low-frequency, pulsed calls to attract females and intimidate other males (Terhune & Ronald 1973; Ballard & Kovacs 1995). No audiogram has yet been made to test their hearing.

4.3.5 Harp seal

The harp seals in Baffin Bay are part of the West Atlantic population that is made up of an estimated 8 million individuals whelping off Newfoundland in 2010 (Hammill & Stenson 2010). In Baffin Bay harp seals are abundant throughout the summer and when the sea ice forms they migrate to the Newfoundland whelping areas (February-April). In March they give birth before moulting in April, after which they spread into Greenlandic and Canadian waters. The harp seals are listed as of 'Least Concern' on the Greenland Red List and the yearly catch of about 15,000 seals per year is considered sustainable.

Harp seal males produce sounds to attract females. The energy varies between 400 Hz to 7 kHz (Serrano 2001) and therefore overlaps with the airgun spectrum. The harp seal hears best between 2-22.9 kHz, but hears well down to 760 Hz and up to 100 kHz (the highest frequency tested) (Terhune & Ronald 1972).

4.4 Seismic surveys and marine mammals

Seismic sources used for hydrocarbon exploration in deep oceanic water are among the most powerful man-made sound sources (Hildebrand 2009). Consequently, they have attracted attention with respect to their possible negative impacts on marine organisms, primarily, but not exclusively, on marine mammals.

4.4.1 Seismic sources

Transmitting sound kilometers into the seabed requires very powerful, low frequency sound sources. The most commonly used seismic sound source is an airgun, which generates a short and powerful sound when air under high pressure is released. Several airguns are combined into an array (**Figure 7** and **Figure 8**) to increase the power output, and direct the sound downwards into the subsurface. The far field on-axis signature consists of a short, sharp onset peak of excess pressure, followed by a negative reflection of the pulse from the surface (surface ghost). Acoustic signatures of individual airguns contain a short, powerful first pressure pulse, followed by a number of longer, smaller pulses caused by the collapsing of air bubbles. By carefully selecting the size of the individual airguns it is possible to achieve a combined far field signature where the contributions from the collapsing bubbles cancels out to a large degree, leaving only the main pulse and the surface ghost (see example in **Figure 9**).

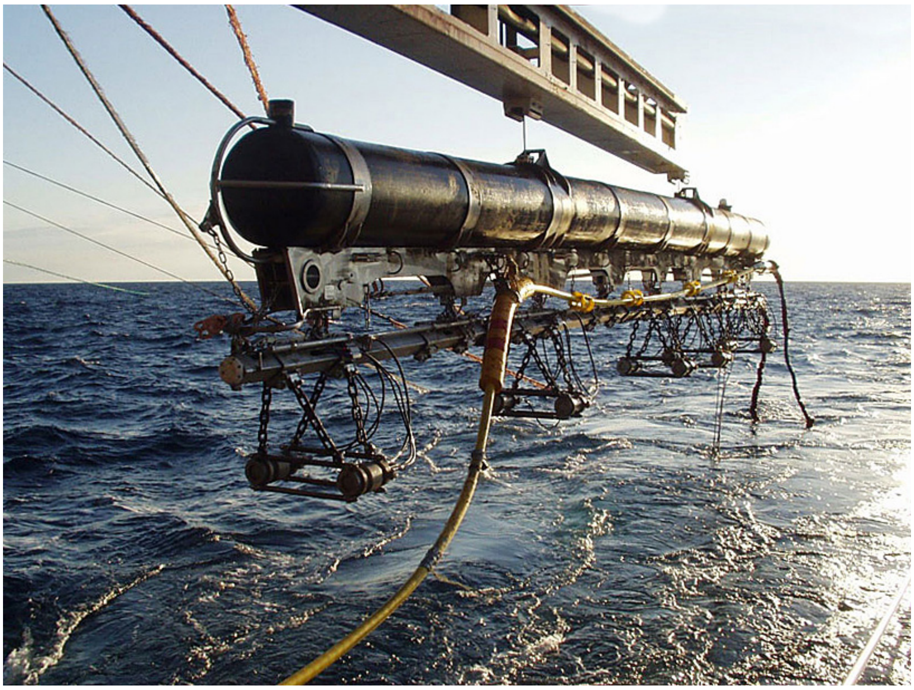

Figure 7. Airgun array. Note the individual airguns hanging pairwise below the frame and pontoon. The yellow hose supplies pressurized air to the array. Photo: www.sercel.com/products/g-gun-2.aspx.

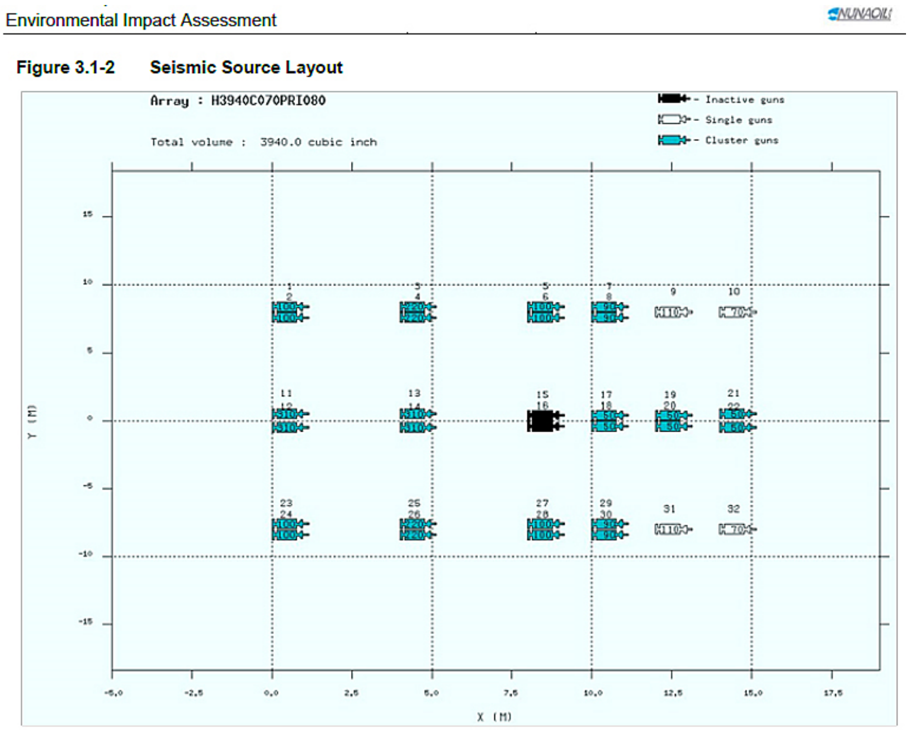

Figure 8. Layout of a large airgun array consisting of 32 airguns with a total volume of 3940 In^3. The figure inside each air gun indicates the individual volumes. From ConocoPhillips EIA (Austin et al. 2010a, p. 74).

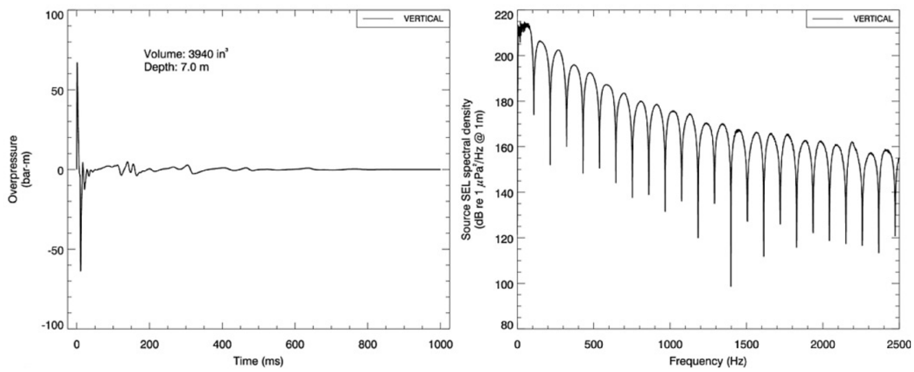

Figure 9. Modeled far-field pressure signature (left) and power density spectrum (right) of a 3940 In^3 seismic array, directly below the array. From ConocoPhillips EIA (Austin et al. 2010a, p.76-77).

4.4.2 Sound propagation in Arctic waters

Estimating the sound exposure that animals will experience at large distances from powerful sound sources is by no means trivial. A number of factors play important roles in determining sound propagation in general, and for airgun arrays and Arctic waters in particular. The signals one can record at some distance horizontally from an array will deviate considerably from the modeled signal shown in **Figure 9**, and received levels will not be predictable in a simple way from the source factor/source level (the sound pressure normalized to a distance of 1 m from the array) and spectrum.

Firstly, off-axis the array is not a point source, but consists of a large number of separate airguns (or clusters of airguns). The signal in **Figure 9** is modeled to be directly below the array at a depth of several times the aperture of the array, which means that the main pulses (and surface ghosts) from the individual airguns are all in phase and add constructively to the signal to form a short and powerful on-axis signal. This will not be the case at other positions horizontal to the array, where there will be different delays to the receiver and consequently a breakup of the main pulse into several smaller pulses.

Secondly, the proximity to the surface will affect sound propagation of low frequencies. The so called Lloyd's mirror effect, where the phase-inverted surface echo interferes destructively with the directly transmitted pulse at distances of up to a few wavelengths from the surface means that the low frequency part of the signal cannot propagate close to the surface. The main energy of the signal in **Figure 9** is below 100 Hz, corresponding to a wavelength of more than 15 m, which means that this part of the signal is strongly attenuated close to the surface at longer distances from the array.

Thirdly, the possibility of a surface duct, with greatly enhanced transmission properties, due to a minimum in the vertical sound speed profile, will duct the sound, which tends to be trapped in the channel, with significantly better transmission than predicted from simple transmission loss models that ignore the sound speed profile (e.g. (DeRuiter et al. 2006; Madsen et al. 2006)).

Lastly, a further complicating factor is the presence of drifting ice, both icebergs from the glaciers and broken up sea ice, which complicates sound transmission even further.

4.5 Noise impact

Noise can result in a variety of detrimental effects whose consequences to marine life, and marine mammals in particular, can range from nil to severe, depending on the type and received level of the sound. See for example (Gordon et al. 2004; Nowacek et al. 2007b; Southall et al. 2007) for recent reviews.

4.5.1 Injury

High sound pressures, such as those generated from seismic airguns, are capable of elevating hearing thresholds, an effect also known as a threshold shift (TS). If the threshold returns to the pre-exposure level after a period of time, the TS is known as a temporary threshold shift (TTS); if the threshold does not return to the pre-exposure level, the TS is called a permanent threshold shift (PTS). The onset of temporary threshold shift (TTS) has been documented in the beluga, where TTS was induced in an individual exposed to a short pulse from a water gun with a sound exposure level (SEL, sound energy) of 186 dB re 1 uPa^2s (Finneran et al. 2000). This signal is comparable to a signal from an airgun and can thus be used to assess the risk of inflicting TTS on belugas during seismic surveys. There are no data available from narwhals, or bowhead whales and Arctic seals, but as narwhals and belugas are closely related, and of comparable size, it appears a reasonable first assumption to use beluga data for narwhals as well. It is therefore expected that narwhals may develop TTS at close ranges to an operating airgun array.

4.5.2 Physiological effects of prolonged noise exposure

It is well known from humans that prolonged exposure to noise at levels below thresholds for acute effects can produce hearing loss and also induce other physiological effects, such as elevated stress hormone concentrations in the blood (Evans & Johnson 2000), increased blood pressure, heart problems and reduced learning capabilities among others (Passchier-Vermeer & Passchier 2000). One study on belugas has shown that blood stress hormone levels increased in response to noise exposure (water guns), and that these levels increased with increasing noise levels (Romano et al. 2004). A recent study on northern right whales showed that they had elevated levels of stress hormones likely as a consequence of intense ship noise in the waters off New England (Rolland et al. 2012). These effects may be relevant for marine mammals in Baffin Bay. The long term consequences of such elevated stress hormone levels are unknown for marine mammals and the risks cannot be assessed.

4.5.3 Changes in behavior and activity

There are few studies on behavioral reactions of Arctic marine mammals to noise from seismic surveys. Where needed, we have therefore included studies where these species have reacted to noise from other sources. Such studies are highly relevant as they may help envision how the species may react to seismic noise.

4.5.3.1 Beluga

Belugas are sensitive to noise (Lawson 2005). They have shown avoidance reactions to seismic operations at distances of up to 20 km from the airgun array, where the received level was calculated to be about 130 dB re 1 µPa (rms) (Miller et al. 2005). From the seismic vessel itself, there were only two sightings (at ranges of 1.5 and 2.5 km) during 1561 hours of daylight observations, while at 20-30 km from the seismic vessel the number of belugas was unexpectedly high (Miller et al. 2005). This was examined by comparing aerial and vessel-born observations collected concurrently during the seismic operations. This study shows that when a species is not observed from seismic vessels in areas where it should be present, it does not mean that there are no animals there, rather that they avoid areas within a certain range of the noise source.

In another study, Finley et al. (1990) showed that belugas react strongly to icebreaker noise: belugas were displaced to ranges of up to 80 km from the icebreaker and they reacted by fleeing rapidly away from the direction of the icebreaker. Their group integrity broke down and their dive pattern changed as the animals joined in large group to make long dives close to or beneath ice edges. Also, their acoustic behavior changed and they made apparent alarm calls at ranges of 80 km to the icebreaker, i.e. long before it was visible.

In Baffin Bay belugas are migrating near ice covered waters. Changes in behavior or travelling routes due to disturbances can be fatal, as belugas can be trapped in the ice. Belugas should be considered as highly sensitive to disturbance from seismic surveys and other anthropogenic activities.

4.5.3.2 Narwhals

There are no studies on reactions of narwhals to seismic noise. However, there is a study on narwhal reactions to an icebreaker which may be indicative of how these animals may react to seismic noise. Finley and colleagues (1990) showed that narwhals disappeared from an area up to 80 km from an advancing icebreaker. Narwhals showed two different reactions in response to the noise: they either huddled together, staying motionless at the surface while remaining in physical contact with each other, seized vocalizations and changed their normal dive behavior in that they sank quietly below the surface; or they fled rapidly in the same manner as belugas in the same area did. The first reaction was more common and was interpreted as a stealth anti-predator strategy, as the same behavior had been observed in response to killer whales. Thus, narwhals seem to interpret icebreaker sounds as a danger and react accordingly. The other reaction could have resulted from panic. About a day after the icebreaker had departed, narwhals returned to the area showing normal behavior. Similar reactions may be expected to seismic noise and therefore narwhals are not likely to be observed from seismic vessels.

Baffin Bay is an important habitat for narwhals as they make two yearly migrations through the bay to their summering or wintering grounds showing high site fidelity. In the fall, four different populations of narwhals migrate to the same general area in the southern part of Baffin Bay (Dietz et al. 2008) to overwinter. It was suggested by Heide-Jørgensen and colleagues that an increase in observations of narwhal groups trapped in the ice in 2008 and 2009-10 could be due to seismic surveys causing a delay in the fall migration (Heide-Jørgensen et al. 2012). Changes in narwhal behavior and migration patterns may be fatal. Narwhals should thus be considered as highly sensitive to disturbances from seismic surveys and other anthropogenic activities.

4.5.3.3 Bowheads

Bowhead whales have shown avoidance behavior during migration at distances of up to 30 km from a seismic array (received levels of 120-130 dB re 1 μPa peak to peak unweighted) (Koski & Johnson 1987; Richardson et al. 1999). In another study some bowheads were observed from the seismic vessel at ranges leading to shutdowns (within 1000 m for that survey) (Miller et al. 2005), however, there were twice as many bowheads observed from the seismic vessel at times with inactive airguns as when the airguns were in operation. Also, the range of the animals to the vessel was significantly shorter when the airguns were inactive. This suggests that some bowheads avoided the area when the airguns were on. Koski et al. (2009) showed that feeding bowheads tolerated differing levels of seismic noise before they disrupted their feeding. Some tolerated levels up to 160 dB re 1 μPa (rms) whereas others tolerated levels up to 170 dB re 1μPa (rms). A recent study showed that bowheads stopped calling when median received levels from airgun pulses reached 116–129 dB re 1 μPa (10–450 Hz) at a median distance of 41–45 km (Blackwell et al. 2013). The difference in behavioral reactions among animals of the same species may be attributed to differences in their physiological state (e.g. hungry vs not hungry, sex, previous experiences, presence of calves, age etc.). Beale and Monaghan (Beale & Monaghan 2004) found that hungry turnstones tolerated greater levels of disturbance than well-fed birds did. The hungry birds had to tolerate the disturbance in order to feed, whereas the more fit animals simply left the area to feed elsewhere or return later. This could be the case for the Bowhead feeding study mentioned above, and is an important point to consider when evaluating behavioral reactions in response to human disturbances.

The fact that the bowhead whale population is listed as near-threatened, together with the knowledge that they utilize Baffin Bay for behaviors important to their fitness and that they are sensitive to airgun noise means that the population is particularly vulnerable to the effects of hydrocarbon exploration.

4.5.3.4 Seals

All seal species are vocal and depend on acoustic cues for a range of behaviors. Bearded seals depend on acoustic communication, especially during the mating season where males holding a territory sing to attract females (Burns 1981). During this period (March-June) bearded seals may be sensitive to acoustic disturbances. Bearded seal calls have the main energy between 500-5000 Hz (Risch et al. 2007), i.e. in the same frequency range as seismic noise and they may therefore experience signal masking. Also hooded and harp male seals produce calls in the frequency range overlapping with airgun noise. As a consequence, seals will have to increase signal source level to be heard at the same distances as without the airgun noise. This may not be possible near strong airgun pulses, and ultimately signal masking could cause a decrease in mating rate for seals exposed to seismic noise during their mating season. Signal change of the caller in response to noise is known as the Lombard effect and has been shown in primates, birds and marine mammals (Tyack 2008). In a single study on effects of airgun noise on seals (Harris et al. 2001), a few bearded seals were observed near a seismic vessel and appeared to tolerate airgun noise well. However, the authors did not state what the expected undisturbed distribution of bearded seals would have been, and it is thus not known if or to what degree some bearded seals actually were displaced from the area. Another study (Blackwell et al. 2004) conducted in connection to pile driving in Alaska (Northstar production island) seems to support that seals (in this case ringed seals) tolerate loud impulsive sounds. Ringed seals are not considered especially sensitive to noise from seismic exploration as ringed seals exposed to seismic ships in other areas showed only little avoidance behavior (Harris et al. 2001; Lee et al. 2005). However, ringed seals may still be subject to masking as the calls males produce to attract females overlap in frequency with airgun noise.

Harp seals and hooded seals are also present in the area but very little is known about their acoustic behavior and even less about possible detrimental effects of noise on these species.

4.6 Seismic program in 2012

The combined activity program proposed by the hydrocarbon companies for the 2012 season was extensive and raised concerns about its possible detrimental effects, especially on the narwhal population in Melville Bay.

4.6.1 Issues of concern

The program suggested in the spring of 2012 consisted of simultaneous 2D and 3D surveys in four license blocks (Qamut, Anu, Napu and Tooq) in northern Baffin Bay. This is by far the largest program proposed in Greenland. The magnitude of the program coupled with the close proximity to the Melville Bay Nature Reserve and the narwhal protection zones (Kyhn et al. 2011) gave reasons for concern. Several effects from seismic noise are possible, of which behavioral disturbance of narwhals in their summering area in Melville Bay is considered the most significant, followed by the autumn migration of belugas southwards along the coast.

Furthermore, a number of factors added to the concern for the marine mammals in the area, compared to other areas (in and outside Greenland):

1) The hydrography and associated vertical sound speed profile in the area is typical of Arctic waters, i.e. with a pronounced sound speed minimum close to the surface (30-50 m). This sound speed minimum will act as a waveguide and trap seismic sounds in the upper layers of the water column (see for example **Figure 29** in Appendix D to ConocoPhillips' EIA 2012) leading to increased sound exposure in the part of the water column where many marine mammals spend significant amounts of time. Further, the Melville Bay is poorly charted both in terms of geophysics and water depths, especially near the glacial fronts where narwhals may concentrate.

2) The narwhals in Melville Bay are recognized as an isolated stock with little or no exchange with the neighboring stock in Inglefield Bredning. Melville Bay is the summering ground for this stock and the whales' presence in the bay would overlap in time with the planned surveys (Heide-Jørgensen et al. 2010b).

3) Although Melville Bay is a very open bay, the seismic operations are distributed across the opening, giving rise to concern that migrating animals (mainly narwhals and belugas) could be prevented from entering the bay or be trapped inside the bay, with few or no alternatives for relocating to less disturbed areas.

4) In the early fall (from 25 September to 25 October) the West Greenland stock of belugas pass through the coastal areas of Melville Bay. This stock summers in the Canadian High Arctic and winters in West Greenland and it currently numbers around 10,000 whales.

The main problem with the above issues is that there are few or no studies on how and at what levels marine mammals, narwhals in particular, react to seismic noise. Furthermore, as outlined earlier, the soundscape resulting from seismic activities in the area may be complex and difficult to predict. Recent studies have underlined the need to use realistic transmission loss modeling estimates, as opposed to simple spherical spreading loss, in predictive modeling (e.g. (Goold & Fish 1998; DeRuiter et al. 2006; Madsen et al. 2006; Diebold et al. 2007; Austin et al. 2012c)). Only a few peer-reviewed studies have been conducted on source properties and transmission losses from large airgun arrays (Tolstoy et al. 2004; Breitzke et al. 2008; Tolstoy et al. 2009), all of which are based on only one or two different depths in the same area, within a few kilometers from the airgun array. As described above, Arctic waters pose special difficulties when it comes to prediction of the sound transmission from a low frequency, powerful sound source. In the summer, melting ice and cold surface temperatures create a low-sound-speed surface layer. This makes it difficult to model attenuation reliably with distance and therefore to calculate the received levels that animals are exposed to with range and depth from an airgun array. The reliability problem is further compounded by a general lack validation via direct measurements.

4.6.2 Anticipated sound exposure

ConocoPhillips, Maersk and Shell were requested to model the expected noise levels in Baffin and Melville Bay for their EIAs. They commissioned JASCO Applied Sciences to carry out acoustic modeling to predict underwater sound propagation from four types of airgun array sources (**Table 1**); an overview of the actual arrays used in 2012 is provided in **Table 2**. A detailed description of the models and their input parameters can be found in appendices of the EIA reports submitted by the seismic companies. Here we provide a brief summary of the models and their findings.

Table 1. Overview of the array sources used in the modeling studies completed by JASCO (Austin et al. 2012a; Austin et al. 2012b; Matthews 2012). * source factors calculated from source levels stated in the EIAs (LGL & Grontmij; InuplanA/S & GolderAssociates 2012; NunaOil & Associates 2012). Note that source levels are assuming the array to be a point source.

	ConocoPhillips	**Shell**	**Maersk**
Exploration license area	Qamut	Anu, Napu	Tooq
Array type	2D	3D	3D
No. of active airguns	30	33; 22	33
Total volume (in^3)	3940	4240; 2940	4240
Peak-peak source factor (dB re 1Pa*m)*	142	143	143
Peak-Peak source level (dB re 1 µPa)	262.4	262.6	262.6
Reference	Austin et al. 2012b	Matthews 2012	Austin et al. 2012a

Table 2. Overview of the seismic surveys conducted in Baffin Bay in 2012. Data largely taken from EIAs (LGL & Grontmij; InuplanA/S & GolderAssociates 2012; NunaOil & Associates 2012)

	Qamut	**Anu + Napu**	**Tooq**
Companies	ConocoPhilips, DONG, Nunaoil	Shell, Statoil, GDF Suez Nunaoil	Maersk Oil Nunaoil
Type	2D	3D	3D
Vessels	*M/V Princess*	*M/V Polarcus Samur* *M/V Polarcus Amani*	*R/V Polarcus Asima*
Airgun type	Sercel G. gun II	Bolt 1500-LL/1900-LLXT	Bolt 1500-LL/1900-LLXT
No. of active airguns	32	33	33
Array size (cubic Inch)	3940	4240	4240
Source level, dB re 1 µPa (peak)	262.4	262.6	262.6
Shot interval	10 sec	11 sec	10-11 sec
Planned effort (km)	3060	14160 8000-9000 km^2	1,900 km^2
Survey start	25-08-2012 (20:33)	01-08-2012 (02:07)	06-08-2012 (06:57)
Survey end	24-09-2012 (09:43)	14-10-2012 (01:59)	01-10-2012 (02:00)

JASCO used two complementary models to predict the underwater acoustic field for the seismic sources: JASCO's Airgun Array Source Model (AASM) (MacGillivray 2006) and JASCO's Marine Operations Noise Model (MONM).

The AASM was used to predict the airgun array pressure signatures and directional source levels, based on array layout, tow depth, the volume and firing pressure of each airgun, and the interactions between individual airguns in the array. The output of the AASM was fed into the MONM to compute received per-pulse Sound Exposure Level (SEL) at a specified depth and range, while incorporating the following environmental properties:

- a bathymetric grid of the area (SRTM30+ v7.0)
- a site-specific sound speed profile (obtained from the US Naval Oceanographic Office's Generalized Digital Environmental Model database, v3.0), and
- a geoacoustic profile based on the composition of the seafloor.

The received SEL at a surface sampling location was taken as the maximum-over-depth received SEL, i.e. the maximum value over all modeled depths at that sampling point. The resultant maximum-over-depth SEL sound fields were presented on bathymetry maps as color contours around the source (e.g. **Figure 10**).

The SELs modeled with MONM were converted to 90% root-mean-square sound pressure levels (rms SPL) and peak sound pressure levels (SPL) with conversion factors obtained using JASCO's Full-Waveform Range-dependent Acoustic Model (FWRAM).

Sound propagation from single seismic shots was modeled at two to four representative sites within each of the three survey areas (**Table 3**, e.g. **Figure 10**). Furthermore, the cumulative sound field over 24 hours of operations was modeled for each of the surveys individually, as well as for all the surveys combined.

Table 3. Location and water depth of the modeled source locations. Shell's Site 1 (bold) lies inside the Qamut block.

Seismic operator	Exploration license area	Site	Latitude	Longitude	Water depth (m)
ConocoPhillips	Qamut	1	75˚ 24.764'N	62˚ 04.253'W	880
ConocoPhillips	Qamut	2	75˚ 15.784'N	63˚ 37.469'W	140
ConocoPhillips	Qamut	3	75˚ 05.467'N	65˚ 38.791'W	340
Shell	**Qamut**	1	75˚ 02.228'N	62˚ 07.415'W	512
Shell	Anu	2	74˚ 42.000'N	61˚ 00.000'W	768
Shell	Anu	3	74˚ 09.000'N	61˚ 59.580'W	612
Shell	Napu	4	73˚ 24.000'N	62˚ 32.760'W	391
Maersk	Tooq	1	73° 56.673'N	58° 56.038'W	110
Maersk	Tooq	2	73° 28.718'N	58° 28.562'W	550

JASCO's models showed that the airgun sounds would be audible at very long ranges (**Figure 10**), probably across the entire Baffin Bay Basin and certainly within the whole of Melville Bay. Levels within Melville Bay, including the nature reserve and the narwhal protection zones, were predicted to be sufficiently high to have the potential to cause behavioral reactions in narwhals and beluga whales, as well as other marine mammals that may be found concomitantly in the area. However, the exact sound exposure levels resulting in behavioral reactions in many of the species are not known for airgun noise. Sound levels sufficiently high to be capable of inflicting immediate, acute effects (such as temporary or permanent hearing loss) were only expected in the close vicinity of the airgun arrays (within a few hundred meters or less). The predicted noise levels from the models were comparable to the actual noise levels measured during the 2011 seismic survey in the Pitu block (Annon. 2012), taking into account that the program in 2011 was of a magnitude comparable to each of the programs intended for Qamut and Tooq. Total noise levels were thus predicted to be considerably higher in 2012, compared to 2011, and at a level that would affect the whole of Melville Bay and therefore result in temporary habitat degradation, likely to affect marine organisms that depend on sound for vital life functions such as orientation, communication and feeding.

Figure 10. Example of JASCO's pre-season modeling: Received maximum-over-depth sound exposure levels (SEL) around a 4240 in^3 3D airgun array at Shell's Site 2. Datum: WGS84; projection: Mercator for the large map and UTM Zone 21 for the inset map. (Modified from (Matthews 2012)). Data from JASCO was provided with the permission of Shell.

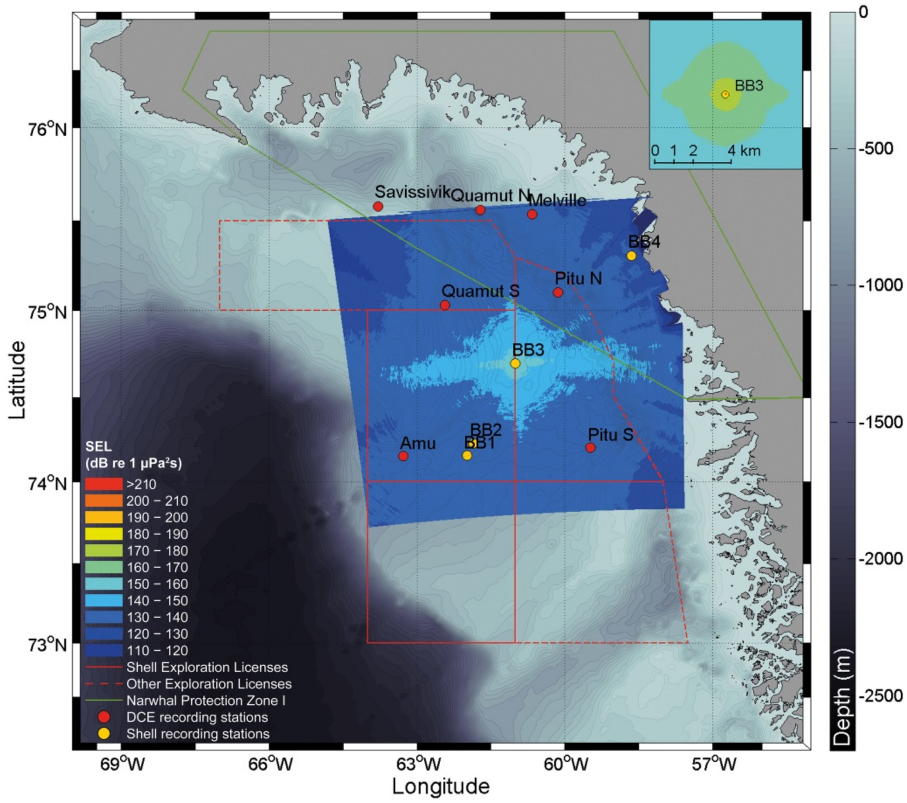

4.7 Motivation for the monitoring program

Predictive modeling of sound exposure with the objective of assessing possible effects on marine mammal behavior is typically part of EIAs for hydrocarbon projects. For Greenland it is further required that all companies model the cumulative noise impact of all the surveys combined. As the last requirement is new, it appeared prudent to evaluate whether this EIA requirement is justified. As a consequence, a monitoring program was established in 2012 with a dual purpose: 1) to assess the actual noise exposure and transmission properties of Melville Bay and 2) to evaluate the quality of the predictive modeling as a tool in the Environmental Impact Assessment procedure. The program was based on measurements of actual noise levels at a number of stations throughout the license blocks and Melville Bay, along with collection of environmental data, such as CTD measurements and actual bathymetry data. The environmental data were to be feed into an advanced sound propagation model developed by collaborators at Woods Hole Oceanographic Institution (WHOI), and the results of the noise recordings where to validate the output of this propagation model. This was meant as an exercise to help point out areas that still present difficulties to underwater acousticians, and that would advance the discussion of how and where the state of the art might be advanced to better meet environmental protection needs in acoustically complex areas. This approach will also enable a verification of the validity of the predictive sound propagation modeling commissioned by the hydrocarbon companies. This step is highly important as it will take the process of predictive modeling for EIAs a step further and hopefully provide suitable alternatives for scenarios where the current predictive modeling can be improved.

5 Materials and methods

Seismic signals were measured during the seismic surveys conducted in 2012. The signals were recorded at short ranges with hydrophones deployed from a rigid hull inflatable boat (RHIB), while at long ranges they were recorded with dataloggers on seven moorings, each with three dataloggers distributed at different depths.

The objective was to record and characterize airgun pulses during the seismic program. Sampling period was limited by datalogger memory and sea ice conditions at the more coastal moorings at both ends of the season. Therefore, data were only recorded concurrently with the seismic program i.e. no data were collected prior to or following the seismic program.

Additional sound recordings were obtained by JASCO for Shell before and during the seismic operations. JASCO had four moorings: one with a single datalogger (deployed later in the season) and three with dataloggers at three different depths. These data were shared by Shell and included in our analysis.

5.1 Experimental setup

5.1.1 Short-range signatures

To determine the short-range characteristics of the airgun pulses, a set of sound recordings was obtained at close range from one of the seismic vessels, *R/V Polarcus Asima* (**Figure 2**), operating for Maersk in the Tooq block (**Figure 1**). Recordings were made in late September 2012 in close collaboration with the crew of *Polarcus Asima*. As no special actions were taken by *Polarcus Asima* during the recordings, and recording schedule was determined by weather and availability of a suitable recording platform (*R/V Sanna*), the data collected represent random samples of the airgun pulses emitted by the seismic vessel during surveys in the Tooq block.

Hydrophone recordings were made from a small RHIB operated from *R/V Sanna*. Data were collected at approximate distances of 0.5, 1, 2, 4, and 8 nmi from the airgun array of *Polarcus Asima*. At the beginning of each recording session, the RHIB was positioned well ahead of *Polarcus Asima* so that recordings could be made at an angle of 90 degrees to the airgun array while *Polarcus Asima* remained on its track line (**Figure 11**). Recordings were thus obtained well ahead of *Polarcus Asima* as well as after the vessel passing at all recording ranges. Recordings were thus made throughout the passage of the *Polarcus Asima.*

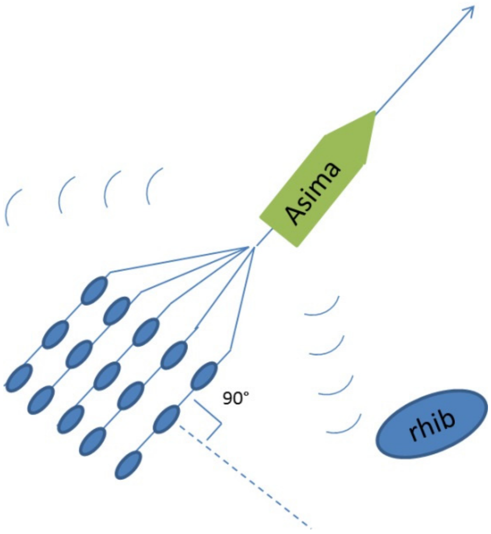

Figure 11. Short-range recording methodology. Hydrophone recordings were made in close proximity to *R/V Polarcus Asima* to obtain a signature of the airgun array. Data were collected from a small RHIB that was positioned so that the airgun array would pass the RHIB at an angle of 90 degrees. The engine and all electronic equipment were turned off in the RHIB during data acquisition.

At ranges of 4 and 8 nmi from the airgun array, sound was recorded with a Reson TC4032 hydrophone (Reson A/S, Slangerup, Denmark; sensitivity of -172 dB re 1V/µPa). The frequency response of the hydrophone is flat (-/+ 2.5 dB) between 10 Hz and 80 kHz, and the hydrophone was calibrated with a pistonphone (Brüel & Kjær 4223) at 250 Hz prior to the field recordings. Hydrophone output was bandpass filtered between10 Hz - 50 kHz using a custom-built amplifier box and relayed to a linear PCM Recorder (Olympus LS-11) sampling at 96 kHz with 16 bit resolution. The TC4032 was suspended at 90m depth, between a large buoy at the surface, and weights mounted below the hydrophone. Ten small trawl floats, attached along the upper part of the cable, acted as a spring to dampen any motion induced by waves and swell (**Figure 12**). The exact recording depth was measured with a Star Oddi data-logger (DST milli T, v 19) (data analyzed in SeaStar v 5.68) attached to the hydrophone. During recordings, all electrical equipment, echosounder and engine were turned off and the RHIB drifted with wind and currents. Its position was continuously logged using a handheld GPS and the range between the airgun array and the RHIB could later be calculated by comparing the GPS data with the shot log of *Polarcus Asima*. For safety reasons, *R/V Sanna* remained 1 nmi from the RHIB with an idling engine. No other vessels were in the vicinity of the seismic vessel during the recording period.

Due to the powerful airgun output a less sensitive hydrophone was used at close ranges (0.5-2 nmi) to avoid clipped recordings. Here, a TC4034 hydrophone (Reson A/S, Slangerup, Denmark, sensitivity of -218 dB re. 1V/µPa), was deployed with an amplifier gain of 40 dB and a recording depth of 9 m. Otherwise, the recording chain consisted of the same equipment and settings as for the longer ranges described above. All recordings were in stereo and the system noise of the recorder was determined from the empty channel.

Figure 12. Deployment of the deep hydrophone (90 m), with trawl balls attached to the cable to act as springs to dampen movements caused by waves and swell.

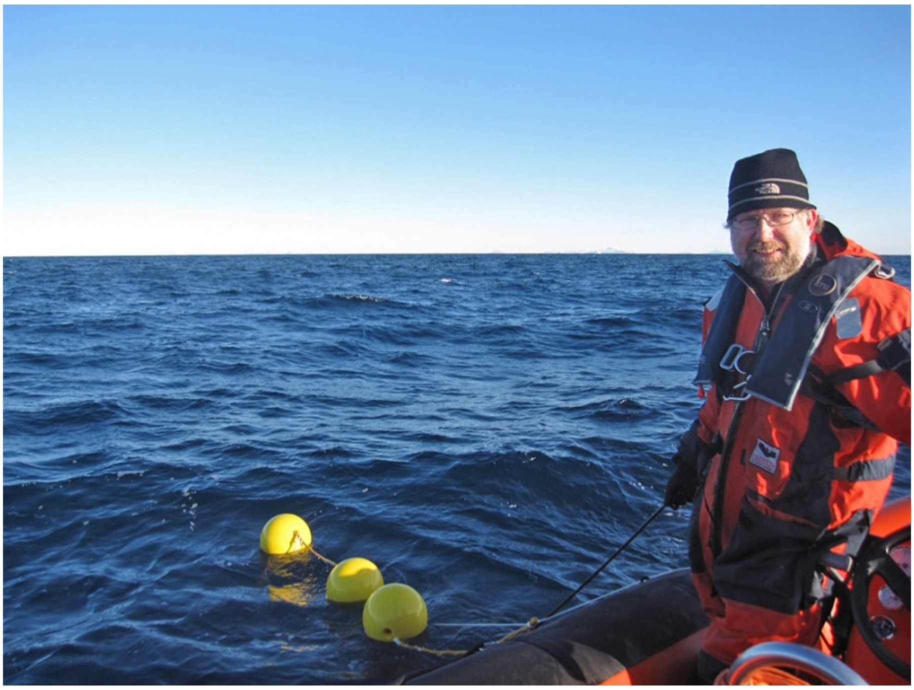

5.1.2 Mid-to-long range characteristics/Moorings

5.1.2.1 Dataloggers

Airgun pulses from the four seismic vessels were recorded under a range of conditions and ranges from survey vessels by automated dataloggers (DSG Ocean, Loggerhead Instruments, Sarasota, Florida) deployed on seven moorings in Baffin Bay in the beginning of August 2012. The DSG Ocean (**Figure 13**) is a low-powered underwater acoustic recorder that records to high capacity SD memory cards and is housed in an aluminum housing allowing deployments at depths up to 3000 m. Dataloggers were equipped with HTI-96-I hydrophone (Hightech Inc, Mississippi, USA) with sensitivity of -210 dB re. 1V/µPa ± 0.5 dB, measured with a pistonphone (type 42AC, G.R.A.S., Copenhagen) fitted with a custom-built coupler, and sound pressures ccherein measured by a standard microphone (type 46AE, G.R.A.S., Copenhagen). The HTI-96-I hydrophone was purposefully chosen to be of low sensitivity in order to avoid overloading by high level signals from nearby seismic surveys. Sampling was carried out with 16 bit resolution at a rate of 80 kHz with a 40 kHz low-pass filter, followed by digital FIR low-pass filtering and decimation by a factor of 2, yielding a usable bandwidth from 16 Hz to 20 kHz. The low-pass filter, however, was not flat and consequently limited the flat frequency response of the system to approximately 16 - 16000 Hz (**Figure 14**). Recordings were made with a 33% duty cycle (1 minute on, 2 minutes off), and 128 GB of memory capacity per datalogger, allowing approximately 60 days of data collection. Power was supplied by 24 alkaline D-cells per datalogger.

Pre-amplifier gain, set at 0, 10 or 20 dB (**Table 4**), was the only parameter varied between the dataloggers. The gain was chosen based on proximity to the seismic surveys conducted in the area.

Table 4. Gain settings for the 21 DSG Ocean dataloggers used in the study.

Station	DSG ID	Hydrophone ID	Position	Gain
Amu	1194	437302	Top	0
	1184	437290	Middle	0
	1175	437297	Bottom	0
Melville	1187	437305	Top	20
	1178	437298	Middle	20
	1176	437303	Bottom	20
Pitu N	1177	437306	Top	20
	1182	437301	Middle	20
	1190	437300	Bottom	20
Pitu S	1185	437309	Top	0
	1179	437307	Middle	0
	1180	437304	Bottom	0
Qamut N	1196	437293	Top	20
	1191	437292	Middle	20
	1181	437311	Bottom	20
Qamut S	1186	437295	Top	0
	1183	437294	Middle	0
	1188	437291	Bottom	0
Savissivik	1189	437299	Top	10
	1193	437310	Middle	10
	1195	437296	Bottom	10

Figure 13. Dataloggers. Three DSG Ocean dataloggers ready to be mounted along the mooring line. The hydrophones to the right are transparent yellow and mounted on the top of each data-logger. All shackles and rings were taped with insulating tape to avoid noise from rattling.

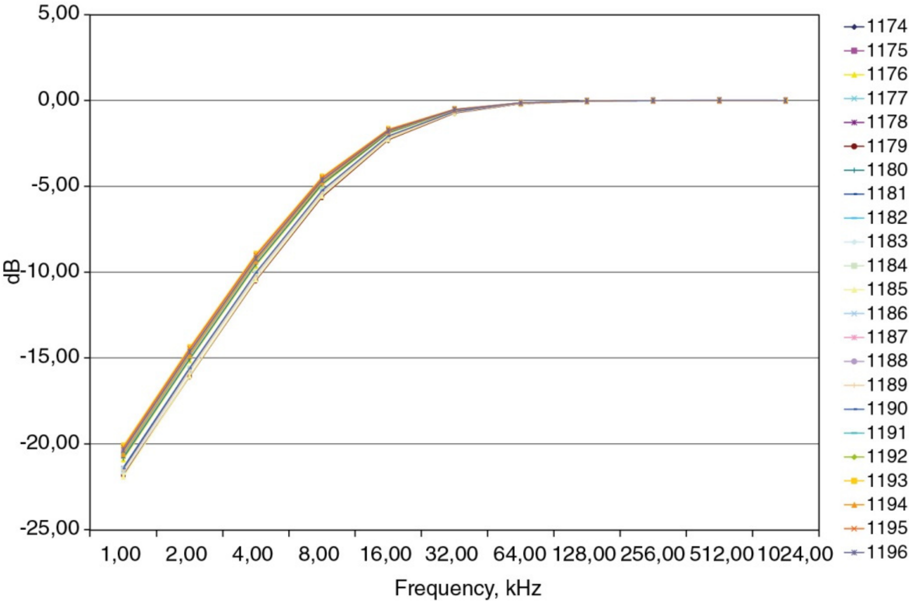

Figure 14. High pass filter of all the used DSG Ocean dataloggers.

5.1.2.2 Mooring design

Three dataloggers were moored at each station, mounted along one common line tethered between a 600 kg anchor and a 30′′ subsurface steel float. Dataloggers were mounted at 40 and 150 m below the surface, and at 30 m above the seabed (**Figure 15**). An acoustic release (Teledyne, Benthos 866-A) was mounted between the deepest datalogger and the anchor. Flotation was mounted at strategic locations along the line as were two weak links intended to break in case the mooring was struck by an iceberg. The design was chosen so that even if both weak links should break, and the mooring thus separated into three parts, the two top dataloggers would float independently while the third logger, nearest to the anchor, would remain at its intended depth to be recovered on its own. The two top units were equipped with a subsurface beacon (KILO, XEOS Technologies) that upon surfacing obtains its position from GPS and transmits it through the Iridium satellite network. The transmitted positions could then be used to track and recover the units. Temperature and temperature+pressure sensors (Star-Oddi Data Storage Tag millli-T and milli-L, respectively) were distributed along the mooring line to log the temperature throughout the recording period at various depths. All moorings had the temperature+pressure sensors at the subsurface float, 150 m depth and 25 m from the sea floor. In addition, three moorings (PituS, Amu and QamutN) had temperature sensors at 50, 150, 200, 250 and 400 m depth.

5.1.2.3 Deployment and recovery

The seven moorings were deployed on 8th-11th August 2012, from *R/V Sanna*. They were deployed top-first using the main winch of the vessel to slowly uncoil the mooring behind the ship that moved ahead with a constant speed of 1.5 knots. In the end, the anchor was released at the intended final position pulling the mooring to the bottom.

Parts of the moorings had detached at the weak links and surfaced before (13th-18th August), the intended recovery date (**Table 5**) presumably due to a combination of bad weather and ice, and too weak links. The detached parts of the moorings were tracked with the beacon signals as they floated with the currents. Some were recovered with the help of the industry vessels or locals, but most were retrieved when the bottom-moored dataloggers were recovered in the period 13th – 18th September 2012 with *R/V Sanna*.

The anchored moorings were released with a Universal Deck Box UDB-9400 and retrieved to the ship after surfacing.

Table 5. Overview of deployments. Stations BB1-BB4 were part of the monitoring program conducted by JASCO for Shell, whose data were subsequently made available for the present analysis.

Station name	Longitude N	Latitude W	Position	Recording start	Detachment	Recovery
Amu	74.15423	63.27795	Top	09-08-2012 21:35	13-08-12 13:02	14-09-2012 06:29
			Middle	09-08-2012 21:35	13-08-12 13:11	14-09-2012 06:29
			Bottom	09-08-2012 21:35	Not detached	13-09-2012 16:44
Melville	75.53500	60.66667	Top	10-08-2012 20:35	18-08-12 04:53	29-08-2012 21:59
			Middle	10-08-2012 20:35	18-08-12 04:53	29-08-2012 23:20
			Bottom	10-08-2012 20:35	Not detached	15-09-2012 09:14
Pitu N	75.03333	60.13217	Top	11-08-2012 16:35	18-08-12 01:23	30-08-2012 11:05
			Middle	11-08-2012 16:35	18-08-12 01:23	30-08-2012 11:05
			Bottom	11-08-2012 16:35	Not detached	15-09-2012 19:26
Pitu S	74.20457	59.47132	Top			Lost
			Middle			Lost
			Bottom	09-08-2012 13:08	Not detached	16-09-2012 14:05
Qamut N	75.56125	61.71467	Top	10-08-2012 16:59	28-08-12 22:11	14-09-2012 17:56
			Middle	10-08-2012 16:59	Not detached	15-09-2012 06:56
			Bottom	10-08-2012 16:59	Not detached	15-09-2012 06:53
Qamut S	75.03133	62.43150	Top	11-08-2012 10:23	16-08-12 07:56	22-08-2012 10:38
			Middle	11-08-2012 10:23	16-08-12 07:56	22-08-2012 10:08
			Bottom	11-08-2012 10:23	Not detached	16-09-2012 06:23
Savissivik	75.57835	63.78405	Top	10-08-2012 11:17	17-08-12 20:32	29-08-2012 21:53
			Middle	10-08-2012 11:17	17-08-12 20:32	29-08-2012 21:53
			Bottom	10-08-2012 11:17	Not detached	14-09-2012 20:05
BB1	74.1585	61.9786		29-07-2012	-	15-10-2012
BB2	74.2310	61.8539		29-07-2012	-	16-10-2012
BB3	74.6997	61.0008		30-07-2012	-	16-10-2012
BB4	75.3072	58.6416		14-08-2012	-	15-09-2012

Figure 15. Design of the DCE moorings, exemplified by the mooring at Qamut N.

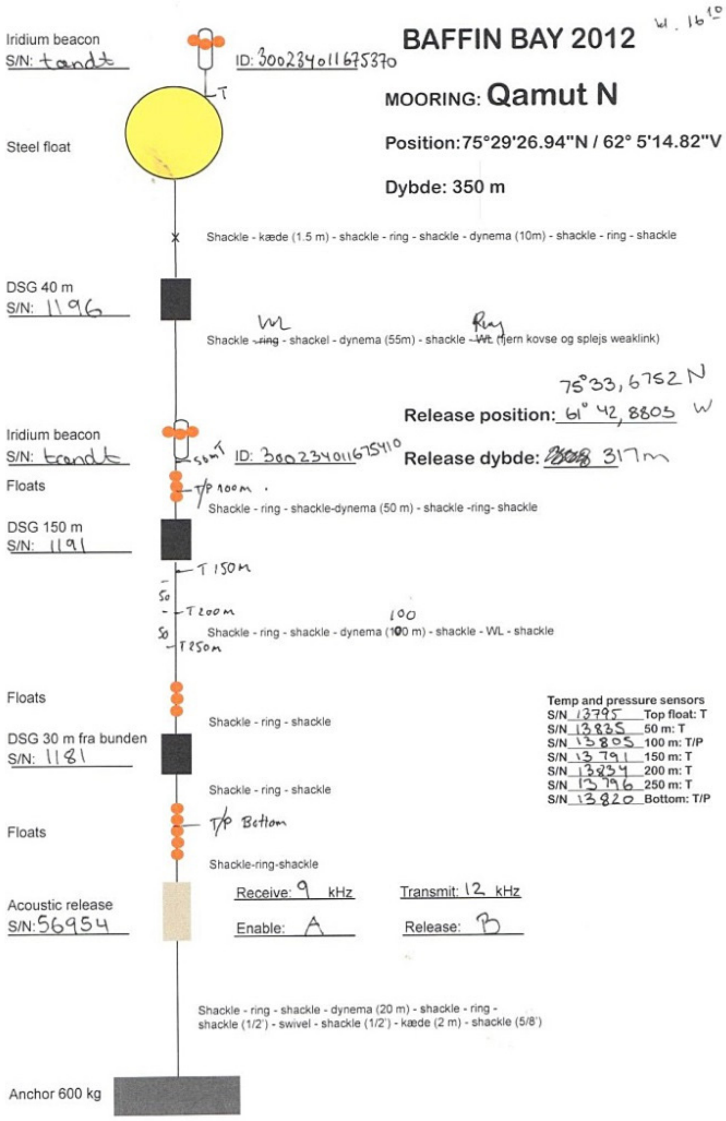

5.1.2.4 Sound speed profiles

CTD profiles were obtained with a SeaBird SBE19plus at each mooring site at the time of deployment and recovery (**Table 6**), and during the close-up recordings of *Polarcus Asima*. In addition, a set of 15 representative sound speed profiles acquired by Shell during their surveys in Anu and Napu blocks was included as input to the post-season modeling (**Table 7**).

5.2 Recording issues

There were a number of technical issues with the recordings which were dealt with in various ways.

1) In the beginning of all DSG-files there was a small and gradually diminishing DC-offset, which was due to the charging of a capacitor in the pre-amplifier. This issue has partly been dealt with by the manufacturer by turning on the power supply to the hydrophone some seconds prior to start of recordings. The remaining DC-offset was removed by fitting an exponential function to the positive values of the initial segment of each 1 minute recording. If the fit was stable (i.e. it resulted in a negative exponent parameter), the file was corrected by subtracting the best fitting curve.

2) After the detachment, ambient noise at the floating hydrophones was elevated.
3) Cable splices of JASCO's vertical array at station BB2 leaked on the hydrophones at 0 and 200 m. Consequently, no useable data from the hydrophones at 200 and 400 m depth were obtained. Details can be found in (Martin & MacDonnel 2013).
4) One of the loggers at JASCO's BB1 station (146-02.8000 deployed at 200 m) seemed to malfunction, in that while the time stamps of the recordings suggest a file saving interval of approximately 15 minutes, the files were 30 minutes long. Data from this logger were therefore not included in this report.

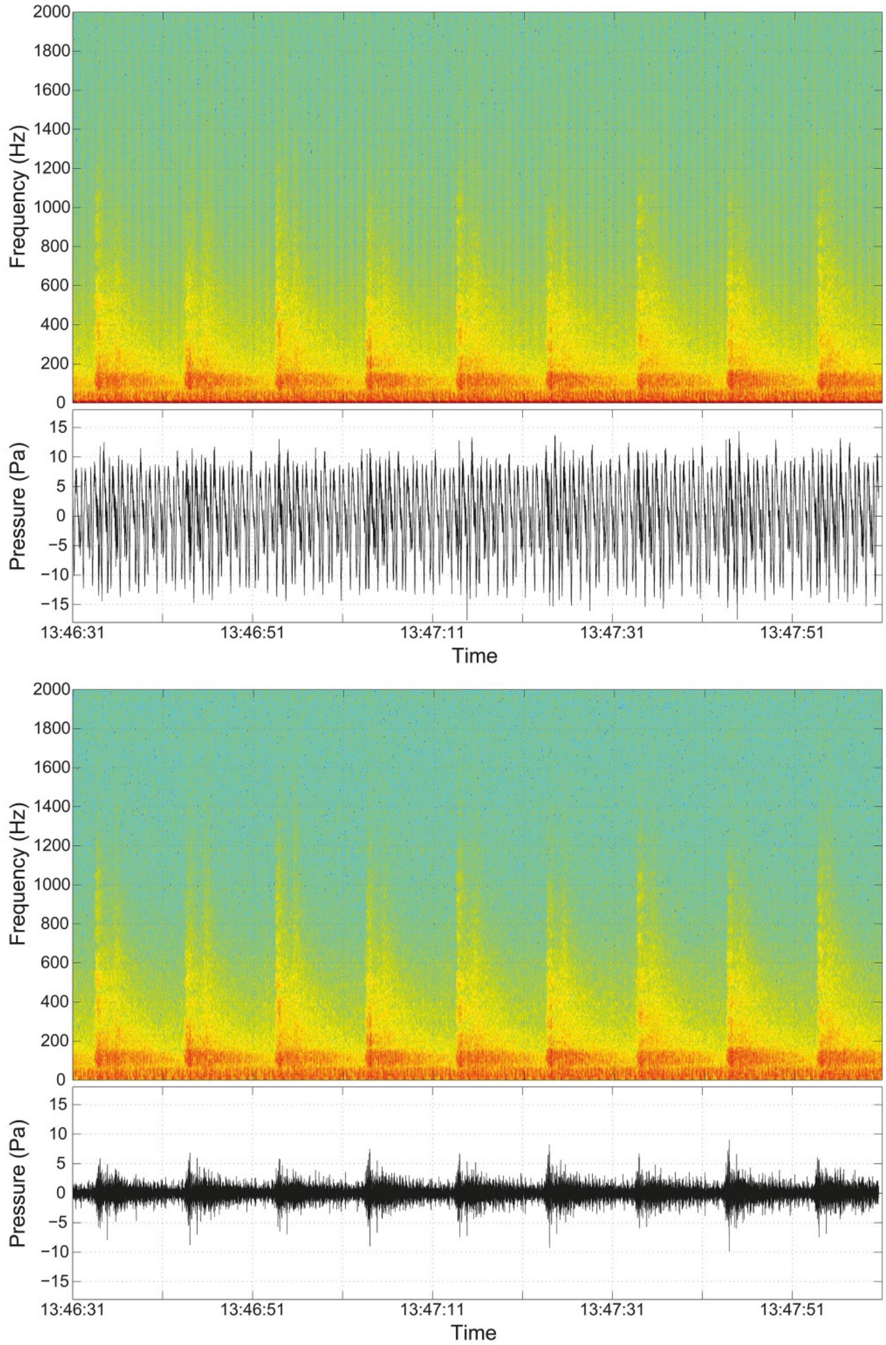

Figure 16. Top panel: A sample of the data from the BB1 recorder collected on August 21st, showing the voltage bias noise. Bottom panel: The same sequence processed with a 4th order Butterworth high-pass filter with a cut off frequency of 10 Hz.

5) Low voltage in the power supply of the recorders at BB1-BB4 resulted in increased self-noise of low frequency (1-5 Hz) in the data after 3-20 days of recording (**Figure 16)**. This noise was removed by JASCO with a high-pass Kaiser filter with cut-off at 10 Hz (Martin & MacDonnel 2013). In the present analysis a 4th order Butterworth filter with cut-off at 10 Hz was used instead (**Figure 17**), which provided -3 dB of attenuation at 10 Hz and -24 dB at 5 Hz. Most of the energy below 10 Hz is from geologic activity and flow noise, and would regardless be filtered away in the initial processing.
6) Some of the DCE dataloggers (Pitu S, Amu, Qamut S) were set with too little gain due to an over-focusing on risk of clipping before the first recordings were obtained from one of the airgun arrays. This means that self-noise dominated the recordings and that level fluctuations appear less pronounced (see appendix E).

5.3 Data analysis

Data analysis centered on assessing noise emissions from the seismic surveys to Baffin Bay and Melville Bay and estimating exposure levels as experienced by marine mammals by combining in situ measurements at selected locations and a sound propagation model for the area. The outputs of the newly-developed model and predictions of JASCO's pre-season modeling study were compared to empirical data from a subset of locations.

Spectral signatures of airgun pulses were characterized using the short-range recordings. The sound budget at each recorder for the whole deployment period was assessed by computing SEL in 1-minute-long windows and daily cumulative sound exposure levels (cSELs) in the full bandwidth, as well as in the frequency band of 10-2000 Hz, which encompasses the dominant sound energy at long ranges (Austin et al. 2012a; Austin et al. 2012b). Marine mammal frequency weighted (m-weighted, (Southall et al. 2007) SEL and cSEL values were also computed to weigh the importance of sound levels at particular frequencies by the receiver's hearing sensitivity, and thus estimate sound levels in frequency bands relevant to marine mammals, narwhals in particular. An automatic pulse detection algorithm, followed by manual inspection was used to find start and end times of individual airgun pulses. Amplitudes of these pulses were computed as SEL (and 90% rms SPL) in the frequency band of 10-2000 Hz to verify the outputs of the modeling studies.

All analyses were performed in MatLab 2007b or MatLab 2013b (Mathworks, MA, USA).

5.3.1 Short-range signatures

From the recordings at close range, time stretches were selected during which the distance to the survey ship could be considered known and constant. For each of the distances to *Polarcus Asima*, 0.5, 1, 2, 4 and 8 nmi, recordings with a suitable gain, and a usable dynamic range were identified, allowing for analysis of the received levels during surveys.

The pulses were found by automated level detection (with subsequent inspection) and cut for analysis in a window starting 5 seconds before the threshold was crossed and ending 5 seconds after time of threshold crossing. Averaged power spectra in 1-Hz-wide bands (PSD) were calculated from discrete Fourier transforms using the full 10 seconds analysis window to arrive at minimum values.

The RMS levels were calculated over the time interval covering 90% of the energy of the pulses. Sound exposure levels were measured in 10 seconds time intervals (one level value for each pulse).

The background noise levels were calculated from a recording made during a pause in the airgun firings. It should be noted, however, that it was still possible to discern faint pulses from distant surveys in the recordings, so at low frequencies the natural background noise level is overestimated.

5.3.2 Mid-to-long range recordings

For the analysis of data from the dataloggers, we split the process of finding suitable airgun recordings into two steps: 1) identification of sound files containing pulses indicative of the presence of seismic activity, and 2) localization of the time of occurrence of individual pulses within such files.

5.3.2.1 Screening of logger data

For the detection algorithm, we chose to use one feature that is relatively constant with distance and over long stretches of time, namely the regularity of occurrence of airgun pulses, with typical inter-pulse intervals slightly longer than 10 seconds (**Table 2**). For detection purposes, the signal was first band-pass filtered to cover only the range of 10-100 Hz. An envelope was formed using the analytical signal and then a chirp z-transform was performed on the resulting instantaneous amplitude data to produce a highly resolved power spectrum covering the range from 0.05 to 0.25 Hz (the reciprocal of 4 to 20 second). The chirp z-transform is a convenient way to arrive at high-resolution spectral estimates in a small frequency range without the need for excessive zero padding, which would have rendered the analysis process very slow.

For the algorithm, we computed a criterion to facilitate the decision of whether or not to include a recording in further analysis. This was designed to eliminate files with no airgun pulses present. The criterion utilized the significance of the peak frequency in the zoomed-in-on energy spectrum of the envelope. The key frequency (KF), was the spectral peak in the range of 0.09-0.11 Hz, corresponding to the range of the reciprocals of the typical pulse intervals used in the surveys. For a file to be included in further analysis, the energy in a 0.025 Hz wide band centered on the KF should have been at least twice as high as the sum of energies in two similar bands centered on 0.67*KF and 1.5*KF (**Figure 17** and **Figure 18**).

The algorithm only reported recordings where pulses from one survey dominated over any other ongoing rhythmic activity. The presence of more than one sequence of signals tended to prevent the recording from being included. The algorithm was largely insensitive to even large impulsive artefacts that would often occur, for instance in the case where a loose recording station would bounce at the surface (**Figure 17**). Such instances did not occur rhythmically and while they did raise the noise floor of the z-transform spectrum, they did not produce any spectral peaks.

Because of inter-pulse variability within the files, stemming from slightly different pathways to the receiver, the screening algorithm could not reliably pinpoint the exact time of occurrence of individual pulses. Thus, once a recording had been classified as containing usable signals, the extraction of the individual pulses was performed by methods that maximized the number of correct detections, while reducing the influence of shorter impulsive disturbances. For this purpose, two different automatic feature detecting routines were used: 1) envelope level detector for recordings from stationary receivers, and 2) a more conservative, smoothed-envelope-based detector for recordings from loose moorings that were prone to containing large impulsive artifacts.

5.3.2.2 Airgun pulse detectors

Level detector

The pre-screened recordings from stationary loggers were dominated by seismic pulses, with only occasional transient noise from calving glaciers or biological sources. Thus, a simple level detection routine was used to locate peaks of individual airgun pulses.

For detection purposes each recording was band-pass filtered between 100-300 Hz (4^{th} order Butterworth filter) and the digital recording units were converted to Pascals (Pa) by applying hydrophone sensitivity and gain settings (**Table 4**; (Martin & MacDonnel 2013)). Signal envelope was then formed and its magnitude examined on a sample-by-sample basis. If the magnitude exceeded a pre-defined threshold, a maximum was searched for in a window starting 1 second before the threshold was crossed and ending 3 seconds after the time of threshold crossing. This maximum envelope level was then compared to the maximum envelope levels of the preceding three pulses. If the envelope level of the candidate pulse was ≥0.5 of the mean of the levels of the preceding pulses, the candidate pulse was saved for further analysis. A 4-second-long window, starting 1 second before the time of maximum amplitude and ending 3 seconds after the peak time, of the non-filtered recording was saved for further analysis. After a confirmed detection, a blanking time of 9 seconds from the initial detection was implemented, i.e. the algorithm would skip over 9 seconds of the recording following the time of threshold crossing. This blanking time was chosen as the maximum time shorter than the shortest shooting interval to limit the number of false alarms and speed up the analysis.

Smoothed-envelope detector

Each pre-screened recording from loose moorings was filtered to the range of 30 to 70 Hz (4^{th} order Butterworth filter), which typically contained the bulk of the energy of the signals of interest. The recording's digital units were converted to Pa, and the envelope was then formed from the analytical signal, the signals were resampled (decimated) with a factor of 10, and the result was low-pass filtered (2^{nd} order Butterworth) with corner frequency = 0.1 Hz. The peaks in the resulting signal marked the positions of the longer duration airgun pulses, whereas even very intensely recorded impulses, stemming from bounces against the water surface, tended to be vastly reduced by this process (**Figure 18**). A 4-second-long window (peak time-1sec: peak time+3sec) of non-filtered data was saved for further analysis.

Figure 17. Detector output for signals with high received level but impulsive noise disturbing detection. The upper left panel shows the raw signal in blue and the bandpass filtered signal in green. The impulses are vastly reduced by filtering, but they are still higher than the shots. The lower left panel shows the smoothed envelope used eventually to extract individual pulses. Extraction in this case is very simple due to the excellent signal-to-noise ratio. The much shorter disturbing impulses are almost completely removed by the smoothing (low pass filtering) of the envelope. The right panel shows the chirp z-transform and the frequency bands used in the criterion. In this case the firing rate around 0.1 Hz is extremely dominating and detection is easy.

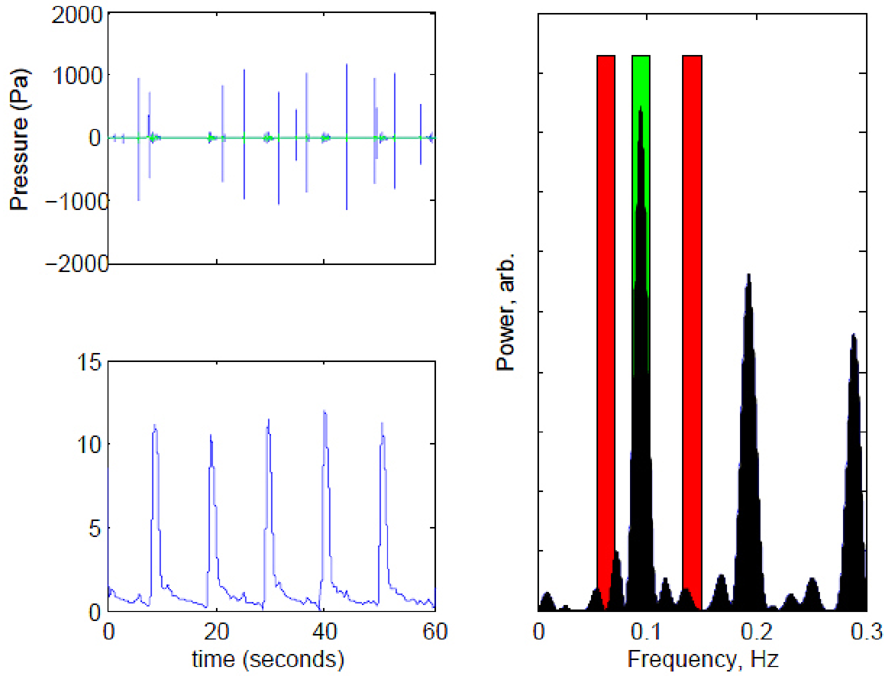

5.3.3 Sound budget

The complex sound propagation conditions in the Baffin Bay resulted in intense reflections that caused long pulse durations. Thus, for ranges longer than 20 km from the source, the duration of individual airgun pulses often exceeded 3 seconds (Martin & MacDonnel 2013). Furthermore, at many of the recording stations activities from several seismic vessels contributed to the soundscape. Total energy per file (corresponding to a 1 minute-long window for the DCE Ocean dataloggers), rather than per pulse, was therefore computed to assess variations in sound budget at each recorder over the deployment period. Accordingly, the 30-minute-long files from the AMAR loggers deployed by JASCO for the Shell monitoring program (Martin & MacDonnel 2013) were divided into 1- minute-long intervals.

The recordings were band-pass filtered between 10 and 2000 Hz, a band that should be dominated by energy from airgun pulses. Sound exposure levels were computed and daily cumulative SELs were estimated by summing (in linear units) the SELs of all the recordings made on a given day. The "1 minute on - 2 minutes off" duty cycle of the DCE Ocean dataloggers was corrected for by linearly interpolating values between the recorded files.

Additionally, mid-frequency (i.e., with low- and high-frequency cut-offs at 150 Hz and 160 kHz, respectively) m-weighted (Southall et al. 2007) SELs and daily cSELs were computed to assess the sound budgets based on sound levels weighted in a manner so as to incorporate hearing sensitivities of toothed whales (and narwhals in particular) found in the Baffin Bay.

Figure 18. Detector output for signals with low received level (RL) and hence low signal-to-noise ratio (SNR) (top) and very low RL and hence very low SNR (bottom). The upper left panel shows the raw signal in blue and the bandpass filtered signal in green. The lower left panel shows the smoothed envelope used eventually to extract individual pulses. Note that the rhythmic firing is in fact visually detectable even though it is not visible in a spectrogram (not shown). The right panel shows the chirp z-transform and the frequency bands used in the criterion. In this case the firing rate around 0.1 Hz is not having enough impact on the spectrum to count as detection. The power within the reference bands is dominating over the 0.1 Hz band.

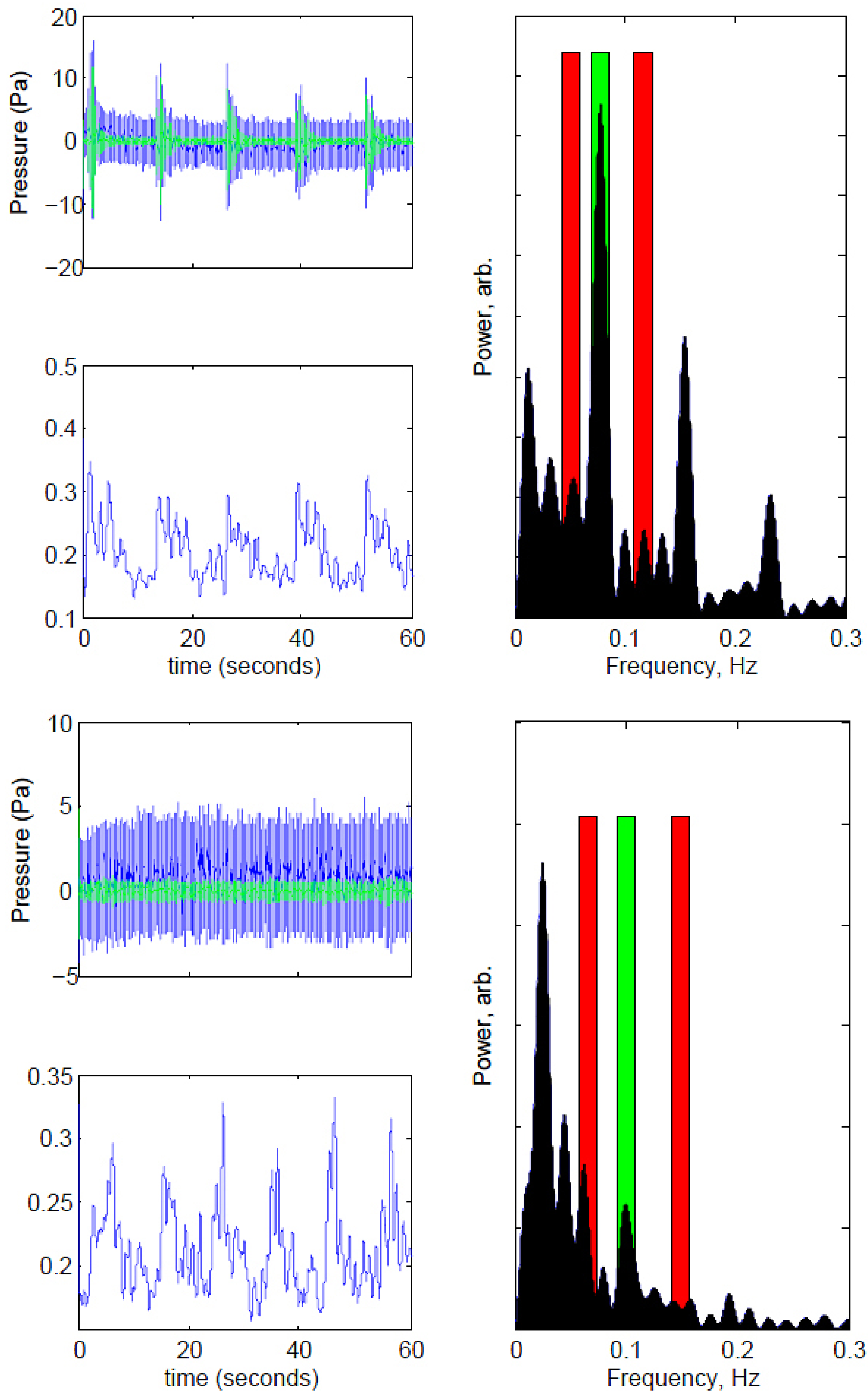

5.4 Modeling of transmission loss

The Ocean Acoustics and Signals Lab at the Department of Applied Ocean Physics and Engineering at Woods Hole Oceanographic Institution (WHOI) carried out theoretical and numerical studies to understand the effects of environmental variability and uncertainty on predicting the underwater sound field resulting from the 2012 seismic surveys in Melville and Baffin Bay. Some deterministic modeling efforts were also devoted to presenting the baseline physics of underwater sound propagation in this complex environment. The purpose of WHOI's input to this study was not to evaluate the Baffin Bay Environmental Impact Assessment process, or third parties' calculations and methods, which are generally "state of the art" and carefully considered. Rather, it was meant as an exercise that would help point out areas that still present difficulties to underwater acousticians, and that would advance the discussion of how and where the state of the art might be advanced to better meet environmental protection needs in acoustically complex areas.

Five main topics were of particular interest in the WHOI studies: 1) variability in the surface mixed layer, 2) 3D acoustic effects, and when those must be considered, 3) uncertainty in transmission loss (TL) due to uncertainty in the bottom geoacoustic model, 4) uncertainty in TL due to rough sea surface and ice scattering effects, and 5) experimental sampling issues for calibrating TL measurements.

5.4.1 Sound propagation model and model parameters

To best render the sound levels propagating from the airgun arrays in the studied area, the WHOI group implemented theoretical analysis of sound propagation uncertainty, and numerical modeling with environmental data collected during the survey and public scientific bathymetric database in the literature. The numerical models were later compared directly to measured data for validating whether the models capture the significant features seen in the data (see section 5.4.3) so we can trust the baseline physics that the models delivered. The transmission loss from the license blocks to the locations and depths of the recorders was modeled. A short description of the numerical techniques that the WHOI model employs is provided below.

A 3D parabolic equation (PE) model (Lin 2013) using the split-step Fourier (SSF) algorithm (Tappert 1977) with a wide-angle PE approximation (Feit & Fleck 1978) was utilized in this study. This 3D PE model can be implemented in either a Cartesian or a cylindrical coordinate system, and the latter was employed here to cover a wide azimuthal aperture in space. The PE solution was obtained with a one-way marching algorithm originating from the receiver position by employing the acoustic reciprocity principle (Rayleigh 1876). Computation of the 3D PE program starts from the model source at the receiver position and marches outward radially. The split-step Fourier technique (Hardin & Tappert 1973) was used to solve the one-way wave equation at each marching step. This technique divides sound propagation over a heterogeneous sound speed field into free space propagation with a fixed reference wavenumber, and applies phase fluctuations due to environmental variability. The free space propagation is handled in the wavenumber domain, and phase anomalies are introduced in the spatial domain. The cylindrical PE model holds a consistent degree of approximation along radials from the model source at each azimuth, but the conventional fixed cylindrical grids will not have uniform model resolution. Two methods were developed by Lin et al. (Lin 2013) and were used here to improve cylindrical PE model resolution; the first method was to utilize an arc-length grid, and the second was to extend angular wavenumber spectra with zeros (zero-padding). In the arc-length grid, the grid interval is fixed to maintain the model resolution. Because the arc-length aperture is also fixed, the model grid will wrap around the entire azimuth near the model source and gradually unwrap as the radius increases, enabling the model to capture all of the signals reaching the area of interest. Because the arc-length grid does not allow Fast Fourier Transform, it will increase the overall efficiency to switch the model grid to the angular grid at a certain distance. This changeover is seamless because both grids have cylindrical geometry. When the computation switched to the angular grid, the zero-padding technique was used to maintain the model resolution by extending the angular wavenumber spectra with zeros.

5.4.2 Modeled scenarios

Sound propagation to receivers at two sites was modeled. Site 1 was selected as the area most suitable for model verification. Site 2 was a coastal location and was closest to the Melville Bay Nature Reserve (**Figure 1**).

Site 1 – Qamut N

For a comparison between the output of the transmission loss model and the empirical data, a peripheral license block and a relatively isolated receiver were sought for, to increase the number of pulses that could be unequivocally assigned to the focal seismic vessel and limit the number of pulses that overlapped with signals from non-focal surveys.

Initially Maersk's seismic survey in the Tooq license block and the Pitu S recording station were selected to be the focus of this study (e.g. **Figure 1** and **Figure 22**). However, the middle and top loggers from the Pitu S station were not retrieved (**Table 5**) and the signal to noise ratios of the pulses recorded on the bottom receiver were low. While this was in agreement with preliminary model results showing large TL towards the bottom logger (Appendix C, **Figure C1**), it rendered further analysis difficult, as very few data points were suitable for comparisons.

Consequently, the analysis was refocused on the seismic activities of ConocoPhillips in the Qamut block as recorded on the Qamut N station. Qamut N was the only DCE station at which both the bottom (275 m) and the 150-m-deep logger remained stationary over the whole deployment period (**Table 5**, **Figure 22**).

Site 2 – BB4

As outlined above, the coastal areas of Melville Bay constitute important summering grounds and migration corridors for narwhals.

Furthermore, the proximity to the coast, and therefore melting glaciers, makes this area an interesting system to study the effects of spatial variability in sound speed profile from a source located in the center of the Bay towards the coast.

While several of the DCE loggers were within the Narwhal Protection Zone I, JASCO's BB4 station was the only recorder located in the vicinity of the Melville Bay Nature Reserve and in close proximity to the coast (**Figure 19** and **Figure 20**).

The model domain was a 67.62° fan with a 148.13 km radius extending from a 100 m deep location in the vicinity of the BB4 station towards the center of the bay where the seismic surveys of ConocoPhillips and Shell were conducted (**Figure 19**).

5.4.3 Model verification

The seismic vessels operated with an average firing interval of approximately 11 s, corresponding to a shot spacing of approximately 25 m, depending on vessel speed. Given such high spatial resolution, a rather conservative approach for the inclusion of shots in the analysis was taken.

Figure 19. Area covered by the WHOI model in scenario 2 with the receiver at station BB4 at 100 m depth. A. Model domain. The long red line denotes 100 m isobath. The model domain is a fan with an opening angle of 67.62 degrees and a radius of 148.13 km. B. Source positions within the model domain included in signal analysis (i.e. positions that could be unambiguously assigned to the focal source and from which the signals did not overlap with pulses from non-focal sources). The logger at station BB4 was deployed later in the season (Table 5; (Martin & MacDonnel 2013)), after Shell's vessels had operated in the north-eastern corner of the Anu block. Datum: WGS84; projection: Mercator.

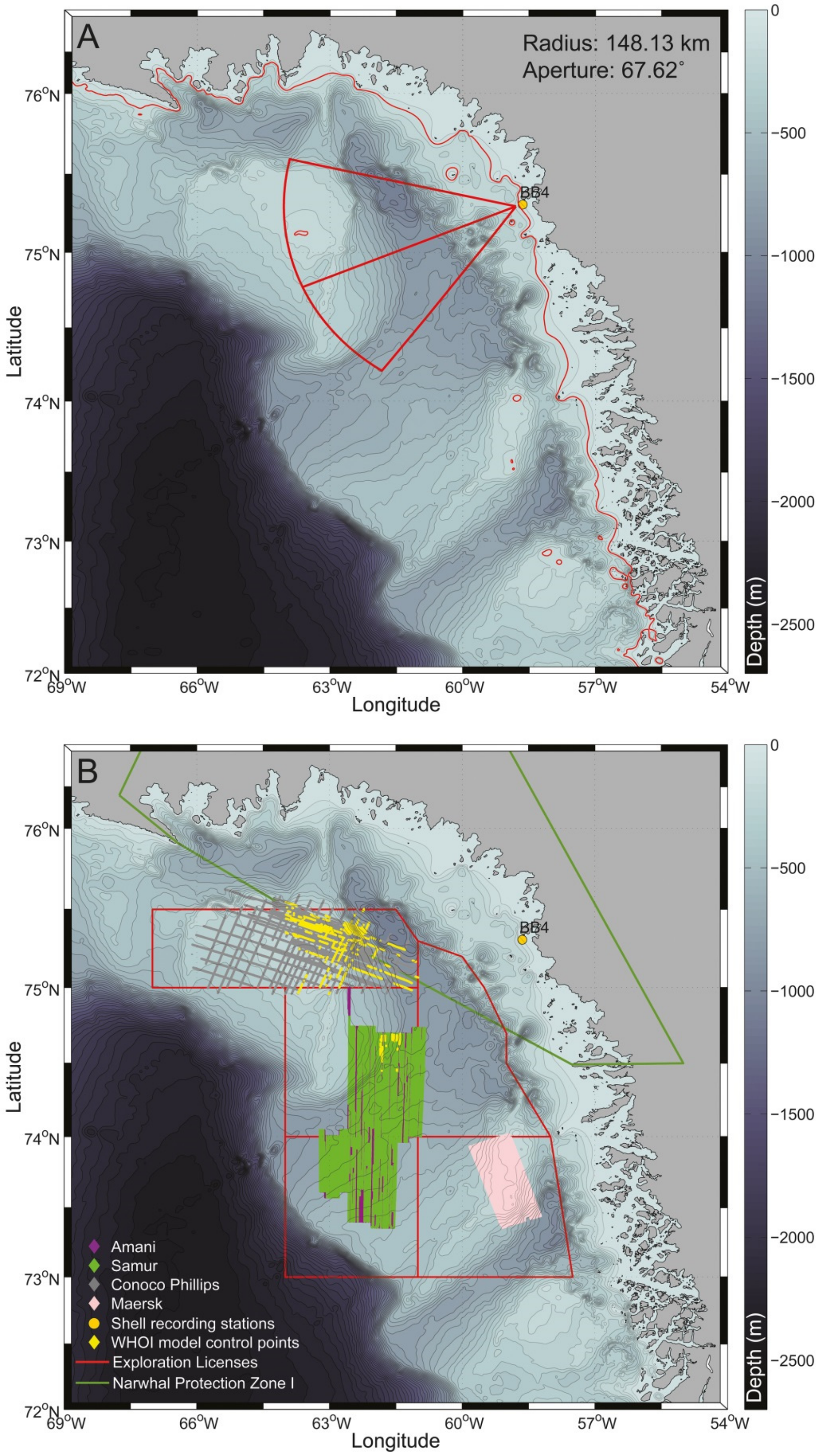

Files recorded during the operation of the focal survey in the area corresponding to the model domain (Figure 19) were found and screened for airgun pulses (see 5.3.2.1). Recordings fulfilling the screening criterion were processed with the airgun pulse detection routines (see section 5.3.2.2). The outputs of the detectors were then inspected manually; detections overlapping with pulses from non-focal vessels and the occasional false alarms were deleted. If pulses from more than one source were present in the recording, and the detections could not be unambiguously assigned to the focal survey, the data entry was excluded from the database. Pulse assignment was based on spectral similarity of the pulses to certain detections within relatively close time periods.

90% rms SPL and SEL in the frequency band of 10-2000 Hz were computed in the 4-second-long (-1:+3 s) time window around the pulse peak (see section 5.3.2.2).

The seismic airgun pulses detected at the BB4 station were of much lower amplitudes and much shorter durations than pulses received at the DCE stations or JASCO's recorders within the Anu and Napu blocks. Consequently, a shorter time window (±0.8 s) around the peak was assumed for the analysis of the BB4 detections.

The sound exposure levels mapped to the source locations were compared to an Nx2D simulation of the output of the transmission loss model.

5.5 Comparison with JASCO's propagation model

JASCO conducted a detailed comparison of the levels measured by the loggers at the BB1-BB3 stations to the pre-season modeling results (**Figure 10**), as part of the "Shell Greenland Acoustic Monitoring of 2012 3D Seismic Surveys in Baffin Bay" study (Martin & MacDonnel 2013). They found a relatively good correspondence between the results measured along a broadside track, ranging from 0.1 to 75 km from Shell's model site 3 (**Table 3**, **Figure 20**), and the levels anticipated by the model (Martin & MacDonnel 2013). Our intent was not to repeat JASCO's measurements, but to expand their results by examining how sound levels received at stations distributed in various parts of Baffin Bay, and at different depths, compared to the maximum-over-depth levels (e.g. **Figure 10**) predicted by the pre-season modeling for all companies. In addition, cumulative SELs originating from the northernmost firing line of ConocoPhillips and recorded at the Qamut N station were measured. Finally, cumulative SELs from Shell's two firing lines considered in the pre-season modeling study, and all other vessels operating during the same time periods, were determined for seven recording stations.

5.5.1 Single-shot sound fields

Levels of shots originating in close proximity to the modeling sites (**Table 3**), as received at the different recording stations, were compared to the predictions of the pre-season modeling. For this purpose, vessel firing positions within a 2 km radius from a given modeling site were found (**Figure 20**). The time delays from these positions to all stations encompassed within the modeled sound field (e.g. **Figure 10**) were estimated assuming an average sound speed of 1465 m/s (average sound speed at Amu - Appendix A, **Figure A7**, panel 3), and sound recordings corresponding to the arrival times of the airgun pulses at the recording stations were identified. The files were then processed in the same way as those used in the verification of the WHOI model, but with less conservative criteria to maximize the number of pulses included in the analysis:

1. Recordings were passed through the airgun pulse detection routines using a threshold of 1.4 Pa.
2. The results were inspected manually and false detections, detections that could not be unequivocally assigned to the focal survey, as well as detections overlapping with pulses from non-focal surveys were deleted.
3. 90% rms SPL and SEL were computed in the 4-second-long time window around the pulse peak (section 5.3.2.2).

Given that the sound field modeled for Maersk only encompassed one of the DCE stations, with high transmission loss (see section 5.4.2), and the BB1-BB3 stations, which were dominated by pulses from the nearby Shell vessels, the modeling results for Maersk were not included in the analysis.

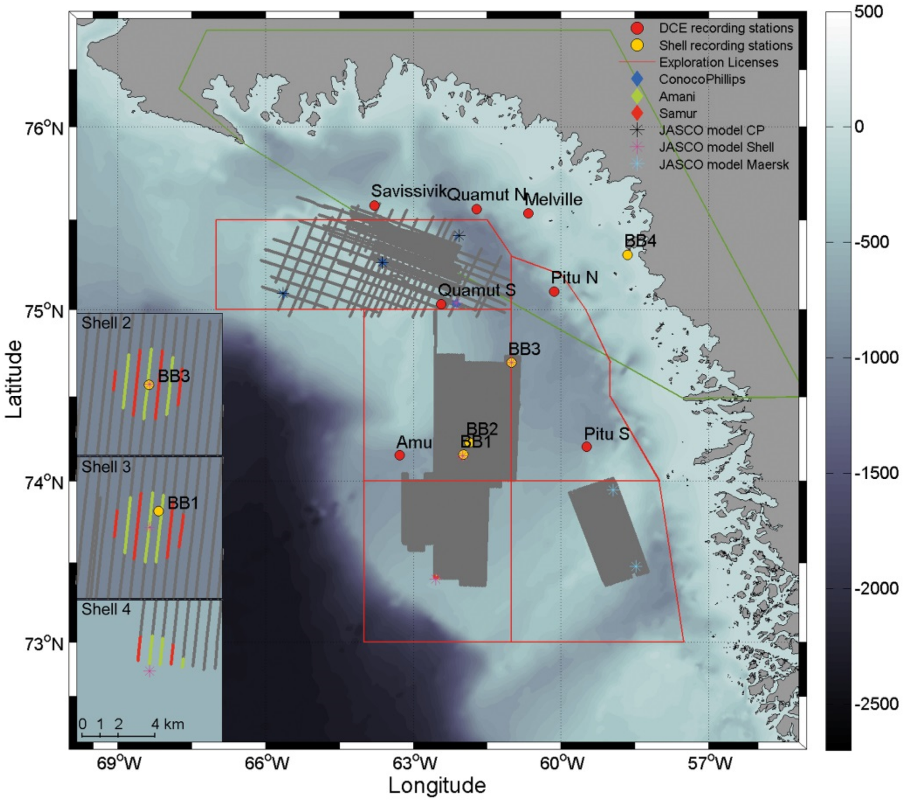

Figure 20. Source positions modeled by JASCO and shots included in model verification. Note that Shell's site 1was within the Qamut block (in the vicinity of the Qamut S recording station), and hence shots from the M/V Princess (ConocoPhillips, blue dots) were used for comparison with the modeled soundscape. Inset maps zoom in on the tracks of the two Shell vessels and the shots selected for the model verification (i.e. within a 2 km radius from the modeled source positions). Large map - datum: WGS84; projection: Mercator. Inserts - datum: WGS84; projection: UTM Zone 21.

5.5.2 Cumulative sound exposure levels

<u>Single source - ConocoPhillips</u>

As detector data for the ConocoPhillips seismic survey recorded on the three loggers at the Qamut N station had already been inspected for verification of the WHOI model (section 5.4.3), cumulative SELs for three different depths were computed and compared to JASCO's pre-season modeling results for pulses emitted along the northernmost firing line (Austin et al. 2012b).

Not all pulses emitted along the firing line passed the inclusion criteria (sections 5.3.2.2 and 5.4.3). For the bottom and the 150-m-deep recorder, the missing data points were therefore linearly interpolated. For the shallowest station this did not produce a valid result and instead it was assumed that the received pulse energy was the same as the energy for the pulse emitted closest in time to the unknown one (in principle sample-and-hold interpolation). This method was verified, and gave identical results to the linear interpolation method used for the two deeper stations where that worked well. The interpolated energy in linear units was then summed and a time correction factor (accounting for the total firing time amounting to less than 24 hours) was added (in dB).

Multiple sources – Shell

In their pre-season modeling, JASCO addressed the requirements for cumulative sound exposure at a regional scale by generating aggregate exposure maps of combined noise contributions from all concurrent seismic activities (i.e. seismic operations of Shell, ConocoPhillips and Maersk). For that purpose, JASCO assumed that the different seismic vessels would operate along the firing lines considered in the single-source-cSEL scenarios (Austin et al. 2012a; Austin et al. 2012b; Matthews 2012). Given that the schedules of the surveys in 2012 did not conform to that assumption, it was not possible to directly verify the results of the model. Instead, 24-hour cSELs from shots emitted along the modeled northernmost firing line of ConocoPhillips (Austin et al. 2012b), together with airgun shots from all other vessels operating during the same time periods, were measured individually. The same was done for Shell. However, Shell's operations along the western modeled firing line were conducted in two transects, hence a total of three scenarios were considered.

Sound exposure levels of the whole recordings taken during the firing periods of interest, rather than a sum of the energy of all individual shots, were measured (see **Figure D1** in Appendix D), as, given the somewhat different firing rates of the vessels operating in different parts of the bay (see for example **Figure D2** in Appendix D), it was not possible to reliably define windows over which to compute the SELs of individual shots. Moreover, given the often long duration of the signals and the overlap of pulses originating from different surveys, this method appeared more accurate (**Figure D1-Figure D2** in Appendix D). Recordings from self-noise-dominated or loose loggers were excluded from the analysis, thereby limiting the dataset to only comprise recordings dominated by the seismic noise. A total of eleven loggers from seven stations (BB1-BB3, Savissivik, Qamut S, Melville and Pitu N) were analyzed.

The energy of individual sound files in linear units was summed and a time correction factor (accounting for the total firing time amounting to less than 24 hours) was added (in dB).

6 Results

All recovered dataloggers had recorded as intended (**Table 5**) and the recordings comprised a total of 4226 hours of continuous recordings. Along with noise recordings, detailed environmental data, such as temperature, depth and salinity profiles, were collected in different parts of Baffin Bay (**Figure 21**). Nearing the end of the seismic program, up and close recordings were made of one of the four seismic vessels to document the signature of one of the airgun arrays in operation. 9 approaches of *Polarcus Asima* were recorded at ranges from 0.5 nmi to 8 nmi.

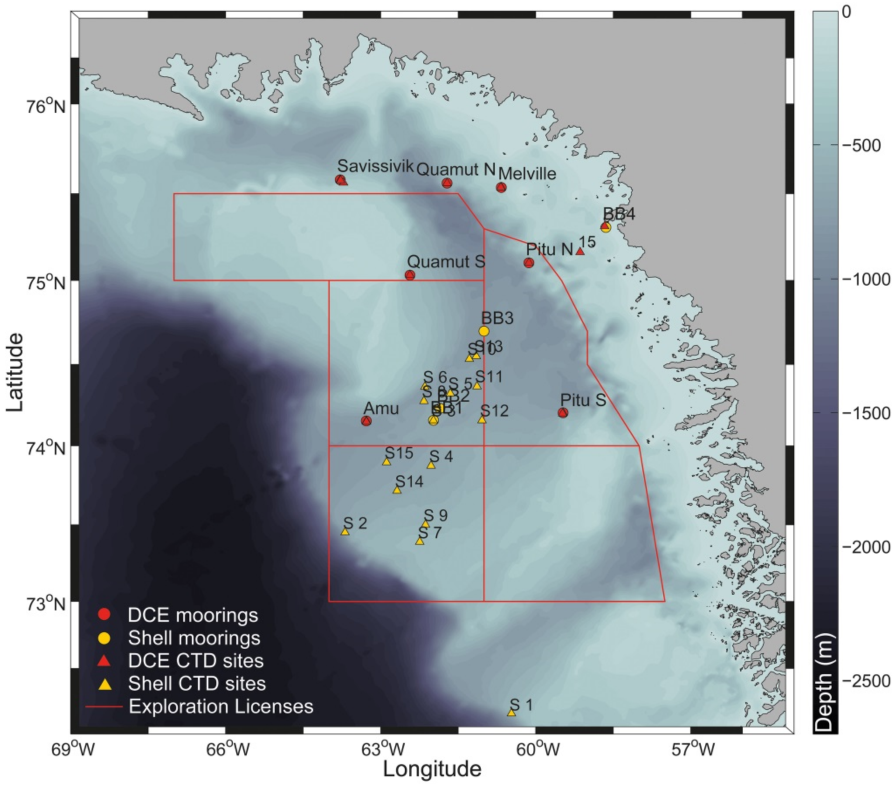

Figure 21. Map of NE Baffin Bay/Melville Bay with the five license blocks, mooring positions and sites where CTD-profiles were acquired by DCE or Shell. DCE CTD-profiles were obtained at deployment and recovery of the moorings (**Table 6**). Shell CTD-profiles were recorded throughout the seismic season (**Table 7**). Datum: WGS84; projection: Mercator.

6.1 Dataloggers and data

Seven moorings, each with three dataloggers, were deployed, and out of these, nineteen loggers were successfully retrieved, all containing usable data. The last two dataloggers were tracked to have washed up on an inaccessible part of the coastline and could not be retrieved. Due to an underestimation of the wave forces generated during storms, all dataloggers in the top of the moorings and all but one of the middle dataloggers detached during the deployment period and floated freely while continuing to record. As all loggers were fitted with GPS transmitters, they could be tracked by satellite telemetry and some of the data could still be included in the analysis. Most of the floating dataloggers were recovered in the middle of September from *R/V Sanna*, some were recovered by support vessels of the seismic operators and two were recovered close to Thule by a local fireman. An overview of the deployments is shown in **Table 5**. In addition to these data, recordings made by JASCO for Shell at four additional locations (**Table 5**) were included in the analysis. **Figure 22** shows a map of the deployment positions and tracks of the floating recorders after the detachment.

Figure 22. Deployment positions (red dots for DCE stations, yellow dots for JASCO's moorings) and tracks of dataloggers that detached from moorings due to storms and drifted freely in the area. The tracks are color-coded with date. Datum: WGS84; projection: Mercator.

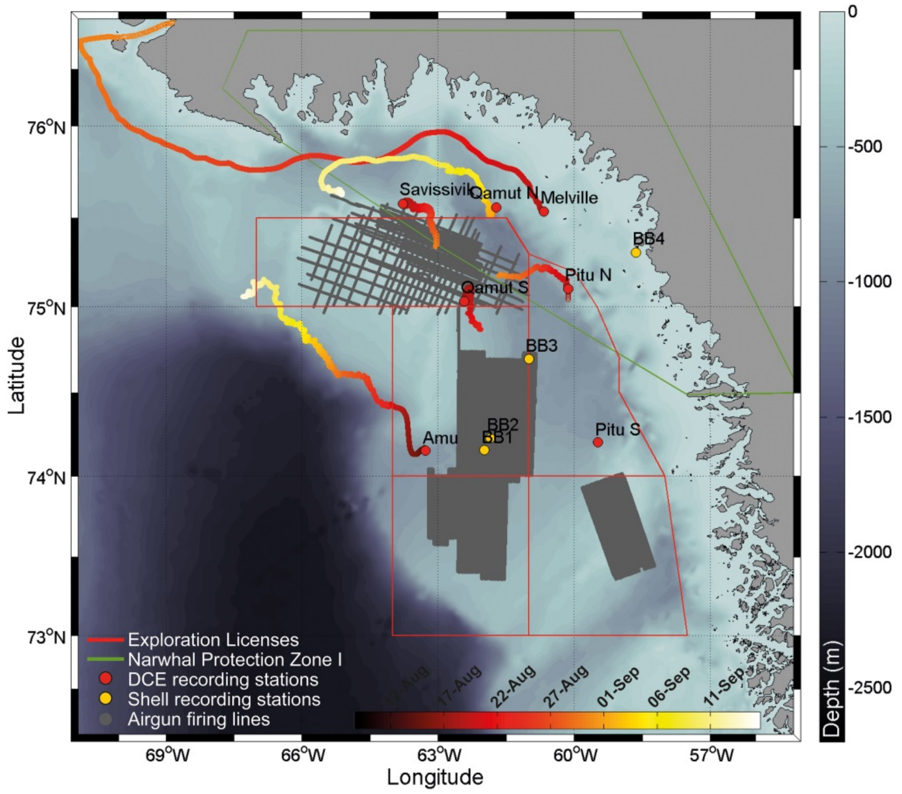

6.2 Environmental data

6.2.1 Sound speed profiles

Sound speed profiles were computed from CTD measurements collected at DCE mooring stations in connection with deployment and again at the time of recovery (**Figure 23**, **Table 6**, Appendix A). In addition, a number of sound speed profiles were measured by Shell during their survey operations (**Figure 23**, **Table 7**) which were made available for the WHOI modeling studies. The basic features of the profiles were similar across the entire Baffin Bay with the exception of the profile obtained at the Depotøerne station (**Figure 23**). This station was in the vicinity of JASCO's BB4 mooring and WHOI's modeling site 2 (**Figure 19**) and located close to the shore and glaciers (**Figure 21**, **Table 5**). The profiles differ significantly from the US Naval Oceanographic Office's Generalized Digital Environmental Model used for JASCO's modeling (Matthews 2012) with the surface duct stronger than anticipated (Martin & MacDonnel 2013), but relatively stable over the entire period (**Figure 23**).

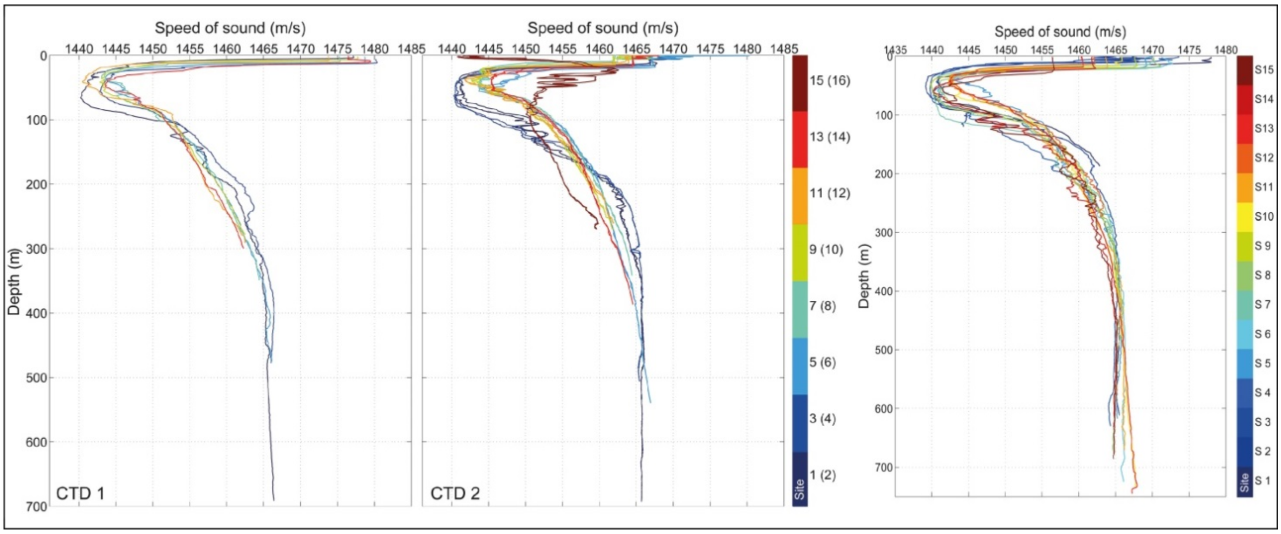

Figure 23. Sound speed profiles collected during the seismic season. Left and middle: DCE measurements acquired at the time of mooring deployment and recovery; right: data obtained by Shell throughout the season. The atypical sound speed profile in the middle panel (brown line) was obtained close to the coast/glaciers at Shell mooring position BB4 (Depotøerne).

Table 6. Location and timing of the CTD measurements taken by the DCE.

Label	Date	Latitude (N)	Longitude (W)	Depth (m)	Mooring site	CTD cast
1	2012-08-09	74.15417	-63.27783	746	Amu	1
2	2012-09-13	74.14983	-63.27750	752	Amu	2
3	2012-08-09	74.20457	-59.47130	581	Pitu S	1
4	2012-09-16	74.20028	-59.47983	583	Pitu S	2
5	2012-08-11	75.10333	-60.13217	590	Pitu N	1
6	2012-09-15	75.10333	-60.13167	600	Pitu N	2
7	2012-08-11	75.03133	-62.43150	390	Qamut S	1
8	2012-09-16	75.03137	-62.43495	388	Qamut S	2
9	2012-08-10	75.55958	-61.71467	317	Qamut N	1
10	2012-09-15	75.56230	-63.71885	320	Qamut N	2
11	2012-08-10	75.57835	-63.78403	335	Savissivik	1
12	2012-09-14	75.57598	-63.77623	300	Savissivik	2
13	2012-08-10	75.53500	-60.66667	446	Melville	1
14	2012-09-15	75.53610	-60.67358	450	Melville	2
15	2012-08-14	75.16500	-59.14167	360	Depotøerne	1
16	2012-09-15	75.31472	-58.66472	358	Depotøerne/BB4	2

Table 7. Location and timing of the CTD measurements taken by Shell.

Label	Date	Latitude (N)	Longitude (W)	Depth (m)
S1	2012-07-27	72.2425	-60.4693	187
S2	2012-07-28	73.4508	-63.6898	120
S3	2012-07-29	74.1583	-61.9794	612
S4	2012-08-05	73.8745	-62.0246	630
S5	2012-08-18	74.3233	-61.6533	617
S6	2012-08-25	74.3636	-62.1442	725
S7	2012-08-28	73.3900	-62.2433	419
S8	2012-09-04	74.2760	-62.1627	679
S9	2012-09-16	73.5000	-62.1333	493
S10	2012-09-17	74.5333	-61.2833	734
S11	2012-09-22	74.3667	-61.1367	670
S12	2012-09-28	74.1583	-61.0400	274
S13	2012-09-30	74.5500	-61.1500	745
S14	2012-10-05	73.7167	-62.6833	632
S15	2012-10-10	73.8967	-62.8867	686

6.2.2 Bathymetry

Comparisons between the bathymetry models used by JASCO and WHOI in the sound propagation studies, and the in situ depth measurements provided by the seismic operators (**Figure 24** and **Figure 25**) showed disagreements. **Figure 24** and **Figure 25** show comparisons for the Qamut license block. Appendix A.2 contains the results for the Anu, Napu and Tooq blocks (**Figure A9.** Deviation between the bathymetry models available prior to study and depths measured during seismic surveys in the Anu and Napu License Areas. Top panel: the bathymetry model used by JASCO for the preseason modelling (SRTM30+ v7.0) sampled at Shell's airgun firing lines. Middle panel: depths measured by Shell's vessels at their firing positions. Bottom panel: difference between the bathymetry model and the measured depths.). Within plateaus the differences between the models and the measurements are relatively minor but may exceed 250 m in areas where the bottom is sloping.

6.2.3 Mooring temperature and depth sensors

This section presents pressure and temperature data measured by the StarOddi loggers that were distributed along the Qamut N mooring. Measurements from the Amu station, (i.e. the only other recovered DCE mooring with multiple StarOddi sensors) are shown in Appendix A, (**Figure A13**).

6.2.3.1 Depth

Both JASCO's vertical arrays and the DCE moorings included top floats intended to minimize possible displacements of hydrophones in the ocean currents (**Figure 15**; (Martin & MacDonnel 2013) and both designs have proven successful in this respect. Pressure sensors deployed along the Qamut N mooring recorded depth variations on the order of ±1 m per day (**Figure 26**). These fluctuations were interpreted as being the result of fluctuations in water depth due to local tides, rather than changes in the orientation of the mooring.

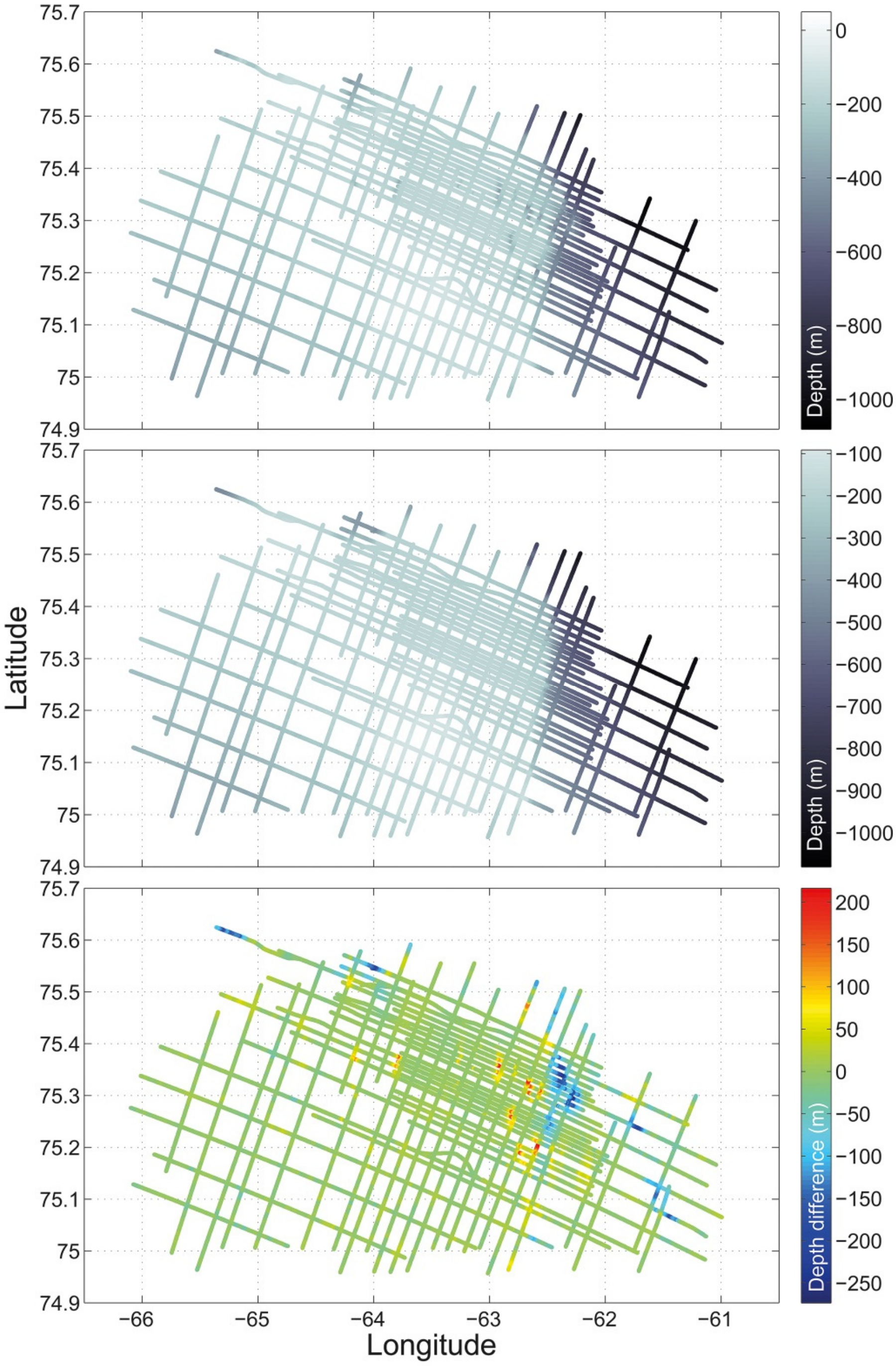

Figure 24. Deviation between the bathymetry model available prior to the study and depths measured during seismic surveys in the Qamut block. Top panel: the bathymetry model used by JASCO for the pre-season modeling (SRTM30+ v7.0), sampled at the ConocoPhillips airgun firing lines. Middle panel: depths measured by the ConocoPhillips vessel at its firing positions. Bottom panel: difference between the bathymetry model and the measured depths. (Measurements courtesy of ConocoPhillips).

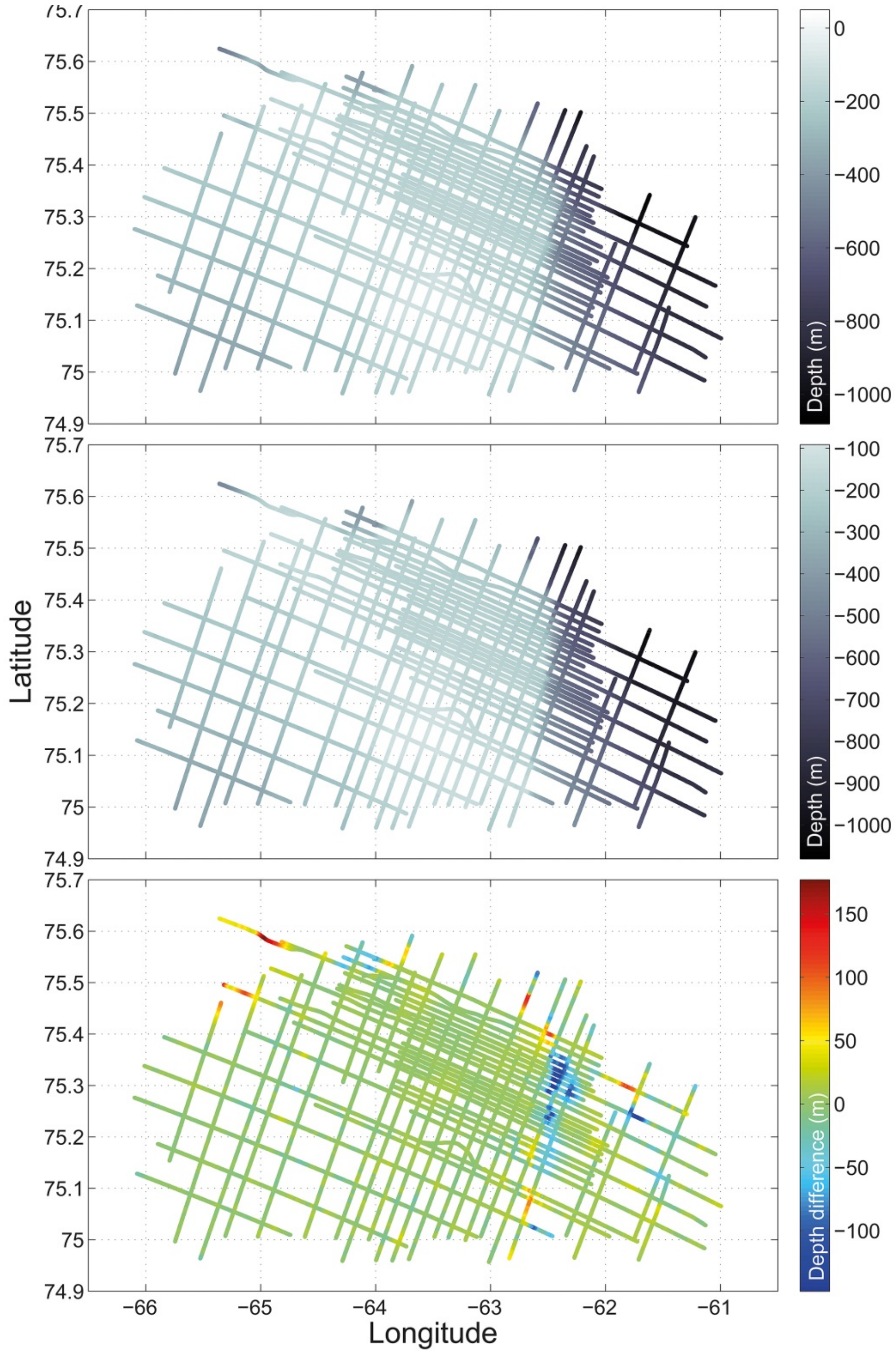

Figure 25. Deviation between the bathymetry model available prior to the study and depths measured during seismic surveys in the Qamut block. Top panel: the bathymetry model used by WHOI (IBCAO v3.0 30 arc second, (Jakobsson et al. 2012) sampled at the ConocoPhillips airgun firing lines. Middle panel: depths measured by the ConocoPhillip's vessel at its firing positions. Bottom panel: difference between the bathymetry model and the measured depths. (Measurements courtesy of ConocoPhillips).

Figure 26. Depth recorded by two of the StarOddi loggers deployed along the Qamut N mooring, in which both the bottom and the 150-m-deep noise loggers remained stationary for the whole period of deployment. Depth variations were on the order of ±1 m per day, most likely due to tide-related changes in water depth. Phases of the moon caused larger variations every two weeks.

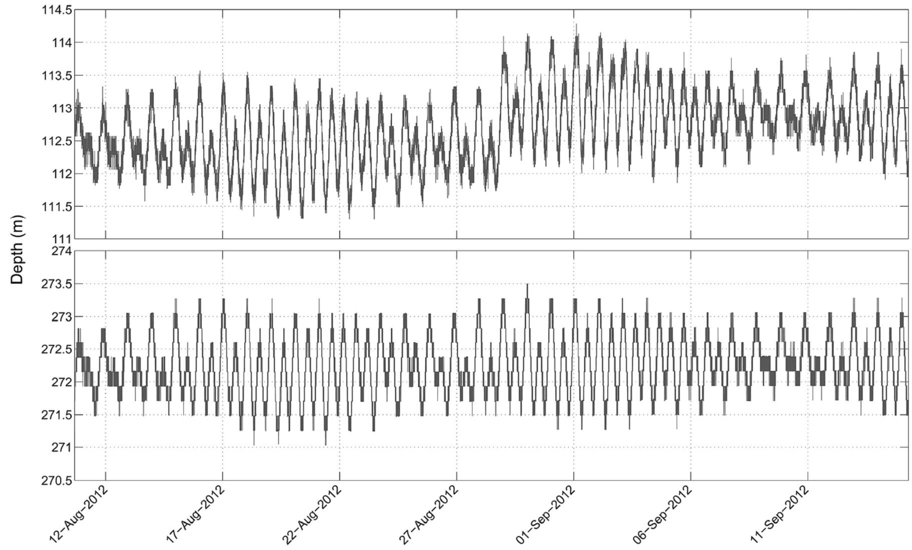

6.2.3.2 Temperature

Overall, there was a good correspondence between the CTD data collected at the times of mooring deployment and recovery, and the temperatures measured by the StarOddi sensors over the 5-week deployment period (**Figure 27**). Both the mean and the range of temperature fluctuations varied significantly with depth: For the water layer below 150 m the mean temperature was 1-2 °C (±<0.2°C). At 25-50 m depth the mean temperature was 1°C (±1°C) (**Figure 27** and **Figure 28**).

Figure 27. Temperature profiles at the location of the Qamut N mooring showing typical temperature variations in the top 300 m of the water column. The profiles are overlaid with data from StarOddi sensors that were attached to the mooring at seven depths. For the top sensor, only data collected prior to detachment are presented. The overall stability of the deeper profile, as well as the variability of the surface mixed layer in between deployment (CTD1) and recovery (CTD2) phases are to be noted.

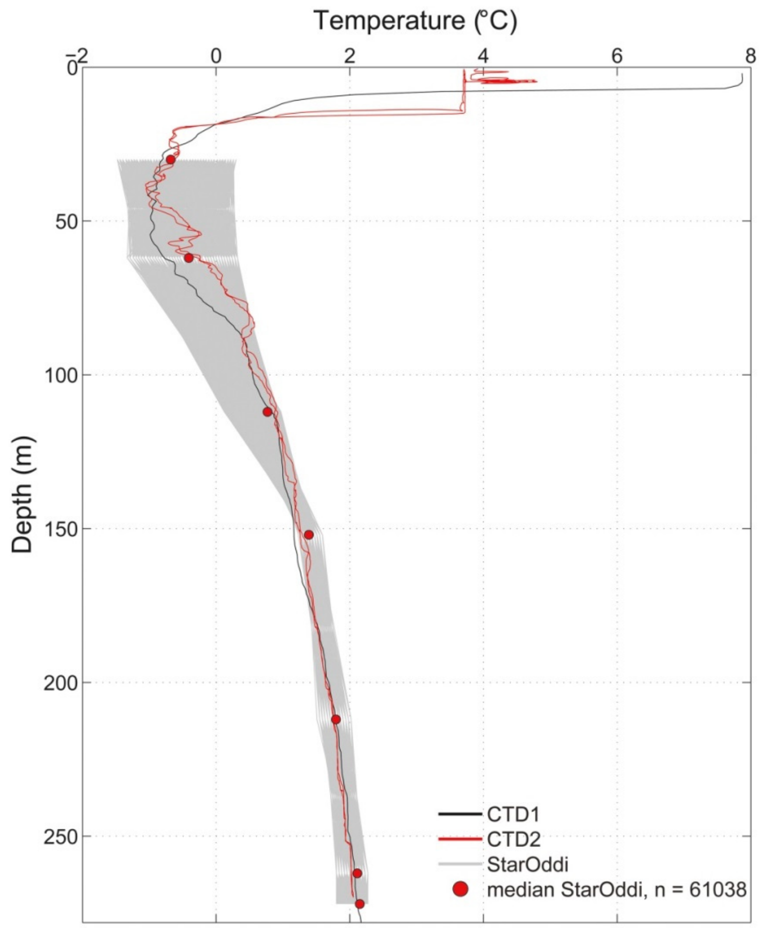

The temperature variations recorded by the deep water sensors seemed to correspond to the above-mentioned tidal depth changes (**Figure 28**).

A detailed discussion of the observed variability in the surface mixed layer and its consequences for the transmission loss is given in Appendix B.

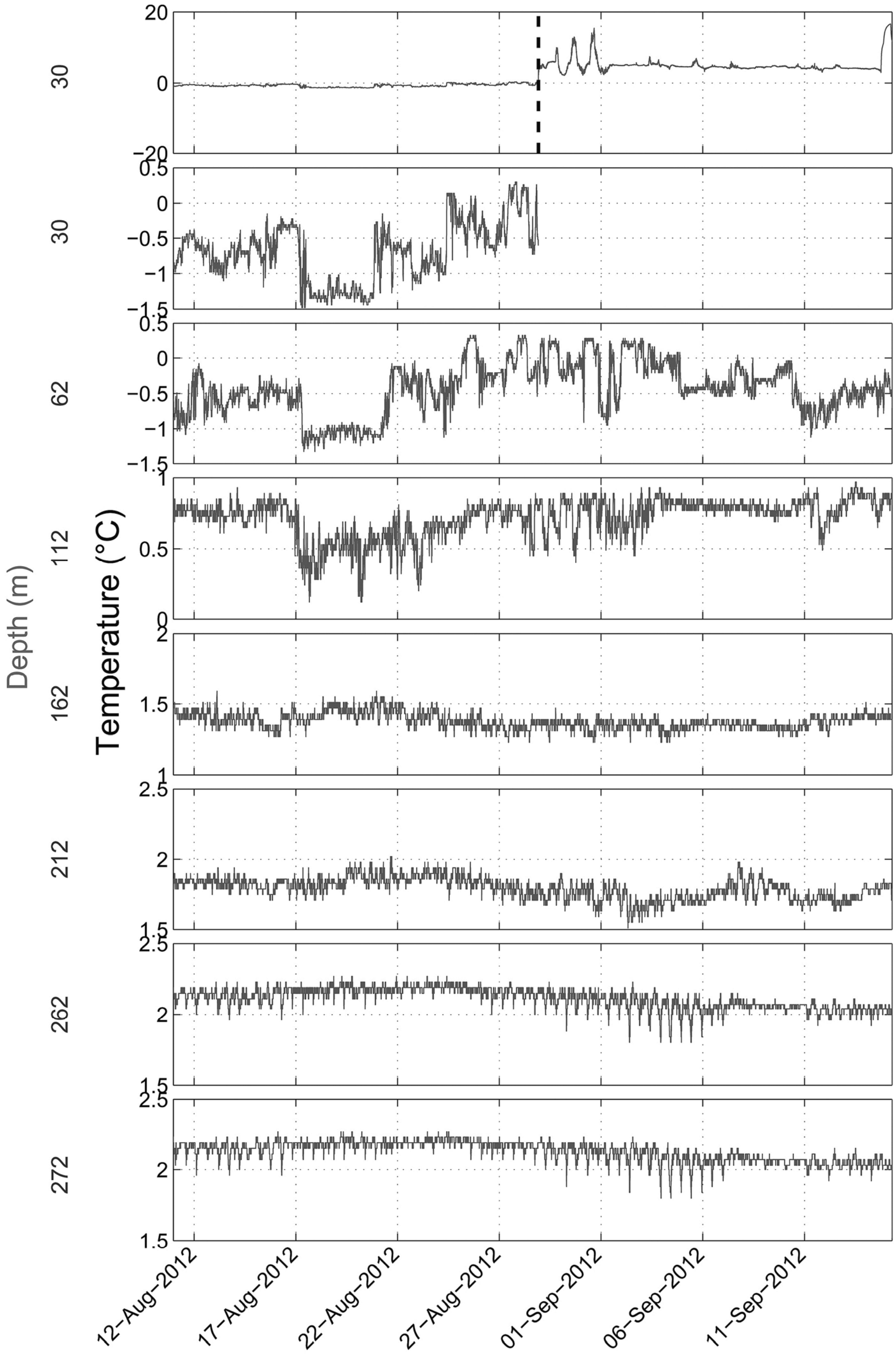

Figure 28. Temperature recorded by the Star-Oddi loggers distributed along the Qamut N mooring. The dashed line in the top panel marks the time of detachment of the top part of the mooring.

6.3 Short-range signatures

The airgun pulses sampled during the close-up recordings, contained significant energy at frequencies all the way up to the limits of the recording device (Nyquist rate of 48 kHz; **Figure 29** and **Figure 30**). Given that the typical time interval between consecutive pulses was close to 10 seconds, the averaged power spectral densities depicted in **Figure 30**, using an integration time of 10 seconds, correspond to the average spectrum levels received at the different ranges from the operating airgun array. A less conservative measurement with an integration window of 1 second centered on the pulse would have led to a 10 dB increase in the reported levels, assuming negligible energy outside the 1-second window.

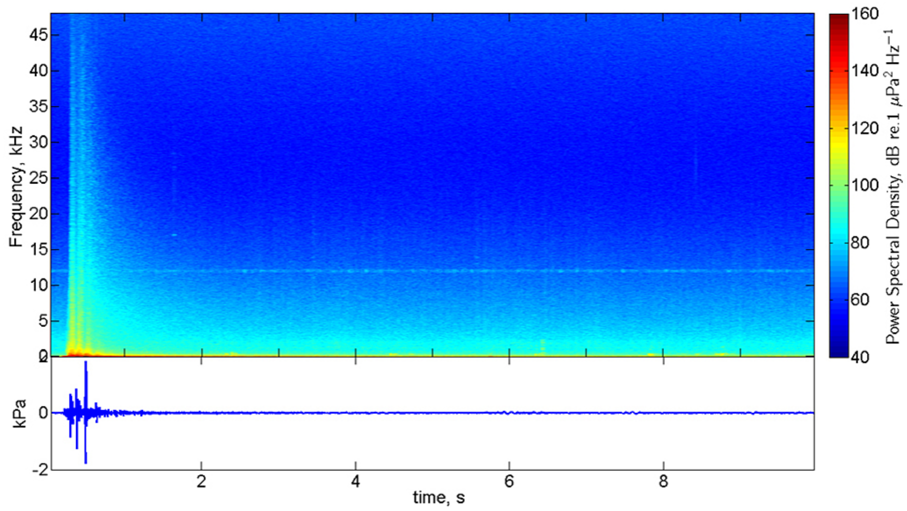

Figure 29. Averaged spectrogram of pulses recorded at a distance of 1 km from the airgun array of R/V *Polarcus Asima*.

At all distances (up to 8 nmi), the spectral levels were elevated above Wenz' maximum (Wenz 1962) up to at least 1 kHz (**Figure 30**). The very high apparent "ambient level" was likely also influenced by a distant survey, and the overall sound level was well above the expected values of Wenz curves for sea state of 0.5-1 during which these recordings were taken.

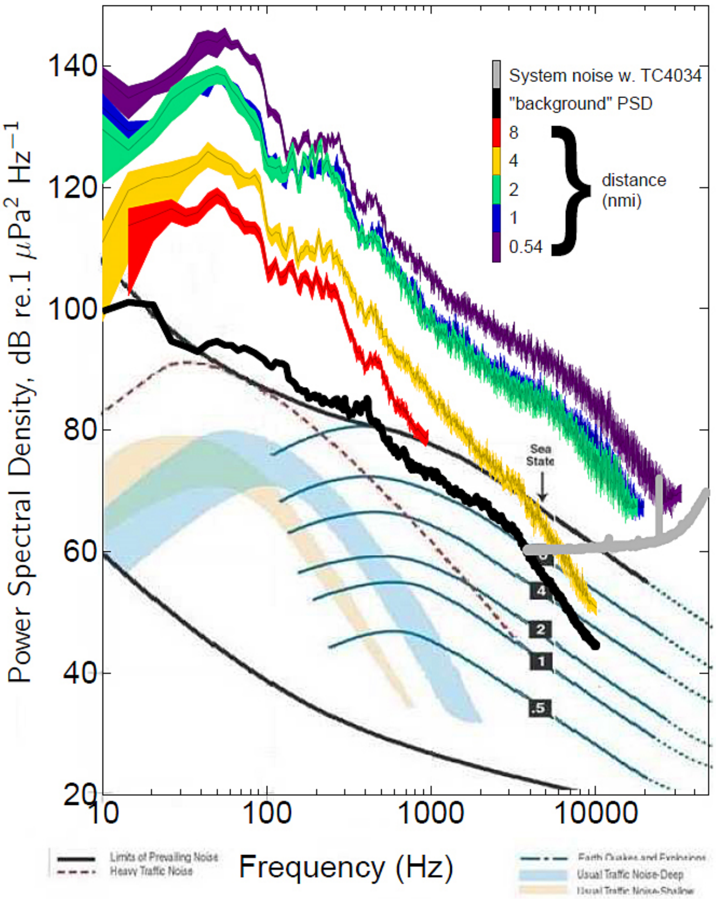

Figure 30. Power spectral density levels (PSD) of the airgun source. The airgun pulses were detected in the recordings automatically (see section 5.3.1) and clipped to fit within a time window of 10 seconds centered on the pulse. The average PSD for all pulses recorded at a given distance was calculated using one large FFT (960000 samples). The resulting 480000 PSD values were averaged together into 8192 bins (58 "original" values in each). The background noise was calculated similarly.
The PSD line stops 6 dB above the limiting noise floor, system (of Reson 4034 recorder) self-noise or "background" noise. The levels recorded during the break are very high compared to the Wenz' curves and when recordings were inspected carefully it was possible to detect another distant survey operation.
The figure is adapted from Wenz, 1962 as shown in (Peerin 2002).

Full-spectrum envelopes of airgun pulses during a 12 second firing interval for ranges of 0.5 to 8 nmi from R/V *Polarcus Asima* (**Figure 31**) show that during the approximately 10-second interval between pulses (1 pulse every 10 seconds), the instantaneous sound intensity did not fall back to the background level, even at the longest distances, although this phenomenon was much more pronounced at ranges below 4 nmi.

Received levels (RL) are shown in **Figure 32**. The mean peak-to-peak RL was highest at the 0.54-nmi range with a maximum of 198 dB re 1 µPa (p-p). There was no difference in the received level between 1 and 2 nmi (193 dB re 1 µPa (p-p)) and there was only 1 dB difference at 4 and 8 nmi with received levels of 174 and 172 dB re 1 µPa (p-p), respectively. The mean rms RL measured over the 90% energy duration followed the same pattern, with levels decreasing with range from 187 dB re 1 µPa (rms) at 0.54 nmi over 183 dB 1 µPa (rms) and 182 dB re 1 µPa (rms) at 1 and 2 nm, 164 dB re 1 µPa (rms) at 4 nmi to 161 dB re 1 µPa (rms) at 8 nm. Mean sound exposure levels (SEL) computed over a 10-second integration window decreased from 174 dB re 1 μPa^2s at 0.54 nmi over 168 and 167 dB re 1 μPa^2s at 1 and 2 nmi, 155 dB re 1 μPa^2s at 4 nmi to 148 dB re 1 μPa^2s at 8 nmi i (**Figure 32**).

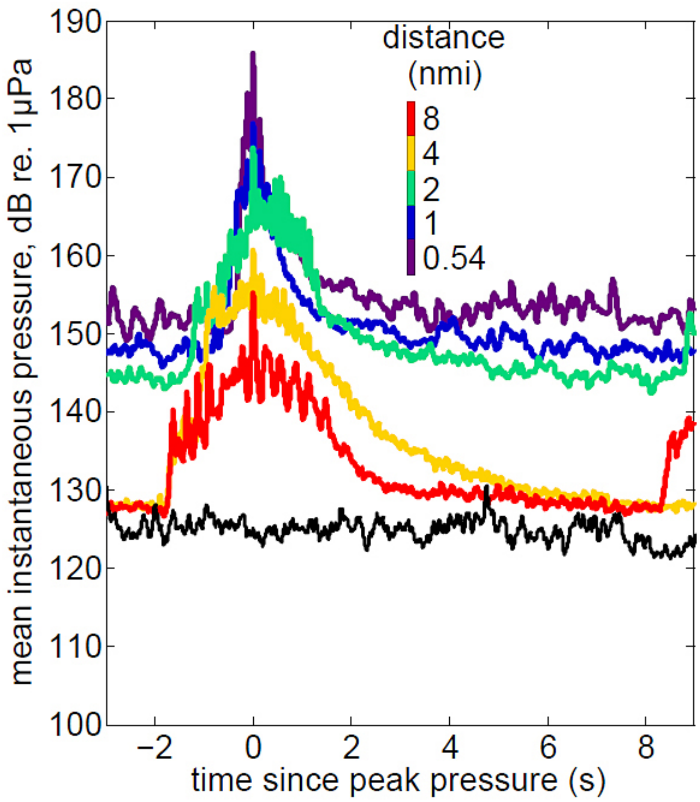

Figure 31. Development of mean instantaneous pressure (envelope) as a function of time after a shot, as measured at various distances (0.54 to 8 nmi) from the source. The envelopes were calculated using the analytical signal (hilbert in Matlab). For each distance, the envelopes of 12 shots were averaged together and thereafter smoothed with a phase neutral low-pass filter (filtfilt in Matlab). The lowest (black) line is a similarly smoothed envelope of the ambient sound recorded during a pause in the seismic operation.

Figure 32. Received levels of airgun signals recorded with handheld hydrophones at close ranges to the seismic vessel *R/V Polarcus Asima.* Top panel shows received levels calculated as peak–to-peak values. Middle panel depicts rms received levels computed using the 90% energy duration time window, and bottom panel depicts sound exposure level in a 10-second time window.

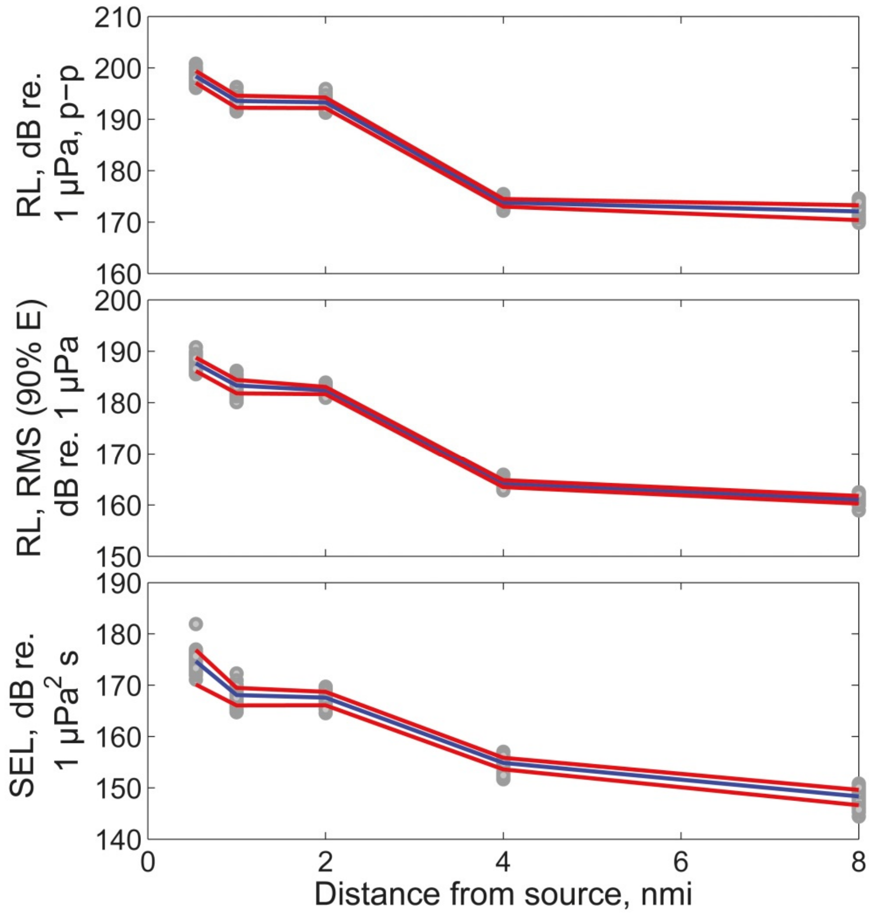

6.4 Long range recordings

6.4.1 Typical recordings

Both the sound speed profile with a strong surface duct (**Figure 23**) and the “fast” (sand or harder material) bottom contributed to the complex sound propagation conditions in the Baffin Bay area (for details see Appendix B). Multiple reflections arriving with short time delays caused long (typically on the order of 4 seconds) effective pulse lengths (e.g. **Figure 33** and **Figure 34**).

Frequently, pulses originating from several seismic vessels would arrive at comparable received levels and overlap in time (**Figure 34**).

Figure 33. Spectrogram and time series of a typical sound recording of airgun pulses received at the bottom hydrophone (logger #1195) at the Savissivik station on 27 August 2012 (see map in **Figure 41** for positions of the seismic vessels relative to the loggers).

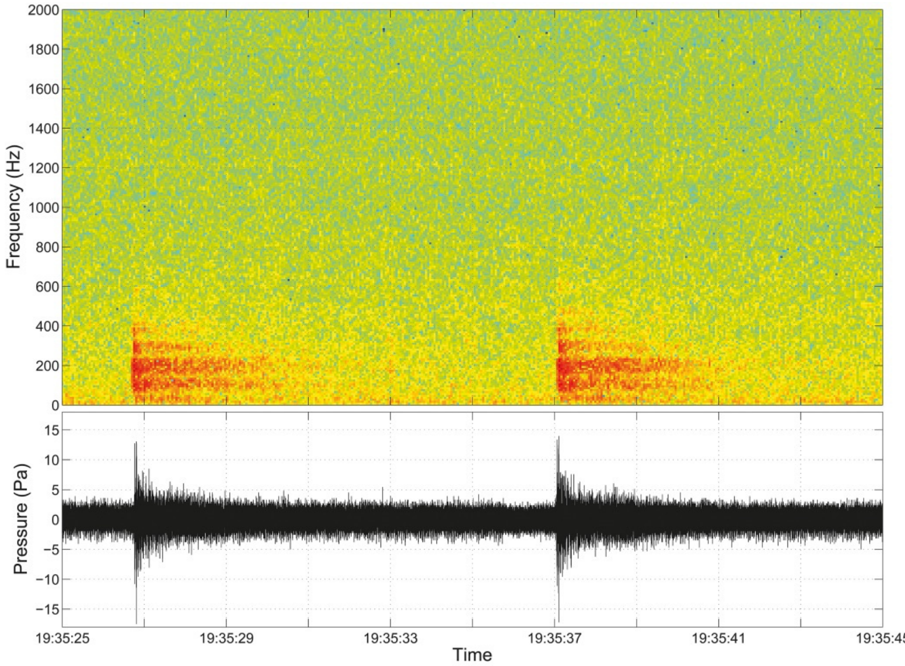

Figure 34. Spectrogram and time series showing overlapping airgun pulses from three seismic vessels (most likely *M/V Princess* (ConocoPhillps), *R/V Polarcus Samur* (Shell) and *R/V Polarcus Amani* (Shell)) received at the middle hydrophone (logger #1191, 150 m deep) at the Qamut N station on 11 September 2012 (see map in **Figure 41** for positions of the seismic vessels relative to the loggers).

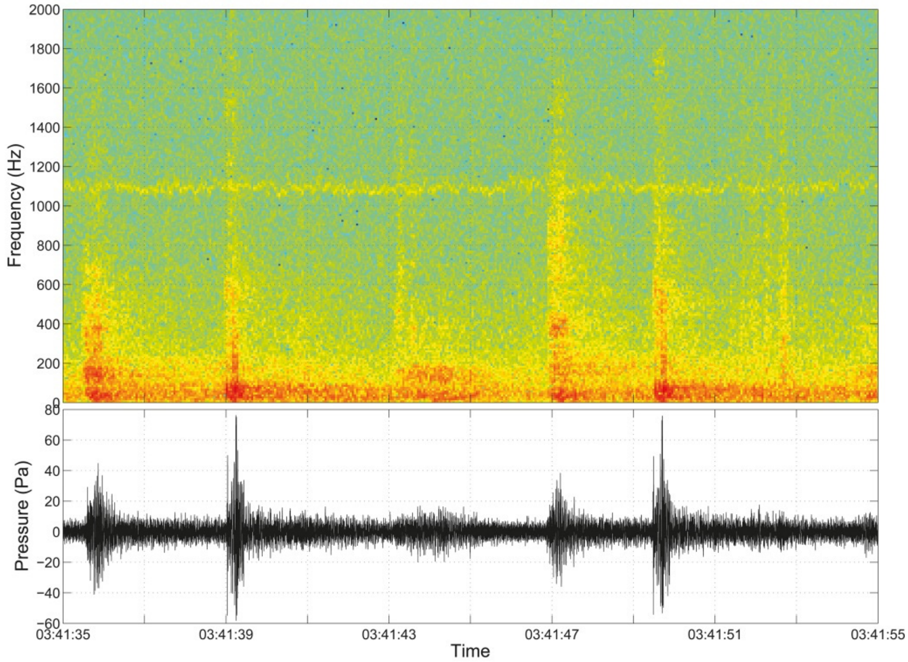

6.4.2 Sound exposure levels

R/V Polarcus Amani and *R/V Polarcus Samur* began their operations in Shell's license blocks on 01 August 2012 (**Table 2**, **Figure 35**-**Figure 40**). Shortly thereafter, on 06 August, they were joined by Maersk's vessel in the Tooq license area. Finally, ConocoPhillips, initiated its operations in the Qamut block on 25 August. The seismic activities in Baffin Bay extended until 14 October, and over the duration of the DCE recordings a maximum seismic-free time interval of 10 hours was recorded.

The commencement of seismic operations was closely reflected in the sound exposure levels recorded at JASCO's hydrophone arrays in the Anu and

Napu blocks, with an approximate 20 dB increase in the daily median SEL and cumulative SEL values (**Figure 35**). The levels remained elevated for the duration of the deployment period of the recording stations (**Figure 35**). While the total SELs (**Figure 35**) and the SELs of recordings band-pass filtered between 10-2000 Hz (**Figure 36**), showed small differences before August 1st for the BB1-BB3 stations, there were no noticeable differences between the two methods hereafter.

The mid-frequency m-weighted SELs within Shell's license blocks (**Figure 37**) were on average approximately 10 dB lower than the total and band-pass filtered values (**Figure 35** and **Figure 36**).

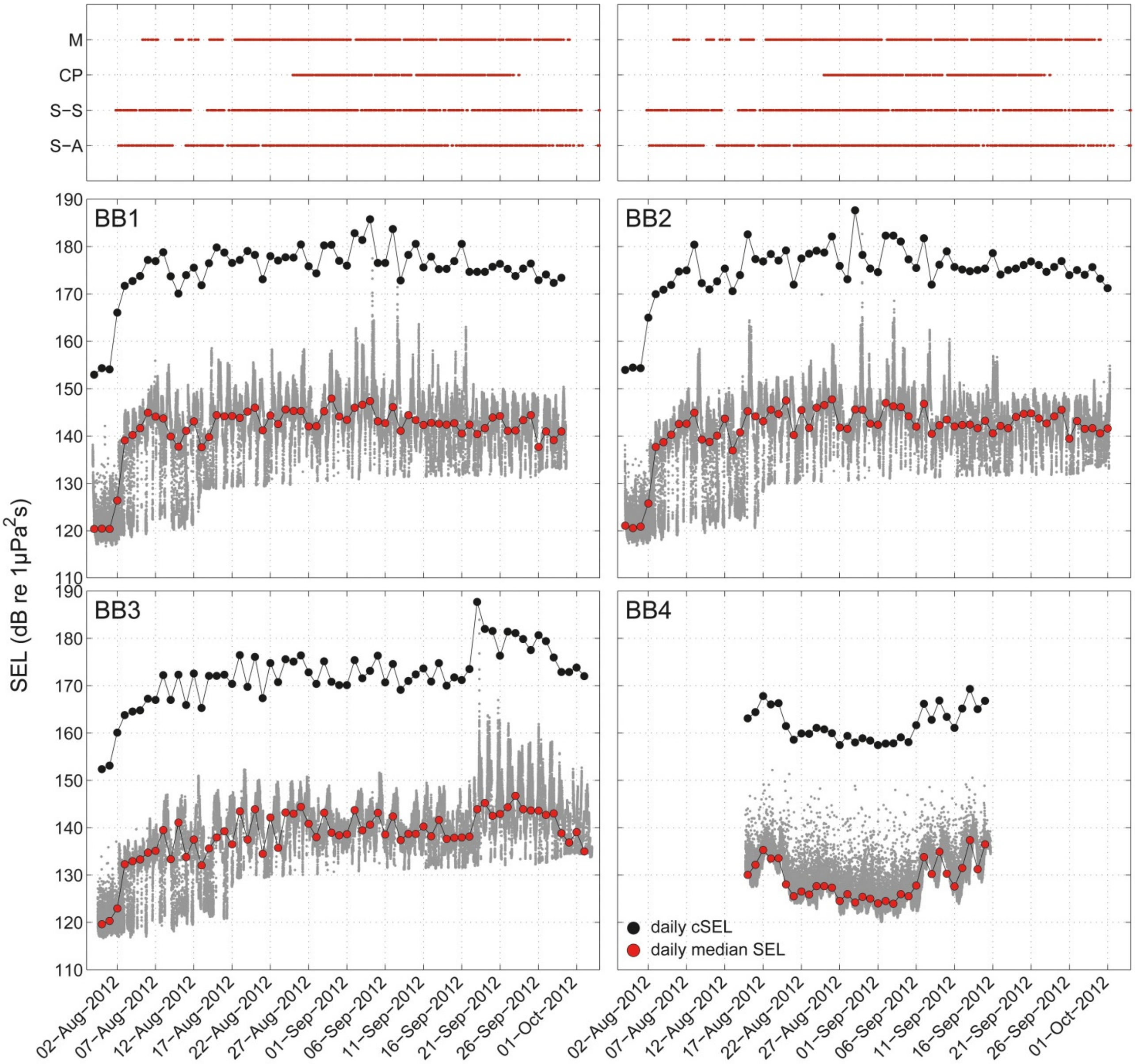

Figure 35. 1-minute full bandwidth (10–32000 Hz) sound exposure levels (SEL; i.e. energy flux density computed for 1-minute-long time periods) at the shallow (100 m for BB1-4) hydrophones at Shell's recording stations. Red circles mark daily median SELs, black circles denote cumulative SEL (cSEL) over 24 hours. Top panel shows time of operation of the seismic vessels (M= Maersk, CP=ConocoPhllips, S-S=Shell Samur, S-A=Shell Amani). The vessels' positions with respect to the moorings every 5 days are shown in the maps in **Figure 41**. Please note that these energy values are calculated over 1 minute. For estimates over a time window of 1 s, subtract 18 dB ($10\log_{10}(60)$).

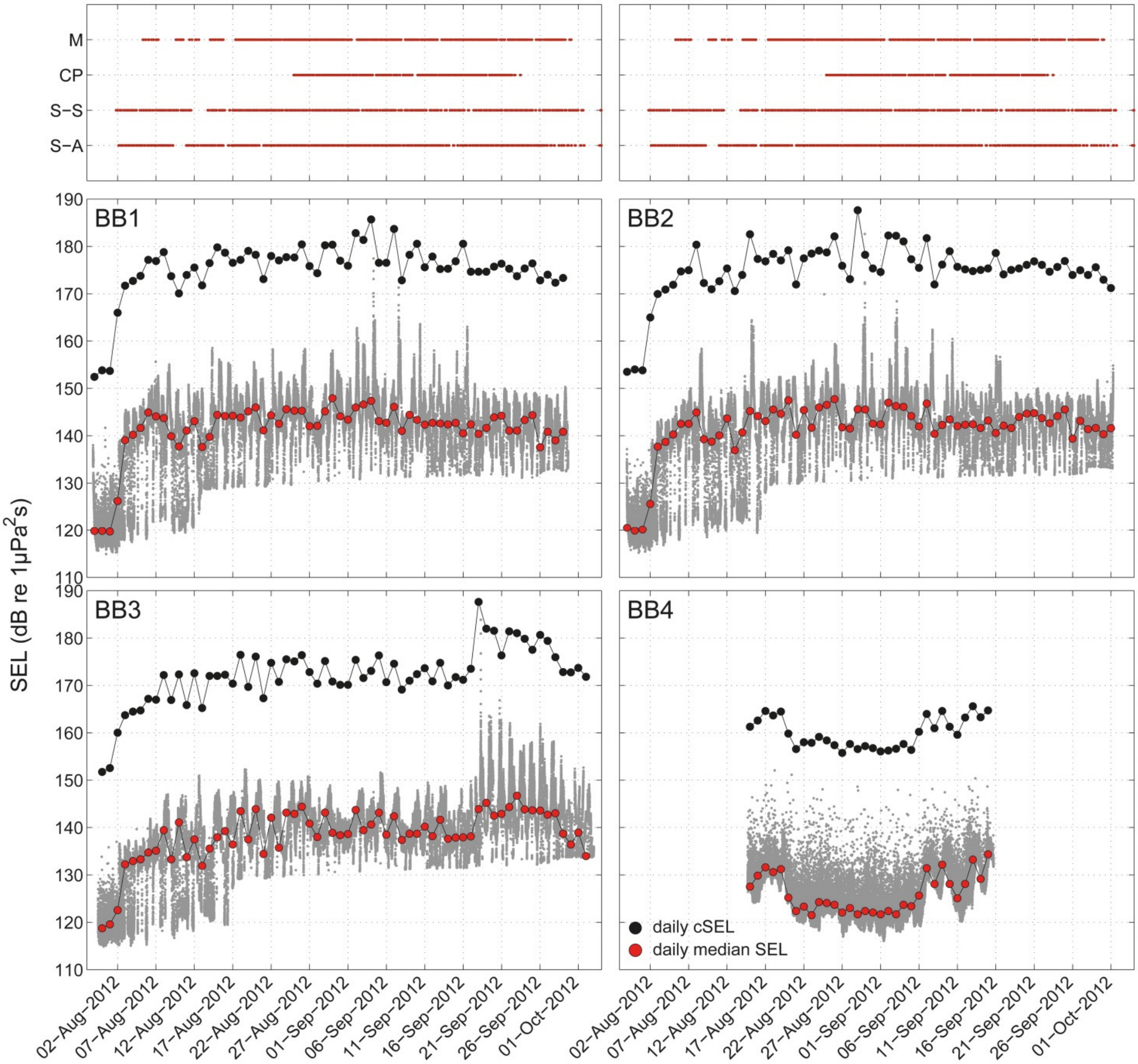

Figure 36. 1-minute sound exposure levels in the frequency band of 10-2000 Hz at the shallow (100 m for BB1-4) hydrophones at Shell's stations. Red circles mark daily median SELs, black circles denote cumulative SEL (cSEL) over 24 hours. Top panel shows time of operation of the seismic vessels (M=Maersk, CP=ConocoPhllips, S-S=Shell Samur, S-A=Shell Amani). The vessels' positions with respect to the moorings every 5 days are shown in the maps in **Figure 41**. Please note that these energy values are calculated over 1 minute. For estimates over a time window of 1 s, subtract 18 dB ($10\log_{10}(60)$).

The daily median and cumulative filtered SELs recorded at the centrally located DCE moorings (**Figure 38**-**Figure 40**) were close to those of the BB1-BB3 stations (**Figure 35**-**Figure 37**). Initially, most of the moorings distributed in the northern part of the Bay (e.g. Qamut N, **Figure 38**) showed on average lower received levels. However, these became significantly elevated at the commencement of ConocoPhillips' seismic survey, thus illustrating a cumulative impact from more than one seismic source.

The vessels' movements relative to the noise loggers (**Figure 41**) gave rise to a characteristic 'jagged' pattern in the recordings, with peak 1-minute SELs of up to 189 dB re 1μPa²s and magnitudes of level variations of up to 50 dB (**Figure 35**-**Figure 37**).

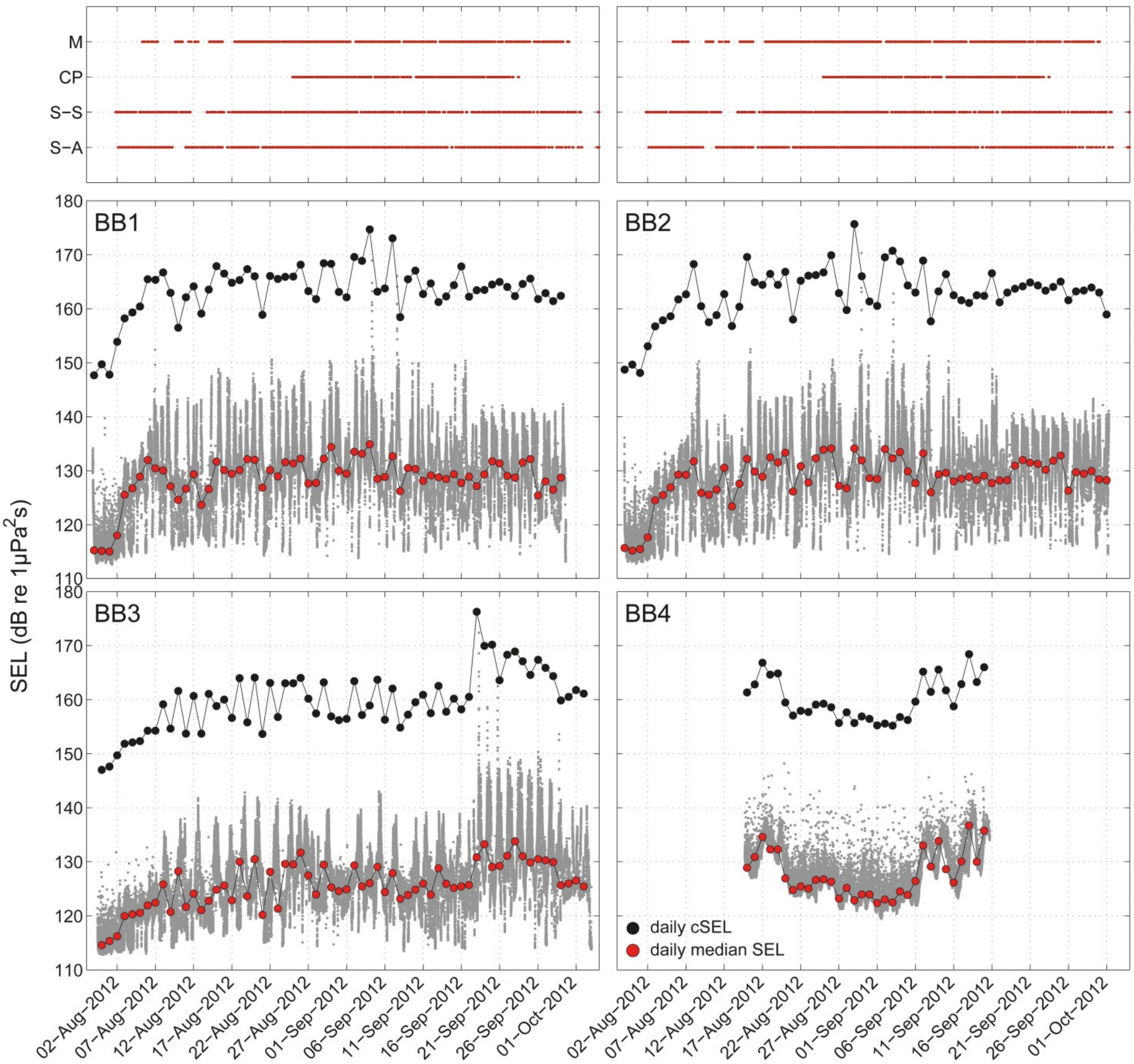

Figure 37. 1-minute mid-frequency m-weighted sound exposure levels at the shallow (100 m for BB1-4) hydrophones at Shell's recording stations. Red circles mark daily median SELs, black circles denote cumulative SEL (cSEL) over 24 hours. Top panel shows time of operation of the seismic vessels (M=Maersk, CP=ConocoPhillips, S-S=Shell Samur, S-A=Shell Amani). The vessels' positions with respect to the moorings every 5 days are shown in the maps in **Figure 41**. Please note that these energy values are calculated over 1 minute. For estimates over a time window of 1 s, subtract 18 dB ($10\log_{10}(60)$).

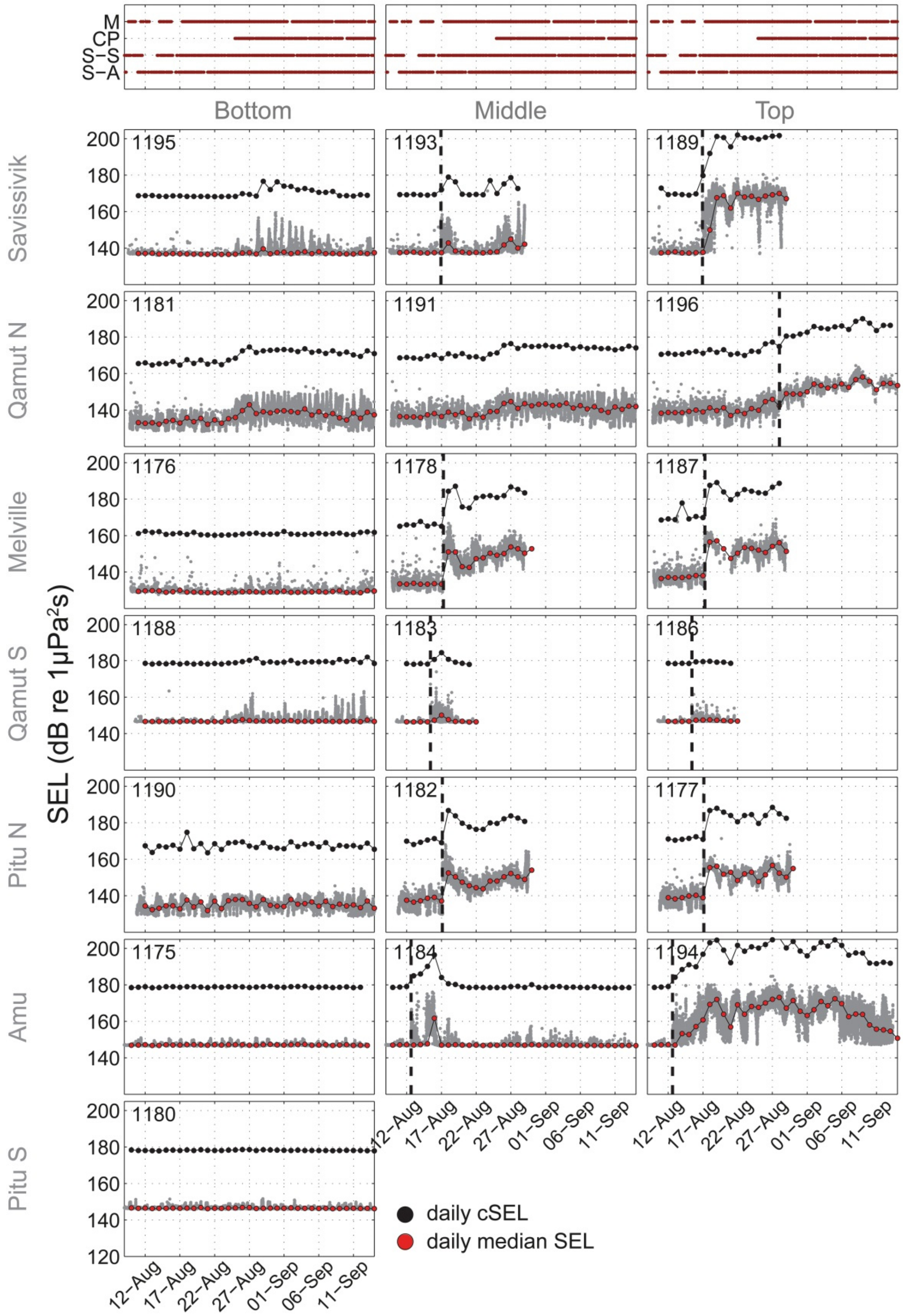

Figure 38. 1-minute broadband sound exposure levels at the DCE moorings over the entire deployment period (SEL; i.e. energy flux density computed for 1-minute-long time periods). Red circles mark daily median SELs; black circles denote cumulative SEL (cSEL) over 24 hours. Top panel shows time of operation of the seismic vessels (M=Maersk, CP=ConocoPhllips, S-S=Shell Samur, S-A=Shell Amani). Dashed lines show when the datalogger detached from the moorings. The plots depict total energy per file (see section 5.3.3), the levels therefore rise after the detachment, as any transient artefacts and flow noise around the loose logger contribute to the energy estimates. The stations Pitu S, Amu and Quamut S were self-noise limited and the amplitude of the increase at each survey start is therefore underestimated. The vessels' positions with respect to the moorings every 5 days are shown in the maps in **Figure 41**. Please note that these energy values are calculated over 1 minute. For estimates over a time window of 1 s, subtract 18 dB ($10\log_{10}(60)$).

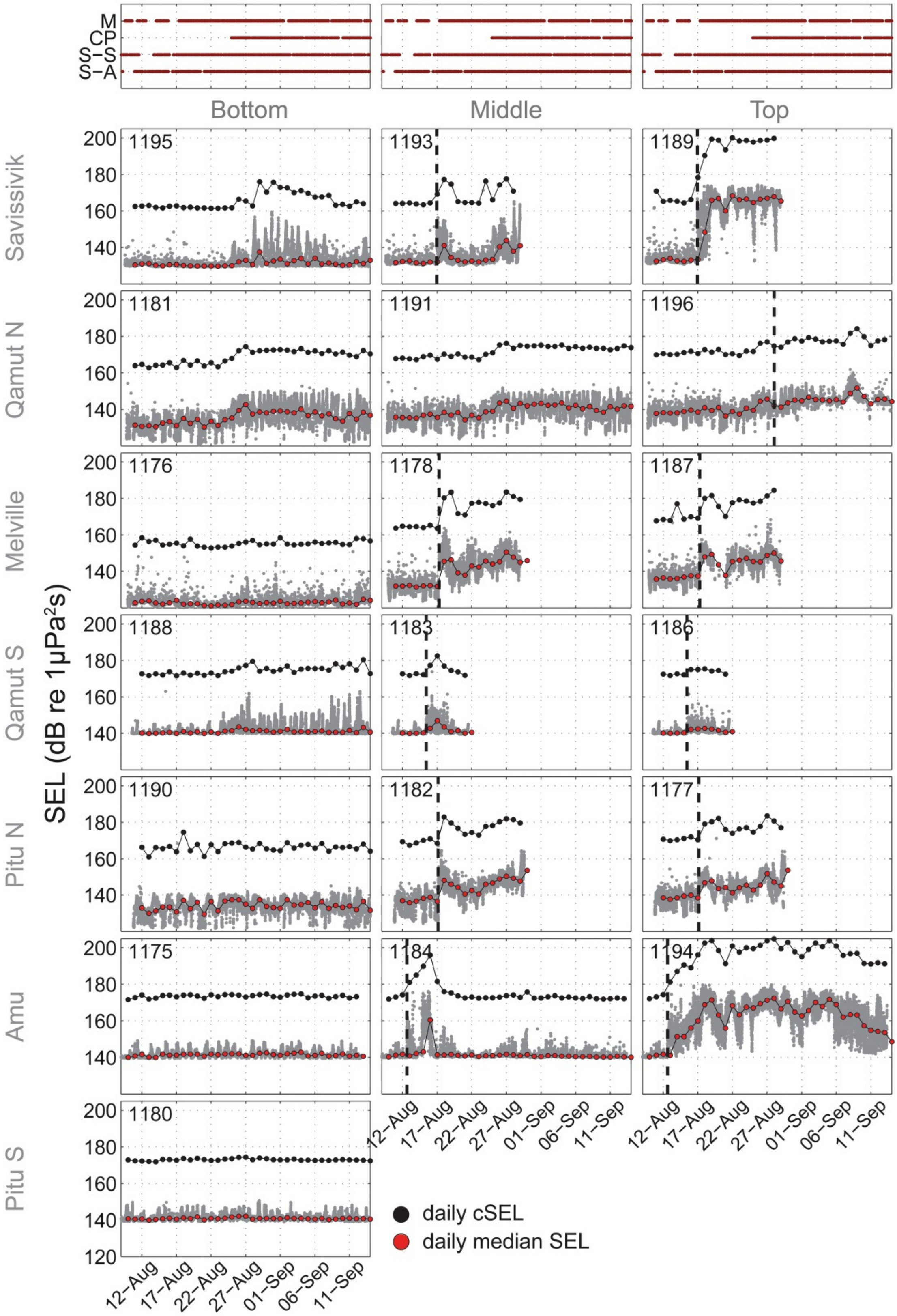

Figure 39. 1-minute sound exposure levels in the frequency band of 10-2000 Hz at the DCE moorings. Red circles mark daily median SELs; black circles denote cumulative SEL (cSEL) over 24 hours. Top panel shows time of operation of the seismic vessels (M=Maersk, CP=ConocoPhllips, S-S=Shell Samur, S-A=Shell Amani). Dashed lines show when the datalogger detached from the moorings. The plots depict total energy per file (see section 5.3.3), the levels therefore rise after the detachment, as any transient artefacts and flow noise around the loose logger contribute to the energy estimates. The stations Pitu S, Amu and Quamut S were self-noise limited and the amplitude of the increase at each survey start is therefore underestimated. The vessels' positions with respect to the moorings every 5 days are shown in the maps in **Figure 41**. Please note that these energy values are calculated over 1 minute. For estimates over a time window of 1 s, subtract 18 dB ($10\log_{10}(60)$).

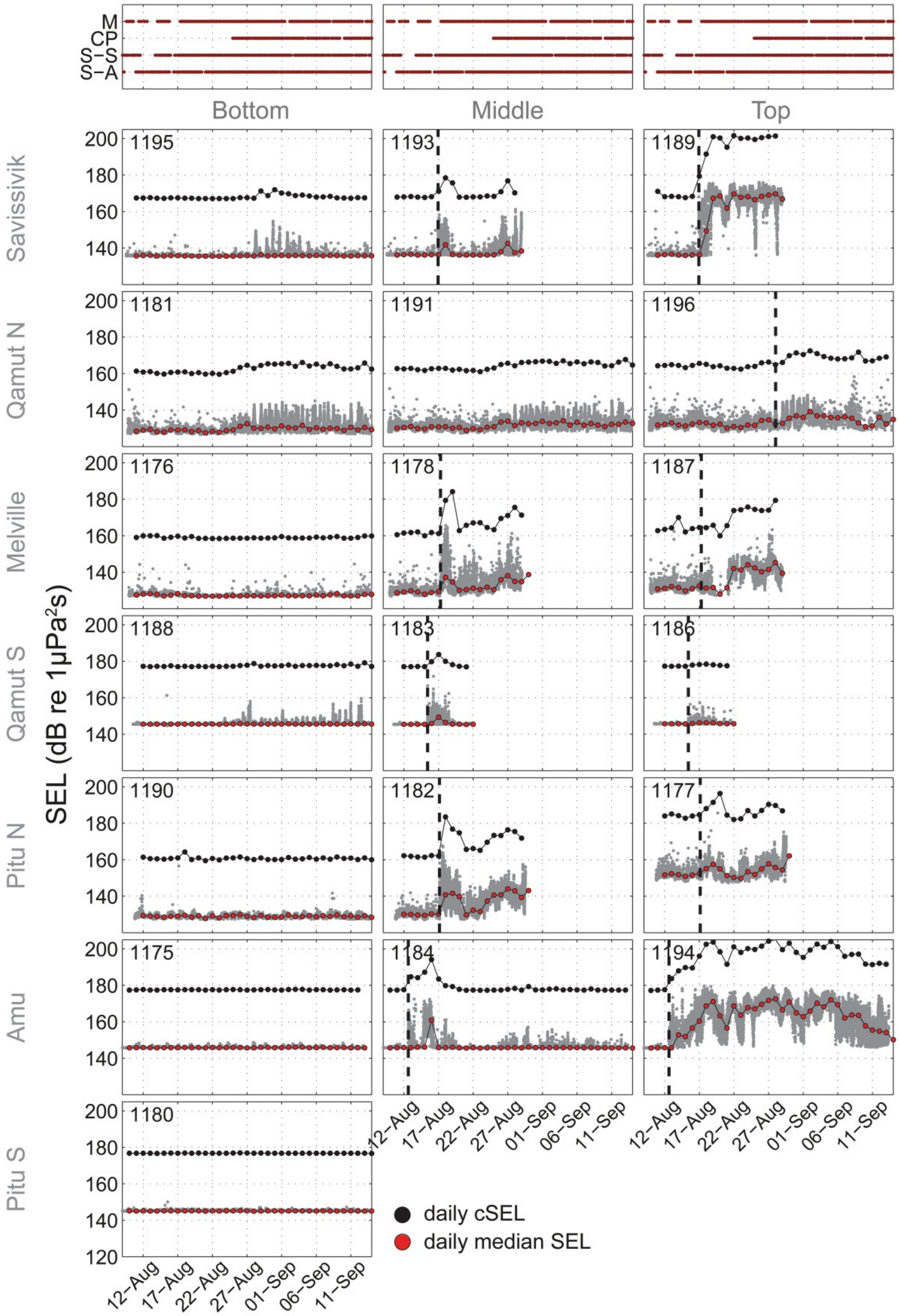

Figure 40. 1-minute mid-frequency m-weighted sound exposure levels at the DCE moorings. Red circles mark daily median SELs; black circles denote cumulative SEL (cSEL) over 24 hours. Top panel shows time of operation of the seismic vessels (M=Maersk, CP=ConocoPhllips, S-S=Shell Samur, S-A=Shell Amani). Dashed lines show when the datalogger detached from the moorings. The plots depict total energy per file (see section 5.3.3), the levels therefore rise after the detachment, as any transient artefacts and flow noise around the loose logger contribute to the energy estimates. The stations Pitu S, Amu and Quamut S were self-noise limited and the amplitude of the increase at each survey start is therefore underestimated. The vessels' positions with respect to the moorings every 5 days are shown in the maps in **Figure 41**. Please note that these energy values are calculated over 1 minute. For estimates over a time window of 1 s, subtract 18 dB ($10\log_{10}(60)$).

M-weigthed mid-frequency sound exposure levels at the DCE moorings (**Figure 40**) were on average 6-10 dB lower than broadband and 10-2000 Hz-filtered sound exposure levels (**Figure 38**- **Figure 39**).

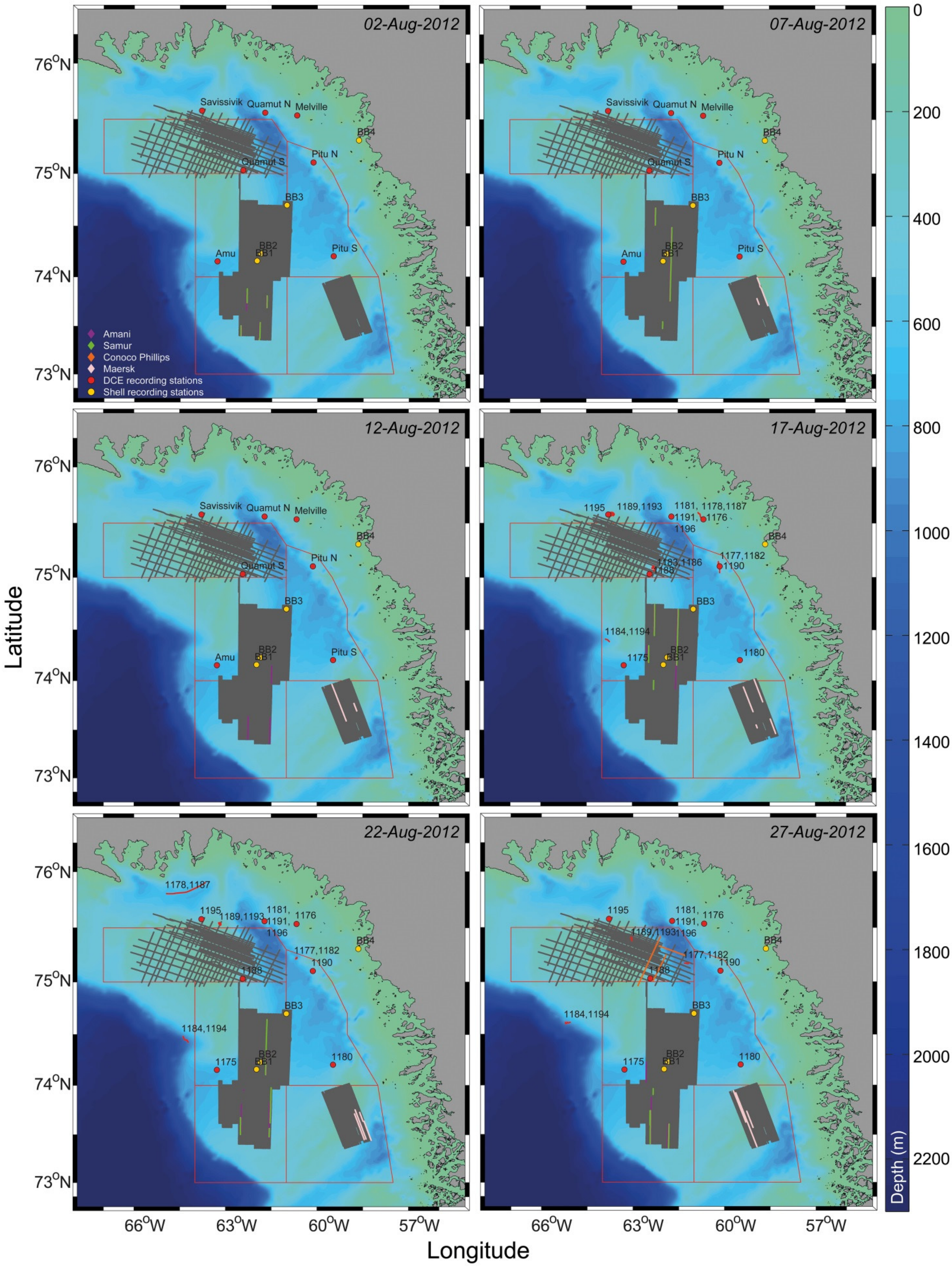

Figure 41 a. Maps showing the distribution of the seismic vessels with respect to the moorings and the loose loggers at 5-day intervals. ConocoPhillips began operation on 25 August. Datum: WGS84; projection: Mercator.

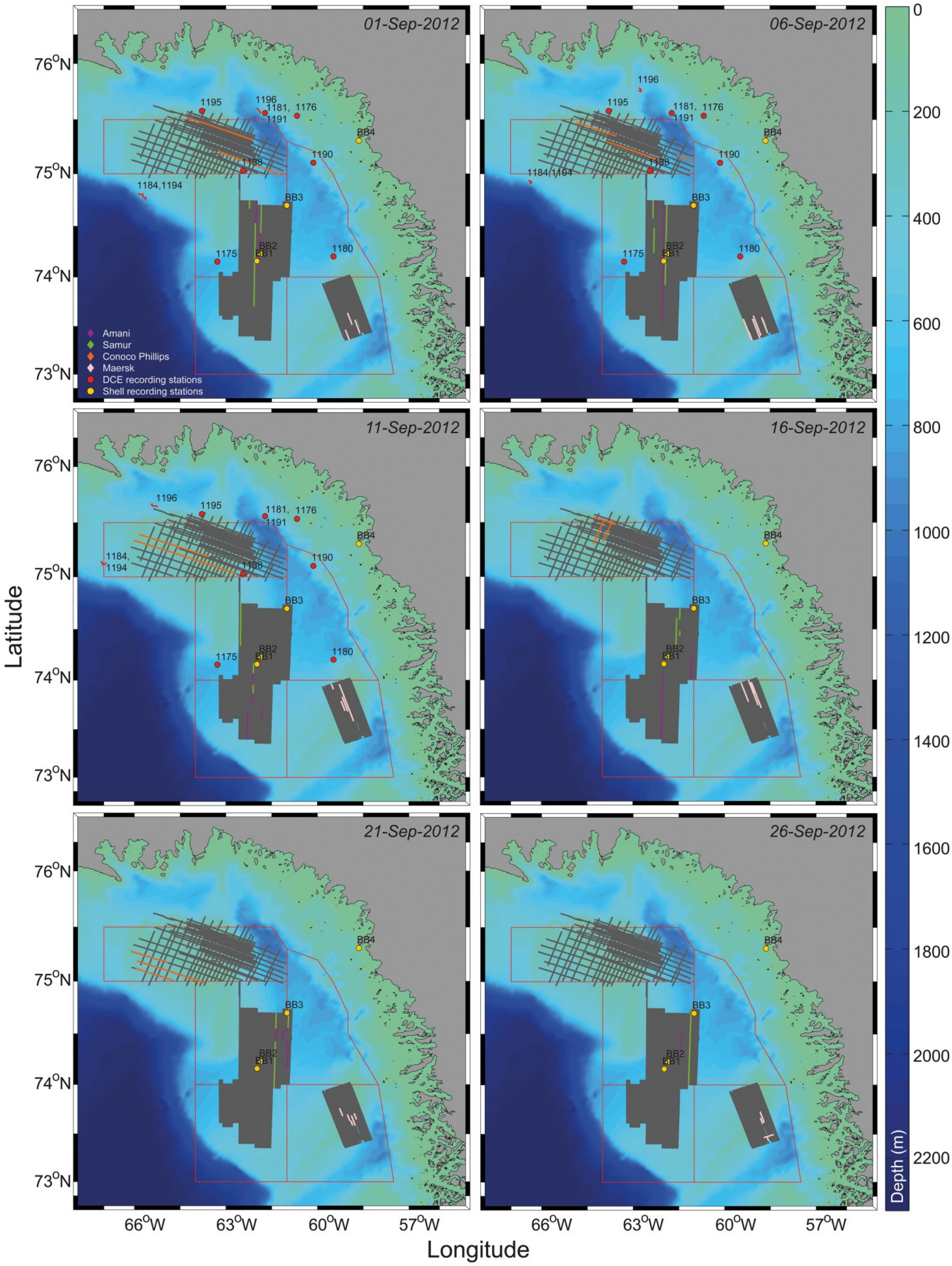

Figure 41 b. Maps showing the distribution of the seismic vessels with respect to the moorings and the loose loggers at 5-day intervals. ConocoPhillips ceased operation on 24 September. DCE dataloggers were retrieved between 13th -16th September. Datum: WGS84; projection: Mercator.

Figure 41 c. Map showing the distribution of the seismic vessels with respect to the moorings and the loose loggers. ConocoPhillips ceased operation on 24 September. DCE dataloggers were retrieved between 13th -16th September. Datum: WGS84; projection: Mercator.

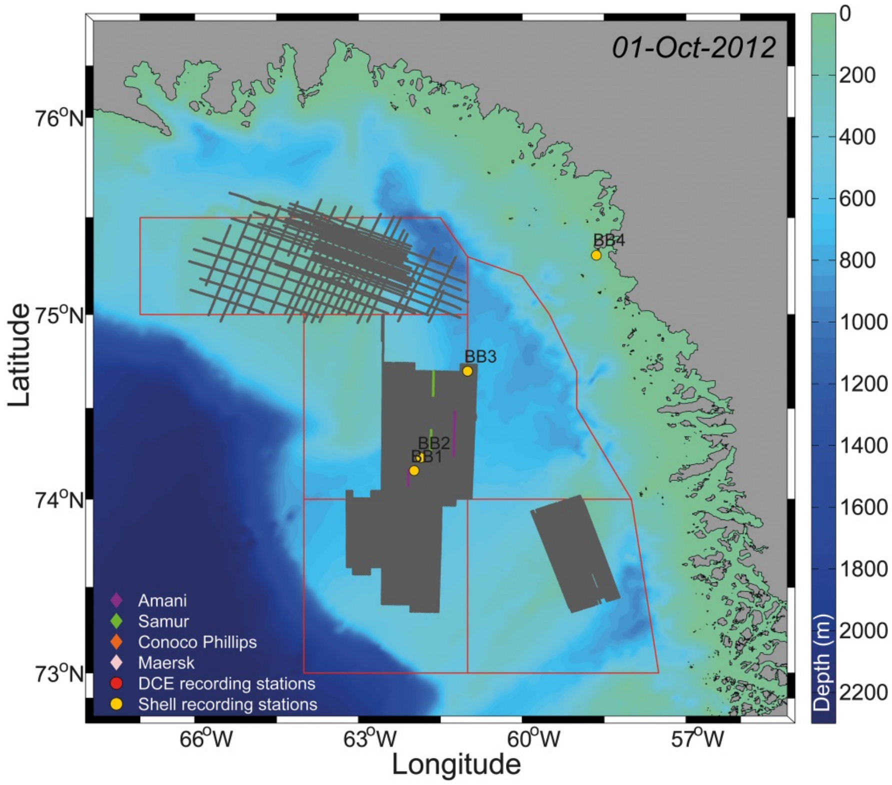

Comparisons of sound exposure levels measured by hydrophones positioned at 100, 200 and 400 m depths along a single mooring. **Figure 42** shows that the topmost logger tends to, but does not always, records the highest levels.

Figure 42. Sound level variation with depth at Shell's BB1 and BB3 stations (400 m black, 200 m blue and 100 m green). Sound levels are expressed in terms of 1-minute sound exposure levels. For estimates over a time window of 1 s, subtract 18 dB ($10\log_{10}(60)$).

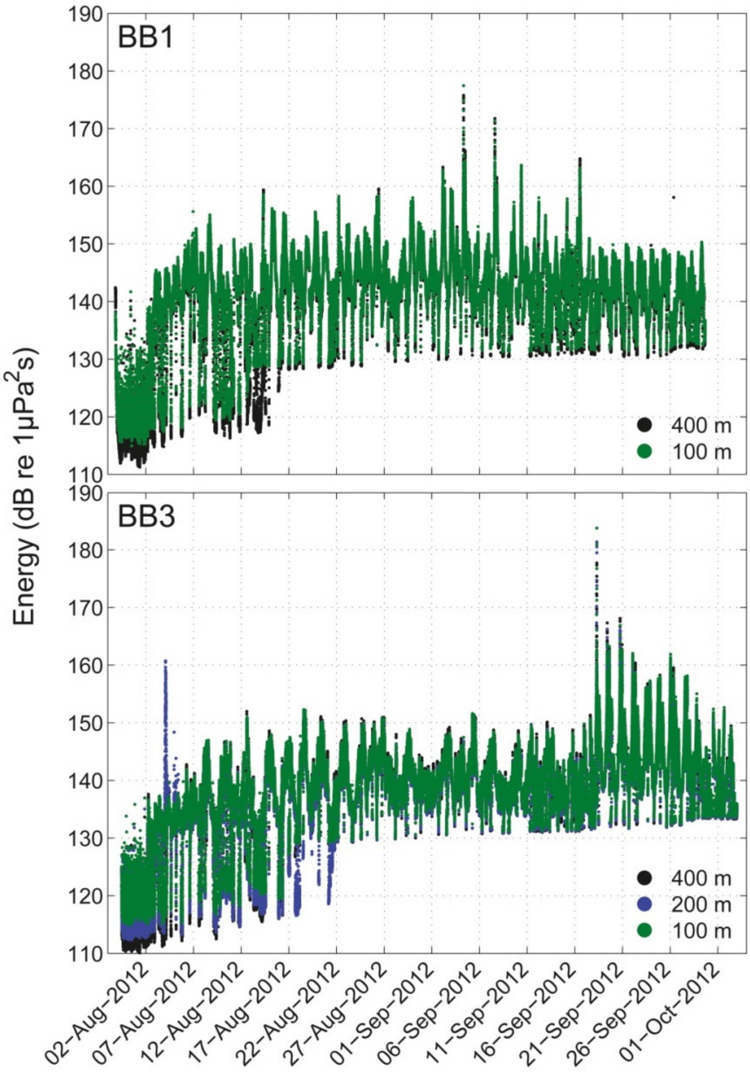

6.5 Modeling of transmission loss

6.5.1 Site 1 – Qamut N

The modeling study for the Qamut N license block identified a region of low transmission loss extending north-south along the edge of the plateau (**Figure 43**).

The presence of such a sound channeling area was also clearly visible in the received levels recorded at the Qamut N noise loggers when the airgun array was operating along that same plateau (**Figure 44**).

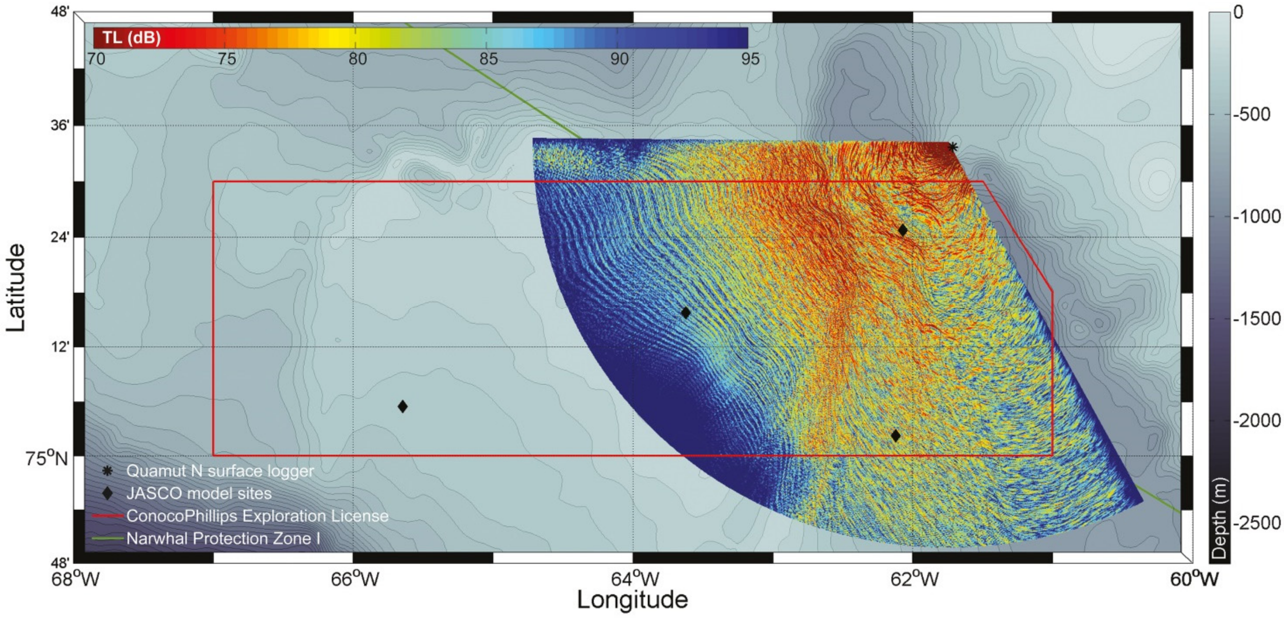

Figure 43. Output of the WHOI model for scenario I: transmission loss from sources located within the Qamut license area, towards a receiver located at the Qamut N station at a depth of 274 m. Datum: WGS84; projection: Mercator.

6.5.2 Site 2 – BB4

Results of the model towards JASCO's coastal station, BB4, suggest that the airgun pulses emitted in the Qamut and Anu blocks are subjected to high transmission loss as they propagate towards the coast (**Figure 45-Figure 46**). This, in addition to 1) the short recording time, due to late deployment, i.e. after Shell's vessels had already operated in the northeastern corner of the Anu block, and 2) the multiple and often overlapping sources, likely contributed to the very few usable points for model verification (**Figure 19b**).

The model assumed a uniform sound speed profile within the model domain, even though CTD casts suggested a significant spatial variability from the coast to the center of the Bay.

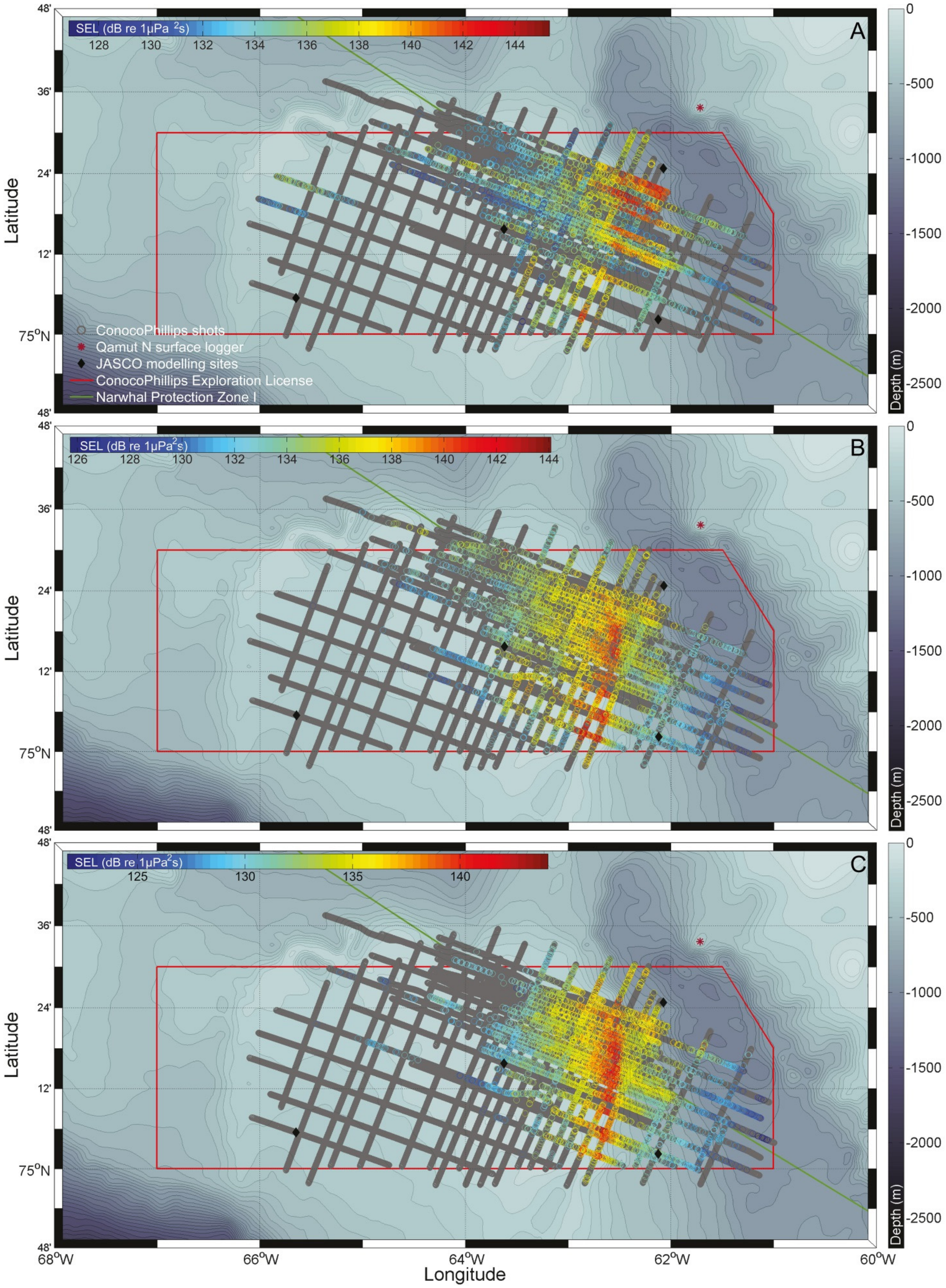

Figure 44. Levels of ConocoPhillips' shots recorded at the top (A), mid-water (150 m; B) and bottom (274 m; C) hydrophones of the Qamut N mooring (red star). The top hydrophone data (depth of 11.5 m) are from the period after detachment and only data points from when the buouy was in the vicinity of the original location were included in the analysis. The data were verified manually to exclude false alarms and signals overlapping with shots from other seismic vessels. Datum: WGS84; projection: Mercator.

Figure 45. Output of the WHOI model for scenario II: transmission loss from sources located within the northeastern corners of the Qamut and Anu license areas, towards a receiver located in the vicinity of the BB4 station at a depth of 100 m. Datum: WGS84; projection: Mercator.

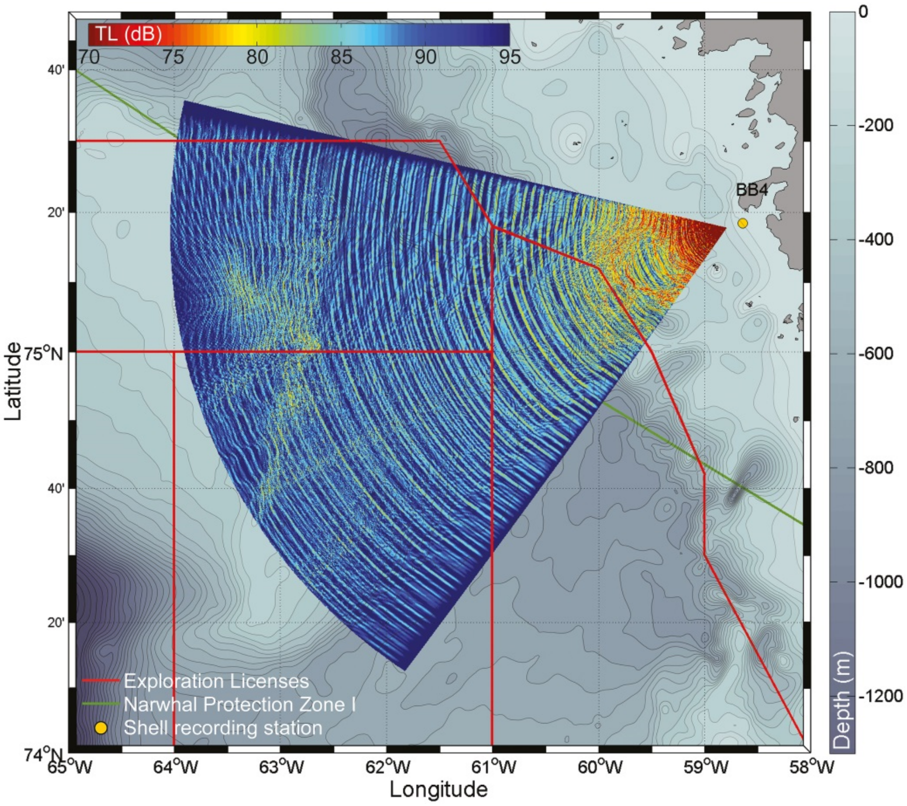

Figure 46. Levels of ConocoPhillips' and Shell's shots encompassed by the WHOI model area for scenario II (**Figure 45**) as recorded at JASCO's BB4 station near the coast (100 m deep). The data were verified manually to exclude false alarms and signals overlapping with shots from other boats. Datum: WGS84; projection: Mercator.

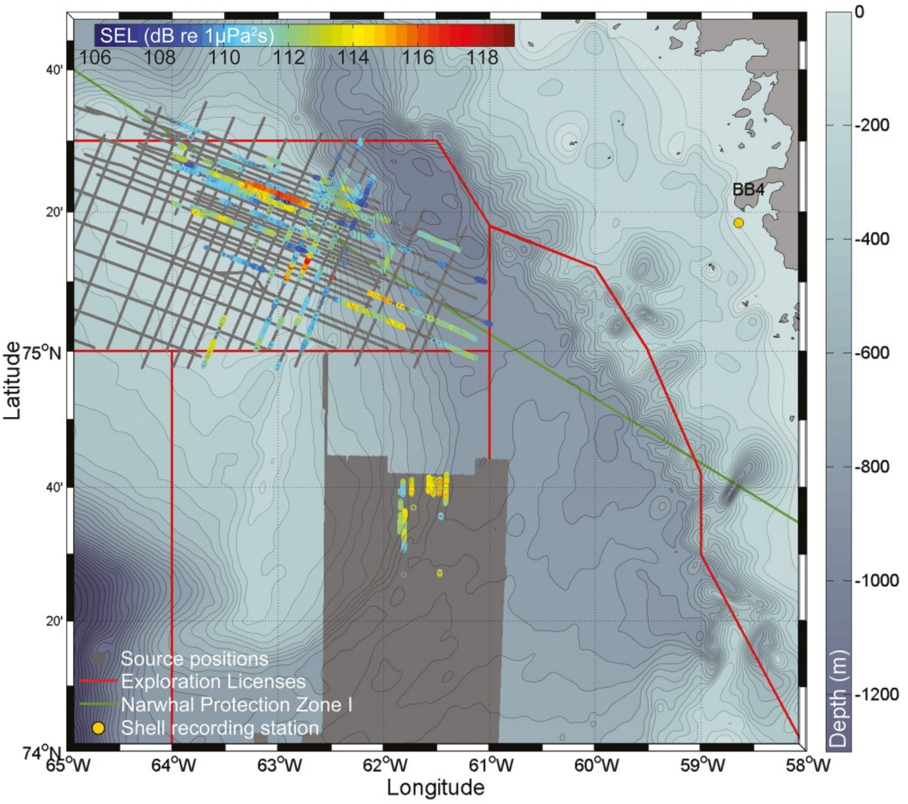

6.6 Comparison with JASCO's pre-season modeling results

6.6.1 Single-shot sound fields

We compared sound levels received at the moorings to the maximum-over-depth sound exposure levels modeled by JASCO, to extend the validation of the model conducted by JASCO for the Anu and Napu blocks (stations BB1-BB3; (Martin & MacDonnel 2013)) to the whole area covered by the model. To ensure that our choice of logger deployment depths did not compromise our ability to capture the maximum-over-depth levels, we plotted the observed SEL variation with depth against the received level profile computed for the model sampling position closest to the position of the mooring in question (**Table D1** in Appendix D; data courtesy of JASCO and Shell). Here we present our findings for Shell's model site 1 (within the Qamut block; **Figure 47**) and Shell's site 3 (in the Anu block; **Figure 48**). Results for ConocoPhillips' sites 1-3 and Shell's sites 2 and 4 are included in Appendix D (**Table 3** - **Table 7**).

Although seemingly many of the recording stations were encompassed by the JASCO model area around Shell's site 1 (**Figure 47**), for quite a few of the loggers, the recording period did not overlap with the time at which the ConocoPhillips vessel operated in the vicinity of site 1. Sound exposure levels measured at the stations (Qamut N: median of 133 dB re 1 µPa^{2}s (middle), 135 dB re 1 µPa^{2}s (bottom), Qamut S: 141 dB re 1 µPa^{2}s (bottom), Pitu N: 127 dB re 1 µPa^{2}s (bottom), BB1 (two loggers):123-126 dB re 1 µPa^{2}s, BB2 (one logger): 126 dB re 1 µPa^{2}s, BB3 (three loggers): 127-128 dB re 1 µPa^{2}s) were within, or below, the ranges predicted by the model (**Figure 47)**.

Similarly, sound exposure levels recorded at stations encompassed by JASCO model area for Shell's site 3 (Qamut N: mean of 128 dB re 1 µPa^{2}s (middle), 122 dB re 1 µPa^{2}s (bottom), Pitu S: 131 dB re 1 µPa^{2}s (bottom), Amu: 137 dB re 1 µPa^{2}s (bottom), BB1 (two loggers): 154-156 dB re 1 µPa^{2}s, BB2 (one logger): 144 dB re 1 µPa^{2}s, BB3 (three loggers)): 127-128 dB re 1 µPa^{2}s were found to be within or below the predicted SEL ranges (**Figure 48**). Mooring BB1 was deployed at merely 1 km from Shell's site 3 (**Figure 48**; (Martin & MacDonnel 2013)). Given that all shots emitted within a 2 km radius surrounding the modeled source position (**Table 3**) were considered in the analysis (see section 5.5.1), the observed SEL variation for the station (**Figure 48**) must to some extend be due to the variable distance between the station and the seismic vessel.

Although Qamut N station was not within the area covered by the pre-season modeling for Shell's site 3, modeling the station was included in the analysis, because it consistently recorded pulses originating in the Anu Block (see e.g. **Figure 34**). Data on predicted variation with depth for the station were, however, unavailable for comparison with the on-site recordings.

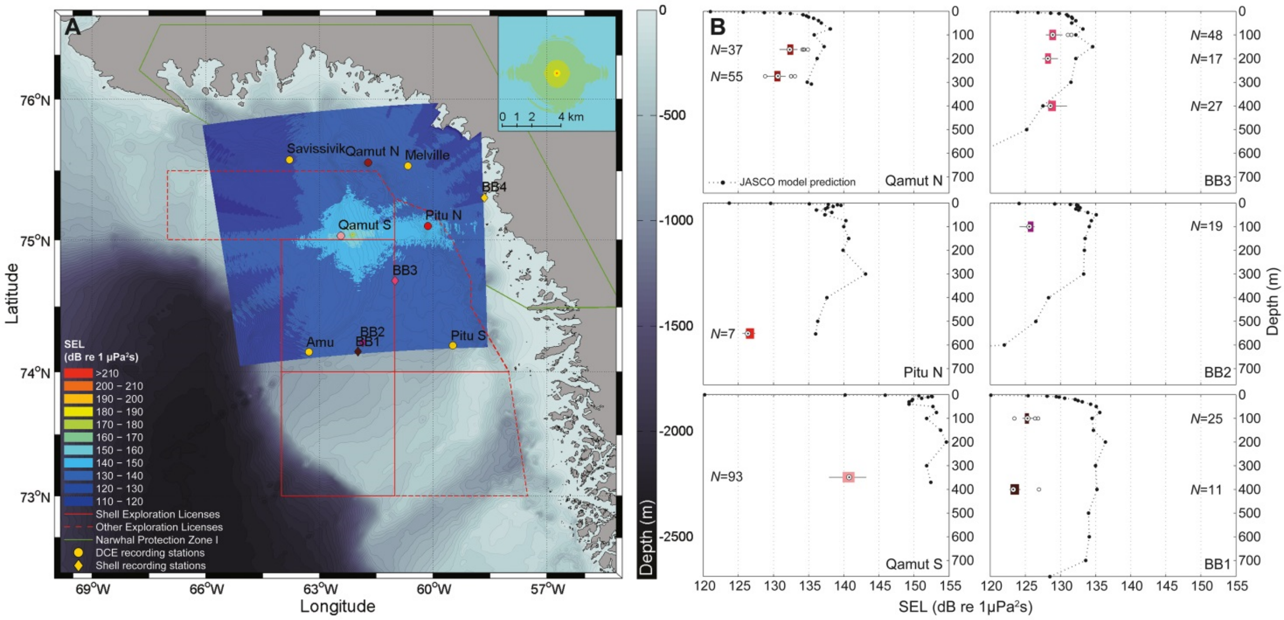

Figure 47. Sound distribution (SEL) modeled by JASCO for Shell's site 1 (A), together with sound exposure levels from airgun signals emitted in the vicinity of the site as recorded at loggers within the modeled area (B). Results of the on-site measurements have been overlaid with SEL-over-depth profiles computed by JASCO for model sampling positions closest to the positions of the moorings. Shell's site 1 was within the Qamut block. Therefore, shots emitted by ConocoPhillips, rather than Shell, were selected for the analysis. All shots fired within a 2 km radius of the modeled source position (**Table 3**) were considered. These shots were emitted late in the season when many of the free-floating surface and mid-water recorders had already been collected. Large map - datum: WGS84; projection: Mercator. Inserts - datum: WGS84; projection: UTM Zone 21. Colors of the boxplots in B correspond to the colors of the recording stations in A.

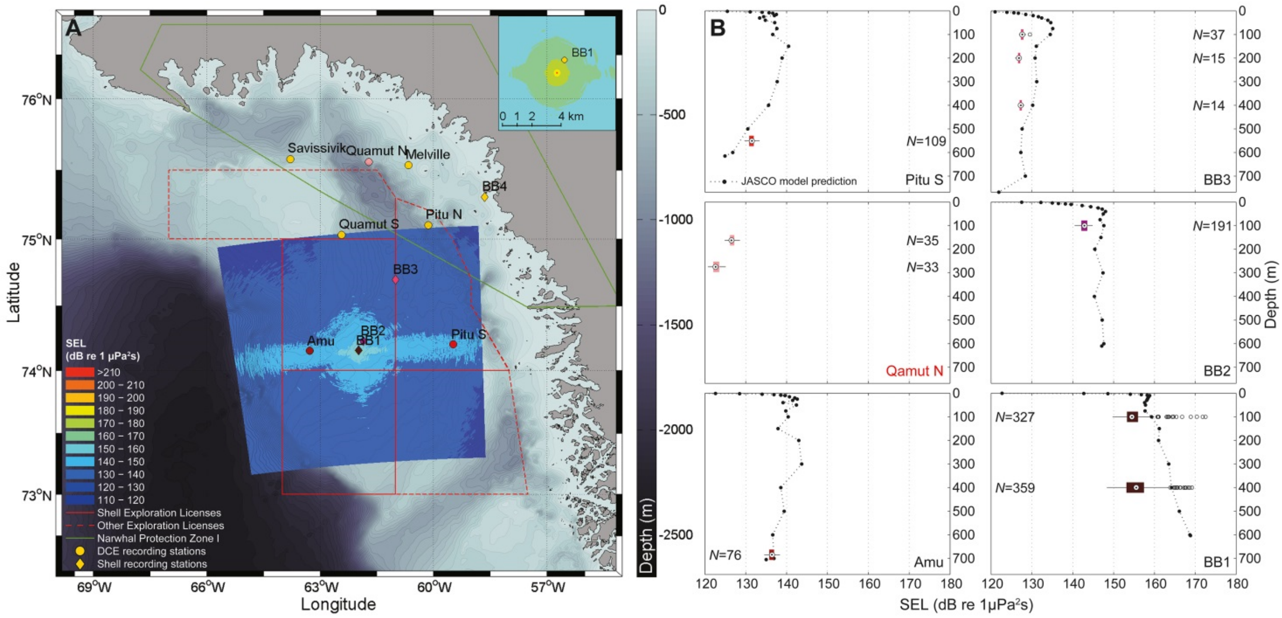

Figure 48. Sound distribution (SEL) modeled by JASCO for Shell's site 3 (A) together with sound exposure levels from airgun signals emitted in the vicinity of the site as recorded at loggers within the modeled area (B). Results of the on-site measurements have been overlaid with SEL-over-depth profiles computed by JASCO for model sampling positions closest to the positions of the moorings. All shots fired within a 2 km radius of the modeled source position (**Table 3**) were considered in the analysis. Note that the Qamut N mooring (in red in B) was outside the modeled area, but was included here, because it consistently recorded signals originating in the Anu block. However, because signals propagating over such long ranges were shorter, we used a shorter time window (±0.8 sec rather than -1:+3 sec, (see section 5.3.2.2). Large map - datum: WGS84; projection: Mercator. Inserts - datum: WGS84; projection: UTM Zone 21. Colors of the boxplots in B correspond to the colors of the recording stations in A.

6.6.2 Cumulative sound exposure levels

The results of JASCO's pre-season modeling of the flat-weighted cumulative SEL over 24 hours for ConocoPhillips' northernmost firing line are presented in the top panel of **Figure 49**. Our estimates of the 24-hour cSEL for all three loggers at the Qamut N station, closest to that particular firing line were within the maximum-over-depth ranges predicted by JASCO with values of 173, 175 and 178 dB re 1µPa^{2}s for the bottom, middle and top recorder, respectively (**Figure 49**). While it was not possible to directly verify the aggregate cSEL for all seismic surveys as modeled by JASCO (**Figure 49**, bottom panel), the best approximation for ConocoPhillips, i.e. the aggregate 24-hour cSELs from shots emitted along ConocoPhillips' northernmost firing line and all coinciding shots from the other vessels operating during the same time period (see section 5.5.2 and **Figure 50**), were close to JASCO's maximum-over-depth estimates. The aggregate cSELs for recordings filtered between 10-2000 Hz were 174, 176 and 179 dB re 1µPa^{2}s for the bottom, middle and top Qamut N loggers, respectively (**Figure 50**). For unfiltered recordings, the values were 175, 176 and 182 dB re 1µPa^{2}s for the bottom, middle and top recorder, respectively.

Similarly, the proximate estimates of the aggregate cSELs from Shell's survey (**Figure 51**) for seven recording stations were within, or below, the maximum-over-depth cSEL ranges predicted by JASCO for Shell's survey only, and for all surveys combined (**Figure 51** and **Figure 52**).

Figure 49. Top panel: Cumulative flat-weighted SEL over 24 hours modeled by JASCO for a 3940 in^3 airgun array operating in August along ConocoPhillips' northernmost firing line (Data courtesy of JASCO and ConocoPhillips; map - datum: WGS84; projection: Mercator). Bottom panel: A detailed view of a part of the modeled field around the Qamut N station. Color-coding as in the top panel. The pink, purple and brown circle outlines mark positions of the three Qamut N loggers. The top part of the mooring was loose at the time of the recordings used for the cSEL estimate and thus the mean position is shown here. All three 24 hour cSEL values (specified next to the logger positions) were within the predicted maximum-over-depth ranges.

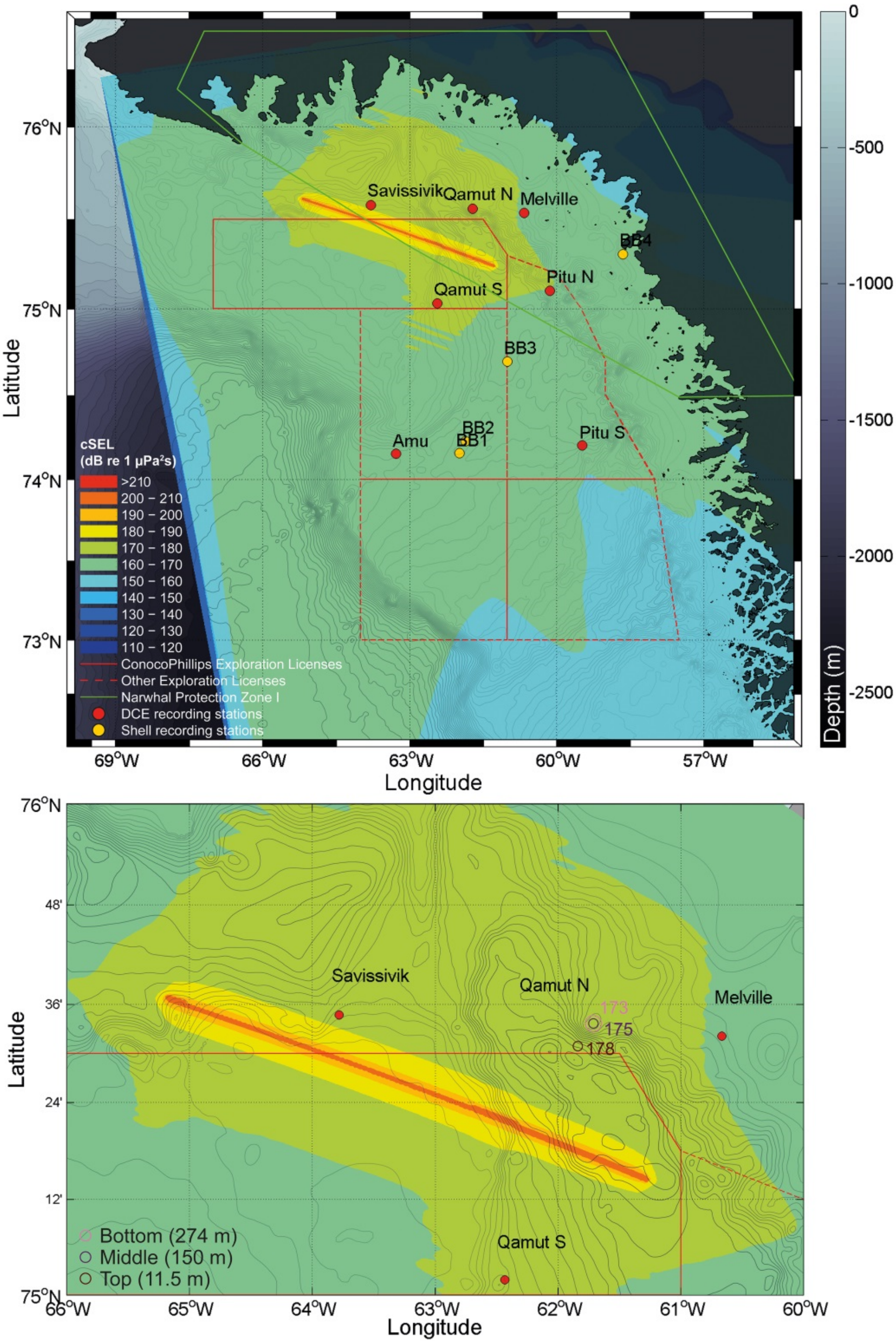

Figure 50. Aggregate cumulative sound exposure levels over 24 hours for shots fired along the northernmost firing line of ConocoPhillips and all coinciding shots from the other surveys as recorded at the Qamut N station. The top datalogger of the mooring (1196) was loose at the time of the recordings used for the cSEL estimate and thus it's mean position is shown here (yellow marker).The recordings were filtered between 10 and 2000 Hz (4th order). The aggregate cSEL for unfiltered data were 175, 176 and 182 dB re 1µPa^{2}s, for the bottom, middle and top loggers, respectively. Datum: WGS84; projection: Mercator.

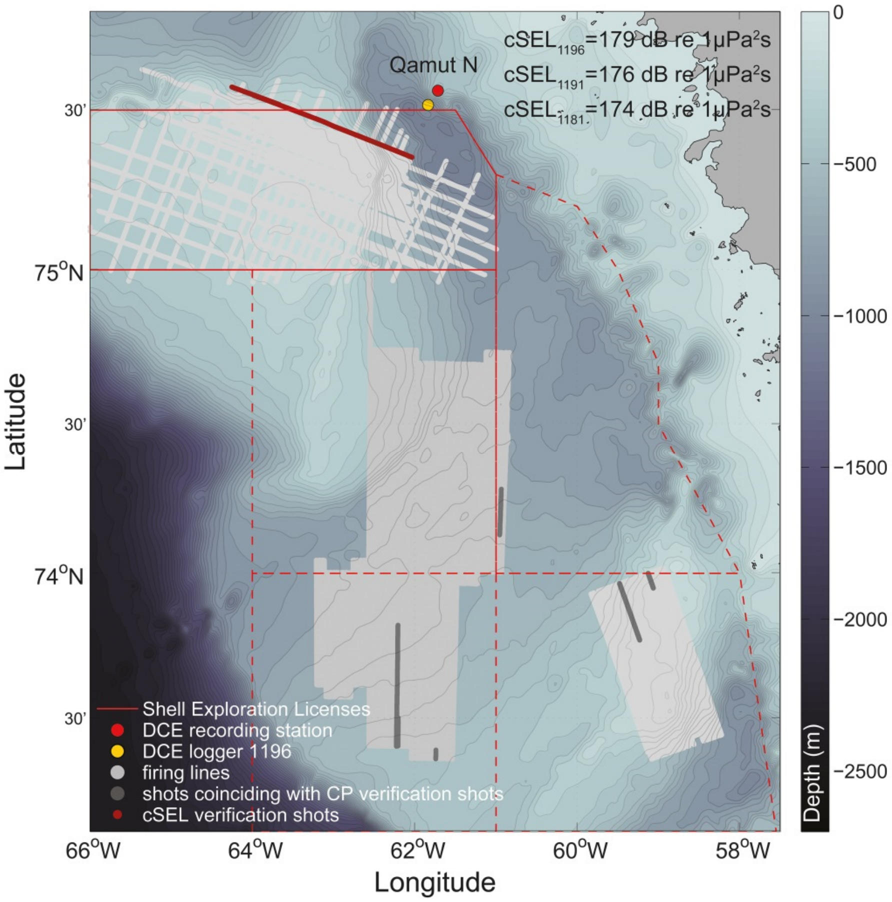

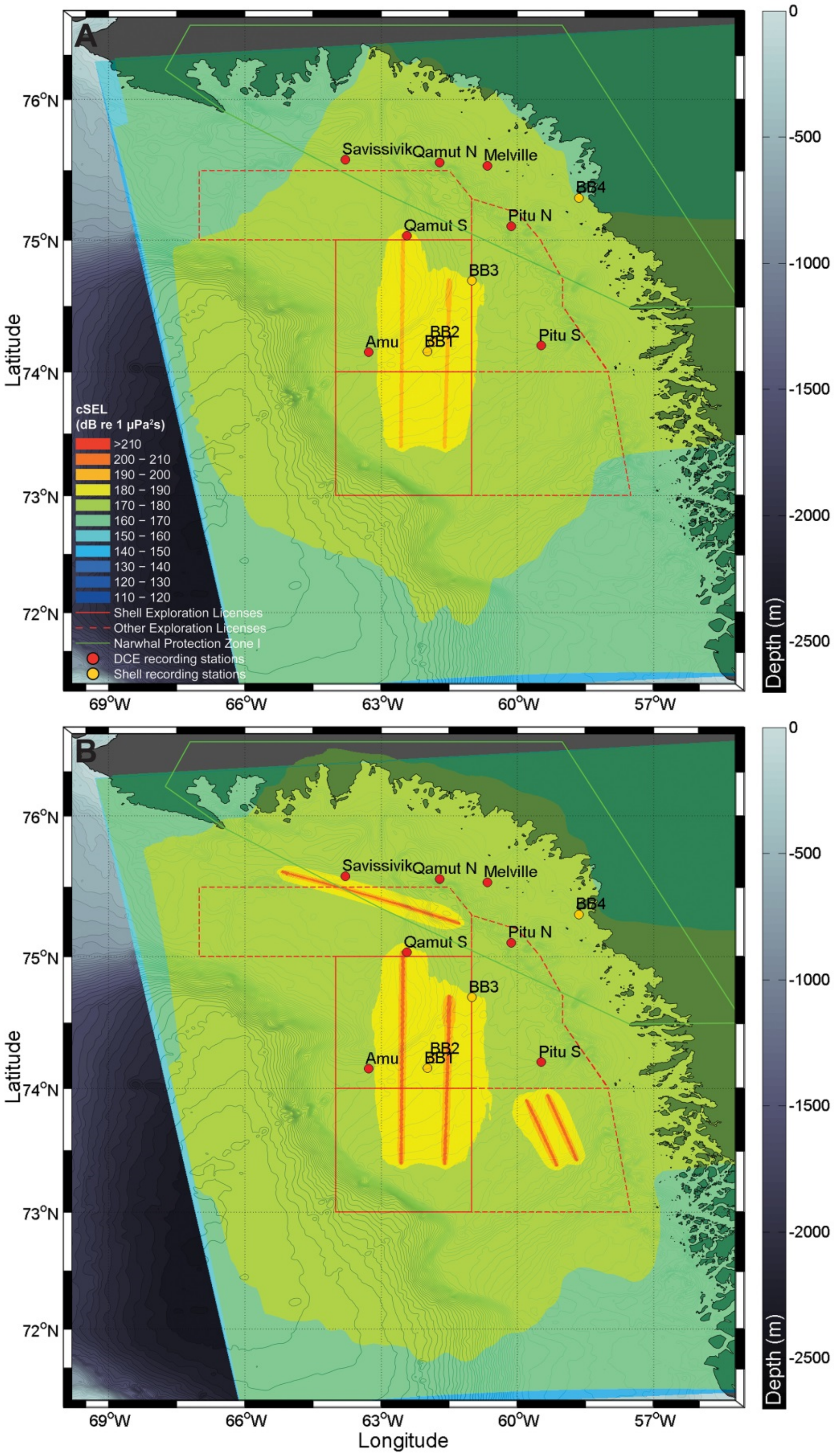

Figure 51. A: Cumulative flat-weighted SEL over 24 hours modeled by JASCO for a 4240 in^3 airgun array operating in August along two firing lines extending over the Anu and Napu blocks (i.e. Shell's license areas; data courtesy of JASCO and Shell; map - datum: WGS84; projection: Mercator). B: Aggregate flat-weighted cSELs over 24 hours for Maersk's, ConocoPhillips', and Shell's seismic survey operations in August. Color-coding as in A.

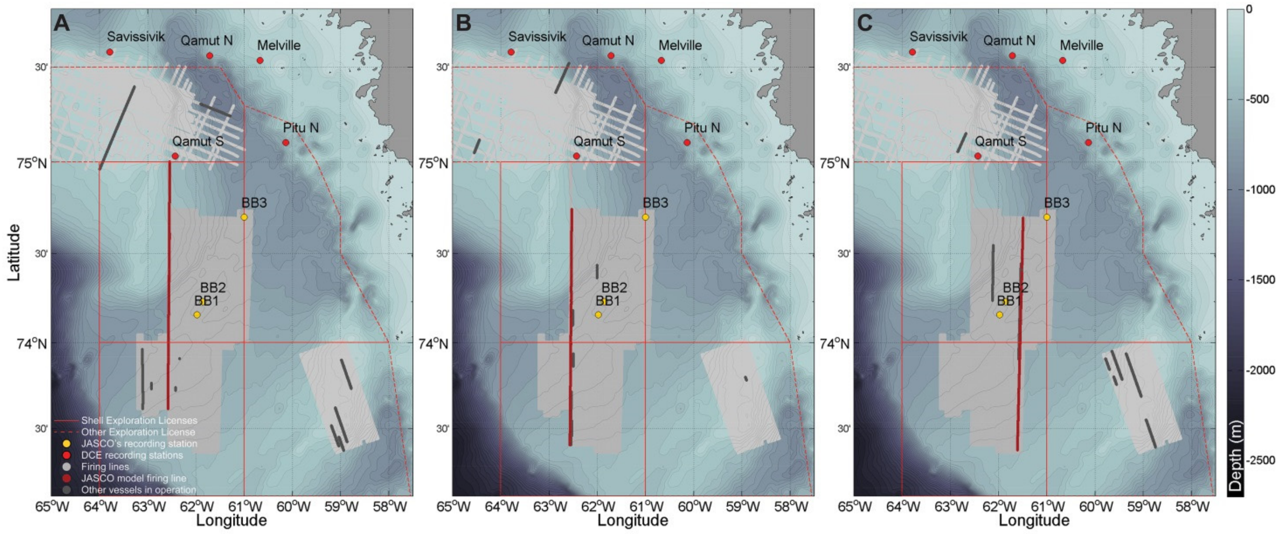

Station	Logger	Depth (m)	cSEL (dB re 1 µPa2s)								
			A (10-2000 Hz)	A (10 Hz HPF)	A (no filter)	B (10-2000 Hz)	B (10 Hz HPF)	B (no filter)	C (10-2000 Hz)	C (10 Hz HPF)	C (no filter)
BB1	146-05.64000	100	176	176		175	175		178	178	
BB1	146-01.8000	400	176	176		175	175		179	179	
BB2	147-01.64000	100	176	176		174	174		179	179	
BB3	148-05.64000	100	172	172		169	169		175	175	
BB3	148-02.8000	200	172	172		169	169		174	174	
BB3	148-01.8000	400	172	172		169	169		175	175	
Savissivik	1195	298.5	162	168	168	170	172	172	163	168	169
Qamut N	1191	162	173	174	174	175	175	175	173	173	173
Qamut N	1181	274.5	170	170	170	174	174	174	169	169	169
Melville	1176	411.5	155	160	161	155	160	161	157	161	162
Pitu N	1190	551.5	166	167	167	167	167	168	167	168	168

Figure 52. Aggregate cumulative sound exposure levels over 24 hours for shots fired along the western (A and B) and eastern (C) firing lines of Shell considered in the pre-season modeling, and all coinciding shots from the other vessels, as recorded at seven stations (data from loose or self-noise-dominated loggers were not included in the analysis). Top panel: positions of the seismic vessels for the three scenarios (maps - datum: WGS84; projection: Mercator). Bottom panel: Aggregate cSEL estimates for recordings filtered between 10 and 2000 Hz (4th order), filtered with a 10-Hz-high-pass filter (4th order) (HPF), or not filtered.

7 Discussion

In the late summer and early autumn of 2012 Baffin Bay and Melville Bay were subject to what is probably the hitherto largest man-made noise exposure to this area. Four large seismic survey vessels commissioned by Shell, ConocoPhillips and Mærsk conducted surveys in the Qamut, Anu, Napu and Tooq license blocks (**Figure 1**). Environmental impact assessments had beforehand predicted substantially elevated noise levels in the region (LGL & Grontmij; InuplanA/S & GolderAssociates 2012; NunaOil & Associates 2012), well within levels thought capable of affecting/disturbing marine mammals (Richardson et al. 1995; Nowacek et al. 2007a). The present noise monitoring program, together with the program conducted by JASCO for Shell, shows that noise levels were indeed considerably elevated during the surveys, and within the levels anticipated in the Environmental Impact Assessments (**Figure 35- Figure 40**).

7.1 Technical issues

Due to mechanical instabilities and the harsh environment of the High Arctic Greenland a few technical issues were encountered during the recordings. The detachment of the upper part of all moorings clearly indicates that the weak links, inserted as a precautionary measure against destruction by icebergs, were too weak. However, the large redundancy of loggers and tracking devices ensured that all but two loggers were recovered. The noise levels recorded by many of the free-floating dataloggers were elevated (**Figure 38**) due to flow noise, waves and wires banging on the hydrophones. In most cases, it was clearly visible when the dataloggers detached in the total SELs of the one-minute-long files (**Figure 38**, detachment time indicated by a dashed line). Nevertheless, airgun pulses could be extracted for the more detailed analysis (e.g. **Figure 44A**) by utilizing the relatively stable firing rate, and all detected airgun pulses were confirmed visually before included in the analysis. Secondly, the gain was set too low on some of the DCE stations, which meant that the recordings at Pitu S, Qamut S, Amu and, to some degree, Savissivik were dominated by self-noise of the recording systems (see Appendix E). This is also the reason why flow noise did not seem to dominate at these stations after detachment (**Figure 38**). This is unfortunate and was based on the bad experiences of Cornell Lab of Ornithology in 2011 (Annon. 2012), when almost all their recordings were clipped during an effort to document the noise levels of a seismic survey in the Pitu block. Recommendations for future monitoring efforts should include using two acoustic dataloggers with different gain settings to allow for the recording of background noise level with a high gain, while maintaining the capability to encompass intense impulsive instances without exceeding the maximum level of the less sensitive channel.

7.2 Airgun signatures

Close-up recordings of the airgun array of *Polarcus Asima* operating in the Tooq licence block were made over a few days and at ranges of 0.54, 1, 2, 4 and 8 nautical miles. Results revealed a complex pattern of variation of received levels with range that did not conform to a logarithmic relationship (**Figure 32**). This was likely due to inclusion of varying numbers of reflections from the water surface and the bottom at the different locations, and convergence.

The close-range signals contained significant energy at high frequencies. Elevated levels were seen at frequencies as high as 48 kHz (**Figure 29**), but even though the recordings were limited at higher frequencies by the system noise of the Reson 4034 hydrophone (**Figure 30**), there is little reason not to think that the curve would extend upwards to 50 kHz or higher. This is in full agreement with close-range recordings of individual airguns made by Goold and Coates (Goold & Coates 2006), who saw energy extending up to 150 kHz in recordings of a 60-cubic-inch- and a 250-cubic-inch airgun 10 m away. DeRuiter and colleagues (2006) also found significant acoustic energy above 500 Hz in airgun recordings obtained at up to 11.5 km from the source. Furthermore, they showed that high-frequency airgun noise could be trapped in low-salinity surface ducts that allow it to propagate with little transmission loss and reach much longer ranges than predicted by simple transmission loss models. Similarly, Austin and colleagues (2012c) measured significant energy up to 5 kHz out to an 8-km range from a small test airgun array. Although high-frequency signal components attenuate rapidly with distance, due to the frequency-dependent absorption, these observations stress the importance of including these higher frequencies (above a few kHz) in assessments of possible effects on marine mammals, and, given their good high-frequency hearing, Odontocetes in particular.

7.3 Noise levels in Baffin Bay in 2012

A direct illustration of the contribution of the seismic surveys to the noise level in Baffin Bay and Melville Bay can be seen in **Figure 35** to **Figure 37**, which show the received energy at JASCO's moorings minute by minute throughout the entire recording period. No recordings were made after the end of the seismic surveys. However, the three stations, BB1-BB3, deployed by Shell before the start of the seismic operations show a stepwise increase in sound exposure levels, justifying the need for cumulative noise models in the EIAs. The first level increase occurred approximately 5 days after the start of recordings (**Figure 35**), coinciding with the onset of Shell's two surveys (**Table 2**, **Figure 41**). A second step in noise level increase followed 5 days later, and coincided with Mærsk starting its activities in the Tooq block (**Table 2**, **Figure 41**), but may also have been due to Shell's vessels operating closer to the recording stations (**Figure 41**). The average SELs remained elevated throughout the seismic season and never returned to the initial values over the course of the seismic season. Similarly, elevation of the background level in between airgun shots was found in the short-range data (**Figure 31** & **Figure 33**). While the total SELs (**Figure 35**) and the SELs of recordings band-pass filtered between 10-2000 Hz (**Figure 36**) for the BB1-BB3 stations showed small differences before August 1st, there were no noticeable differences between the two methods thereafter. This indicates that the received levels due to seismic activities were dominated by frequencies in the range between 10 Hz and 2 kHz. Consequently, the comparatively large differences between the two SEL estimates seen at JASCO's BB4 station seem to imply that this coastal area (e.g. **Figure 19a**) was dominated by energy outside of the typical airgun frequency range, which could be from the numerous icebergs in this area, as well as from movements of glaciers in the vicinity of the station.

The same pattern was seen at the DCE stations over the course of the season with stepwise increases in SEL (**Figure 38**-**Figure 40**), though, we did not have any background recordings prior to the seismic surveys. The stepwise increase was most evident at the northern stations, Savissivik, Qamut N and Qamut S, where the start of ConocoPhillips' survey was visible as a strong elevation in the received sound energy. However, it should be kept in mind that the station Qamut S and to a much lesser degree Savissivik were self-noise limited and the amplitude of the increase is therefore underestimated. The jagged appearance of the curves likely reflected a combination of Shell and ConocoPhillips' seismic vessels moving back and forth along the transect lines (**Figure 41**) and local interference effects in the form of shadow and convergence zones (see similarity between the Qamut N and Pitu N moorings before August 25th and the dissimilarity between Qamut N and Savissivik in **Figure 38**). However, another important factor in the varying levels may be local bathymetry effects, for example local areas of higher or lower transmission loss, as seen on a larger scale along the north-south running sound channel (**Figure 43**). Depending on the orientation of the seismic vessel with respect to the recording station such bathymetry effects will vary in influence. The variation in received levels at the southern stations, Pitu S and Amu, were affected by the high self-noise of these stations (**Figure E1**- **Figure E3** in Appendix E) and the low transmission loss northward form the Tooq block as suggested by the transmission loss modeling (see Appendix C, **Figure C1**). The level fluctuations due to the seismic surveys therefore appeared less pronounced (**Figure 38**) with the lower bound of variations limited by self-noise whereas the upper bounds most likely were a genuine effect of the lower transmission loss northward from the Tooq block. Regardless of the cause, we can conclude that both stations did record airgun pulses, but most of the arriving signals were of low received level (below about 150 dB re 1 $\mu Pa^2 s$) (**Figure 38**). In contrast, the noise levels registered at the northern stations, Quamut N and Pitu N, were high, in the case of Qamut N, nearly as high as those recorded at the BB3 mooring (**Figure 35** and **Figure 48**). Due to the North-South low-sound-speed channel extending northwards from Shell's operation sites (**Figure 43** and **Figure 44**), the airgun shots from Shell's two vessels were almost constantly present in these recordings (see e.g. **Figure 34**). Shell's BB4 station near the coast also recorded airgun pulses originating from Anu and Qamut blocks (**Figure 46**), despite being dominated by natural sounds from icebergs. Airgun pulses were further opportunistically recorded on three dataloggers deployed near Disko in the southern part of Baffin Bay (**Figure 53**). We do not have received levels for these recordings, but airgun pulses were present 8-100% of the time in August and September 2012, with no airgun signals recorded in July (**Figure 53**), which points to the four simultaneous seismic surveys in Northern Baffin Bay as the most probable source of the signals. It is therefore likely that the four seismic surveys were audible in the entire Baffin Basin.

Figure 53. Airgun pulses from the four seismic surveys recorded near Disko in the southern part of the Baffin Bay (Bottom panel). Three dataloggers were deployed here and recorded from October 2011 to September 2012 with a sample rate of 16kHz, and a duty cycle of 17 min every other hour. The top panel shows the percentage recording periods per day with seismic detections on the moorings deployed at 71°09N / 64°26W). GINR, Preliminary results. Bottom panel shows exploration licenses and position of the three dataloggers (D1-3) in the southern part of Baffin Bay. (map - datum: WGS84; projection: Mercator).

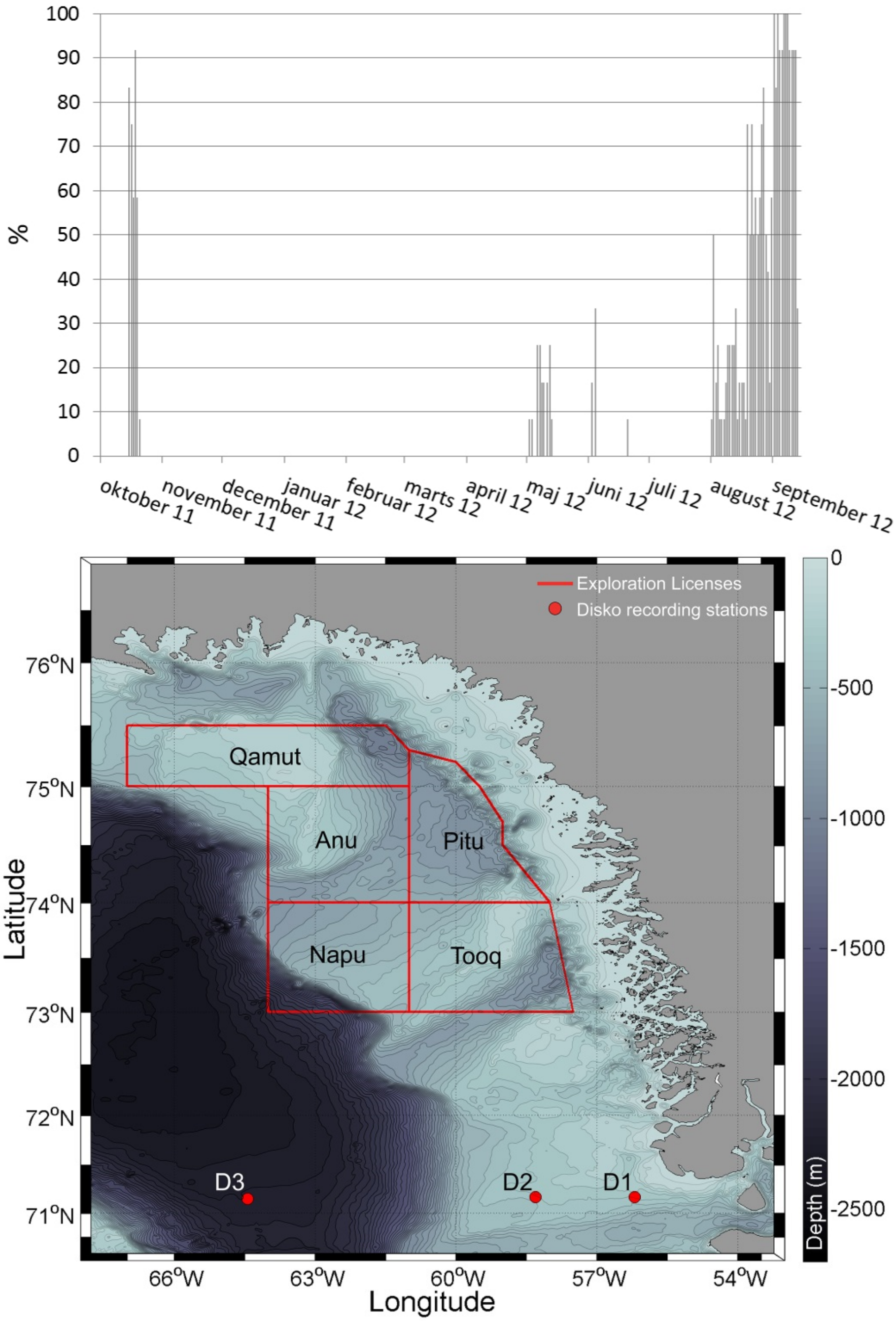

Before the start of the seismic activities, the per-minute ambient noise energy level was approximately 120 dB re 1 µPa²s (**Figure 35**). However, these recordings seem to have been dominated by the self-noise of JASCO's dataloggers (**Figure 54** and **Figure E4** - **Figure E5** in Appendix E). Thus, the SEL of the ambient noise before the onset of the surveys must have been lower than measured here by JASCO. The median third octave levels (TOLs) received at the BB2 and BB3 stations during the three days with the lowest SELs (**Figure 55**) were lower than TOLs reported for Disko Bay in May (about 90 dB re 1µPa (rms) between 25 and 7000 Hz and approximately 75 dB re 1µPa (rms) at 20 kHz) and August (ranging from 75 dB re 1µPa (rms) at 1 kHz to between 95 and 100 dB re 1µPa (rms) at 10-20 kHz) (Simon 2010). It seems, however reasonable to assume that the levels here were higher than the very low noise levels recorded in the protected Kobbefjord on the southwestern coast of Greenland (58 – 68 dB re 1µPa (rms)) (Simon 2010). Following the commencement of the seismic surveys, the SELs at the BB1-

BB3 stations were therefore on average at least 20 dB higher than the pre-exposure level, and sometimes increased by more than 70 dB compared to the pre-season levels (**Figure 35**). The highest SELs of up to 189 dB re 1 μPa²s (**Figure 35**) coincided with the passage of the survey vessel close to the data-loggers. Cumulative SEL over 24 hours increased from about 120 dB re 1 μPa² s to up to 189 dB re 1 μPa²s (**Figure 35**-**Figure 40**). This is an increase in background noise energy of more than six orders of magnitude.

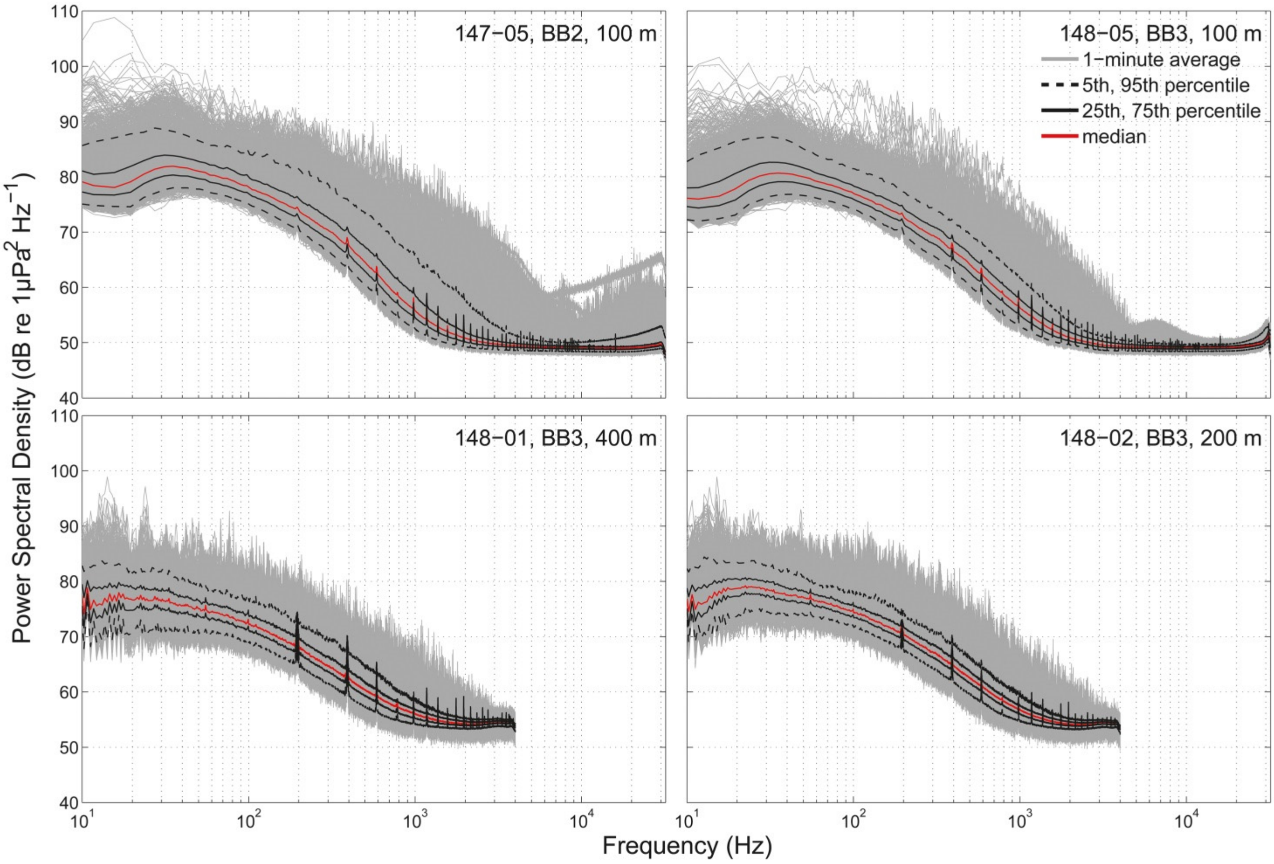

Figure 54. Power spectral density (PSD) levels of ambient noise recorded with four loggers, at two stations, during three days with the lowest median sound exposure levels (**Figure 35**) before the start of the seismic activities in Baffin Bay. The loggers were selected for easy comparison with the two self-noise datasets provided by JASCO (**Figure E4** - **Figure E5** in Appendix E). Note that logger 147-01.8000 did not render any usable data due to leakage along the BB2 mooring cable. Instead, recordings from a different logger deployed along the same mooring are presented here, together with data from all three loggers from the BB3 station to look at variation with sampling rate and deployment depth.

One station, the BB4, located close to the coast at Depotøerne (e.g. **Figure 19A**), recorded markedly lower levels of noise (median 1 minute SEL of 124-138 dB re 1 μPa²s) (**Figure 35**) than the rest of JASCO's stations, reflecting of course the greater distance from the seismic sources but also the complex conditions for sound propagation with melting ice and very uneven bathymetry near the coast. It is worth noting that the only sound speed profile which deviated markedly from the rest was also from this area (**Figure 23**), implicating how the varying bathymetry and melting ice affected the sound propagation near the coast.

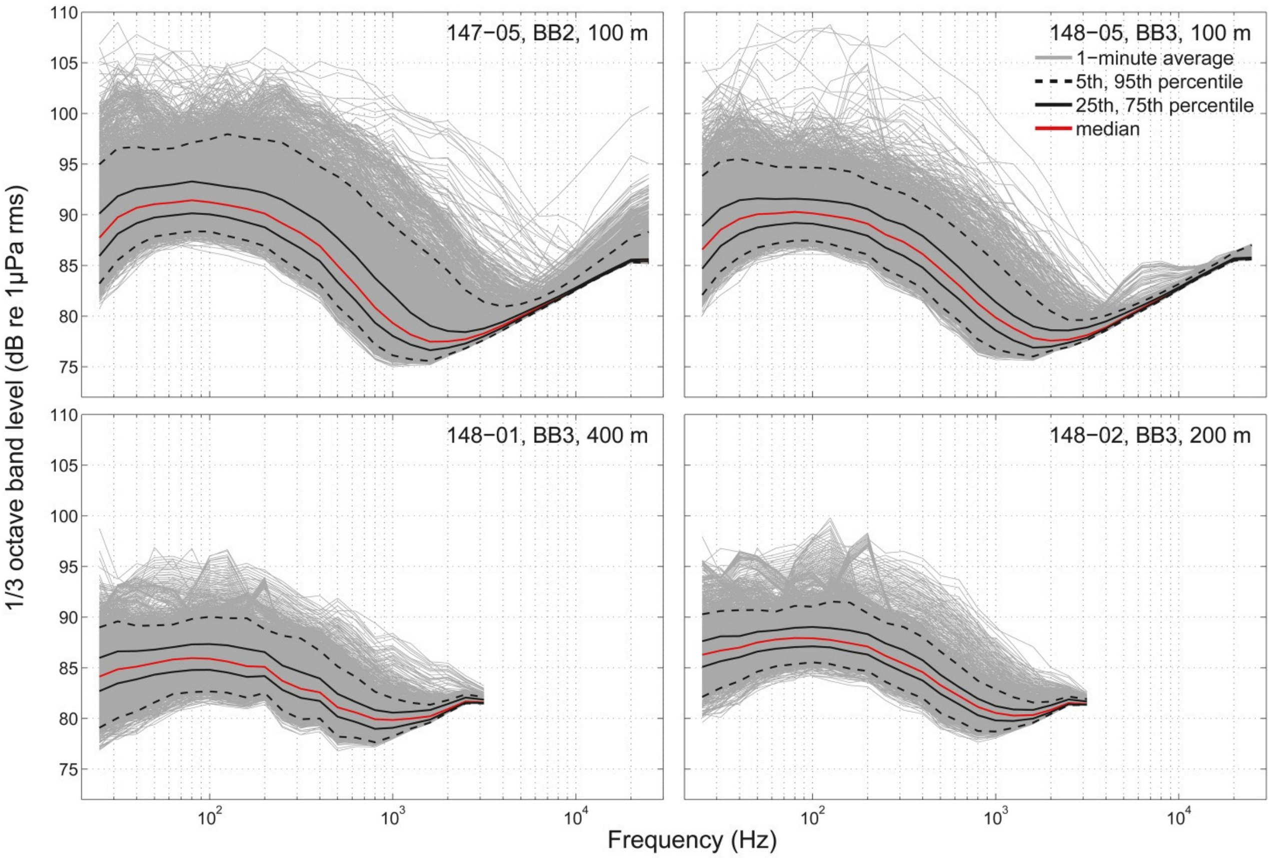

Figure 55. Third-octave received levels (TOL) of ambient noise recorded with four loggers, at two stations, during three days with the lowest median sound exposure levels (**Figure 35**) before the start of the seismic activities in Baffin Bay. See justification for datalogger choice in **Figure 54**.

Another important observation was the joined effect of the reflective properties of the bottom of Baffin Bay and the water surface that together gave rise to long effective pulse lengths, typically on the order of 4 seconds and sometimes up to 10 seconds (**Figure D1** in Appendix D), when multiple reflections arrived at the receivers with short time delays (e.g. **Figure 33** and **Figure 34**). This is highly relevant when considering cumulative effects of pulses originating from several seismic vessels, as those arrived at comparable received levels and overlapped in time (**Figure 34**), which effectively led to very short breaks without any airgun noise, and is discussed below in relation to marine mammals.

7.4 Sound propagation conditions

The recordings made by the moored dataloggers showed large variations in received levels over time (**Figure 35-Figure 40**), mainly attributable to the distance to the nearest seismic source. However, in a number of recordings, illustrated most clearly in **Figure 42** with data from the BB1 and BB3 stations, there were deviations which could not be explained by source distance alone. In most recordings, the uppermost datalogger registered the highest sound levels, on account of the top logger being the closest to the low-sound-speed channel. However, there were instances where the middle or the bottom datalogger showed the highest received levels (**Figure 42**). These were likely due to changes in the sound propagation path from the source to the receiver, reflecting the physical phenomena linked to the change in sound speed with depth and bathymetry. The combined effects of reflection and refraction resulted in the creation of shadow zones, with sound levels lower than expected from simple propagation models, and convergence zones with elevated sound pressure levels (Medwin & Clay 1998). Thus, the received noise levels deviated markedly from simple predictions of transmission loss with distance. The three-dimensional location of the shadow and convergence zones depends not only on the sound speed profile but also on the distance to the source (Medwin & Clay 1998), which, again, may lead to non-monotonic relationships between distance to source and received levels at a fixed position (i.e. at a particular receiver). The short range recordings present an example of this with a non-monotonic relationship between range to source and received level with about 1 dB difference in received level between 1 and 2 nmi and between 4 and 8 nmi (**Figure 32**). This is important to keep in mind when considering different zones of impact (Richardson et al. 1995) in relation to mitigation of the effects of seismic noise on marine mammals in Environmental Impact Assessments.

The 3D transmission loss modeling performed by WHOI demonstrated that the acoustic environment of the north-eastern Baffin Bay and Melville Bay was highly complex. The model outputs showed regimes where they could be strongly influenced by the accuracy of the environmental inputs. In particular, the near-surface sound ducting, the geoacoustic properties of the bottom, and the detailed bathymetry in shallow and high-gradient regions, could produce large effects on the predicted transmission loss. One rather common source of error in acoustic modeling studies is the lack of correct bathymetry information, which is especially true in regions with appreciable bottom slope. In such areas, it is a common experience that multiple bathymetric measurements disagree. This was also found here in comparing the depth charts available for the predictive modeling and the depths actually obtained during the seismic surveys (**Figure 24**-**Figure 25** and **Figure A9**-**Figure A12** in Appendix A), with the greatest disagreement along the north-south running deep channel in the Qamut license block (**Figure 24**-**Figure 25**). This channel provided complexity to the acoustic environment, as the modeling showed lower sound speed in this channel. The channel runs along a deep slope and, due to the poor bathymetrical mapping of the area beforehand, it was not possible to predict it in the EIA modeling. However, with more accurate bathymetric inputs, the WHOI model was able to point to the existence of the low-sound-speed channel (**Figure 43**) and the finding was later validated by the DCE measurements at the Qamut N station (**Figure 44**). This clearly illustrates the importance of valid environmental data as inputs to propagation models, as well as the limitation of predictive modeling in poorly known areas.

We were not able to reliably verify WHOI's modeling results from the coastal areas (**Figure 45**). There are several reasons for this. First of all there were few points to verify the model with and there were no control points in the region with the largest received level variations, west of 63°. Secondly, the station positions were inaccurate in terms of bathymetry. The bathymetry chart available for the WHOI modeling was actually not deep enough at the position of BB4 and the modeled receiver had to be moved somewhat to fit the chart (**Figure 19**). The bathymetry of the coastal part of Baffin Bay is generally not well described, which is a prerequisite for accurate modelling. This means that if seismic activities are to take place in coastal northwest Greenland (and likely most parts of coastal uninhabited Greenland) data on bathymetry must be obtained well in advance to allow for reasonable predictive EIA modeling. Such data should also include bottom substrate and CTD profiles for the seismic season. The latter was also an issue for the verification of the WHOI modeling as they had to use a constant CTD profile, where in fact the profile changes a lot due to melting icebergs and calving glaciers in the area (as observed at BB4 (**Figure 23**)). The constant approach may therefore be too simplistic. Changing CTD profiles will therefore be implemented in the next version of the 3D model. These issues all relate to the purpose of this study, which was designed to look at oceanic propagation of airgun noise, as this was considered the best starting point for the present models, not the coastal areas. Furthermore, wave and ice conditions were not factored into the models, partly due to lack of good input data, but also because these effects are not yet well represented in parabolic equation models. The WHOI 3D model was also narrowband, as a full 3D broadband model has not yet been produced. When this is achievable, the next step will be to extend the models to coastal Arctic areas which again only can be done by obtaining solid environmental data on ice, waves, bottom properties and CTD profiles along with noise recordings in order to be able to predict sound levels for example inside the protection zones, which is important in relation to EIAs. It is our opinion that, while standard Nx2D, broadband parabolic equation models give good results on the average, there are still a number of potential "hot spots" in the propagation, that the community needs more advanced models and input data to address (see discussion on Appendix B).

7.5 Post-season 3D propagation model

A detailed discussion of the WHOI modeling efforts may be found in Appendices B and C. Below we present a brief synopsis of the results found in those Appendices with a treatment of their implications.

7.5.1 Bottom limiting and surface ducting

The variability in the ocean surface layers, affects bottom limiting and near-surface ducting. It is seen that for sources near the surface, such as seismic sources, a sound speed at the source depth that is greater than or equal to the sound speed at the bottom will lead to bottom limiting, which will attenuate sound more effectively, and can limit the exposure to marine mammals. A second issue is the significant below-surface sound speed duct (axis located at ~50m) which was seen in the summer. This can trap sound effectively, especially if the source is not bottom limited, and thus increase the exposure risk for marine mammals. The issue of how the surface water sound speed profile evolves both seasonally and even on a daily basis (due to mixing by wind events) is thus an important one to address from the point of view of ocean measurements. At present, modeling of near surface oceanography is not adequate to give a good daily estimate of the sound speed profile. Thus, daily measurements with CTDs during seismic surveys are recommended.

7.5.2 Geoacoustic model of the bottom

Another important consideration for the Baffin Bay study (and indeed coastal studies) is having an adequate geoacoustic model of the bottom, so that one may accurately estimate the bottom loss component of the transmission loss. It was noted in Appendix B that the basic seismic survey data - coupled with near-surface sediment samples and Hamilton's regression equations - could probably supply an adequate estimate of the near-surface sediment sound speed and density. However, the attenuation (including the effective attenuation due to scattering) and shear properties are harder to measure, and it might not be amiss to think in the future of some field measurements that could address these, to be made along with a survey. One can estimate what the effects of bottom geoacoustic model error are via repeatedly running a forward model (e.g. the JASCO Nx2D model) within a reasonable range of geoacoustic model parameter values, and then determining the spread in transmission loss estimates. This is a crude, computer intensive approach, and we therefore show how one could use a simple extension of the plane wave reflection coefficient for a fluid bottom to estimate the bottom loss per reflection, with the geoacoustic parameters being very explicit and easily changed. This reflection coefficient model, combined with a ray trace model that would only need to be run once, would be adequate for obtaining a good estimate of how transmission loss estimates would vary with bottom model error, and thus which degree of accuracy one would need for the bottom model, given a certain criterion for accuracy in the transmission loss.

7.5.3 3D effects

A third important consideration in modeling transmission loss in a bathymetrically variable coastal region is 3D effects. It is now well known that 3D lateral refraction of energy in coastal regions is important, and can cause focusing and defocusing of energy (hot and cold spots) that is not predictable by Nx2D methods. 3D modeling has also advanced to a point where one can model an entire area like Baffin Bay with a 3D full wave code like parabolic equation (PE). The output of such a model is shown in Appendix C. There are two issues that remain to be addressed with 3D modeling, which we have not fully resolved in this study. The first is the issue of creating a broadband 3D code. Our present results for this study are narrowband, which make them difficult to compare with the broadband Nx2D results from JASCO. However, even the narrowband 3D result shows that significant lateral deflection occurs in certain areas, so that there is an advance being made. Use of direct Fourier synthesis of a broadband pulse is a very computer intensive route, and currently some thought is being given to possible simpler alternatives. A second issue to consider is when and where one should go through the effort of creating a fully 3D calculation. Even in its narrowband implementation carnation, a 3D code is non-trivial to run, and the question of the degree to which the gains in knowledge are sufficiently high is not unreasonable to ask. To address that question, a simple, approximate way of calculating where 3D effects are important is presented. A variant of this method can also be found in the textbook on shallow water acoustics by Katsnelson et al. (Katsnelson et al. 2012). Performing this simpler calculation can inform a user as to whether or not they should use a full 3D calculation.

7.5.4 Effects of bathymetry error on transmission loss

A fourth topic that is discussed by the WHOI group in Appendix B is the effects of bathymetry error on transmission loss. Again, one can run full parabolic equation models to address this, and get exact results, but such an approach is inefficient. Instead, we present a simple approximate method for determining the degree of accuracy needed in bathymetry charts to get good estimates of transmission loss.

7.5.5 Future research

Two topics that we did not manage to address in the report, due to insufficient data, were: 1) ice cover and surface wave effects and 2) sampling issues. As to the former, the ice cover was not modeled due to there not being sufficient data available on either the areal cover or physical properties of the ice in the area. The surface waves were generally small during operations, but even smaller waves do have some attenuating and scattering effects. However, at present, 3D parabolic equation models do not handle these waves, and so we decided not to address them. As to sampling issues, one of the topics mentioned many times previously was the issue of "hot and cold spots" versus average behavior. We argue that the hot and cold spots issue is a serious one that needs to be addressed. At present, the models can be run with the resolution to address this, as per our 3D study. However, we do not have any data that can shed light on this from Baffin Bay, or anywhere else. Testing the detailed variability of the acoustic field, as opposed to a simple "averaged out" version, is one of the challenges for future research in this area

7.6 Predictive modeling

The 24-hour cumulative sound exposure levels of 173-178 dB re 1µPa^{2}s measured at the Qamut N station for the northernmost track of the ConocoPhillips survey were within the range of 170-180 dB re 1µPa^{2}s predicted for the same area by JASCO's pre-season modeling study (**Figure 49**). However, it should be noted that JASCO's results represent maximum-over-depth values (Austin et al. 2012b), with no indication of the depths at which the maxima occurred. The variation observed in our recordings along the vertical plane, i.e. when comparing received levels at three dataloggers distributed along the same mooring, was on the order of 5 dB, with the highest levels recorded on the top logger (**Figure 49**). Though, there is no certainty that the depth of the top logger coincided with JASCO's depth of maximum cSEL. Nonetheless, there was a good correspondence between the SEL-depth profiles, supplied by JASCO for Shell's modeling sites and model sampling positions closest to the locations of the moorings encompassed by the model (data courtesy of JASCO and Shell), and the variation observed in measurements of individual airgun pulses made at different depths along those moorings (**Figure 47**-**Figure 48** and **Figure D6**-**Figure D7** in Appendix D). This suggests that the distribution of the dataloggers along the moorings provided reliable data for comparison with the maximum-over-depth estimates. In general, the SELs of airgun pulses that originated in an area within a 2-km radius of JASCO's modeling sites and were registered at the different recording stations agreed well with the values predicted by the pre-season modeling study (**Figure 47** - **Figure 48** and **Figure D3**-**Figure D7** in Appendix D). The measured energy levels were almost always below the maximum-over-depth levels predicted by JASCO (Austin et al. 2012b). The exceptions were the somewhat higher levels recorded at Pitu N for ConocoPhillips' site 1 (**Figure D3**), and Qamut S and Qamut N for ConocoPhillips' site 2 (**Figure D4**).

One more exception may have been the relatively high received levels (122-127 dB re 1µPa^{2}s) of pulses propagating from Shell's site 3 to the Qamut N station (**Figure 48**) located at the end of the North-South channel identified by WHOI's transmission loss model (**Figure 43**), though, this station was not included in the predictive modeling for that site. This illustrates the influence and importance of bathymetry and geoacoustic properties on sound propagation.

JASCO's model missed the 3D acoustic effects observed in the results of WHOI's transmission loss study for the Qamut license area (**Figure 43** and **Figure 44**), and may therefore have significantly underestimated the sound exposure levels at the Qamut N station, and possibly the region north of it (see, for example, the local variation around JASCO's southernmost modeling site in **Figure 44** and compare to the predictions in **Figure 47**). This was probably mostly due to the limited number of source locations (between two and four per license block (**Figure 20**; (Austin et al. 2012a; Austin et al. 2012b; Matthews 2012) and the choice of these locations to be spread out over the license blocks and represent the ranges of water depth in the area. This meant that JASCO's model was, for instance, not able to assess the importance of local bathymetric features, also because the bathymetric charts available for JASCO's modeling were not precise, as discussed in chapter 7.5.4. A detailed discussion on, and guidelines to, when and where one should consider 3D acoustic effects can be found in Appendix B. It is, nevertheless, encouraging that an overall good correspondence between the preseason model and the on-site measurements was found, especially considering that the predictive modeling was based on input data with poor accuracy and resolution, simply because no better data were available.

In their monitoring report (Martin & MacDonnel 2013), JASCO compared the modeled rms SPL computed using a predicted 90% energy duration time window (Matthews 2012) (termed T90 by Martin and MacDonnel) with the received levels measured along a radial, from approximately 150 m from the source at station BB1 to 75 km at station BB3. From 300 m outwards the measured results were also consistently lower than the prediction, by an average of >5 dB. When the model results were adjusted to incorporate a more realistic T90 rms duration as well as the measured sound speed profile, the difference was still greater than 3 dB. This was, most likely due to the difficulties in predicting the geoacoustic properties of the area without proper bathymetric charts.

It was not possible to directly verify the aggregate cSEL values modeled by JASCO for all four vessels combined (**Figure 51**, bottom panel), because the survey schedules did not comply with the modeled scenario. Instead, 24-hour cSELs from shots emitted along the northernmost firing line of ConocoPhillips and the two modeled firing lines of Shell, together with airgun shots from all other vessels operating during the same time periods, were measured individually (**Figure 50** and **Figure 52**). For all stations considered, the measured levels were within, or below, the predicted ranges (**Figure 50** and **Figure 51**-**Figure 52**). For most stations, however, the cSEL was measured at a single depth, as due to the elevated levels at the loose loggers, data from the top and middle recorders were excluded from the analysis. Variations with depth of up to 15 dB could be expected (**Figure 47** and **Figure D6**-**Figure D7**, Appendix D), but were not observed at the stations with two (Qamut N for Shell) and three (Qamut N for ConocoPhillips and BB3 for Shell) loggers distributed along the same mooring (**Figure 50** and **Figure 52**).

The highest 24-hour cSELs of 189 dB re 1µPa^{2}s (**Figure 35**) were recorded from shots fired along transects located in close proximity to the recording stations (**Figure 41**). Again, these values were close to JASCO's predictions (**Figure 49**-**Figure 51**). With contributions of equal energy from another vessel these estimates would be 3 dB higher (see e.g. **Figure D2**, appendix D), but would still fall within the predicted received level ranges (**Figure 51**). In general, the 24-hour cSELs measured at all loggers that were not loose or self-noise dominated (**Figure 35** and **Figure 38**-**Figure 39**) agreed well with the values predicted by the pre-season modeling study (**Figure 51**).

7.7 Predictive modeling in the environmental impact assessment process

In Greenland, guidelines for Environmental Impact Assessments of seismic and drilling activities require that each applying company models the noise exposure expected from its planned activity, as well as the cumulative noise exposure from all concurrent activities proposed in the same general area (Kyhn et al. 2011). Since this requirement is new, it is prudent to evaluate whether it is justified given the currently available data. **Figure 35** to **Figure 37** present examples of cumulative impacts from more than one seismic vessel. The fact that the noise contributions from the different seismic surveys tend to add up, supports the validity of the current EIA requirements. Future noise exposure models should aim at combining all industrial activities in a wide area that may well cross national borders. In the Greenlandic part of Baffin Bay, for instance, it is relevant to include activities occurring on the Canadian side of the bay as well, whenever these activities are powerful enough to increase noise levels in Greenlandic waters above the existing ambient conditions.

The fact that JASCO was able to estimate noise exposure from the planned seismic operations fairly accurately also indicates that the requirement of predictive modeling as part of the EIA is worthwhile, even for areas that are relatively poorly characterized in terms of, for example, bathymetry. Nonetheless, there are very good reasons to increase the effort of collecting high-quality environmental data and making them available to the companies prior to the EIA-process, as the limiting factors for model precision are the quality and quantity of the input data (Appendix B). This was also the case for the Baffin Bay models, as there was very little hydrographical and bathymetric information available for the EIA-modeling. Comparison between sound speed profiles used in the EIA-models (Austin et al. 2012a; Austin et al. 2012b; Matthews 2012) and the actual measurements taken in 2012 (**Figure 23**) showed that the magnitude of the near-surface low-sound-speed channel was underestimated in the EIA-models (Martin & MacDonnel 2013). It was also clear that the bathymetry had not been mapped in detail as evidenced by the large deviations of the depths measured during the seismic surveys from the depth charts available for predictive modeling (**Figure 24** and **Figure 25** and **Figure A9**-**Figure A12** in Appendix A).

7.7.1 Nx2D broadband modeling

It is encouraging that the Nx2D broadband model, developed for the Environmental Impact Assessment did have an overall good correspondence with our measurements. However, the collected environmental data were rather sparse overall, and we were not able to experimentally examine a number of potentially important environmental effects in sufficient detail, such as ice cover, water column sound speed ducting, geoacoustic model variability and error, and 3D effects in regions with large bathymetric gradients. The latter three of these effects were studied via computer modeling instead and the findings summarized here: As regards to the water column ducting, a near surface duct could produce a very good propagation condition, and also reduce bottom loss, so that more seismic noise would propagate. Even simple models show this as being important, so assessment of the potential for ducting conditions during the profiling might be advisable. As to the bottom property measurement accuracy, again, simple models show that one cannot tolerate large errors in the bottom model, especially where there is shoaling bathymetry such as in coastal regions. However, it is felt that the basic bottom model for the Baffin Bay study, just based on the near surface bottom material, was good enough to predict the bottom loss in this case. The study of the 3D propagation effects using the WHOI 3D PE model pointed out that regions with large bathymetric gradients could show different focusing and shadow zones from an Nx2D analysis, and thus if "hot spots" are of interest, it would be advised to use a 3D analysis in such areas. The WHOI 3D PE analysis needs to eventually be implemented in broadband mode, but even as a narrowband result, it is indicative. Overall, this work calls for a discussion on how scenarios for predictive modeling should be chosen, i.e. to what degree they should focus on average or typical scenarios (location of sources and receivers, i.e. ships and animals) in contrast to focusing on extreme (worst case) conditions.

7.8 Impact on marine mammals

The present study focused primarily on propagation of airgun pulses. Its original motivation, however, were concerns about potential effects of seismic activities on marine mammals. In this section, we therefore put our findings into the context of what is known about marine mammals in the Baffin Bay area. Only one station was placed close to the shore inside the narwhal protection zone (e.g. **Figure 20**), because the modeling efforts were prioritized, and these could best be validated relatively close to the source and in regions for which depth charts were available beforehand. Hence, we were not able to examine the effects of the surveys on narwhals. By and large, the noise levels measured during the seismic operations were within the ranges where effects on marine mammals are possible. Quantifying these impacts, however, is extremely difficult, as there is very limited information available on the behavior of narwhals, belugas, bowhead whales and most seals, including – and perhaps especially – on how they react to noise exposure over extended periods.

7.8.1 Temporary hearing loss

Loud sounds can affect the inner ear of marine mammals permanently, and the first physiological sign that this has taken place, is a temporary threshold shift (TTS). TTS has been studied extensively in bottlenose dolphins (see (Southall et al. 2007) for a review and (Finneran & Schlundt 2013) for the latest results), but only one study is available for belugas and none for narwhals. The single study on the beluga (Finneran et al. 2002) showed that it was possible to induce TTS by single water gun pulses, with frequency spectra not unlike those of airgun signals, at a received sound exposure level of 186 dB re 1 µPa^{2}s. The mean SEL of pulses recorded at a distance of 1 km from *R/V Polarcus Asima* was about 174 dB re 1 µPa^{2}s (**Figure 32**), i.e. 12 dB below the threshold for TTS for belugas (and likely also narwhals given their genetic similarity). These numbers imply that animals were at risk of experiencing TTS from a single airgun pulse when within a range of 260 m of one of the airgun arrays used in the Baffin seismic surveys. However, under the assumption of a leaky integrator model for sound perception (Popov et al. 2014), a TTS can also be elicited by exposure to several pulses with a total cumulative SEL above the TTS threshold. Assuming a TTS onset level of 186 dB re 1 µPa^{2}s a beluga or a narwhal would have been at risk of experiencing threshold shift after being exposed to 14 airgun pulses (corresponding to an exposure time of less than 162 seconds (**Table 2**)) at a range of 1 km from the array. The number of pulses needed to induce TTS increases with range (4 times as many pulses per doubling in range to cause TTS when assuming spherical spreading) and at 2 km from the source, the animals would have to have received 54 airgun signals to experience TTS, corresponding to a 11-12 min period (**Figure 32**). As neither the survey vessel nor the whales were likely to be stationary, the risk that a wary animal was exposed to more than a handful of very powerful pulses appears low, but the risk of TTS is nevertheless real for nearby animals as they would have to cover long ranges in a short time to avoid summing of levels to a value that causes TTS. This means that most of the exposed narwhals and belugas will likely not experience TTS from airgun operations, given that they are shy and keep their distance (none were seen by the MMSOs in Qamut, Napu or Apu blocks (Vanman & Durinck 2012; Lacey et al. 2013) where narwhals otherwise are present in summer-autumn (Dietz & Heide-Jørgensen 1995); however, that animals (including bowheads and pinnipeds (Southall et al., 2007) within some nautical miles from the array will face the risk of TTS. As many seals were observed during active shooting (e.g. 1884 seals observed by Shell MMSOs in the survey blocks alone (Vanman & Durinck 2012) it is likely that some of them experienced TTS.

One way to decrease the risk of TTS as well as permanent hearing damages is to reduce the output of the airgun array source level. This can be done either permanently from onset of the seismic survey or it can be adjusted in accordance with the actual on site propagation conditions (see section 7.5.1). By decreasing the source level 6 dB the ensonified area will be halved and the survey will then only affect ¼ of the original area and 1/8 of the original water volume, hereby greatly reducing the risk of exposure leading to TTS for animals in these areas. It is therefore of great importance to test and choose the source level beforehand as well as assessing the source level continuously underway as the bottom reflectivity and properties become known.

7.8.2 Changes in behavior and distribution

Another, potentially much more important impact of seismic surveys on marine mammals is the possible negative effects on behavior and distribution of the animals. Such adverse effects are poorly understood for narwhals and belugas, but the scant data support the notion that these two species can be affected even at very low received levels of noise (Finley et al. 1990; Miller et al. 2005). If the animals experience a temporary habitat loss during the seismic surveys, or important behaviors (such as foraging, mating or nursing of calves) are interrupted at critical times, these effects could propagate through generations and contribute to a less favorable conservation status via loss of population fitness. Harbor porpoises, for instance, have recently been shown to react to seismic survey noise by decreasing their foraging rate (Pirotta et al. 2014). Such effects may be detrimental if they persist over long periods of time.

The substantial increases in SEL during the four seismic surveys (**Figure 35** to **Figure 38**) indicate that during the seismic season of 2012 marine mammals in Baffin Bay experienced habitat degradation. The jagged pattern, resulting from the changing received levels at the recording stations, further implies that the animals were constantly subjected to changes in the background noise level that they had to adapt to. For example, if they wanted to escape the noise, they would have had to move away from the noise in changing directions. The generally higher noise levels in the top layers of the water column also meant that the animals would have experienced an increasing noise level before arriving at the surface to rest.

As mentioned above, there are no studies to date on the effects of seismic noise on narwhal behavior. Therefore, to assess the risk of behavioral disturbance we shall use threshold levels established for other noise sources and species. Finley and colleagues (Finley et al. 1990) found that narwhals reacted to icebreaker noise at received levels as low as 94-105 dB re 1 µPa rms in the 20-1000 Hz frequency band. The harbor porpoise who, like the narwhal, has the reputation of being wary (Olesiuk et al. 2002; Brandt et al. 2012), has been shown to react to seismic noise (Pirotta et al. 2014) as well as vessel noise (Barlow 1988) at low received levels of around 123 dB re 1 µPa rms (M-weighted) (Dyndo et al. in prep). Harbor porpoises also react to the transient pulses arisen from ramming of wind farm piles, by evacuating a zone with received levels higher than 140 dB re 1 µPa p-p around the pile driving site (Tougaard et al. 2009). The highest noise levels measured at the stations closest to the narwhal summering areas, Melville and Savissivik (e.g. **Figure 38**), were 124 and 155 dB re 1 µPa (rms), respectively (**Figure 56**). It is therefore very possible that narwhals reacted behaviorally during the surveys. Circumstantial evidence of this exists in the form of missing MMSO narwhal observations (Vanman & Durinck 2012; Lacey et al. 2013) from the seismic vessels in areas where narwhals normally may be present at this time of the year (Dietz & Heide-Jørgensen 1995). Heide-Jørgensen and colleagues conducted three visual surveys of narwhals in and just outside the Melville Bay Nature Reserve during the 2012 seismic season and found that narwhals during the second and third survey (conducted during the seismic surveys) were distributed significantly closer to shore and in a smaller area in the central part of the Melville Bay in relation to a survey conducted there in 2007. In 2007 narwhal groups were distributed more widely in north- and southerly direction. Also they found that narwhal groups were significantly more closely spaced in 2012 than in 2007 (Heide-Jørgensen et al. 2013a). This change in distribution may be related to the seismic surveys, but could also be caused by random differences between the years in for example ice distribution or glacier activity in the area. A lack of distributional response does not necessarily imply a lack of behavioral response; however, there is neither sufficient information on the natural behavior of the animals, nor adequate fine-scale movement data available to allow for any quantitative predictions at this point. It is therefore a priority to collect information on the natural behavior of these animals, as well as on how they distribute in space and utilize the marine environment with and without airgun exposure. Effort should be put into obtaining these data through carefully designed field studies, such as those involving Passive Acoustic Monitoring (see section 7.8.4 below) for example coupled with visual surveys and controlled exposure studies where animals equipped with an acoustic and behavioral datalogger are exposed to a known and relevant dose of seismic noise. State of the art dataloggers suiting this purpose are for example Dtags which has previously been used specifically for this purpose (Madsen et al. 2006; Johnson et al. 2009). Another unknown in the determination of the impact of seismic activities on the Baffin Bay narwhal population is the propagation conditions close to shore in Arctic waters as described above in section 7.4. This information is necessary in order to predict the potential effects with range into the narwhal protection zone amongst others.

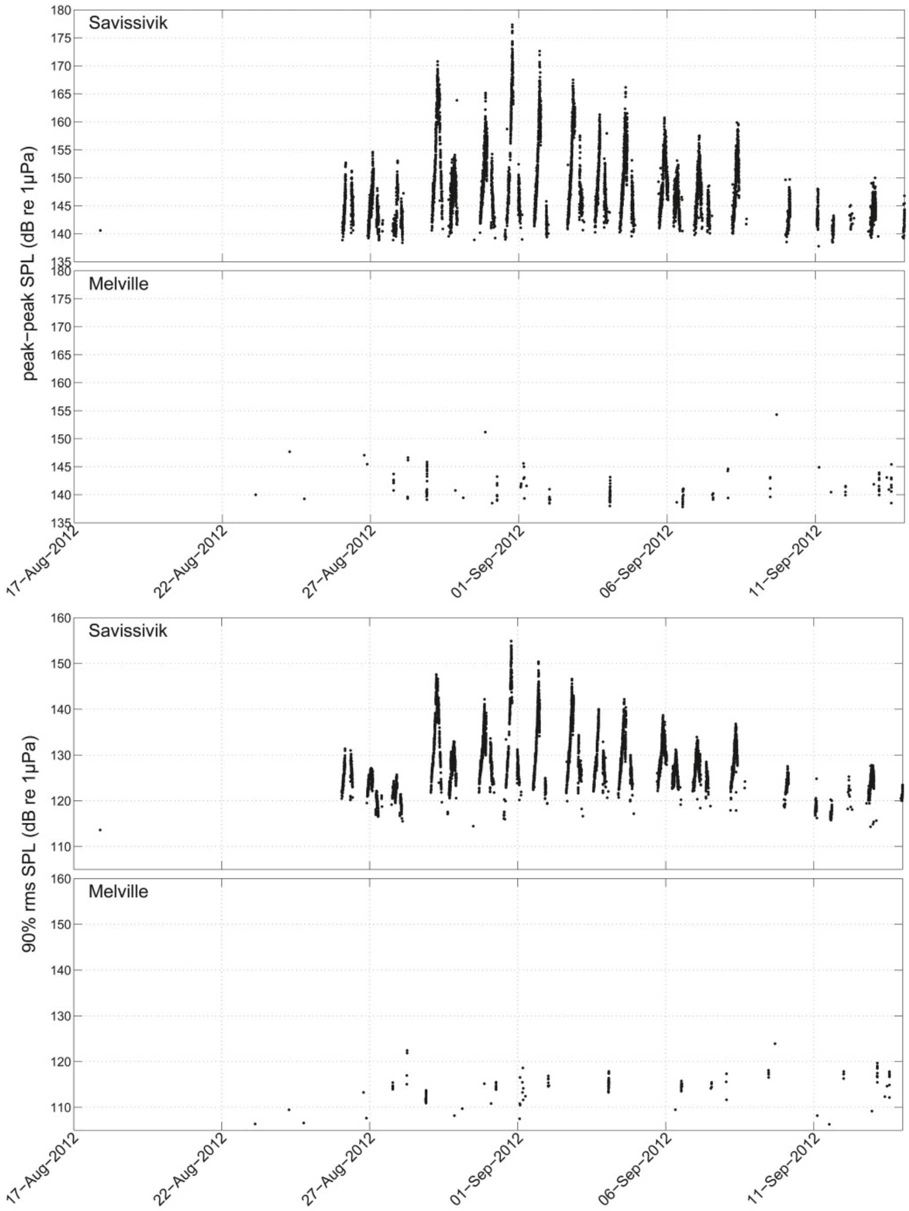

Figure 56. Received levels (p-p top and 90% rms bottom) calculated for airgun pulses received at Savissivik and Melville, the two stations closest to the Melville Bay Nature Reserve.

7.8.3 Masking

Masking of communication signals and other sounds could for some species, in particular the baleen whales and seals, be the most detrimental effect of seismic noise. Masking is very difficult to address experimentally, except in very well-controlled conditions in captivity, and it has yet to be convincingly demonstrated in a natural setting. This, however, does not imply that it does not occur. When considering masking by seismic sources, the main focus is at low frequencies, below 5 kHz, as this is where the main energy of the pulses is concentrated. This is also the part of the spectrum that propagates the farthest from the source. Bowhead whales, narwhals and belugas all have communication signals in this frequency range, as do a number of seal species (see section 4.3).

One way to look at masking is to calculate the range reduction factor, i.e. the reduction in hearing range caused by an increase in background noise level (Møhl 1981). Received levels registered at JASCO's recordings stations during the seismic surveys showed a roughly 15 dB increase in M-weighted SEL compared to the pre-season measurements (**Figure 37**). Thus, narwhals residing in the vicinity of the moorings would have on average experienced an 86% reduction in hearing range at lower frequencies.

During the entire time of our recordings there were only two breaks of more than ten hours with no airgun activities. Furthermore, our data showed that multiple reflected airgun signals arrived at a given receiver with short time delays, causing long (typically on the order of 4 seconds) effective pulse lengths (e.g. **Figure 33** and **Figure 34**), and that one pulse would not fade to background noise levels before the arrival of the next seismic signal (**Figure 34**). Both these findings meant that marine mammals had very little time to receive and emit communication signals during a seismic survey. Also, in our study, it was frequently observed that pulses originating from several seismic vessels arrived at comparable received levels and overlapped in time (**Figure 34**). With multiple simultaneous seismic surveys, the time available for communication was, thus, reduced even further. Seismic surveys seem therefore to entail a considerable reduction in communication space and time for marine mammals in their proximity. However, at present, and until experimental methods that can quantify the effects on the animals become available, not much can be done except keeping this *ad notam* as a potentially significant impact.

7.8.4 Prospects of passive acoustic monitoring (PAM)

The dataloggers used by JASCO in the Shell monitoring program (Martin & MacDonnel 2013), recorded narwhal clicks and whistles on station BB3 on one occasion, and narwhal buzzes on station BB4. They also recorded sperm whale clicks on stations BB1-BB3. None of these detections matched well with the MMSO sightings. However, the two facts: 1) that recorders were able to record narwhal vocalizations and 2) that none were seen by MMS-observers, raise hope that it is feasible to envision a monitoring program for narwhal and beluga based on PAM.

8 Conclusion

This DCE/GNIR monitoring program has demonstrated that the noise exposure to Melville Bay and Baffin Bay from the 2012 seismic surveys was severe, but corresponded to, or was below, the levels anticipated from the modeling performed in connection with the Environmental Impact Assessments for the surveys. This supports the usefulness of such predictive models of acoustic exposure as a valuable tool to assess potential impact on marine life and thus increase the scientific basis for decisions by regulators in future permitting processes.

Significant energy above ambient noise at high frequencies was present in the airgun pulses, up to and possibly beyond 50 kHz at close ranges. At intermediate ranges (up to 8 nmi, i.e. the maximum distance where independent, RHIB-based measurements were made), significant energy could be measured up to several kHz. Thus, although most of the energy of the pulses was below 250 Hz, and hence relatively inaudible to odontocetes, such as the beluga and the narwhal, the increasing sensitivity of these species' hearing with increasing frequency means that the energy at higher frequencies could have added significantly to the audibility of the airgun signals. This observation stresses the need for including higher frequencies in assessment of possible detrimental effects of seismic activities, such as temporary hearing loss and adverse behavioral reactions, at close to medium ranges to airgun sources.

Close to the airgun array of the Mærsk survey, which was the target of the RHIB-based measurements, the noise level was elevated above ambient at all times during shooting, even between individual shots. This was clearly evident up to 2 nmi, and possibly up to 8 nmi from the array. The same rise in ambient noise in between airgun shots was apparent from the other seismic surveys as well. This general rise in background noise has the potential to mask other sounds in the frequency range of 1-10 kHz, including sounds of importance to the animals, such as communication signals.

Measurements from JASCO's moorings inside Shell's license areas (Anu and Napu) documented very variable sound exposure levels, clearly modulated by the movement of the survey vessels towards and away from the moorings. The noise levels were significantly elevated above ambient. Overall average sound exposure levels were increased by at least 20 dB during most of the seismic season, as compared to the period prior to arrival of the first survey vessel. A similar, albeit smaller, increase in overall median noise levels was seen in the DCE recordings from the Qamut block and was attributable to the survey conducted by ConocoPhillips, which started later in the season and added to the already elevated levels caused by Shell's survey.

Recordings from both JASCO and DCE stations showed large fluctuations in received levels of airgun noise. A major part of these fluctuations could be explained by the variable distance to the source as the seismic vessels sailed back and forth along the survey lines. The remaining fluctuations in time and also with depth of individual dataloggers, were likely attributable to changes in the sound propagation path from source to receiver, reflecting interactions of physical phenomena related to the change in sound speed with depth and bathymetry. A combination of reflection and refraction created shadow zones, with sound levels lower than expected from simple propagation models, and convergence zones with elevated sound pressure levels.

It is encouraging that the Nx2D broadband predictive model developed for the Environmental Impact Assessment did have an overall good correspondence with our measurements. However, the data were rather sparse, and it was therefore not possible to experimentally examine in sufficient detail a number of potentially important environmental factors, such as ice cover, water column sound ducting, geoacoustic model variability and error, and 3D effects in regions with large bathymetric gradients. The latter effect was studied by the WHOI group via computer 3D modeling, which showed significant deviations between the predictive modeling and the WHOI model in connection to particular bathymetric structures. Most pronounced was a higher than anticipated sound conduction along an undersea structure from the Anu and Napu blocks into Melville Bay. This calls for a discussion on how scenarios for predictive modeling should be chosen, i.e. to what degree they should focus on average or typical scenarios (location of sources and receivers, i.e. ships and animals) in contrast to focusing on extreme (worst case) conditions.

The limiting factor in all models is the quality and resolution of input data, and this was clearly the case for the Baffin Bay models. Prior to the actual surveys and measurements in 2012 there was very little hydrographical and bathymetric information available for the EIA-modeling. Comparison between sound speed profiles used in the EIA-models and the actual measurements made in 2012 showed that the magnitude of the sound speed minimum was underestimated in the EIA-models. Similarly, it was found that there were inconsistencies between bathymetric models used as model input parameters and the actual bathymetric data obtained by the seismic vessels during the surveys. This stresses the need for collection and dissemination of high-quality data on hydrography, bathymetry and sediment properties, as well as statistics on ice coverage and surface roughness (waves) prior to the impact assessment procedure.

The noise levels during the surveys in 2012 were clearly elevated to levels where effects on behavior of narwhals and belugas could be expected, based on the sparse information available from studies on impacts of other noise sources on these species. The sound exposure levels close to the seismic sources were also sufficiently high to likely cause temporary threshold shifts in narwhals, belugas and seals, where it must be expected that seals did experience TTS. To what degree animals may have habituated to the noise and/or found shelter in less exposed areas (within the ice, behind islands etc.) is unknown. This question must be answered by dedicated studies where the abundance and behavior of animals can be closely coupled to the sound exposure experienced by the animals. One option to elucidate this would be the use of passive acoustic monitoring of both noise and vocalizations of animals in areas known to be of importance to them. PAM can be supplemented with visual surveys to obtain data on group behavior and density. Ideally, the effect of seismic noise on narwhals (or another focal species) should be tested in a controlled exposure study, where animals purposefully are exposed to a known and realistic dose of seismic noise and their reactions quantified. Such data can for example be obtained by exposing animals equipped with dataloggers, logging acoustic behavior, dive pattern, roll, pitch, position, breathing, foraging behaviour and more (for example DTAGs (Madsen et al. 2006; Johnson et al. 2009).

The broad-band recordings made by JASCO for Shell proved to contain not just airgun pulses but also animal vocalizations. The ability of the instruments to record not only the very powerful sounds of sperm whales but also echolocation clicks from narwhals raises prospects for the feasibility of designing dedicated passive acoustic monitoring programs for narwhals, and possibly also belugas. The fact that the recording station within the narwhal reserve (Depotøerne) could pick up feeding buzzes from narwhals demonstrates that it is possible not only to assess abundance of animals, but also make inferences about their behavior with and without noise loads.

In conclusion, the measurements presented here have resulted in a significantly improved understanding of sound propagation conditions in the area and the limiting factors for predictive modeling of noise exposure.

9 Acknowledgements

This project was sponsored by the Bureau of Minerals and Petroleum, Greenland, through financial contributions from Shell Kanumas A/S, Maersk Oil Kalaallit Nunaat A/S and ConocoPhillips Global NVE Greenland LTD.

We would like to thank Shell, ConocoPhillips and Maersk for funding as well as their employees for very good collaboration during this project, in the field as well as at the planning stage. JASCO, Koen Broker, Mads Peter Heide-Jørgensen and Anders Mosbech are thanked for comments to an earlier version of this report. Mafalda de Freitas is thanked for her valuable comments and help editing the previous version of this report. Tenna Boye and Morten Heilmann and the crew of *R/V Sanna* are thanked for invaluable help in the field. The crew of *R/V Polarcus Asima*, *Polarcus Amani* and *Polarcus Samur* are thanked for good collaboration in the field.

10 References

Allen, R. C., and I. Keay. 2006. Bowhead whales in the Eastern Arctic, 1611-1911: Population reconstruction with historical whaling records. Enviro. Hist. 12:89-113.

Andersen, J. M., Y. F. Wiersma, G. Stenson, M. O. Hammill, and A. Rosing-Asvid. 2009. Movement Patterns of Hooded Seals (*Cystophora cristata*) in the Northwest Atlantic Ocean During the Post-Moult and Pre-Breeding Seasons. J. Northw. Atl. Fish Sci 42:1.

Annon. 2012. Passive Acoustic Monitoring: Measurement of Marine Sound Exposure Levels to Seismic Activity Baffin Bay 10th July – 19th September 2011. Cornell, Lab of Ornithology.

Au, W. W. L., R. H. Carder, D. A. Penner, and B. L. Scronce. 1985. Demonstration of adaptation in beluga whale echolocation signals. J Acoust Soc Am 77:726-730.

Austin, M., G. Warner, and M. A. 2012a. Underwater Sound Propagation Acoustics Technical Report: Maersk Oil Kalaallit Nunaat A/S 2012 3-D Seismic Program Block 9 (Tooq). Version 2.0. JASCO Applied Sciences.

Austin, M., G. Warner, and A. McCrodan. 2012b. Underwater Sound Propagation Acoustics Technical Report: ConocoPhillips 2012 2-D Seismic Program, Qamut Block. Version 2.0. JASCO Applied Sciences.

Austin, M. E., A. O. MacGillivray, and N. R. Chapman. 2012c. A coustic Transmission Loss Measurements in Queen Charlotte Basin. Canadian Acoustics 40:27-31.

Awbrey, F. T., J. A. Thomas, and R. A. Kastelein. 1988. Low-frequency underwater hearing sensitivity in belugas, *Delphinapterus leucas*. J Acoust Soc Am 84:2273-2275.

Ballard, K. A., and K. M. Kovacs. 1995. The acoustic repertoire of hooded seals (*Cystophora cristata*). Canadian Journal of Zoology 73:1362–1374.

Barlow, J. 1988. Harbor porpoise, Phocoena phocoena, abundance estimation for California, Oregon, and Washington. I. Ship surveys. Fishery Bulletin 86:417-432.

Beale, C., and P. Monaghan. 2004. Behavioural responses to human disturbance: a matter of choice? Animal Behaviour 68 1065–1069.

Blackwell, S. B., C. R. J. Greene, and W. J. Richardson. 2004. Drilling and operational sounds from an oil production island in the ice-covered Beaufort Sea. J Acoust Soc Am 116:3199-3211.

Blackwell, S. B., C. S. Nations, T. L. McDonald, C. R. Greene Jr., A. M. Thode, M. Guerra, and A. M. Macrander. 2013. Effects of airgun sounds on bowhead whale calling rates in the Alaskan Beaufort Sea. Mar Mamm Sci 29:E342–E365.

Boertmann, D., J. Tougaard, K. Johansen, and A. Mosbech. 2010. Guidelines to environmental impact assessment of seismic activities in Greenland waters. 2nd edition. NERI Technical Report

Born, E. W., M. P. Heide-Jørgensen, F. Larsen, and A. R. Martin. 1994. Abundance and stock composition of narwhals (*Monodon monoceros*) in Inglefield Bredning (NW Greenland). Meddelelser om Grønland, Bioscience 39:51.

Bradstreet, M. S. W. 1982. Occurrence, habitat use, and behavior of seabirds, marine mammals, and Arctic cod at the Pond Inlet ice edge. Arctic 3:28-40.

Brandt, M. J., C. Höschle, A. Diederichs, K. Betke, R. Mautuschek, S. Witte, and G. Nehls. 2012. Far-reaching effects of a seal scarer on harbour porpoises, *Phocoena phocoena*. Aquatic Conserv: Mar. Freshw. Ecosyst. 23:222-232.

Breitzke, M., O. Boebel, S. A. Naggar, W. Jokat, and B. Werner. 2008. Broad-band calibration of marine seismic sources used by R/V Polarstern for academic research in polar regions. Geophys. J. Int. 174:505–524.

Burns, J. J. 1981. Bearded seal - *Erignathus barbatus* Erxleben 1777. Pages 145-170 in S. H. Ridgway, and R. J. Harrison, editors. Handbook of Marine Mammals. Seals. Academic Press, New York.

DeRuiter, S. L., P. L. Tyack, Y.-T. Lin, A. E. Newhall, J. F. Lynch, and P. J. O. Miller. 2006. Modeling acoustic propagation of airgun array pulses recorded on tagged sperm whales. J Acoust Soc Am 120:4100–4114.

Diebold, J. B., M. Tolstoy, P. J. Barton, and S. P. Gulick. 2007. Propagation of Exploration Seismic Sources in Shallow Water. American Geophysical Union.

Dietz, R., and M. P. Heide-Jørgensen. 1995. Movements and swim speed of narwhals, Monodon monoceros, equipped with satellite transmitters in Melville bay, Northwest Greenland. Can J Zool 73:2106-2119.

Dietz, R., M. P. Heide-Jørgensen, P. Richard, J. Orr, K. Laidre, and H. C. Schmidt. 2008. Movements of narwhals (*Monodon monoceros*) from Admiralty Inlet monitored by satellite telemetry. Polar Biol 31:1295–1306.

Dietz, R., M. P. Heide-Jørgensen, P. R. Richard, and M. Acquarone. 2001. Summer and Fall Movements of Narwhals (*Monodon monoceros*) from Northeastern Baffin Island Towards Northern Davis Strait. Arctic 54:244-261.

Dyndo, M., D. M. Mariaiśniewska, L. Rojano-Doñate, and P. T. Madsen. In prep. Harbour porpoises react to low levels of high frequency vessel noise.

Evans, G. W., and D. Johnson. 2000. Stress and open-office noise. J.Appl.Psychol. 85:779-783.

Feit, M. D., and J. A. J. Fleck. 1978. Light propagation in graded-index fibers solution of nonlinear and variable coefficient wave equations,. J. A. , Appl. Opt. 17:3990–3998.

Finley, J. K., G. W. Miller, R. A. Davis, and C. R. Greene. 1990. Reactions of belugas, *Delphinapterus leucas*, and narwhals, *Monodon monoceros*, to ice-breaking ships in the Canadian high Arctic. Pages 97-117 in T. Smith, D. St. Aubin, and J. Geraci, editors. Advances in research on the beluga whale, Delphinapterus leacas. Canadian Bulletin of Fisheries and Aquatic Sciences.

Finneran, J. J., and C. E. Schlundt. 2013. Effects of fatiguing tone frequency on temporary threshold shift in bottlenose dolphins (Tursiops truncatus). J. Acoust. Soc. Am. 133:1819-1826.

Finneran, J. J., C. E. Schlundt, D. A. Carder, J. A. Clark, J. A. Young, J. B. Gaspin, and S. Ridgway. 2000. Auditory and behavioral responses of bottlenose dolphins (*Tursiops truncatus*) and a beluga whale (*Delphinapterus leucas*) to impulsive sounds resembling distant signatures of underwater explosions. J Acoust Soc Am 108:417-431.

Finneran, J. J., C. E. Schlundt, D. A. Carder, and S. H. Ridgway. 2002. Auditory filter shapes for the bottlenose dolphin (Tursiops truncatus) and white whales (Delphinapterus leucas) derived with notched noise. J Acoust Soc Am 112:322-328.

Gjertz, I., K. M. Kovacs, C. Lydersen, and Ø. Wiig. 2000. Movements and diving of bearded seal *(Erignathus barbatus)* mothers and pups during lactation and post-weaning. Polar Biol. 23:559-566.

Goold, J. C., and R. F. W. Coates. 2006. Near Source, High Frequency Air-Gun Signatures. IWC SC 58:1-7.

Goold, J. C., and P. J. Fish. 1998. Broadband spectra of seismic survey air-gun emissions, with reference to dolphin auditory thresholds. J Acoust Soc Am 103:2177-2184.

Gordon, J. C. D., D. Gillespie, J. Potter, A. Frantzis, M. P. Simmonds, R. Swift, and D. Thompson. 2004. A review of the effects of seismic survey on marine mammals. Marine Technology Society Journal 37:14-32.

Hammill, M. O., and G. B. Stenson. 2010. Abundance of Northwest Atlantic harp seals (1952-2010). DFO Can. Sci. Advis. Sec. Res. Doc.

Hardin, R. H., and F. D. Tappert. 1973. Applications of the split-step Fourier method to the numerical solution of nonlinear and variable coefficient wave equations. Siam Rev 15:423.

Harris, R. E., G. W. Miller, and W. J. Richardson. 2001. Seal repsonses to airgun sounds during summer seismic surveys in the Alaskan Beaufort Sea. Marine Mammals Science 17:795-812.

Heide-Jørgensen, M., R. Guldborg-Hansen, K. Westdal, R. Reeves, and A. Mosbech. 2012. Narwhals and seismic exploration: Is seismic noise increasing the risk of ice entrapments? Biological Conservation 158:50-54.

Heide-Jørgensen, M. P. 2004. Aerial digital photographic surveys of narwhals (*Monodon monoceros*) in Northwest Greenland. Mar Mamm Sci 20:246-261.

Heide-Jørgensen, M. P., and M. Acquarone. 2002. Size and trends of the bowhead whale, white whale and narwhal stocks wintering off West Greenland. Pages 191-210 in M. P. Heide-Jørgensen, and Ø. Wiig, editors. White whales in the North Atlantic and the Russian Arctic. NAMMCO Scientific Publications.

Heide-Jørgensen, M. P., and R. Dietz. 1995. Some characteristics of narwhal, *Monodon monoceros*, diving behaviour in Baffin Bay. Canadian Journal of Zoology 73:2120-2132.

Heide-Jørgensen, M. P., R. Dietz, K. L. Laidre, and P. Richard. 2002. Autumn Movements, Home Ranges, and Winter Density of Narwhals (*Monodon monoceros*) Tagged in Trenblay Sound, Baffin Island. Polar Biology 25:331-341.

Heide-Jørgensen, M. P., R. Dietz, K. L. Laidre, P. Richard, J. Orr, and H. C. Schmidt. 2003a. The migratory behaviour of narwhals (*Monodon monoceros*). Canadian Journal of Zoology 81:1298-1305.

Heide-Jørgensen, M. P., R. G. Hansen, S. Fossette, N. H. Nielsen, M. V. Jensen, and P. Hegelund. 2013a. Monitoring abundance and hunting of narwhals in Melville Bay during seismic surveys in 2012. GREENLAND INSTITUTE OF NATURAL RESOURCES.

Heide-Jørgensen, M. P., K. Laidre, D. Borchers, F. Samarrra, and H. Stern. 2007. Increasing abundance of bowhead whales in West Greenland. Biology Letters 3:577-580.

Heide-Jørgensen, M. P., K. Laidre, Ø. Wiig, M. V. Jensen, L. Dueck, H. C. Schmidt, and R. Hobbs. 2003b. From Greenland to Canada in ten days: Tracks of bowhead whales, *Balaena mysticetus*, across Baffin Bay. Arctic 56:21-31.

Heide-Jørgensen, M. P., and K. L. Laidre. 2010. Studies of bowhead whales in relation to the Disko West environmental assessment, 2009-2010. GINR report to DMU for the Disko West Environmental Forum. Greenland Institute of Natural Ressources (GINR).

Heide-Jørgensen, M. P., K. L. Laidre, M. L. Burt, D. L. Borchers, T. A. Marques, R. G. Hansen, M. Rasmussen, and S. Fossette. 2010a. Abundance of narwhals (*Monodon monoceros* L.) on the hunting grounds in Greenland. Mammalogy 95:1135-1151.

Heide-Jørgensen, M. P., K. L. Laidre, M. L. Burt, D. L. Borchers, T. A. Marques, R. G. Hansen, M. Rasmussen, and S. Fossette. 2010b. Abundance of narwhals (*Monodon monoceros*) on the hunting grounds in Greenland. Journal of Mammalogy 91:1135-1151.

Heide-Jørgensen, M. P., K. L. Laidre, M. V. Jensen, L. Dueck, and L. D. Postma. 2006. Dissolving stock discreteness with satellite tracking: Bowhead whales in Baffin Bay. Mar Mamm Sci 22:34-45.

Heide-Jørgensen, M. P., H. Lassen, J. Teilmann, and R. A. Davis. 1993. An index of the relative abundance of wintering belugas, Delphinapterus leucas, and narwhals, *Monodon monoceros*, of West Greenland. Canadian Journal of Fisheries and Aquatic Sciences 50:2323-2335.

Heide-Jørgensen, M. P., and R. R. Reeves. 1996. Evidence of a decline in beluga, *Delphinapterus leucas*, abundance off West Greenland. ICES J. Mar. Sci. 53:61-72.

Heide-Jørgensen, M. P., P. R. Richard, R. Dietz, and K. L. Laidre. 2013b. A metapopulation model for Canadian and West Greenland narwhals. Animal Conservation 16:331-343.

Hildebrand, J. 2009. Anthropogenic and natural sources of ambient noise in the ocean. Mar Ecol Prog Ser 395:5-20.

ICES. 2006. Report of the Working Group on ICES/NAFO Working Group on Harp and Hooded Seals (WGHARP). ICES, ICES Headquarters.

InuplanA/S, and GolderAssociates. 2012. Maersk Oil Kalaallit Nunaat A/S 2012 Program Block 9 (Tooq) 3D-Seismic Survey and Hydrographic Survey Environmental Impact Assessment. Page 103. Inuplan A/S Golder Associates.

IUCN. 2010. 2010 IUCN Red List of Threatened Species.

IWC. 2008. The 2008 Scientific Committee report. Cetacean Res. Manage 10.

IWC. 2012. The 2012 Scientific Committee report. Cetacean Res. Manage 10.

Jakobsson, M., L. A. Mayer, B. Coakley, J. A. Dowdeswell, S. Forbes, B. Fridman, H. Hodnesdal, R. Noormets, R. Pedersen, M. Rebesco, H.-W. Schenke, Y. Zarayskaya, D. Accettella, A. Armstrong, R. M. Anderson, P. Bienhoff, A. Camerlenghi, I. Church, M. Edwards, J. V. Gardner, J. K. Hall, B. Hell, O. B. Hestvik, Y. Kristoffersen, C. Marcussen, R. Mohammad, D. Mosher, S. V. Nghiem, M. T. Pedrosa, P. G. Travaglini, and P. Weatherall. 2012. The International Bathymetric Chart of the Arctic Ocean (IBCAO) Version 3.0. Geophysical Research Letters 39:1-6.

Katsnelson, B. G., V. G. Petnikov, and J. F. Lynch 2012. Fundamentals of shallow water acoustics. Springer.

Klishin, V. O., V. V. Popov, and A. Y. Supin. 2000. Hearing capabilities of a beluga whale, Delphinapterus leucas. Aquatic Mammals 26:212–228.

Koski, W. R., and R. A. Davis. 1994. Distribution and numbers of narwhals *(Monodon monoceros)* in Baffin Bay and Davis Strait. Meddelelser om Grønland, Bioscience 39:15-40.

Koski, W. R., D. W. Funk, D. S. Ireland, C. Lyons, K. Christie, A. M. Macrander, and S. B. Blackwell. 2009. An Update on Feeding by Bowhead Whales near an Offshore Seismic Survey in the Central Beaufort Sea. IWC SC 61.

Koski, W. R., and S. R. Johnson. 1987. Behavioral studies and aerial photogrammetry. in Annon., editor. Responses of bowhead whales to an offshore drilling operation in the Alaskan Beaufort Sea, autumn 1986. LGL Ltd. and Greeneridge Sciences inc., Anchorage, AK.

Kyhn, L. A., and D. Boertmann. 2011. Cairn's ansøgning om "3D-seismic survey in Pitu, 2011". Danish Centre for Environmnet and Energy. Bureau of Minerals and Petroleum, Greenland, Roskilde, Denmark.

Kyhn, L. A., D. Boertmann, J. Tougaard, J. K., and A. Mosbech. 2011. Guidelines to environmental impact assessment of seismic activities in Greenland waters. Page 62.

Lacey, C., S. Travers, and M. Unwin. 2013. Marine mammal and seabird observer's report during 2D seismic survey in Qamut Block, Eastern Baffin Bay, Greenland for ConocoPhillips. RPS Energy.

Laidre, K. L., and M. P. Heide-Jørgensen. 2011. Life in the lead: Extreme densities of narwhals *(Monodon monoceros*) in the offshore pack ice. Marine Ecology Progress Series 423:269-278.

Lawson, J. 2005. Overviews: Beluga whale and noise. Page 53. J JCNB/NAMMCO 2005. Joint Scientific Meeting Nuuk, Greenland, October 13-16, 2005. J JCNB/NAMMCO.

Lee, K., K. Azetsu-Scott, S. E. Cobanli, J. Dalziel, S. Niven, G. Wohlgeschaffen, and P. Yeats. 2005. Overview of potential impacts from produced water discharges in Atlantic Canada. Pages 319-342 in A. e. al., editor. Offshore oil and gas environmental effects monitoring. Approaches and technologies. Batelle Press, Columbus, Ohio.

LGL, and Grontmij. Shell Kanumas A/S Environmental Impact Assessment 2012 Anu-Napu 3D Seismic Survey in Baffin Bay Blocks 5 and 8. Page 157. LGL Ltd. environmental research associates. Grontmij A/S.

Lin, Y. T. 2013. A higher-order tangent linear parabolic-equation solution of three-dimensional sound propagation. J. Acoust. Soc. Am. 134.

MacGillivray, A. O. 2006. An Acoustic Modelling Study of Seismic Airgun Noise in Queen Charlotte Basin. Page 98. University of Victoria, Victoria, BC.

Madsen, P. T., M. Johnson, P. J. O. Miller, N. Aguilar Soto, and P. L. Tyack. 2006. Quantitative measures of air-gun pulses recorded on sperm whales (*Physeter macrocephalus*) using acoustic tags during controlled exposure experiments. J Acoust Soc Am 120:2366–2379.

Martin, M., and J. MacDonnel. 2013. Shell Greenland Acoustic Monitoring of 2012 3-D Seismic Surveys in Baffin Bay. Page 124. JASCO.

Matthews, M.-N. R. 2012. Underwater Sound Propagation from an Airgun Array in Baffin Bay: Shell 2012 Seismic Surveys in Baffin Bay Blocks 5 & 8. Version 3.0. . JASCO Applied Sciences.

Medwin, H., and C. S. Clay 1998. Fundamentals of Acoustic Oceanography. Academic, San Diego.

Miller, G. W., V. D. Moulton, R. A. Davis, M. Holst, P. Millman, and A. MacGillivray. 2005. Monitoring seismic effects on marine mammals – southeastern Marine Mammal Noise Exposure Criteria 491 Beaufort Sea, 2001-2002. Pages 511-542 in S. L. Armsworthy, P. J. Cranford, and K. Lee, editors. Offshore oil and gas environmental effects monitoring: Approaches and technologies. Battelle Press, Columbus, OH.

Miller, L., J. Pristed, B. Møhl, and A. Surlykke. 1995. The click sounds of narwhals (*Monodon monoceros*) in Inglefield Bay, North West Greenland. Mar Mamm Sci 11:491-502.

Mosbech, A., K. L. Anthonsen, A. Blyth, D. Boertmann, E. Buch, D. Cake, L. Grøndahl, K. Q. Hansen, H. Kapel, S. Nielsen, N. Nielsen, F. Von Platen, S. Potter, and M. Rasch. 2000. Environmental Oil Spill Sensitivity Atlas for the West Greenland Coastal Zone. Page 279. Ministry of Environment and Energy, The Danish Energy Agency.

Muench, R. D. 1971. The physical oceanography of the northern Baffin Bay region. The Baffin Bay-North water project. Page 150. Project Scientific report Number 1. Arctic Institute of North America, Montreal.

Møhl, B. 1981. Masking effects of noise; their distribution in time an d space in N. M. Peterson, editor. The question of sound from ice-breaker operations: Proceedings from a workshop (Arctic Pilot Projrect, Calgary, Aberta).

Nowacek, D. P., L. H. Thorne, D. W. Johnston, and P. L. Tyack. 2007a. Responses of cetaceans to anthropogenic noise. Mammal Review 37:81-115.

Nowacek, D. P., L. H. Thorne, D. W. Johnston, and P. L. Tyack. 2007b. Responses of cetaceans to anthropogenic noise Mammal Review 37:81-115.

NunaOil, and G. Associates. 2012. ConocoPhillips Global NVE Greenland LTD. 2012 Program Block 2 (Qamut) Environmental Impact Assessment. Page 101. NunaOil Golder Associates.

O'Corry-Crowe, G. M. 2002. Beluga whale in W. Perrin, B. Würzig, and J. G. M. Thewissen, editors. Encyclopedia of Marine mammals. Academic Press, San Diego.

Olesiuk, P. F., L. M. Nichol, M. J. Snowden, and J. K. B. Ford. 2002. Effect of the sound generated by an acoustic harassment device on the relative abundance and distribution of harbour porpoises (*Phocoena phocoena*) in the Retreat Passage, British Columbia. Mar Mamm Sci 18:843-862.

Passchier-Vermeer, W., and W. F. Passchier. 2000. Noise Exposure and Public Health. Environmental Health perspectives 108:123-131.

Peerin, W. 2002. Encyclopedia of Marine Mammals. Academic Press.

Perry, J., V. Allen, and C. Jones. 2011. Capricorn Greenland Preliminary Environmental Impact Assessment, 3D Seismic Survey Programme for Pitu, Offshore West Greenland. Page 172. Environmental Resources Management Limited.

Pirotta, E., K. L. Brookes, I. M. Graham, and P. M. Thompson. 2014. Variation in harbour porpoise activity in response to seismic survey noise. Biological Letters 10:20131090.

Popov, V. V., A. A. Supin, V. V. Rozhnov, D. I. Nechaev, and E. V. Sysueva. 2014. The limits of applicability of the sound exposure level (SEL) metric to temporal threshold shifts (TTS) in beluga whales, *Delphinapterus leucas*. The Journal of Experimental Biology 217:1804-1810.

Rayleigh, L. 1876. On the application of the Principle of Reciprocity to acoustics. Proc. Roy. Soc. A 25:118-122.

Richardson, W. J., J. Greene, C. R., C. I. Malme, and D. H. Thomson 1995. Marine Mammals and Noise. Academic, San Diego, CA.

Richardson, W. R., G. W. Miller, and C. R. Greene. 1999. Displacement of migrating bowhead whales by sounds from seismic surveys in shallow waters of the Beaufort Sea J Acoust Soc Am 106:2291.

Risch, D., C. W. Clark, P. J. Corkeron, A. Elepfandt, K. M. Kovacs, C. Lydersen, I. Stirling, and S. M. Van Parijs. 2007. Vocalizations of male bearded seals, *Erignathus barbatus:* classification and geographical variation. Animal Behaviour 73:747-762.

Rolland, R. M., S. E. Parks, K. E. Hunt, M. Castellote, P. Corkeron, D. P. Nowacek, S. K. Wasser, and S. D. Kraus. 2012. Evidence that ship noise increases stress in right whales. Proc.R.Soc.Lond.B. 279:2363–2368.

Romano, T. A., M. J. Keogh, C. Kelly, P. Feng, L. Berk, C. E. Schlundt, D. A. Carder, and J. J. Finneran. 2004. Anthropogenic sound and marine mammal health: measures of the nervous and immune systems before and after intense sound exposure. Can. J. Fish. Aquat. Sci. 61:1124–1134.

Serrano, A. 2001. New underwater and aerial vocalizations of captive harp seals (*Pagophilus groenlandicus*). Can J Zool 79:75–81.

Simon, M. J. 2010. The sounds of whales and their food: Baleen whales, their foraging behaviour, ecology and habitat use in an arctic habitat Page 171. Aarhus University, Greenland Institute of Natural Resources, Nuuk, Greenland, Aarhus, Denmark.

Southall, B. L., A. E. Bowles, W. T. Ellison, J. J. Finneran, R. L. Gentry, C. R. Greene, D. Kastak, D. R. Ketten, J. H. Miller, P. E. Nachtigall, W. J. Richardson, J. A. Thomas, and P. L. Tyack. 2007. Marine Mammal Noise Exposure Criteria: Initial Scientific Recommendations. Aquatic Mammals 33:411-521.

Stenson, G. B., R. A. Myers, H. I. Ni, and W. G. Warren. 1996. Pup production of hooded seals *(Cystophora cristata*) in the Northwest Atlantic. NAFO Sci.Coun. Studies 26:105-114.

Stirling, I. 1973. Vocalizations in the ringed seal (*Phoca hispida)*. Journal of Fisheries Board of Canada 30:1592-1594.

Tang, C. L. C., C. K. Ross, T. Yao, B. Petrie, B. M. DeTracey, and E. Dunlap. 2004. The circulation, water masses and sea-ice of Baffin Bay. Page 60. Bedford Institute of Oceanography, Ocean Sciences Division, Fisheries and Oceans Canada, Dartmouth, Nova Scotia, Canada.

Tappert, F. D. 1977. The parabolic equation method, in Wave Propagation and Underwater Acoustics. Pages 224–286 in J. B. Keller, and J. Papadakis, editors. Lecture Notes in Physics. Springer-Verlag, New York.

Taylor, M. K., S. Akeeagok, D. Andriashek, W. Barbour, E. W. Born, W. Calvert, H. D. Cluff, S. Ferguson, J. Laake, A. Rosing-Asvid, I. Stirling, and F. Messier. 2001. Delineating Canadian and Greenland polar bear (*Ursus maritimus*) populations by cluster analysis of movements. Can J Zool 79:690-709.

Terhune, J., and K. Ronald. 1972. The harp seal, Pagophilus groenlandicus (Erxleben, 1777). III. The underwater audiogram. Can J Zool 50:565-569.

Terhune, J., and K. Ronald. 1975. Underwater hearing sensitivity of two ringed seals (*Pusa hispida*). Canadian Journal of Zoology 53:227-231.

Terhune, J. M., and K. Ronald. 1973. Some hooded seal -Cystophora cristata! sounds in March. Can. J. Zool. 51:319–321.

Tervo, O. M., S. E. Parks, and L. A. Miller. 2009. Seasonal changes in the vocal behavior of bowhead whales *(Balaena mysticetus*) in Disko Bay, Western-Greenland. J Acoust Soc Am 126:1570–1580.

Tolstoy, M., J. Diebold, L. Doermann, S. Nooner, and S. C. Webb. 2009. Broadband calibration of the R/V Marcus G. Langseth four-string seismic sources. Geochem. Geophys. Geosyst. 10:1-5.

Tolstoy, M., J. B. Diebold, S. C. Webb, D. R. Bohnenstiehl, E. Chapp, R. C. Holmes, and M. Rawson. 2004. Broadband calibration of R//V Ewing seismic sources. Geophysical Research Letters 31:1-4.

Tougaard, J., J. Carstensen, and J. Teilmann. 2009. Pile driving zone of responsiveness extends beyond 20 km for harbour porpoises *(Phocoena phocoena* (L.)). J Acoust Soc Am 126:11-14.

Tougaard, J., L. A. Kyhn, A. Mosbech, M. Malene, M. P. Heide-Jørgensen, and F. Ugarte. 2012. Regarding marine mammals and proposed seismic surveys in Baffin Bay 2012. Pages 1-13. Danish Centre for Environment and Energy, Greenland Institute of Natural Ressources, Roskilde.

Turl, C. W., D. J. Skaar, and A. W.W.L. 1991. The echolocation ability of the beluga (*Delphinapterus leucas*) to detect targets in clutter. J Acoust Soc Am 89:896-901.

Tyack, P. L. 2008. Implications for marine mammals of large-scale changes in the marine acoustic environment. Journal of Mammalogy 89:549-558.

Valeur, H. V., C. Hansen, K. Q. Hansen, L. Rasmussen, and N. Thingvad. 1996. Weather, sea and ice conditions in eastern Baffin Bay, offshore Northwest Greenland. A review. . DMI Technical Report No. 96-12.

Vanman, C., and J. Durinck. 2012. 3D Marine Seismic Survey Polarcus Anu (Block 5) & Napu (Block 8) Licence Blocks Greenland, Melville Bay Area. Marine Mammal and Seabird Report rev.01 17th July – 20th October 2012. South West Surveys.

Wenz, G. M. 1962. Acoustic Ambient Noise in the Ocean: Spectra and Sources. J Acoust Soc Am 34:1936-1956.

Appendix A. Environmental Data

A.1 CTD Data and Sound Speed Profiles

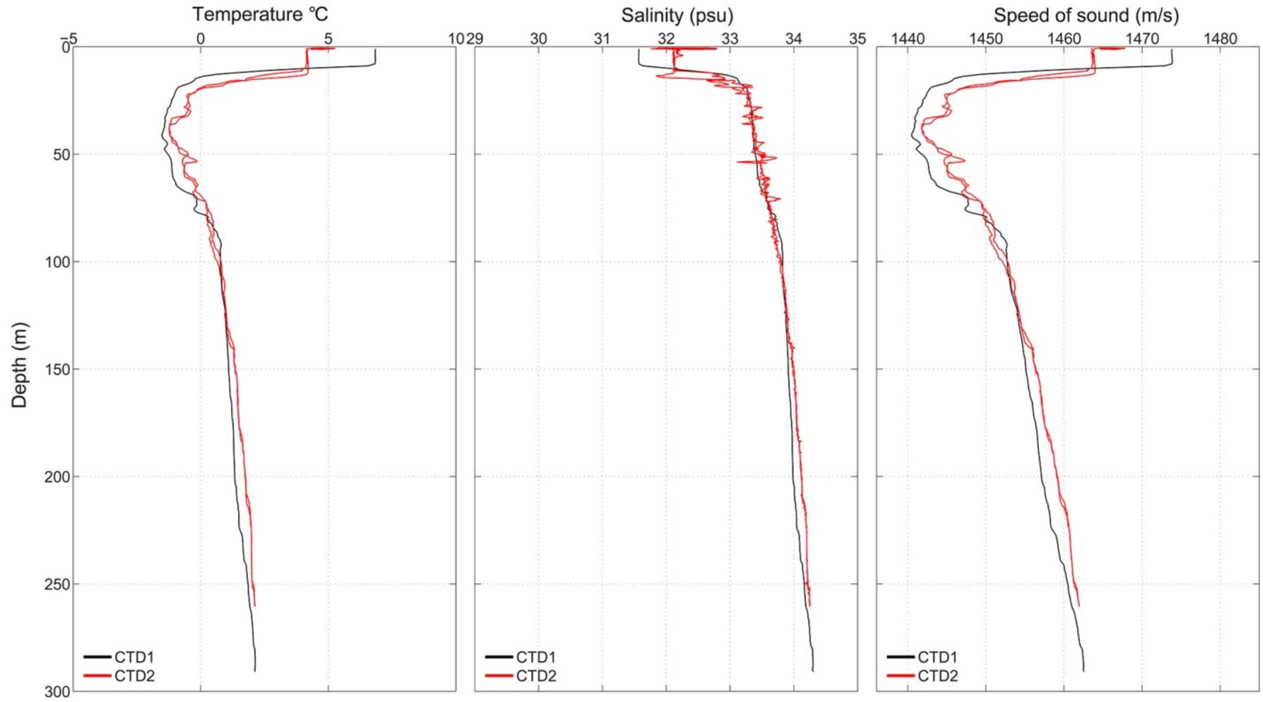

Figure A1. CTD and sound speed profiles obtained during deployment (CTD1) and recovery (CTD2) of the mooring at the Savissivik site. For details on the exact time and location of the measurements see **Table 7** and **Figure 21**.

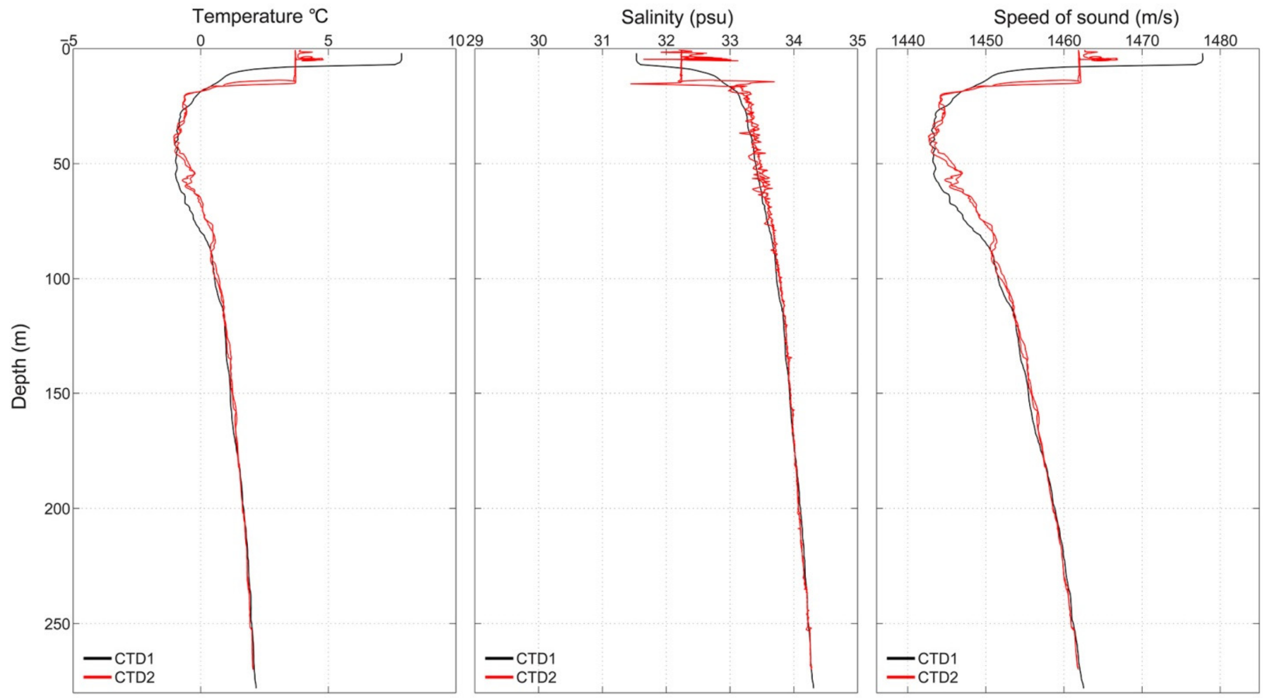

Figure A2. CTD and sound speed profiles obtained during deployment (CTD1) and recovery (CTD2) of the mooring at the Qamut N site. For details on the exact time and location of the measurements see **Table 7** and **Figure 21**.

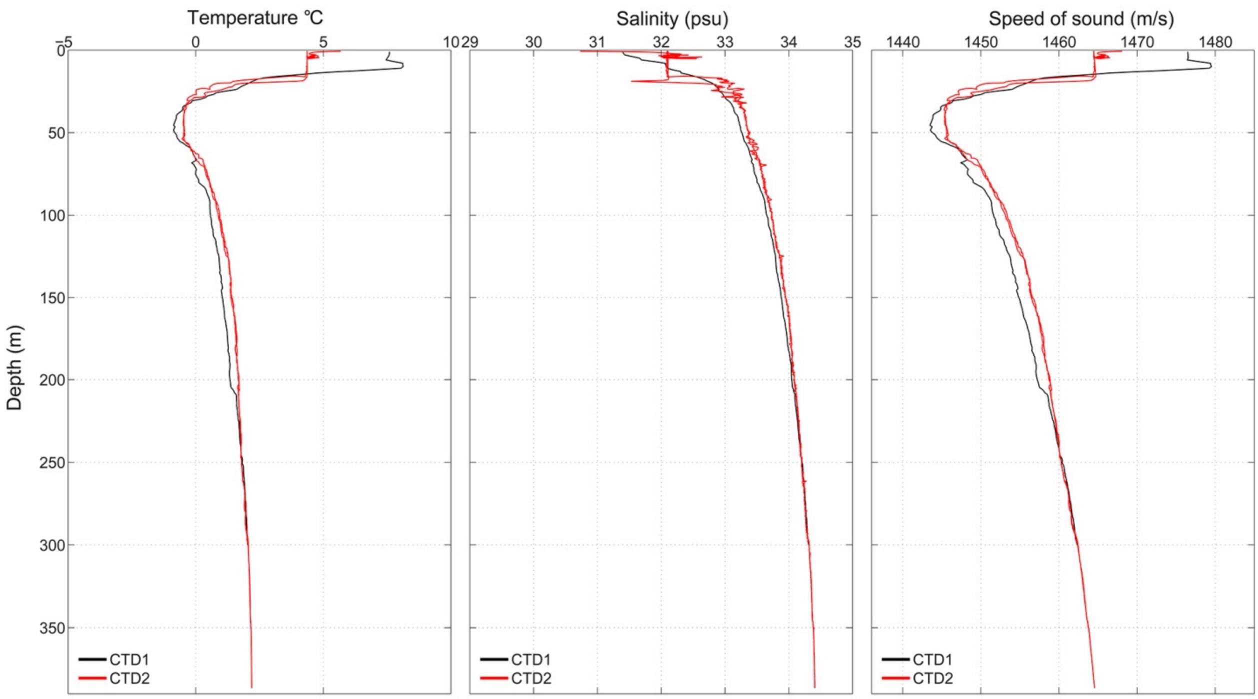

Figure A3. CTD and sound speed profiles obtained during deployment (CTD1) and recovery (CTD2) of the mooring at the Melville site. For details on the exact time and location of the measurements see **Table 7** and **Figure 21**.

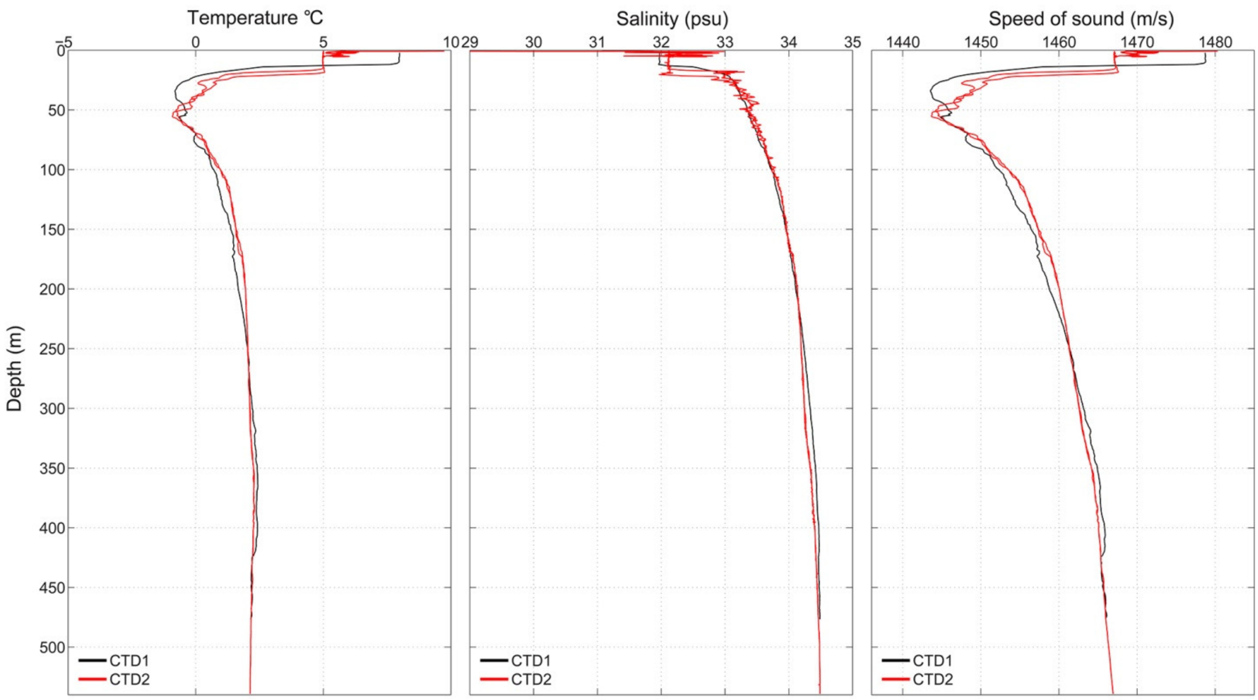

Figure A4. CTD and sound speed profiles obtained during deployment (CTD1) and recovery (CTD2) of the mooring at the Pitu N site. For details on the exact time and location of the measurements see **Table 7** and **Figure 21**.

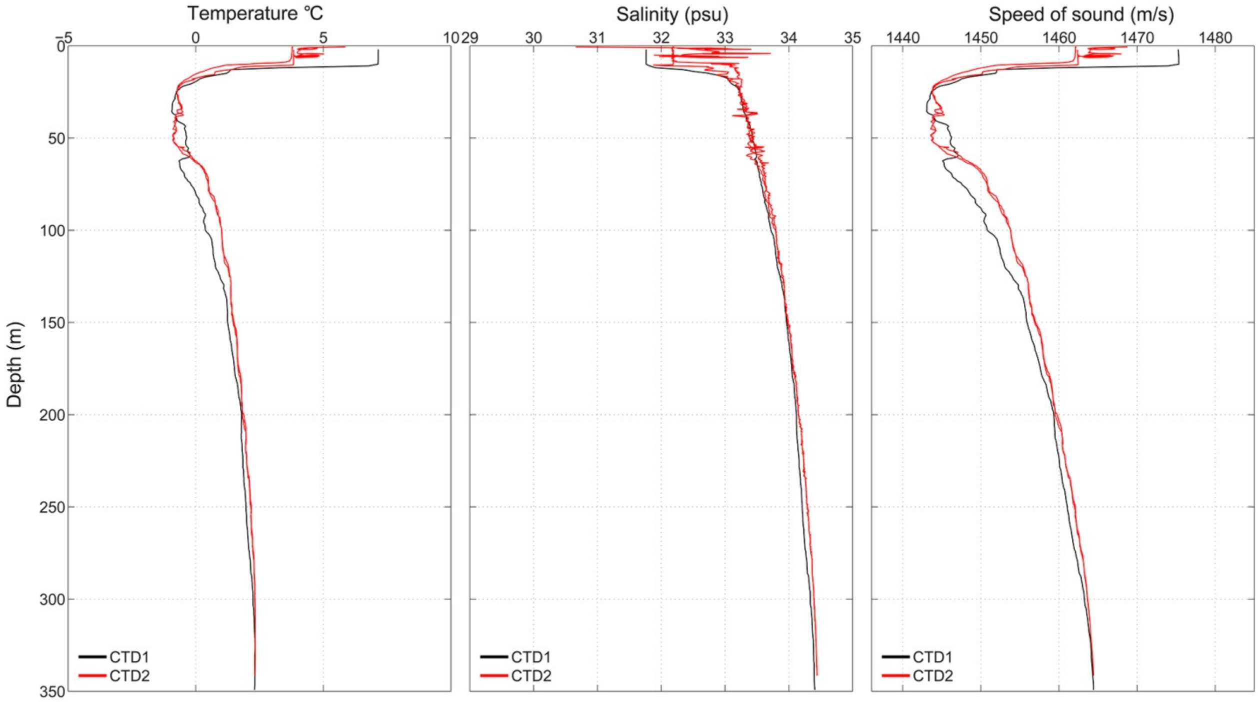

Figure A5. CTD and sound speed profiles obtained during deployment (CTD1) and recovery (CTD2) of the mooring at the Qamut S site. For details on the exact time and location of the measurements see **Table 7** and **Figure 21**.

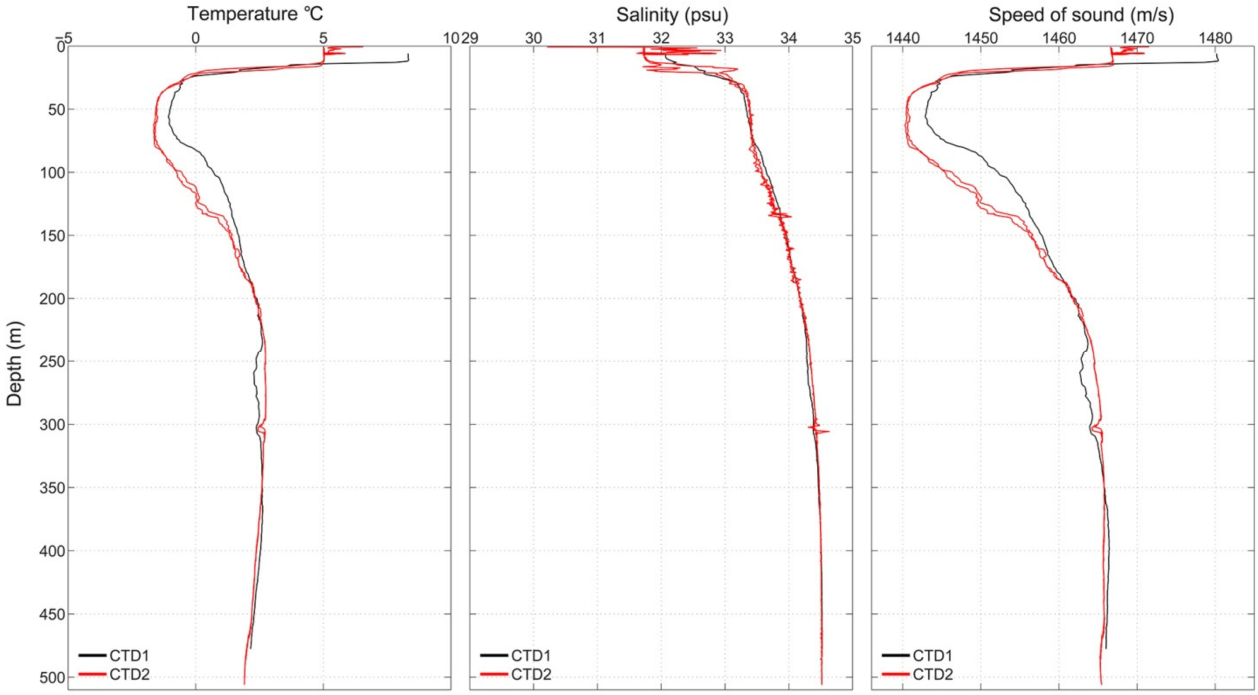

Figure A6. CTD and sound speed profiles obtained during deployment (CTD1) and recovery (CTD2) of the mooring at the Pitu S site. For details on the exact time and location of the measurements see **Table 7** and **Figure 21**.

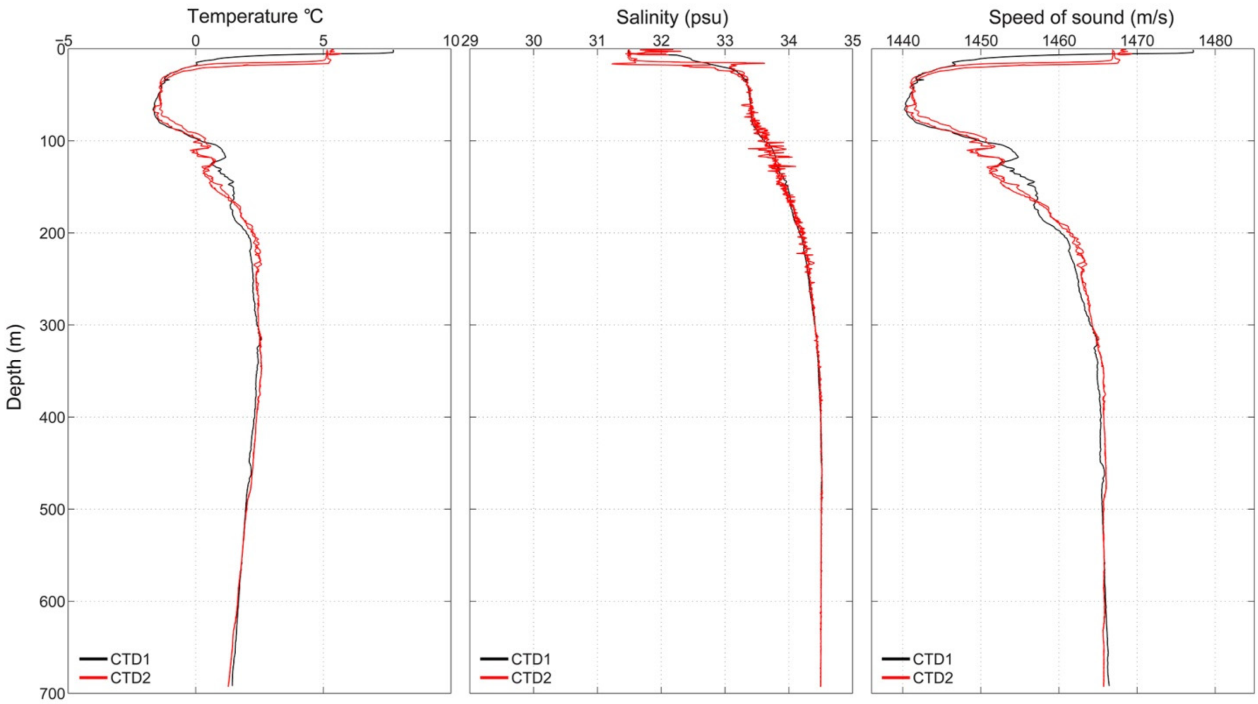

Figure A7. CTD and sound speed profiles obtained during deployment (CTD1) and recovery (CTD2) of the mooring at the Amu site. For details on the exact time and location of the measurements see **Table 7** and **Figure 21**.

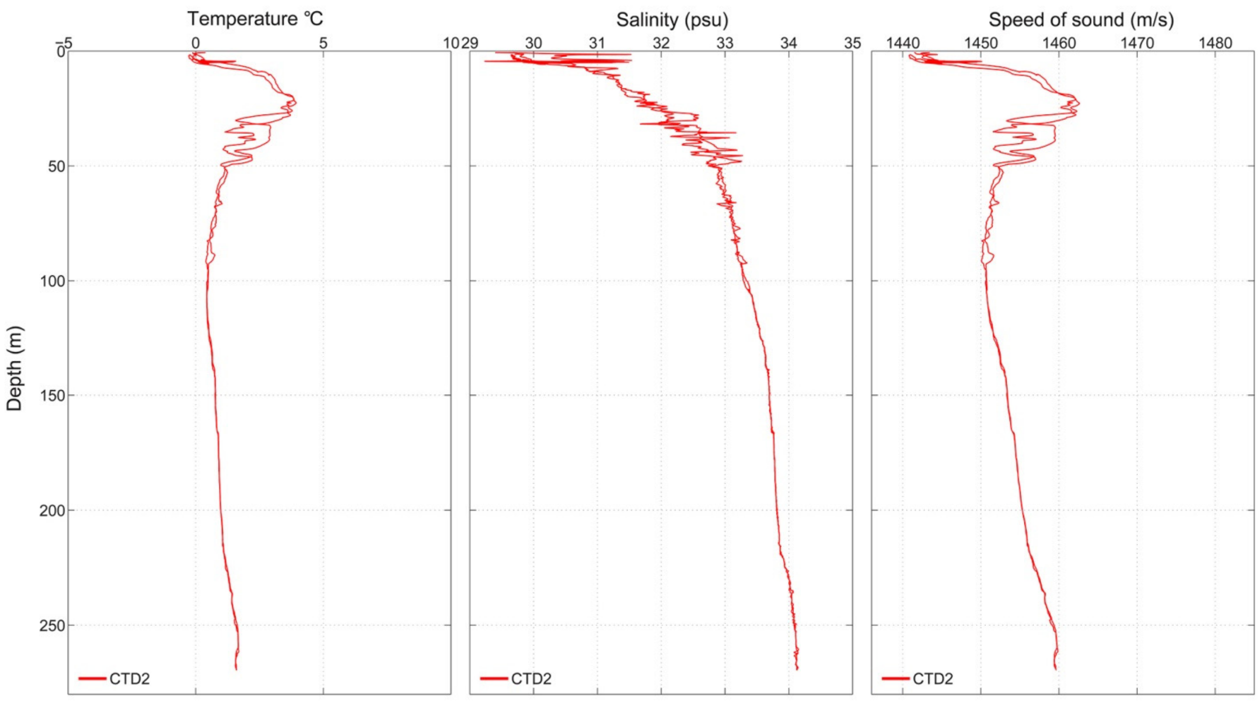

Figure A8. CTD and sound speed profiles obtained at Depotøerne, a location inside the Narval Reserve in the vicinity of Shell's sound monitoring station BB4. For details on the exact time and location of the measurements see **Table 7** and **Figure 21**.

A.2 Bathymetry

A.2.1 Shell

Figure A9. Deviation between the bathymetry models available prior to study and depths measured during seismic surveys in the Anu and Napu License Areas. Top panel: the bathymetry model used by JASCO for the pre-season modelling (SRTM30+ v7.0) sampled at Shell's airgun firing lines. Middle panel: depths measured by Shell's vessels at their firing positions. Bottom panel: difference between the bathymetry model and the measured depths.

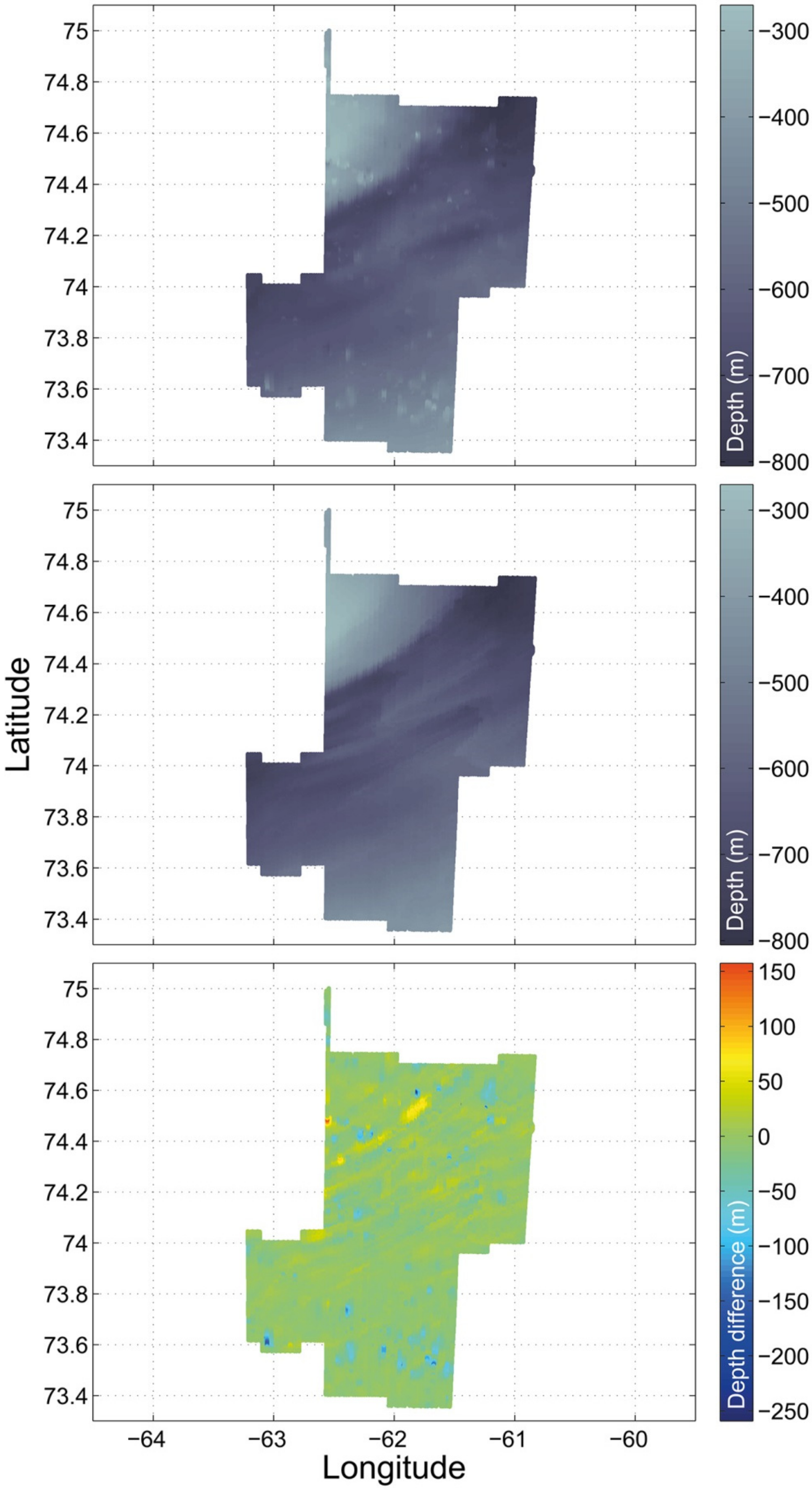

Figure A10. Deviation between the bathymetry models available prior to study and depths measured during seismic surveys in the Anu and Napu License Areas. Top panel: the bathymetry model used by WHOI (IBCAO v3.0 30 arc second, Jakobsson et al. 2012) sampled at Shell's airgun firing lines. Middle panel: depths measured by Shell's vessels at their firing positions. Bottom panel: difference between the bathymetry model and the measured depths.

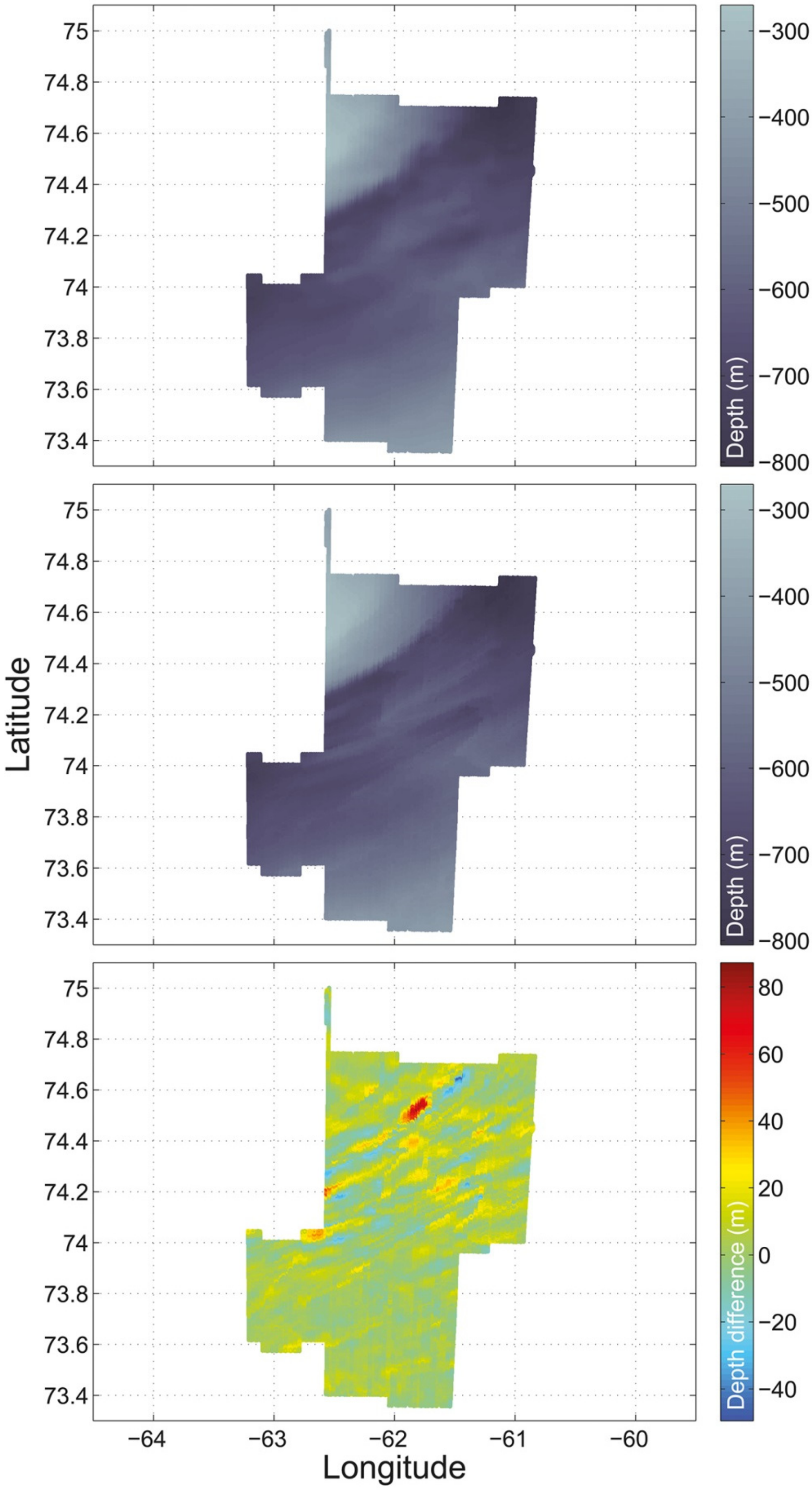

A.2.3 Maersk

Figure A11. Deviation between the bathymetry models available prior to study and depths measured during seismic surveys in the Tooq License Area. Top panel: the bathymetry model used by JASCO for the pre-season modelling (SRTM30+ v7.0) sampled at the Maersk airgun firing lines. Middle panel: depths measured by the Maersk vessel at its firing positions. Bottom panel: difference between the bathymetry model and the measured depths.

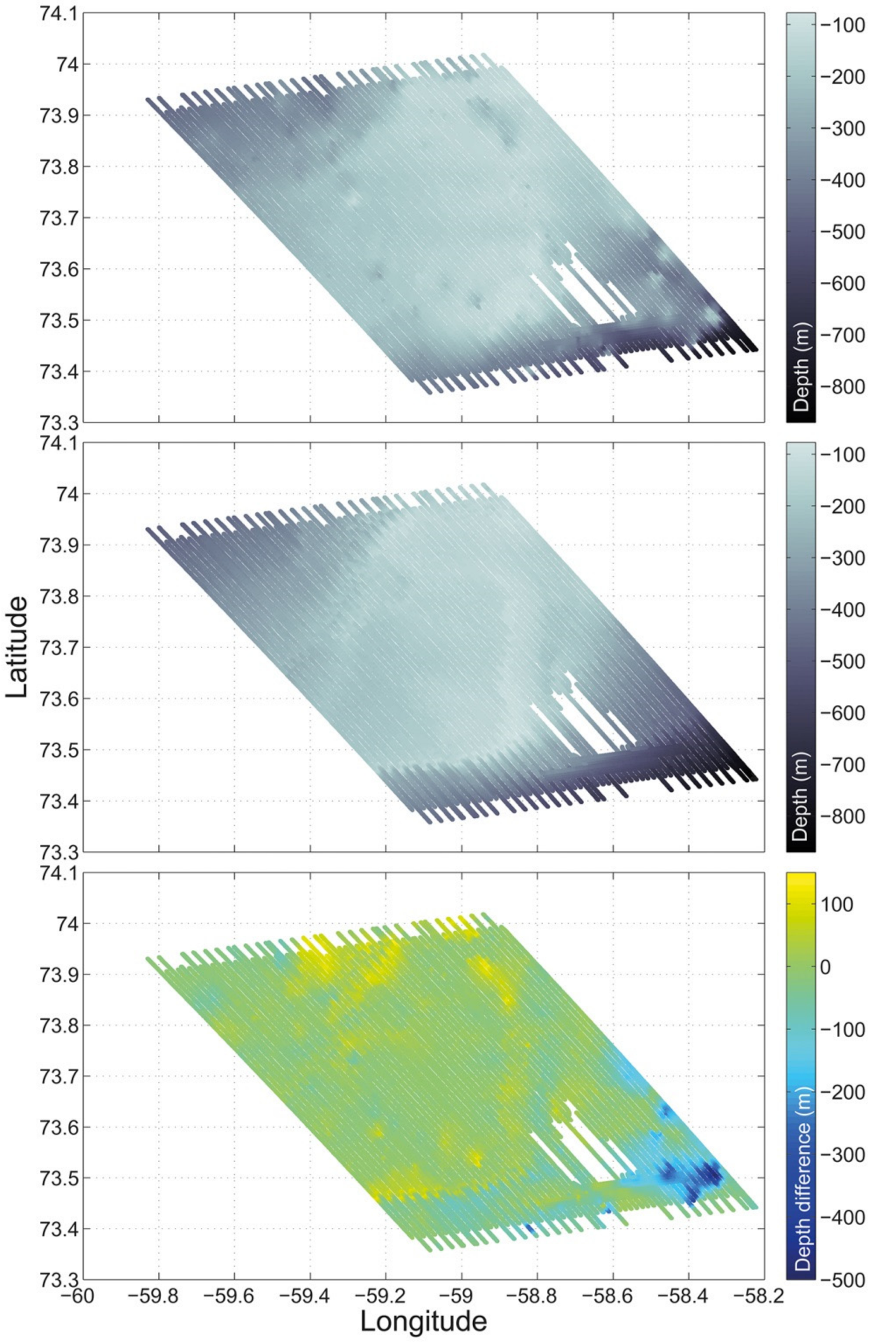

Figure A12. Deviation between the bathymetry models available prior to study and depths measured during seismic surveys in the Tooq License Area. Top panel: the bathymetry model used by WHOI (IBCAO v3.0 30 arc second, Jakobsson et al. 2012) sampled at the Maersk airgun firing lines. Middle panel: depths measured by the Maersk vessel at its firing positions. Bottom panel: difference between the bathymetry model and the measured depths.

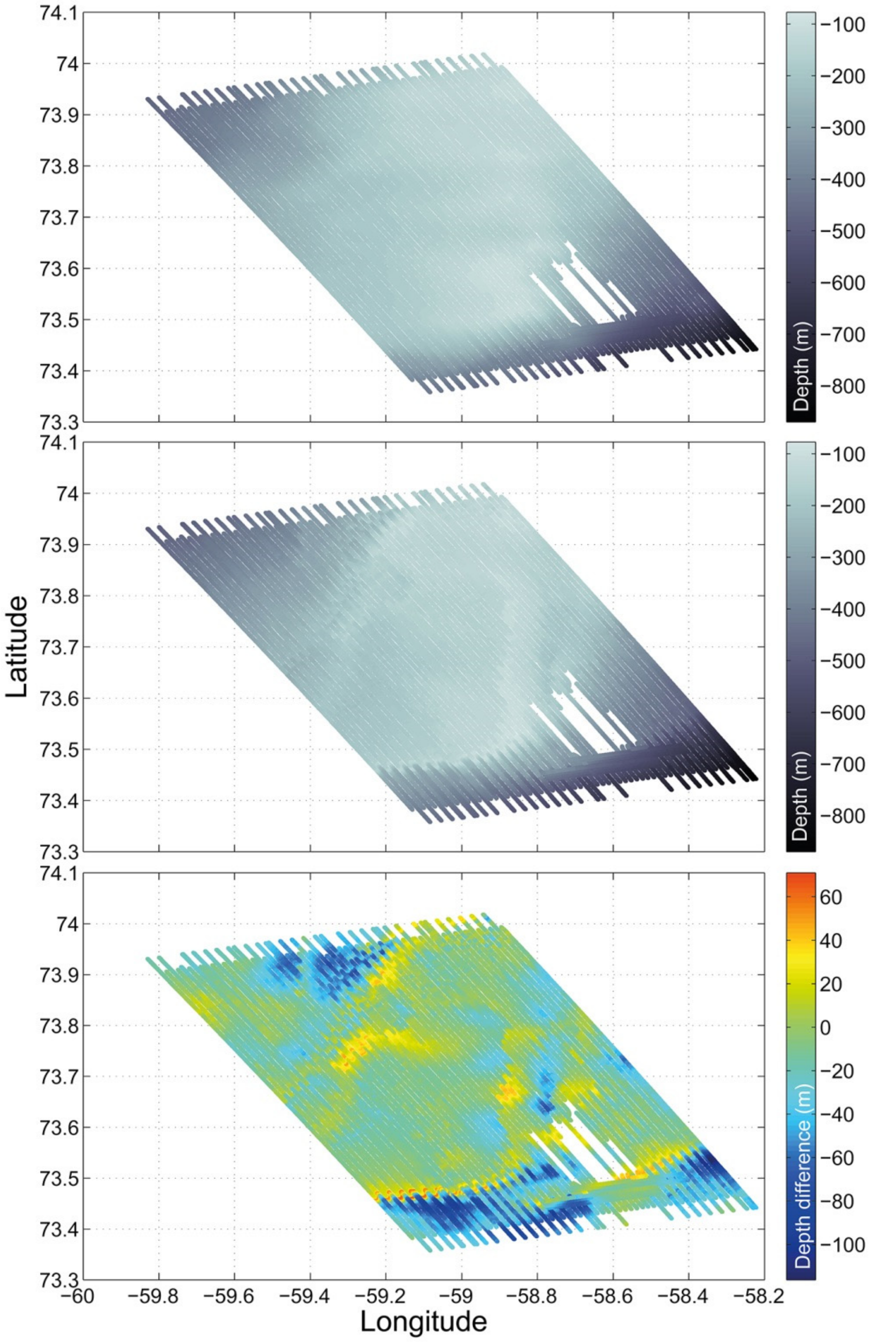

A.3 Temperature

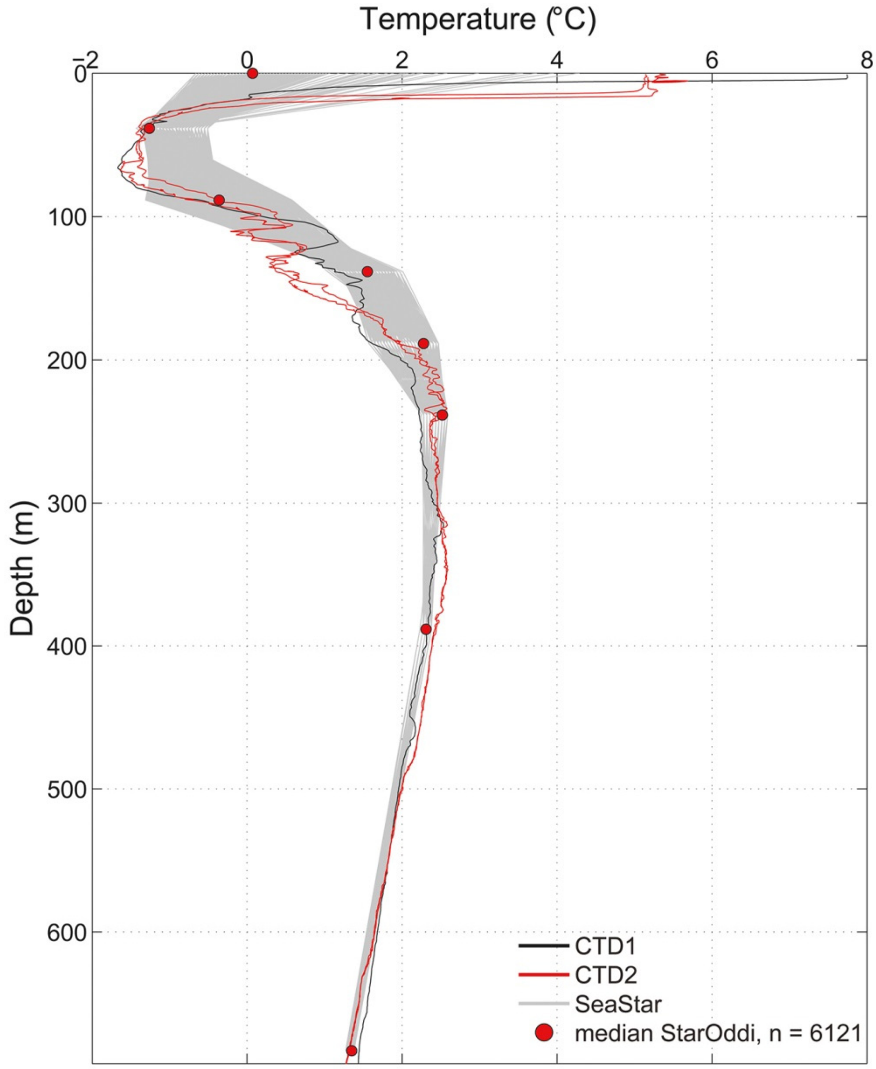

Figure A13. Temperature profiles at the location of the Amu mooring showing typical temperature variations in the 700-m-deep water column. The profiles are overlaid with data from Star-Oddi sensors that were attached to the mooring at eight depths. For the top sensor, only data collected prior to detachment are presented. The overall stability of the deeper profile, as well as the variability of the surface mixed layer in between deployment (CTD1) and recovery (CTD2) phases are to be noted.

Appendix B. WHOI manuscript outline: "Issues in predicting transmission loss for marine mammal exposure in the context of Baffin Bay."

Content of the manuscript

An outline of this report material is as follows:

a. Introduction
b. Variability in the surface mixed layer
c. Uncertainty in transmission loss (TL) due to uncertainty in the bottom geoacoustic model
d. 3D acoustics effects – guideline when and where to examine them
e. Uncertainty in bottom bathymetry.

Introduction

While there is now almost a century of background in underwater acoustics, and a vast literature in the area, the fact remains that our ability to estimate transmission loss (TL) in many areas of the world's oceans remains imperfect. Coastal areas in the Marginal Ice Zone (MIZ) are particularly hard to quantify, and in these following sections, we discuss some of the inherent problems, concentrating specifically on the recent study of seismic exploration sound transmission in Baffin Bay. The intent of this is not to criticize the Baffin Bay environmental impact assessment (EIA) process, calculations, or methods, which are generally "state of the art" and carefully considered. Rather, we wish to point out areas that still present difficulties to underwater acousticians and discuss how and where the state of the art might be advanced to better meet environmental protection needs in acoustically complex areas.

Four main topics will be of interest. They are: 1) variability in the surface mixed layer, 2) uncertainty in TL due to uncertainty in the bottom geoacoustic model, 3) uncertainty in TL due to bathymetric uncertainty, and 4) 3D acoustic effects, and when and where to examine them. In future work, we will also examine: 1) uncertainty in TL due to rough sea surface and ice scattering effects and 2) experimental sampling issues for calibrating TL measurements.

Variability in the surface mixed layer, and it's effects on transmission loss (TL)

Seismic sources are designed so that the airgun arrays beam most of their energy straight down into the bottom, and that this energy is primarily of lower frequency (the 10-200 Hz being typical.) However, due to being pulsed sources, these airgun arrays inevitably must emit some higher frequency energy, with a rolloff of ~6dB per octave being typical from their peak frequency response. This higher frequency energy does not just travel downwards, but also leaks out sideways due to "repeat major lobes" or "grating lobes." These lobes are due to the source array elements being spaced so as to provide Nyquist sampling at the peak frequency (and thus lower frequencies as well), but not at the higher frequencies. These grating lobes allow the higher frequency energy to propagate sideways (primarily in the water column) as opposed to just downward.

Seismic airgun sources are also typically used near the surface (~7m depth) to facilitate towing and to avoid needing to worry about pressure compensation effects. However, due to the temperature and salinity (and thus soundspeed) fluctuating considerably in the surface mixed layer (ML) in an MIZ region like Baffin Bay, this means that the source array can see large differences in soundspeed at its depth. This is important, as we will see, in that it determines whether the acoustic propagation is water column ducted (a good propagation condition for longer range propagation) or bottom limited (a poorer propagation condition for longer range propagation, as energy is lost to bottom interaction).

Bottom limiting occurs when the soundspeed at the source depth is equal to the soundspeed at the bottom, and there are no regions in between those depths that have a higher soundspeed. This means that a ray launched at 0 degrees grazing angle will just interact with the bottom at 0 degrees, by Snell's Law. This implies that all rays will bottom interact, and thus lose considerable energy that way. If the soundspeed at the bottom is any higher than at the surface, however, some of the sound will be refracted away from the bottom, i.e. water column ducted.

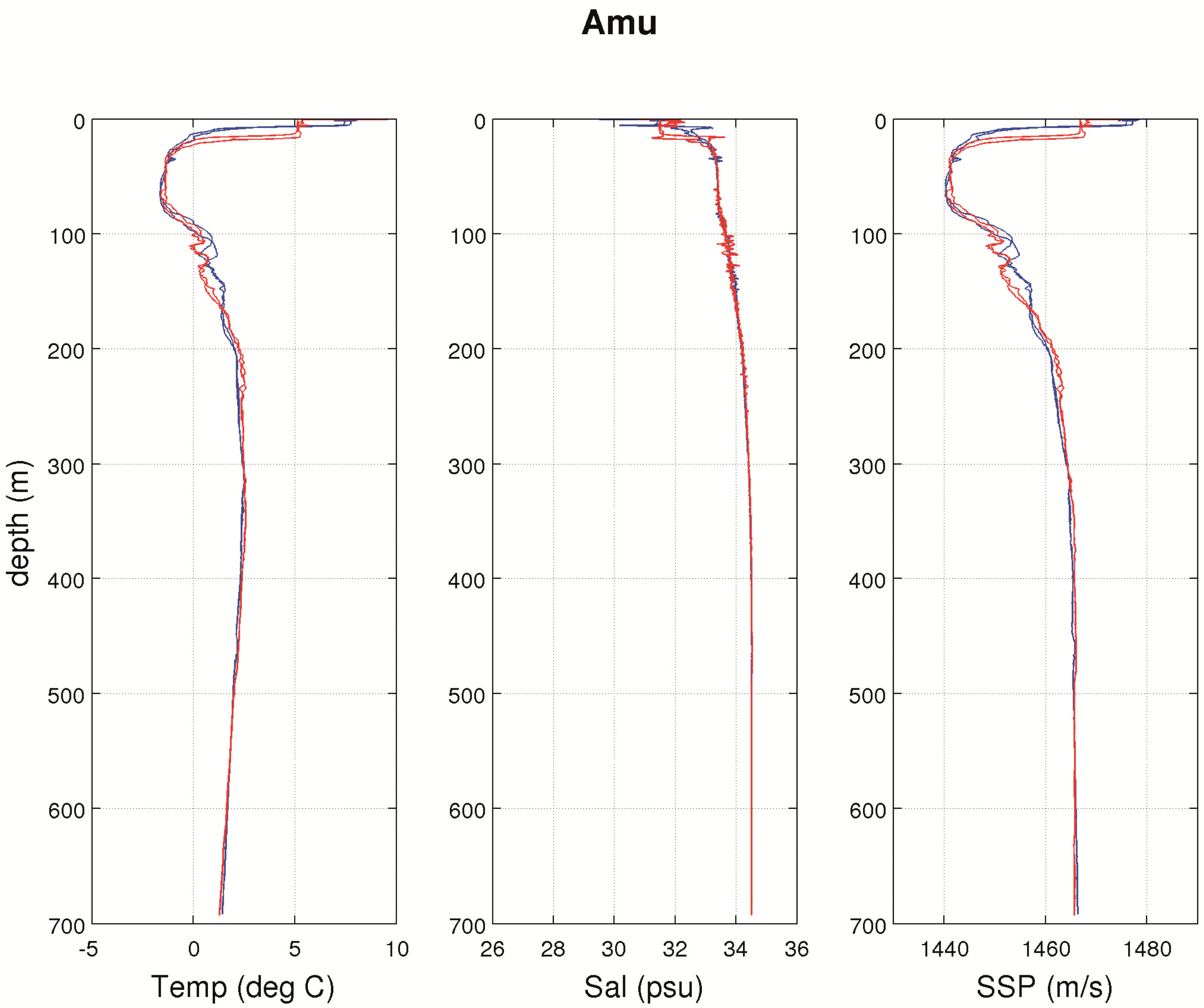

Figure B1. The T, S (and thus c) versus P (depth) profiles from the CTD's taken during the mooring deployment and recovery phases of the experiment at site Amu. Red is deployment, and blue is recovery.

The bottom limiting depth can be determined by examining the soundspeed profile at the source. The T, S (and thus c) versus P profiles from the CTD's taken during the experiment are the key profiles to consider for this acoustics work, since they have the level of vertical resolution we need (order 1-2 meters). We show representative CTD profiles from the Baffin Bat deployment and recovery in **Figure B1**. We should mention that these profiles are "typical" for the region at that time of year; the basic features stay more or less the same over the whole Bay during the month of the experiment.

The temperature profile is intriguing, in that it shows that warmer summer water (greater than 0 degrees) has been mixed down below 100-150 m over the years, but that colder water, due to exposure to the very cold recent winter surface temperatures, predominates above 150 m, thus creating a strong "cold water subsurface duct." The salinity profile is also important, as the near surface freshening (by ~ 3 psu) contributes about -4 m/s to the near surface soundspeed. This slightly counters the near surface heating effects on sound speed, and makes the physical explanation of the profile somewhat more complicated.

A more detailed look at the temperature profiles over the top 200 m of the water column, which shows the moored sensor profiles as well as the deployment and recovery CTD's, is shown in **Figure B2**. This figure demonstrates that the general profile shape was indeed stable over the deployment, but also that the near surface mixed layer changes appreciably in between the mooring deployments and recoveries. This was due to a wind event mixing the warmer surface waters down.

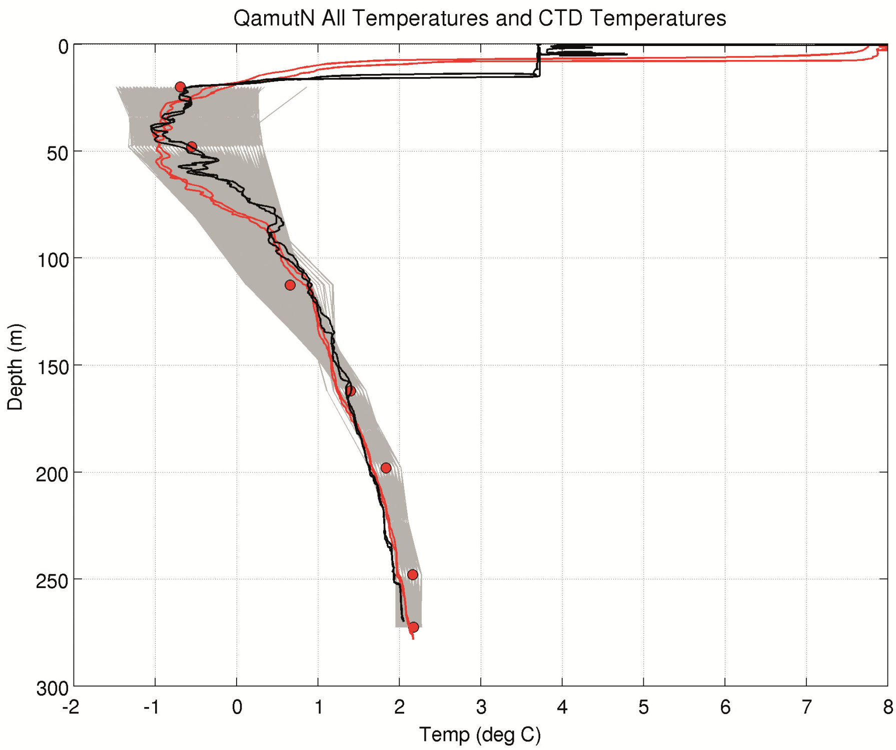

Figure B2. Temperature profiles during the Baffin Bay deployment, emphasizing the top 300 m of the water column. The overall stability of the deeper profile, as well as the variability of the surface ML in between deployment and recovery phases are to be noted.

In the figure above, the surface water is quite warm at deployment (~8 deg C) and has a layer thickness of ~6.5 m, just above the acoustic source. This, in the high frequency ray approximation, will not cause the rays to be bottom limited, as the source is just outside the warm layer. The HF acoustic energy will be ducted in the cold water duct in this case. (Low frequency sound is not as affected by the layer, as we will see.) After a few days, a strong wind event mixes the warm surface water downward, and we then see an ~15m thick layer, but diluted down to 4 deg C temperature. The source is now in the duct, and as its temperature (and thus soundspeed) is greater than that at the bottom (270m for this case), the high frequency sound will be bottom limited.

Given the soundspeed curves above, we can now create a “bottom-limiting” curve for the region, which is shown below in **Figure B3**.

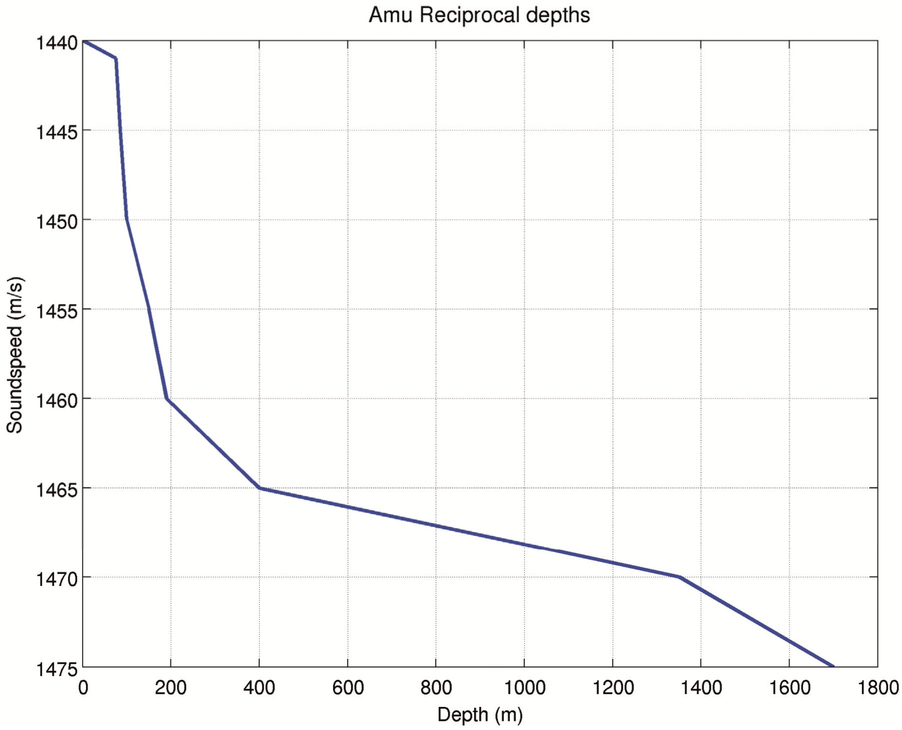

Figure B3. Bottom limiting depth versus soundspeed curve from the Amu CTC profile. Note that 1460 m/sec corresponds to 200 m, the most likely water depth to be encountered in the area where the sources were deployed.

If we now look at what the depth of the Bay was at the locations where the source arrays were towed, we get the distribution seen in **Figure B4**. We note that the most likely water depth is at 200m and that the preponderance of the depths are less than 350m. Thus, if the source is placed in 1460 m/sec soundspeed (or higher) water, the propagation is likely to be bottom limited. Thus the bottom is expected to play an important role in reducing horizontal sound propagation intensity levels in the region.

The implications of bottom limiting due to the surface mixed layer for acoustics are very frequency dependent. To show this, we look at two examples of propagation using the deployment and recovery profiles, i.e. source above and below the mixed layer. A low frequency (125 Hz) and a high frequency (1000 Hz) will be examined for each case.

Figure B4. Distribution of depths seen at the source positions during the Baffin Bay experiment. Peak is just below 200m depth.

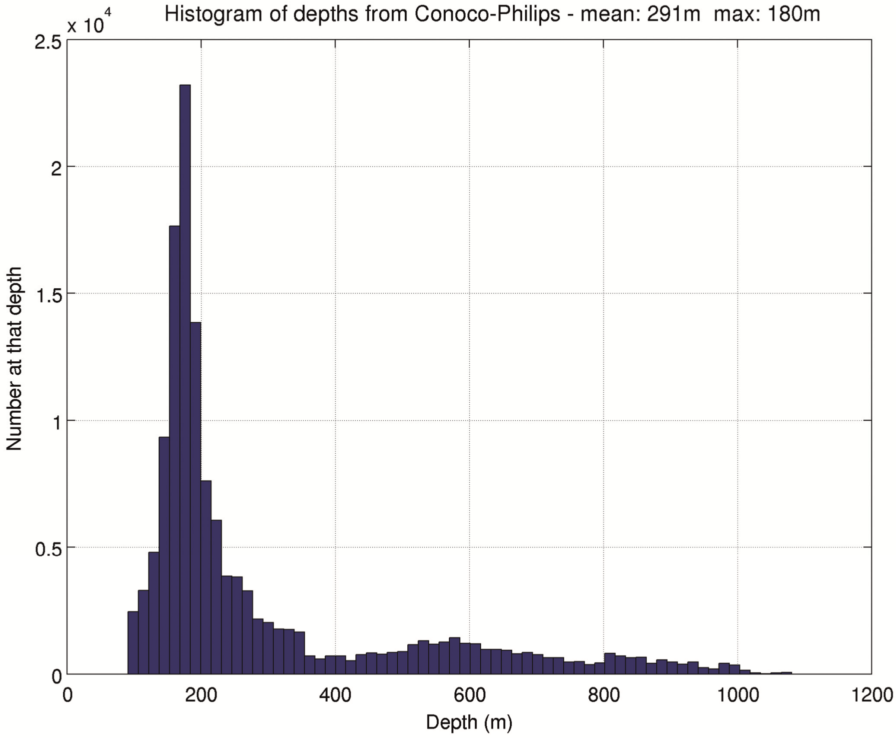

In the **Figure B5** panels, we see the source just underneath the ML, so that in the high frequency limit, the sound energy should be ducted in the cold water duct. At 125 Hz, the 6m wavelength is larger than the ~1/2 meter separating the source depth and the bottom of the ML, and so it "sees/samples" the ML to a good extent. This leads to one seeing bottom limiting, with only a faint hint of surface ducted energy. At 1000 Hz, the acoustic wavelength is 1.5 m, and so the source really feels it is below the ML. We thus see appreciable ducting of this higher frequency sound by the cold water duct.

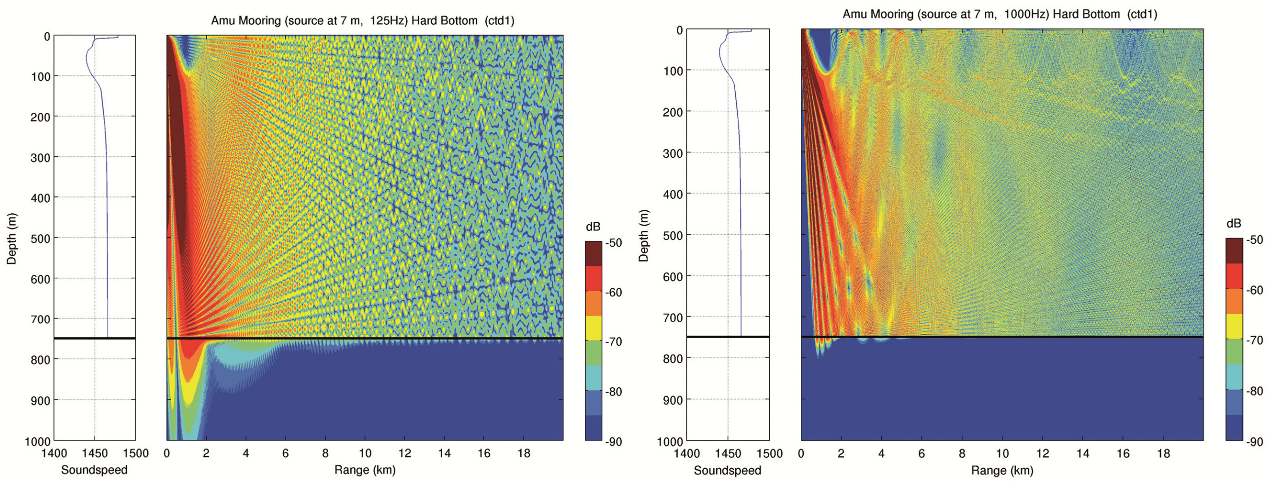

Figure B5. Acoustic intensity as calculated by a parabolic equation for source at 7 m depth and bottom of mixed layer at 6.5 m, i.e. source below the ML. The left hand panel is 125 Hz propagation, and the right hand panel is 1000 Hz propagation.

In the **Figure B6** case, the ML has been mixed down by a wind event to 15 m, and the acoustic source now feels it is comfortably "in the ML" for low and high frequencies. In both cases, the sound propagation is bottom limited. Intriguingly, one sees some high near surface intensities in the high frequency plot, but these are just convergence zone focusing effects for the various multipaths.

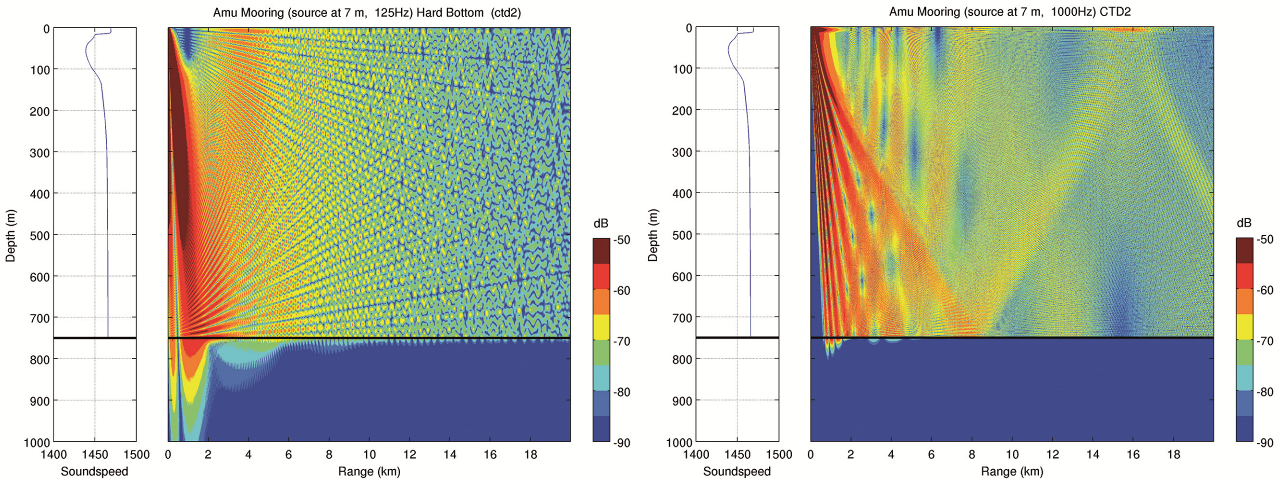

Figure B6. Acoustic intensity as calculated by a parabolic equation for source at 7 m depth and bottom of mixed layer at 15 m, i.e. source below the ML. The left hand panel is 125 Hz propagation, and the right hand panel is 1000 Hz propagation.

Aside from the ducting caused by the ML pushing sound into the ducting directly below (a summer condition), there is seasonal near surface ducting. This can be examined looking at the seasonal climatology of soundspeed, as shown in **Figure B7**, which is from NODC (National Ocean Data Center) climatology.

Figure B7. NODC seasonal climatology for Baffin Bay soundspeed.

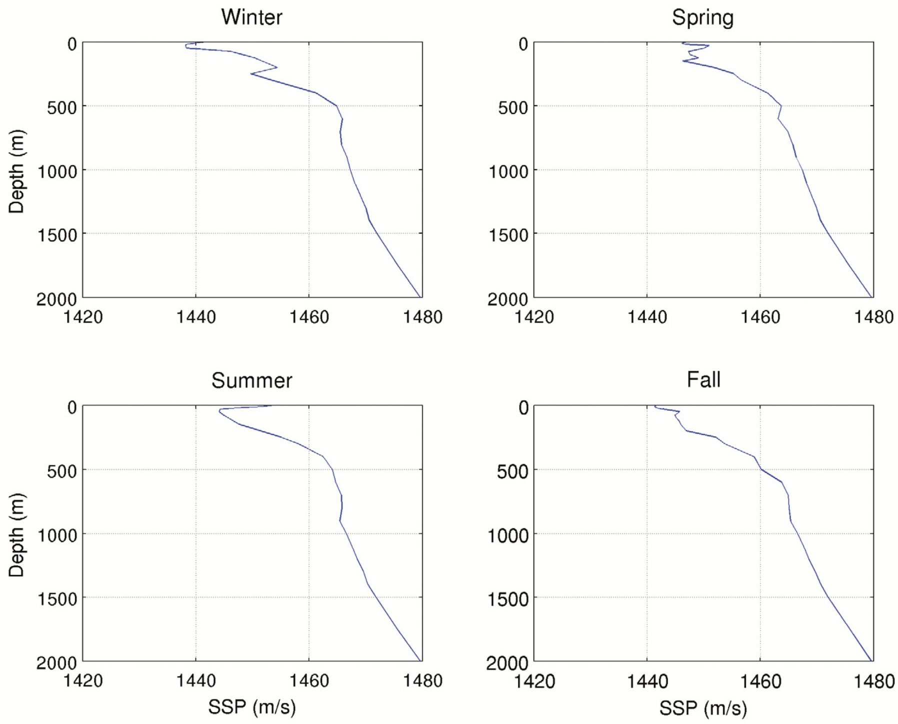

The fall and winter climatologies show the sound channel axis being near the surface, so that one has strong surface ducting for these seasons, which is typical of polar regions. However, in the spring, the duct from 1-200m appears again, due to surface warming and wind mixing. In the summer, we see the profile type previously discussed, i.e. one with a relatively warm surface layer that can cause bottom limiting. In terms of seismic surveying, winter and fall conditions are very harsh due to wind, waves and ice cover, so that one is not likely to have to worry about sound being ducted in the upper water column where the animals are likely to be. However, the spring condition and parts of the summer condition can very possibly produce strong near surface ducting of sound, which can have a greater impact on marine mammals. Thus it is important to know the near surface (0-200m) soundspeed profile when doing seismic work, as the ducting conditions can significantly affect propagation ranges and intensities.

The question thus arises: How do we predict the near surface ML, or do we just measure it and use precautions if a ducted condition exists? There is an extensive literature on predicting the ML, but it is not an easy oceanographic problem, and it takes both some historical data (for initialization) and a model with a lot of environmental input (wind, waves, insolation, cloudiness, etc.) to make any sensible predictions. And even so, most of the current models are 1D (z direction), and do not include lateral variability of the environment. Moreover, modeling the ML near the MIZ is not a current capability, though progress is being made. Thus, our guess is that forecasting the ML is not a profitable direction, at least in the context of typical seismic exploration activities and EIA's.

However, measuring the upper 200m of the ocean with a CTD is very simple for any ship, and this is actually the best, highest resolution data anyway. Moreover, this can be done at multiple sites and times during a survey. Our recommendation would be to include this as a routine activity during exploration cruises, which would allow one to better keep track of the propagation condition for mitigation purposes.

Uncertainty in TL due to uncertainty in the bottom geoacoustic model

One of the most usual uncertainties in shallow water acoustics (which is what we are dealing with in Baffin Bay, as the animals are largely on the continental shelf) is the exact geoacoustic model for the seabed. The compressional wave speed and attenuation, as well as the density, are very often known poorly (we can ignore shear in the sediments in many cases).This in turn leads to large uncertainties in TL, particularly for sound propagating upslope.

We will first look at what the Baffin Bay EIA bottom estimates are, and how they are arrived at. This is done to try to quantify error, and also to suggest possible improvements in methods. We will then study the sensitivity of the error in TL to the error in the bottom geoacoustic model parameters. By modifying the well-known Rayleigh reflection coefficient to include attenuation, we can study directly how changes in the geoacoustic parameters translate into changes in TL. This in turn informs us as to how much error in estimating the geoacoustic parameters is tolerable, given that one insists on a certain measurement accuracy for TL. The mathematics for this will be presented here. Simple cases will be shown, both for general scenarios and for

Baffin Bay in particular, in later work, as the illness of one of the authors precluded its inclusion in the present report.

The Shell seismic data we have so far indicates a "fast" (sand or harder material) bottom, with a water/sediment interface soundspeed of ~1700-1800 m/s, as shown in **Figure B8** below. The seismic profiles give us some idea of the soundspeed profile in the bottom, though far deeper than we need and with less vertical resolution of the near surface sediments. Indeed, most seismic surveys disregard near surface data, as the interest is in deeper oil and gas deposits. And even if there were more interest, the most energy going through the bottom is at the peak frequency of the airgun response, which is ~100 Hz. This gives, using a crude 1λ criterion for vertical resolution, about a 15m resolution length in the vertical direction in the sediments. The higher frequencies we are interested in also need bottom resolution on the order of their wavelengths for good accuracy in estimating bottom loss, and thus TL. Thus, the lower frequency seismic data, while useful, is not fully adequate for the horizontal direction TL studies we are pursuing.

Figure B8. Baffin Bay bottom soundspeed profile from Shell data - 6 profiles averaged and smoothed.

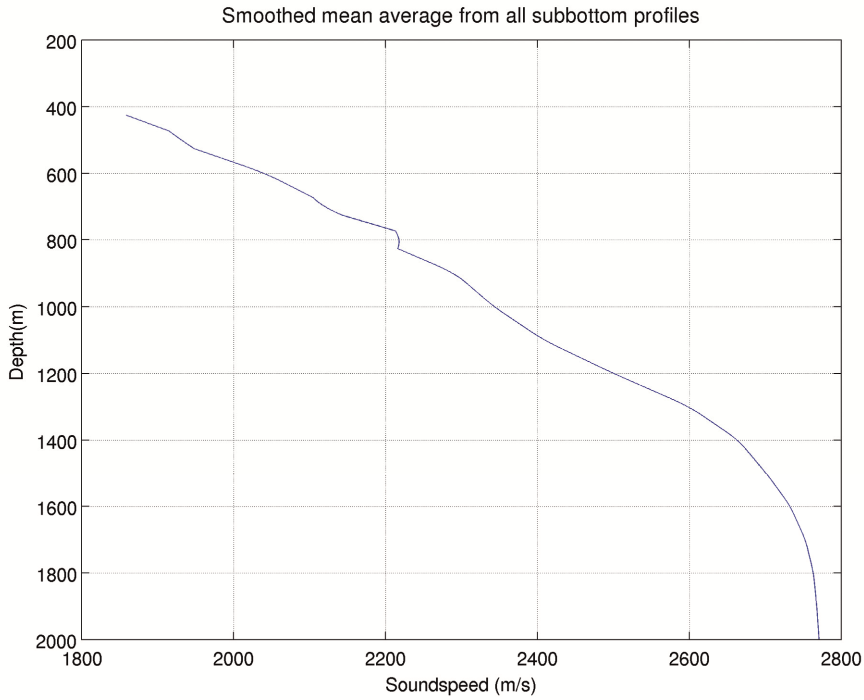

Moreover, the seismic data do not provide either the compressional wave attenuation or the bottom material density. Thus we need some ancillary information to get the bottom (fluid medium) geoacoustic model. Fortunately, work done by Edwin Hamilton (Hamilton 1980) and his collaborators in the late 1970s and early 1980s give some reasonable estimates for the bottom soundspeed and density and their near-surface gradients, given the bottom material and its porosity. Bottom attenuation estimates are less reliable, but again can be approximated if one knows the bottom material. For a sandy bottom like the Baffin Bay case, one can use a first order estimate of a water-sediment interface speed of ~1750 m/s, a shallow sediment soundspeed gradient of ~1 m/s/m, and a water sediment density of ~1.75 gm/cc (a density that matches the soundspeed, i.e. $\rho \sim 0.001c$, where c is in m/s and ρ is in gm/cc.) An attenuation of 0.01 to 0.1 dB/λ is often included, but it again must be stressed that the attenuation numbers generally are the least well known. Moreover, the bottom attenuation is not easy to estimate without careful experimentation, as it is easily confused with surface and bottom scattering effects, as well as any bottom shear. That being said, it is still useful to try to estimate the bottom geoacoustic model, as it can be used over the full range of frequencies that we are interested in.

We note that the **Figure B8** values for the soundspeed profile *are* in fact in line with the Hamilton regression analyses, i.e. the water-sediment interface soundspeed is on the order of 1700 m/s, and the gradient is also close to 1 m/s/m, as per Hamilton. This gives us some confidence that the seismic data can be used as check on the Hamilton regressions for soundspeed and its gradient, or independently, if one has absolutely no knowledge of the bottom material (which is unlikely). However, density and attenuation still need to be measured or estimated.

We next turn to the fluid medium model of the bottom reflection coefficient, which allows us to calculate the bottom loss component of the TL. We will limit ourselves to an infinite bottom halfspace model for now, as: 1) we are looking at near-surface sediments (roughly one acoustic wavelength thick), and so can to first order ignore the vertical profile, and 2) it is simpler and one can more easily relate errors in the geoacoustic parameters to errors in the bottom loss and TL. To look at this quantity, we need to define some auxiliary terms first.

First, we define the complex wavenumber in the bottom (i.e. one that includes its attenuation) as:

$$k_1 = \frac{\omega}{c_1}\left(1 + \frac{i\alpha}{2}\right) = kn_1(1 + \frac{i\alpha}{2})$$

In the above equation, the subscript "1" indicates values in the bottom, and lack of a subscript denotes values in the water column. The relative index of refraction n_1 shown above is defined by:

$$n_1 \equiv \frac{c}{c_1}$$

This is the same, in index of refraction terms, as treating c_1 as complex. It can also be treated as a complex index of refraction, i.e.

$$n_1 \rightarrow n_1\left(1 + \frac{i\alpha}{2}\right)$$

If we square this index of refraction, and keep terms only to order α, we get a term that is useful for the Rayleigh reflection coefficient, i.e.

$$n_1^2 \rightarrow n_1^2(1 + i\alpha)$$

In terms of our previous estimate of attenuation in dB/λ, which we can call β, the α used above is $\beta\left(\frac{dB}{\lambda}\right) = 27.3\alpha$ (Katsnelson et al. 2012).

One more term is needed, i.e. the ratio of the densities in the water and the sediment, given by

$$m_1 \equiv \frac{\rho_1}{\rho}$$

With these terms in hand, we can write the magnitude of the plane wave reflection coefficient for a bottom grazing angle χ and frequency $f = \omega/2\pi$ as (Katsnelson et al. 2012):

$$|V(\chi)| = \left|\frac{m_1 \sin\chi - \sqrt{n_1^2(1+i\alpha) - cos^2\chi}}{m_1 \sin\chi + \sqrt{n_1^2(1+i\alpha) - cos^2\chi}}\right|$$

The bottom loss (BL) per bottom reflection is then given by

$$BL = 20log_{10}|V|$$

We now can look at what sort of reflection coefficient we should get from the Baffin Bay sand bottom, as well as how the error in individual parameters affects the BL. Examples of this will be provided at a later date, due to author illness.

When and where one should include 3D acoustics effects

The standard way one models acoustic propagation for a fully 3D ocean and seabed environment is Nx2D acoustics, i.e. 2D acoustic slices of a 3D environment. This allows one to sample the 3D nature of the environment, but confines the acoustics to the source-receiver plane, i.e. suppresses any out of plane propagation. This is what was done for the Baffin Bay EIS, and is reasonable much of the time.

But, in point of fact, there are many ocean and seabed features that can cause out of plane acoustic propagation in the coastal ocean (bathymetric slopes, fronts, eddies, internal waves, etc.) In these cases 3D acoustics (whether ray theory, mode theory, or parabolic equation) is appropriate. As 3D effects can produce large TL changes, and change the spatial intensity distribution pattern, it is important to include them in such cases. However, it is not obvious exactly when and where one needs to use 3D acoustics, and given that 3D codes are both difficult to run and machine time intensive (compared to their Nx2D counterparts), it would be useful to have some criterion for determining when one should invoke the full force of 3D modeling. We present a simple criterion for including 3D effects here, in hopes that it will be useful for future marine mammal exposure work, among other things.

If one looks at parabolic equation codes, the only way to differentiate between Nx2D and 3D results is to run both codes, a rather inefficient process, especially as the 3D effects are frequency dependent. Ray theory is somewhat better, in that if one defines a given source to receiver track, it is easy in theory to trace a ray starting along that track both in 2D and in 3D. If the 3D track deviates along the S/R track by more than a Fresnel Zone width horizontally, where $R_F = \sqrt{\lambda R}$, then the propagation should be described in 3D. However, ray theory has the characteristic of being a high frequency, and frequency independent, approximation, and it is well known at this point in time that 3D effects can depend on frequency. To incorporate both the ease of ray tracing, and also incorporate the frequency dependence of the 3D propagation, we can use the "vertical modes/horizontal rays" formalism of Weinberg and Burridge (1974). In this formalism, the vertical structure of the acoustic field is given by the (frequency dependent) acoustic normal modes, whereas the horizontal structure of the field is determined by a 2D x-y plane ray trace that uses the modal eigenvalues to determine the 2D index of refraction (also frequency dependent.) This allows one to see how important

3D effects are versus both frequency and the vertical angle of the energy. We will look very briefly at how this works below. We will first look at 3D effects caused by bottom bathymetric steering (probably the predominant effect, especially in Baffin Bay), and then show how to generalize to a combination of ocean and seabed effects.

If we consider bathymetric steering as the dominant effect, we can look with profit at the case of an isovelocity water column (e.g. we can take the average of the water column soundspeed profile) over an acoustically hard bottom. For this case, the acoustic normal mode eigenvalues are easily found (Clay & Medwin 1977). The vertical acoustic wavenumber is given by:

$$\gamma_n = (n - \frac{1}{2})\frac{\pi}{H}$$

where n is the mode number and H is the local water depth. The normalized acoustic normal modes for this case are simply given as

$$\varphi_n = \sqrt{\frac{2}{H}} \sin \gamma_n z$$

and the acoustic field can be written as a simple sum of such modes. More interestingly, in discussing the 3D effects, the horizontal wavenumber is written as

$$k_n = \sqrt{k^2 - \gamma_n^2}$$

where $k = \omega/c$ is the "water wavenumber." This explicitly contains the frequency dependence through the ω. This also leads directly to creating a 2D index of refraction for the "modal rays" (i.e. the horizontal ray corresponding to each mode at a given frequency) via

$$\frac{k_n(\vec{r})}{k_n(\overrightarrow{r_0})} = \frac{c(\overrightarrow{r_0})}{c(\vec{r})}$$

Thus, one obtains from the local (x-y plane) eigenvalues a relative index of refraction field which one can use for tracing 2D, x-y plane modal rays. If these rays deviate from the original source-to-receiver path by more than a Fresnel zone, then 3D effects are important.

The first order way to do this is to use a standard 2D ray tracing program, and then monitor the deviation of the individual modal rays from the straight line path between source and receiver. This calculation just requires standard codes, and a small additional piece of code to calculate the perpendicular distance from the modal ray to the straight line S/R path. The criterion that the ray remains within the Fresnel zone region is graphically shown in **Figure B9**.

Figure B9. Fresnel zone region in which an along-y-axis modal ray retains its identity.

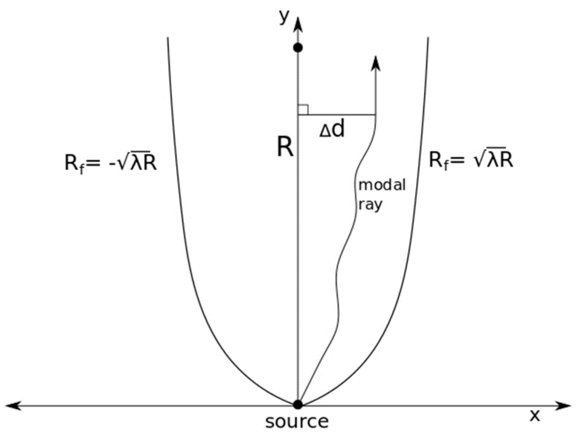

Figure B10. Horizontal deflections along a source to receiver track. The soundspeed gradient along the track is assumed to be approximately constant.

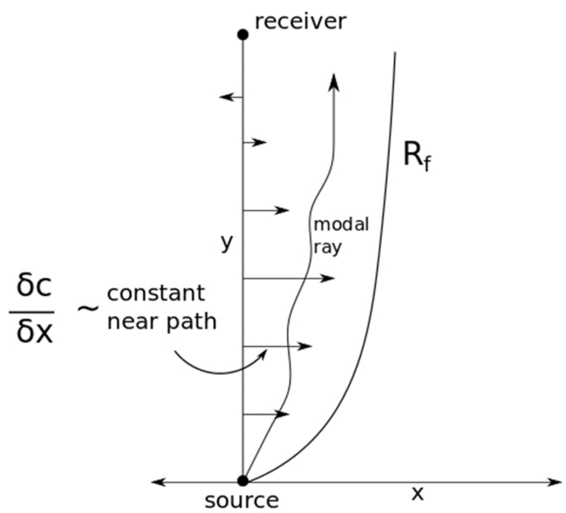

However, with the slight additional assumption that the lateral gradient of the relative index of refraction remain approximately constant within the vicinity of the straight line S/R raypath (see **Figure B10**), one can greatly simplify the criterion for determining whether or not one needs 3D acoustics calculations.

Figure B11. Geometry for considering deflection of a modal ray in a constant gradient region.

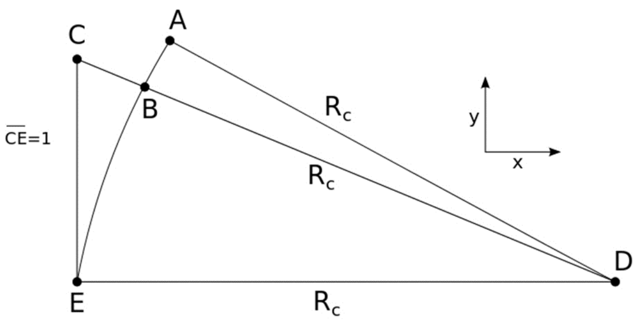

If we remember that in a constant gradient region, a raypath is circular, we can draw a diagram such as **Figure B11**. In this figure, line EC is a unit distance along the source to receiver track. Over that distance, the local horizontal gradient $g = \partial c_{rel,E}/\partial x$ deflects the modal ray some distance to the side (out of plane). This is along the arc of a circle whose radius of curvature is given by

$$R_{curv} = c_{rel,E}/g$$

From the geometry shown in **Figure B11**, one sees from the Pythagorean theorem that

$$\overline{(EC)}^2 + R_{curv}^2 = [\Delta d + R_{curv}]^2$$

Squaring the bracketed term, and then ignoring terms of order $(\Delta d)^2$, which is appropriate if $\overline{EC} \ll R_{curv}$, we obtain that

$$\Delta d \sim \overline{(EC)}^2/2R_{curv}$$

This is a very straightforward thing to calculate. If one now sums (integrates) the Δd as one traverses the straight path from source to receiver, one can see if the deviation along the path is greater than R_F. We note that the deviation can be +/-, as the radius of curvature is a signed quantity. Thus, one could really talk about $|R_F|$ as being the quantity of interest. We should also note that this scheme is susceptible to breakdown in the vicinity of the crest of a hill or ridge, where the horizontal gradients will change quickly in the x-direction. **Figure B12** shows the horizontal bathymetry gradients one encounters in the Baffin Bay region. These results will be used in the near future to predict where one would see the biggest 3D acoustics effects.

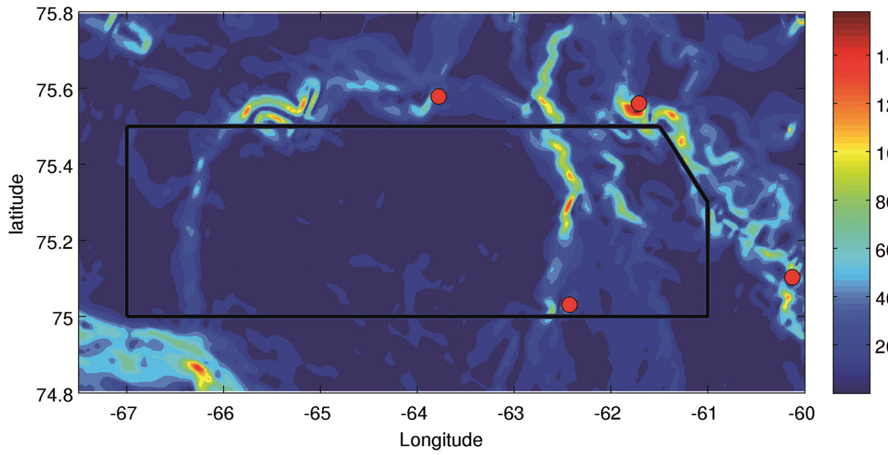

Figure B12. Horizontal bathymetry gradients in the Baffin Bay study area. Units are m/km.

The above scheme just needs the bathymetry and acoustic frequency as inputs, and the mode and ray equations, being very simple, take care of the rest. However, the above only considers the 3D effects of the bathymetry, and if we wish to include the water column soundspeed profile (and its variations!), there is one more simple device we can use. Specifically, we can add a perturbation to the modal wavenumbers due to the perturbation of the water column soundspeed about the "mean soundspeed" in the water column, i.e.

$$\Delta k_n(x,y) = \frac{1}{k_n^0}\int_0^\infty \rho_0^{-1}|\varphi_n^0(z;x,y)|^2 \frac{\omega^2}{c_0^3}\Delta c(z;x,y)dz$$

By adding this perturbation to the k_n for the hard bottom isovelocity case discussed above, one also includes the water column profile, which can depend on the x,y coordinate if that is appropriate. Thus one can fully include both water column and oceanographic effects on 3D propagation.

This approach has further limits in that it is adiabatic mode theory based, rather than fully coupled modes.

Effects of bathymetry error

One rather common error, especially in regions with appreciable bottom slope, is mis-measurement of the bathymetry. This is often discounted, as bathymetric measurements are the result of rather simple and well known echosounder technology. However, it is a very common experience that multiple bathymetric measurements in sloping areas disagree. As an example, the report previously showed two measurements of bathymetry from the Baffin Bay survey site. At the locations of the biggest slope, there was disagreement. While this is "fixable" disagreement, given enough effort, one often has to deal with bathymetry numbers with some error in them.

We present here a simple argument for estimating the effects of bathymetric variability on TL estimation, and also the error in estimating such variability. As with some of our previous arguments, it uses an average, isovelocity water column soundspeed profile. This emphasizes the effects of rays/modes that have turning points at both the surface and the bottom. Paths that do not interact (or interact very weakly) with the surface and bottom are not described by this argument.

Consider the scenario where a source at depth z_s emits energy at a grazing angle θ_0. In a modal picture, this energy will change its angle to the bottom, $\theta(r)$ as a function of range r along the path. This can be expressed as a simple differential equation

$$\frac{d\theta(r)}{dr} = \frac{2\alpha(r)}{\Delta(\theta,r)}$$

where $\alpha(r)$ is the bottom slope as a function of range, and $\Delta(\theta,r)$ is the local ray/mode cycle distance. (We can use the ray cycle distance to first order, as the mode cycle distance generally differs from it by only a small amount, given by the "beam displacement.") This expression can be integrated to give an equation for $\theta(r)$, i.e.

$$\theta(r) = \theta_0 + \int \frac{2\alpha(r)}{\Delta(\theta,r)}dr$$

If we use the definition of the slope, $\alpha(r) = -dH(r)/dr$, where the minus sign comes from the depth convention, and also the definition of the local cycle distance, $\Delta(r) = 2H(r)/\tan\theta(r)$, we get the integral equation

$$\theta(r) = \theta_0 - \int \frac{\tan\theta(r)}{H(r)}dH(r)$$

This equation can be solved by simple iteration in range. If we take n as the index of the nth range step, we can write

$$\theta(r_{n+1}) = \theta(r_n) - \int \frac{\tan\theta(r_n)}{H(r_n)} dH(r_{n,n+1})$$

This can be stepped out in range from the origin to give the local ray angle, and also the local cycle distance, and any range r. One can easily include an error term in this by changing $H(r) \rightarrow H(r) + \Delta H_{err}(r)$. This will change both the denominator and the differential in the equation above. Both these changes (each of which contraibutes an error term) are of about the same order and should be kept, whereas the second order term containing the denominator change and the slope change both together can be ignored.

To get the bottom loss, one writes

$$BL = 20log_{10}|R_B|$$

And to get bottom loss per unit distance at range r, one writes

$$d\big(BL(r)\big) = \frac{BL(\theta(r))}{\Delta(r)}$$

The total bottom loss is simply

$$BL_{tot} = \int d\big(BL(r)\big) = \int \frac{BL(\theta(r))}{\Delta(r)} dr$$

Again, examples of this error as applied to the Baffin Bay study will be created after this report is finalized, due to author health issues.

References

Clay, C.S. and Medwin, H. "Acoustical Oceanography: Principles and Methods." J. Wiley and Sons, New York. 544 pages. (1977).

Hamilton, E.L. Geoacoustic modeling of the seafloor. J. Acoust. Soc. Am. 68, 1313-1340 (1980).

Katznelson, B., Petnikov, V. and Lynch, J. Fundamentals of shallow water acoustics, ONR series book, Springer Verlag, 520 pages. (2012

Weinberg, H. and Burridge, R. Horizontal ray theory for ocean acoustics. J. Acoust. Soc. Am. 55, 63-79 (1974).

Appendix C. WHOI transmission loss modeling. Supplementary material

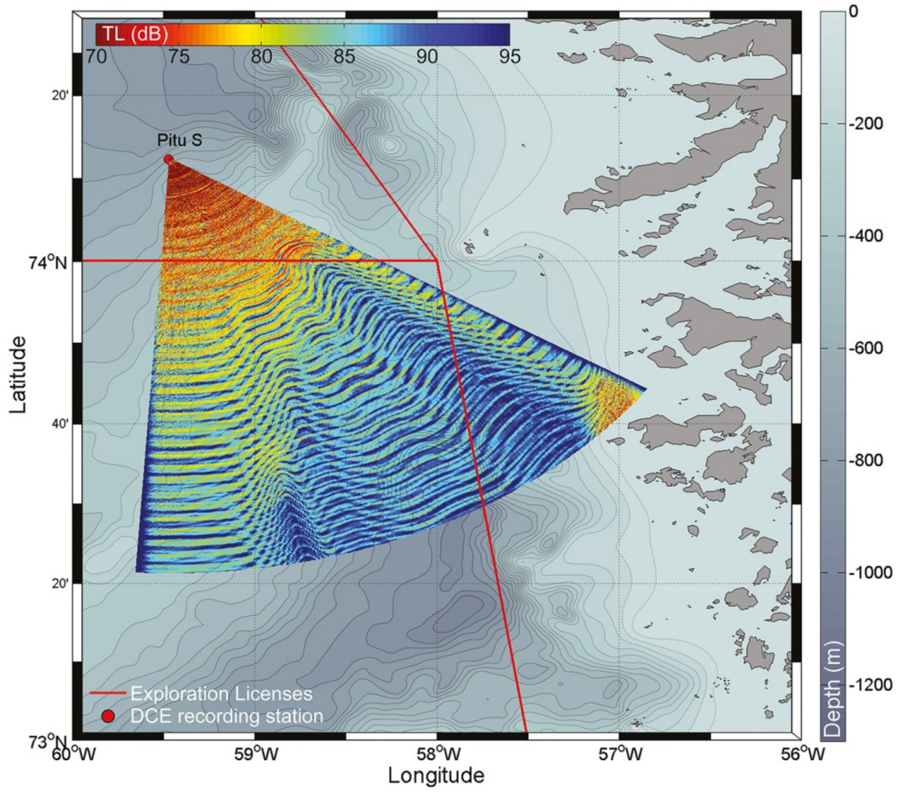

Figure C1. Results of the WHOI PE model for the Tooq license block: transmission loss from sources located within Maersk's license area towards a receiver located at Pitu S station at 50 m. Datum: WGS84; projection: Mercator.

Appendix D. Comparison with JASCO's pre-season modeling results. Supplementary material

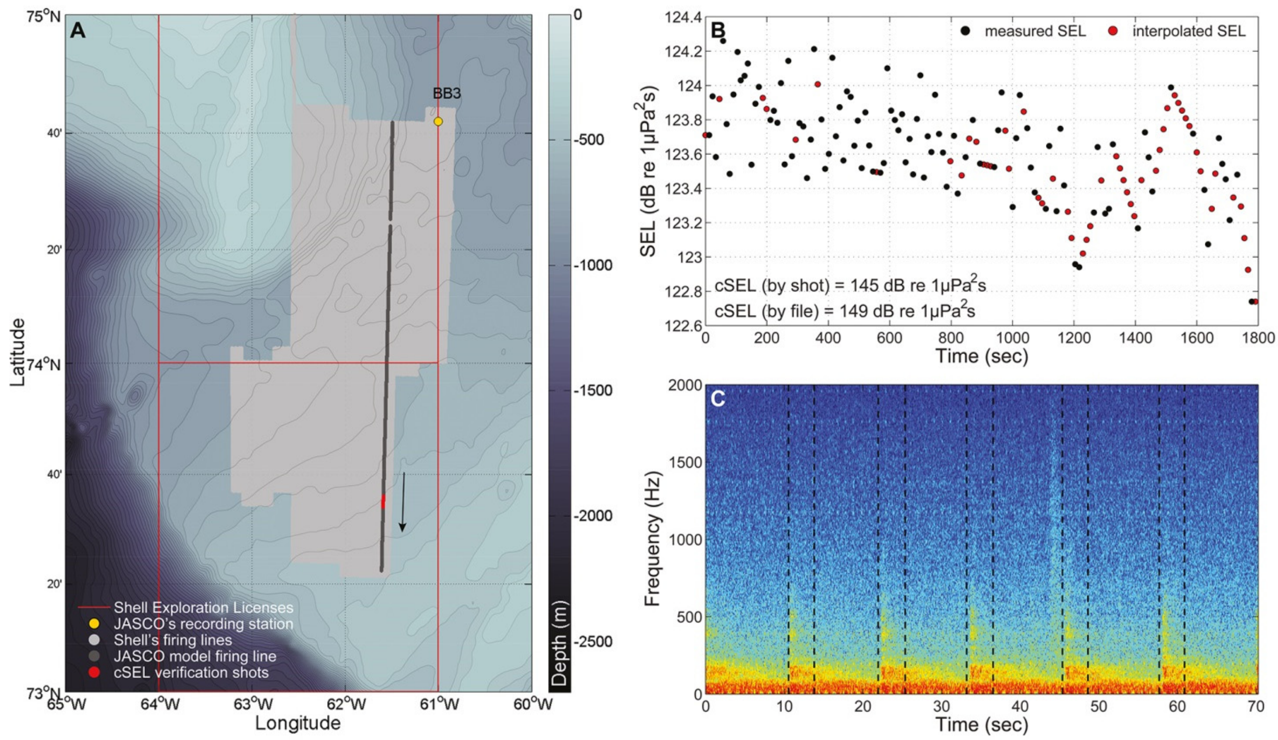

Figure D1. Comparison of two methods of obtaining the cumulative sound exposure levels (cSEL) from Shell's eastern firing line considered in the pre-season modeling: 1) by shot, i.e. summation of the SEL of individual shots recorded during the time period of interest, 2) by file, i.e. SEL of the whole recording within the time window of interest. Shots emitted by *R/V Polarcus Samur* along the eastern survey line during 10 minutes with no other vessels active (red in A; the arrow indicates the array tow direction) and recorded at JASCO's BB3 station were considered here. For both methods, the recordings were filtered between 10 and 2000 Hz. For the by-shot method, SEL of individual shots were computed, based on their 95% rms SPL in a 4-second-long time window (C). Not all pulses emitted along the firing line passed the inclusion criteria (sections 5.3.2.2 and 5.4.3). The missing data points were therefore linearly interpolated (B). The resultant cSEL value was 4 dB lower than that of the whole 10-minute-long recording. The reason for this was most likely the long duration and low levels of the recorded shots, resulting in a significant part of the shot energy not being contained by the 4-second-long rms windows (C). The by-file method seemed therefore more reliable here. Map in A - datum: WGS84; projection: Mercator.

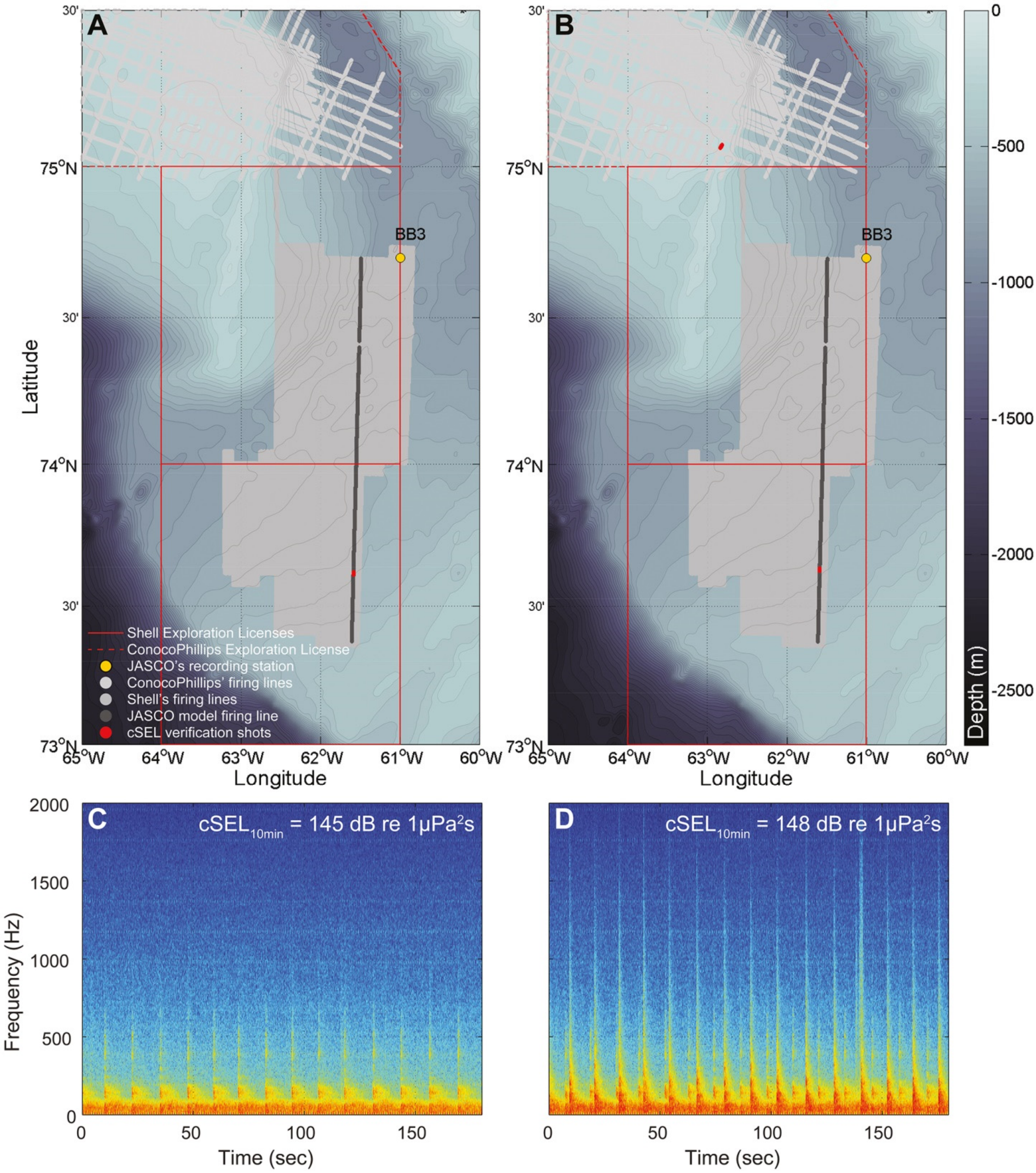

Figure D2. Summation of noise energy from two separate seismic sources. Sound exposure levels (SEL) were estimated for 10-minute-long snippets of recordings within a single sound file from the BB3 station: 1) with a single vessel in operation (A and C) and 2) with two surveys active (B and D). There was a 3 dB (i.e. two-fold) difference between the SEL estimates, as expected for pulses arriving at similar received levels. Maps in A and B - datum: WGS84; projection: Mercator.

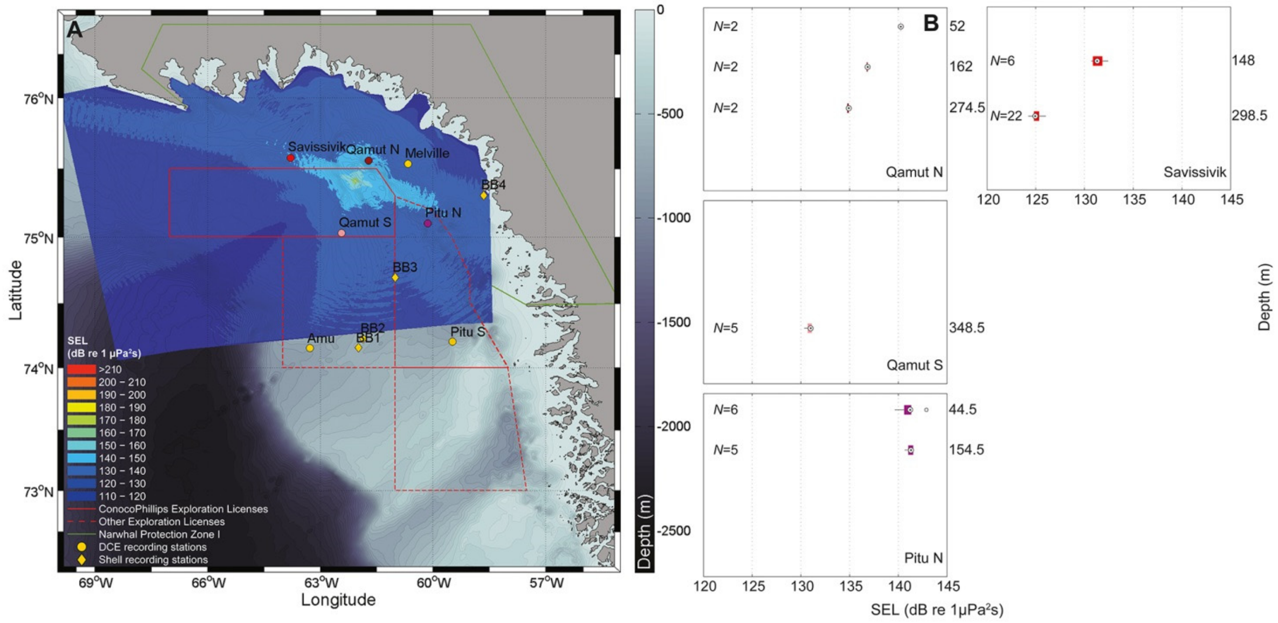

Figure D3. Sound distribution (SEL) modeled by JASCO for ConocoPhillips' site 1 (A), together with sound exposure levels from airgun signals emitted in the vicinity of the site as recorded at loggers within the modeled area (B). All shots fired within a 2 km radius of the modeled source position (**Table 3**) were considered. Datum: WGS84; projection: Mercator. Colors of the box-plots in B correspond to the colors of the recording stations in A.

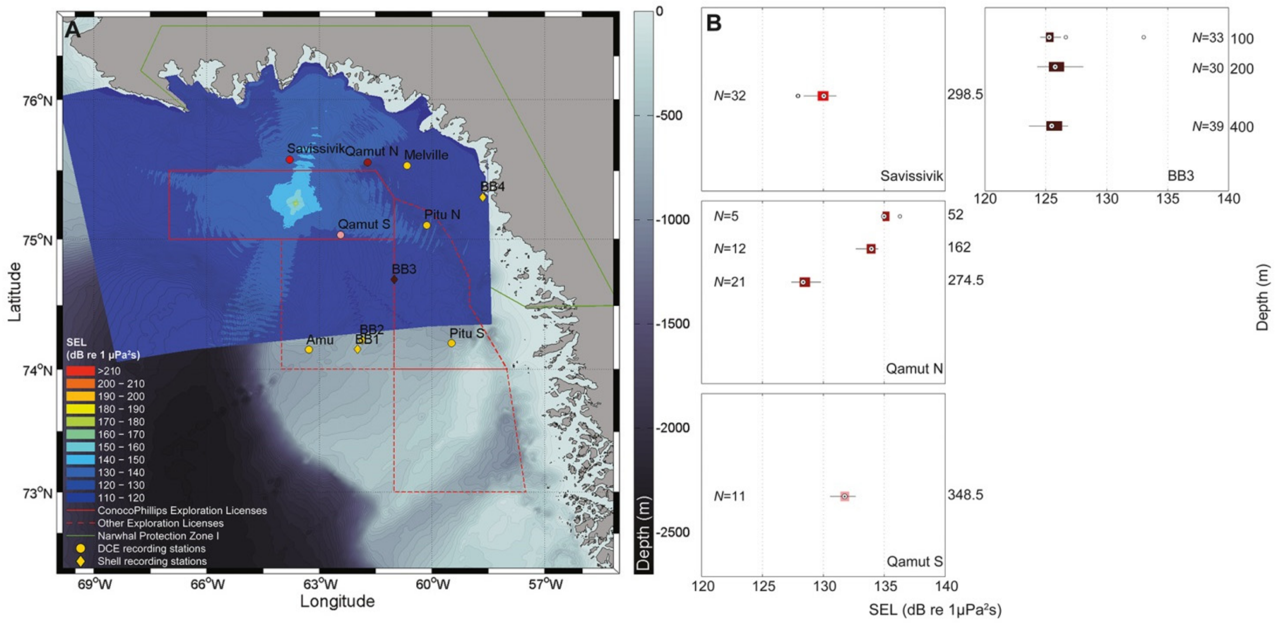

Figure D4. Sound distribution (SEL) modeled by JASCO for ConocoPhillips' site 2 (A), together with sound exposure levels from airgun signals emitted in the vicinity of the site as recorded at loggers within the modeled area (B). All shots fired within a 2 km radius of the modeled source position (**Table 3**) were considered. Datum: WGS84; projection: Mercator. Colors of the box-plots in B correspond to the colors of the recording stations in A.

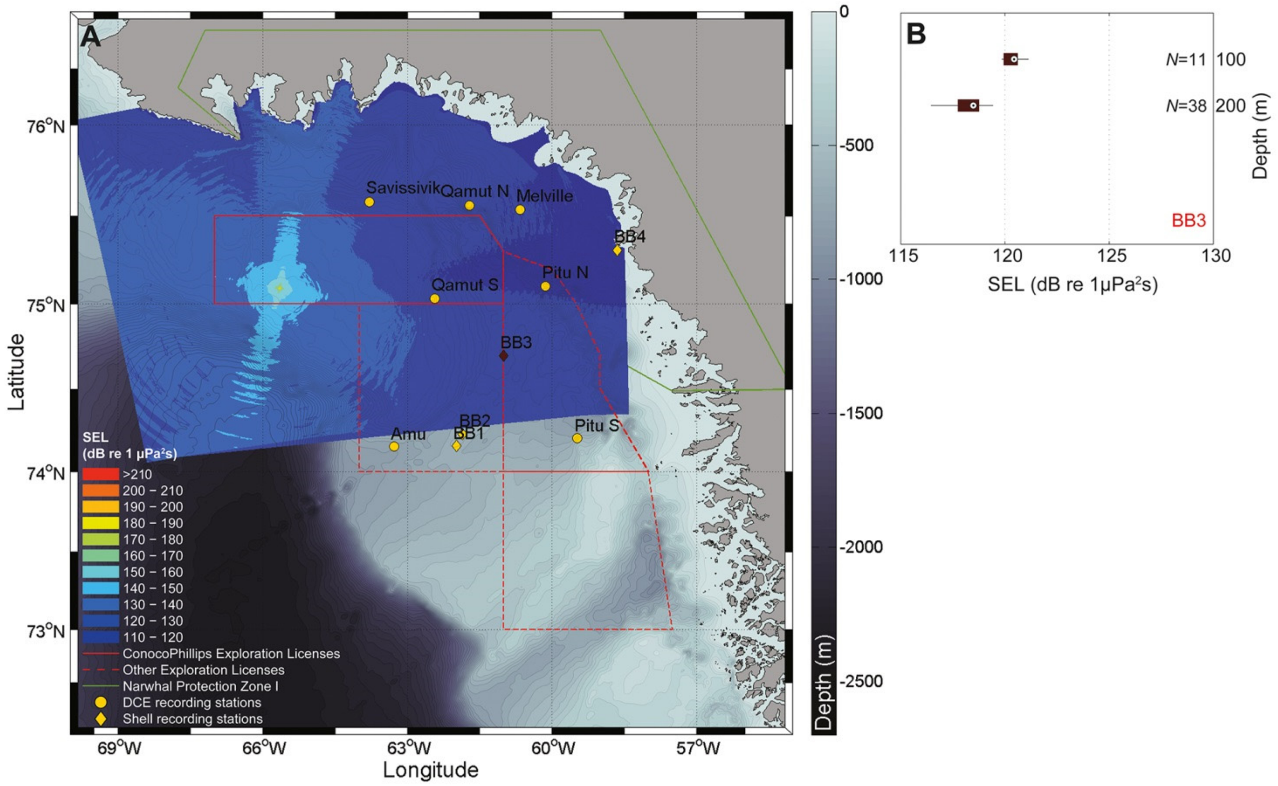

Figure D5. Sound distribution (SEL) modeled by JASCO for ConocoPhillips' site 3 (A), together with sound exposure levels from airgun signals emitted in the vicinity of the site as recorded at loggers within the modeled area (B). All shots fired within a 2 km radius of the modeled source position (**Table 3**) were considered. The airgun pulses detected at the BB3 station were of low amplitudes and much shorter durations than pulses used in verification of the other modeling sites. Consequently, a shorter time window (±0.8 s) around the peak was assumed for the analysis. Datum: WGS84; projection: Mercator. Colors of the boxplots in B correspond to the colors of the recording stations in A.

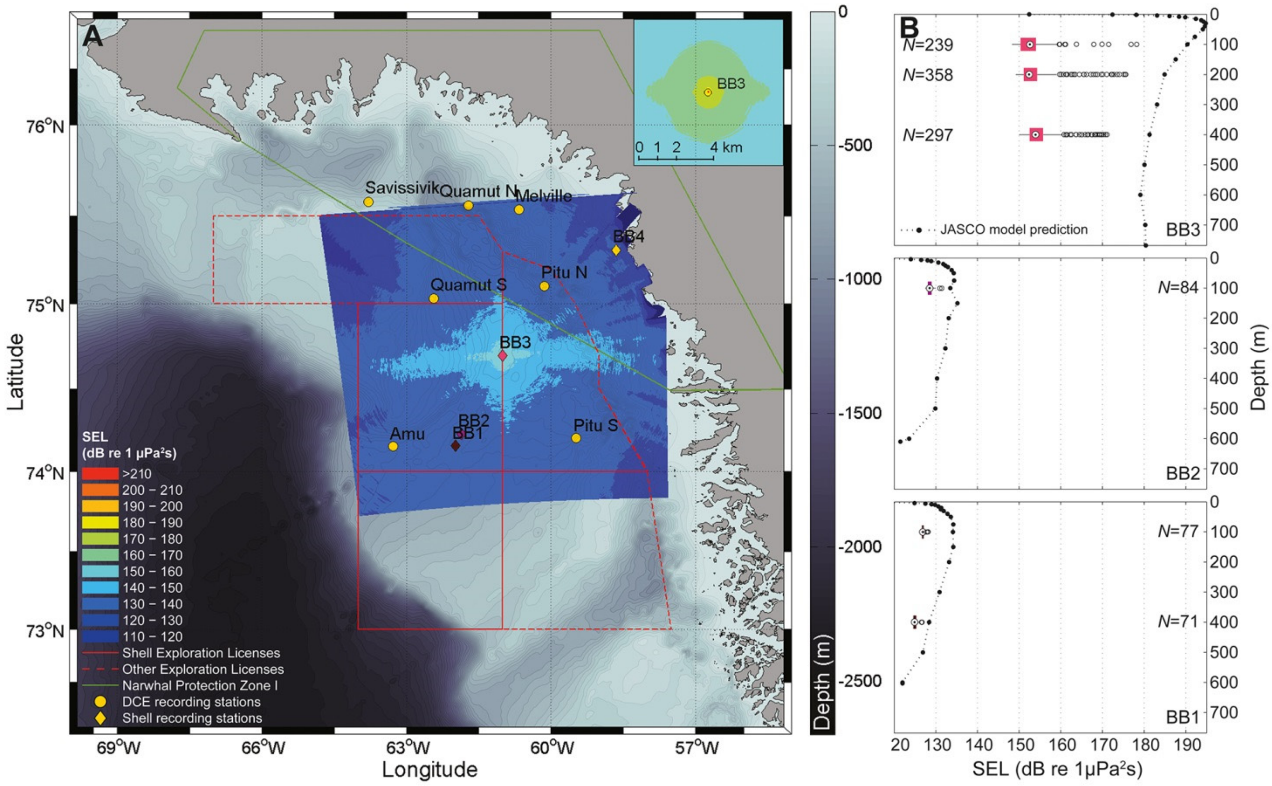

Figure D6. Sound distribution (SEL) modeled by JASCO for Shell's site 2 (A), together with sound exposure levels from airgun signals emitted in the vicinity of the site as recorded at loggers within the modeled area (B). Results of the on-site measurements have been overlaid with SEL-over-depth profiles computed by JASCO for model sampling positions closest to the positions of the moorings. All shots fired within a 2 km radius of the modeled source position (**Table 3**) were considered. Large map - datum: WGS84; projection: Mercator. Inserts - datum: WGS84; projection: UTM Zone 21. Colors of the boxplots in B correspond to the colors of the recording stations in A.

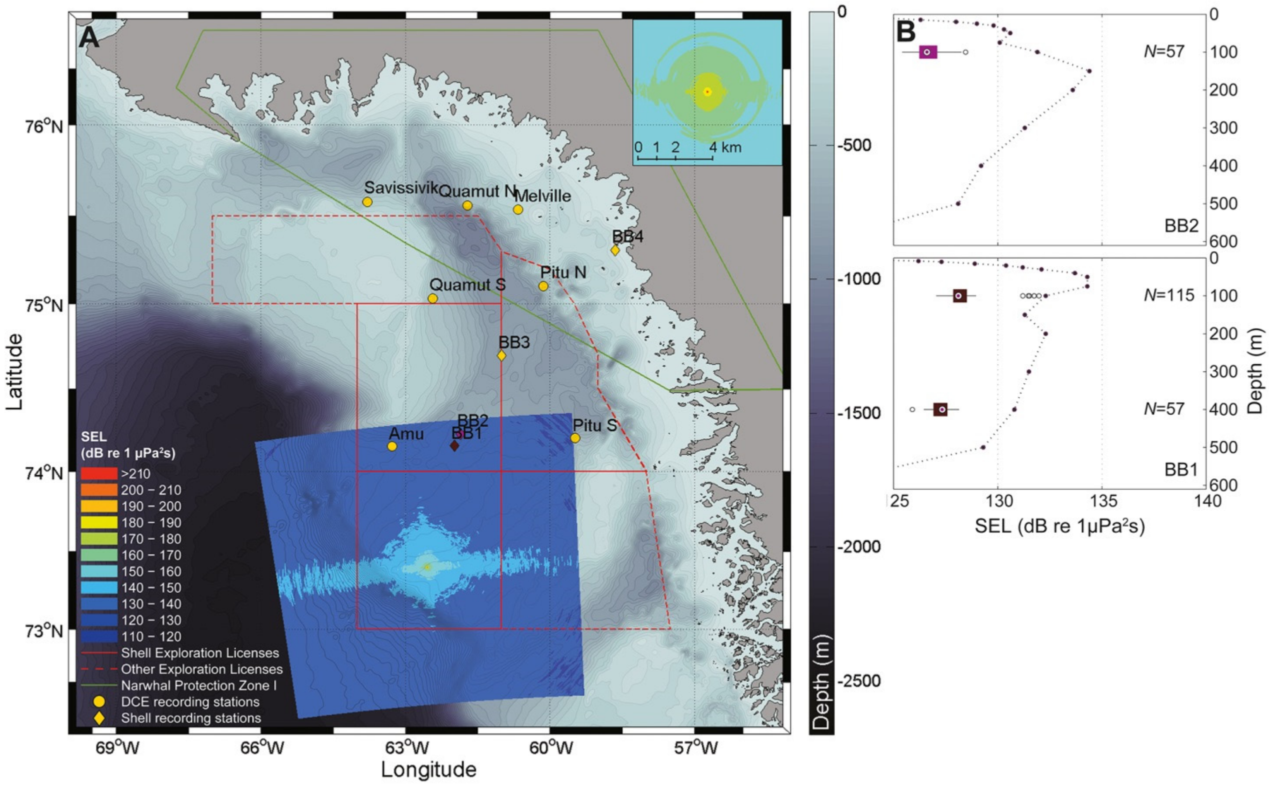

Figure D7. Sound distribution (SEL) modeled by JASCO for Shell's site 4 (A), together with sound exposure levels from airgun signals emitted in the vicinity of the site as recorded at loggers within the modeled area (B). Results of the on-site measurements have been overlaid with SEL-over-depth profiles computed by JASCO for model sampling positions closest to the positions of the moorings. All shots fired within a 2 km radius of the modeled source position (**Table 3**) were considered. Large map - datum: WGS84; projection: Mercator. Inserts - datum: WGS84; projection: UTM Zone 21. Colors of the boxplots in B correspond to the colors of the recording stations in A.

Table D1. Overview of the mooring and JASCO's model sampling positions used to verify the modelled variation of received levels with depth shown in

JASCO Source	DCE Station	DCE Station Easting (UTM21N)	DCE Station Northing (UTM21N)	Modeled Easting (UTM21N)	Modeled Northing (UTM21N)	Water Depth (m)
SH1	Qamut N	368904.6	8391455.8	368906.7	8391425	308
SH1	Qamut S	343604.9	8334269.9	343606.7	8334225	370
SH1	Pitu N	409745.6	8329709.5	409706.7	8329725	553
SH1	BB1	348464.3	8236059.3	348506.7	8236025	603
SH1	BB2	352910.8	8243809.6	352906.7	8243825	610
SH1	BB3	382239.3	8294069.2	382206.7	8294025	768
SH2	BB1	348464.3	8236059.3	348464.9	8236100.5	603
SH2	BB2	352910.8	8243809.6	352864.9	8243800.5	610
SH2	BB3	382239.3	8294069.2	382239.2	8294070	768
SH3*	Qamut N	368904.6	8391455.8	368947.5	8335151	308
SH3	Amu	308986.1	8239323.4	308947.5	8239351	705
SH3	Pitu S	424931.9	8236419	424947.5	8236451	615
SH3	BB1	348464.3	8236059.3	348447.5	8236051	603
SH3	BB2	352910.8	8243809.6	352947.5	8243851	610
SH3	BB3	382239.3	8294069.2	382247.5	8294051	768
SH4	BB1	348464.3	8236059.3	348479.4	8236101	603
SH4	BB2	352910.8	8243809.6	352879.4	8243801	610

*Qamut N located too far outside of modelled area for model location SH3. Model data not valid.

Appendix E. Self-noise

Figure E1. Self-noise of the 1177 logger (deployed at the Pitu N station; **Table 4**) with no gain (top panel) and 20 dB gain (bottom panel). The self-noise recordings were conducted in an anechoic room at the Department of Electrical Engineering at the Technical University of Denmark. The same recording settings as during the deployment were used in the anechoic room, with the exceptions of calibrating with 0 or 20 dB gain. The psd were computed in 10-second-long windows.

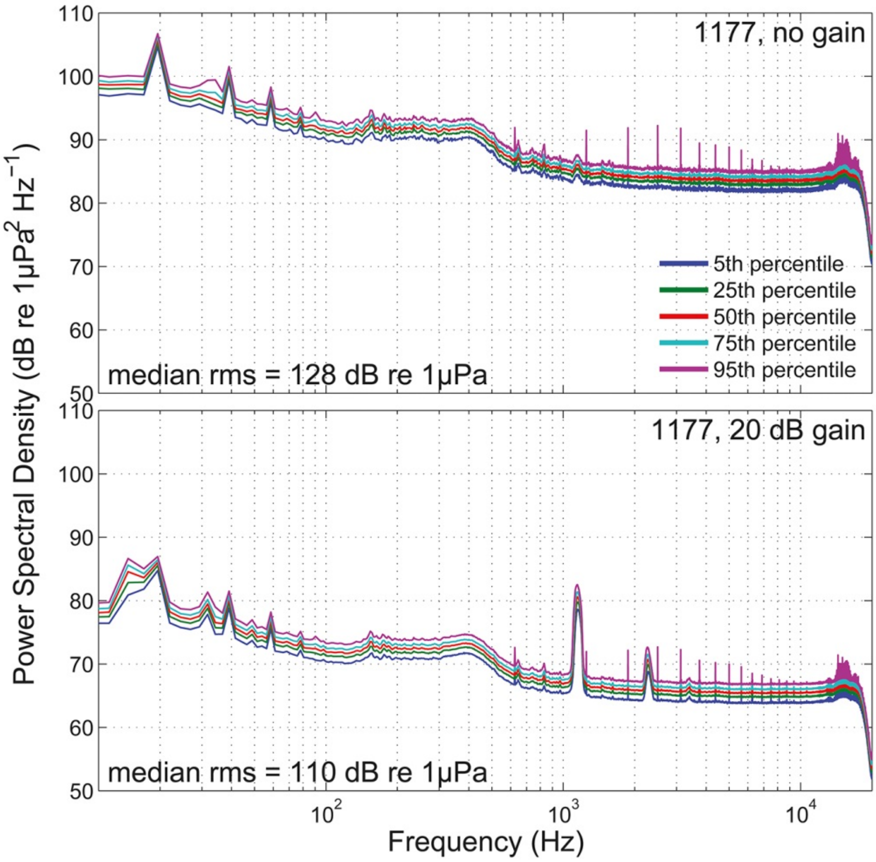

Figure E2. Self-noise of the 1183 logger (deployed at the Qamut S station; **Table 4**) with no gain (top panel) and 20 dB gain (bottom panel). The self-noise recordings were conducted in an anechoic room at the Department of Electrical Engineering at the Technical University of Denmark. The same recording settings as during the deployment were used in the anechoic room, with the exceptions of calibrating with 0 or 20 dB gain. The psd were computed in 10-second-long windows.

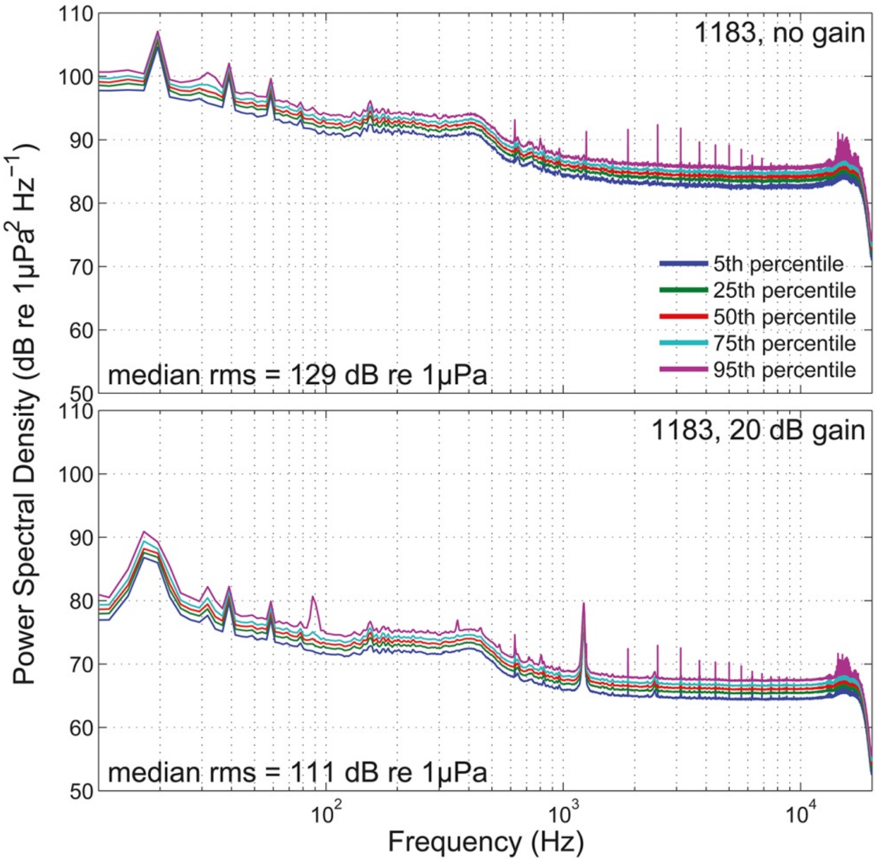

Figure E3. Self-noise of the 1186 logger (deployed at the Qamut S station; **Table 4**) with no gain (top panel) and 20 dB gain (bottom panel). The self-noise recordings were conducted in an anechoic room at the Department of Electrical Engineering at the Technical University of Denmark. The same recording settings as during the deployment were used in the anechoic room, with the exceptions of calibrating with 0 or 20 dB gain. The psd were computed in 10-second-long windows.

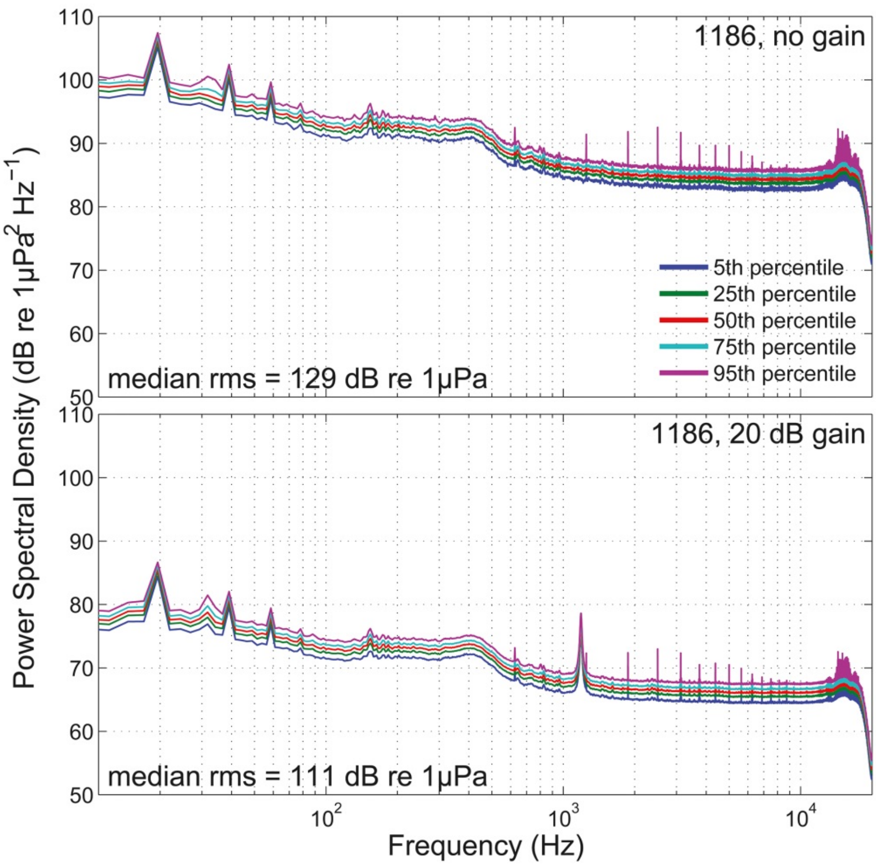

Figure E4. Self-noise of JASCO's 147-01.8000 logger (deployed at the BB2 station, but recovered with no usable data due to leakage along the mooring) with the same gain settings as during its deployment in Baffin Bay. Courtesy of JASCO.

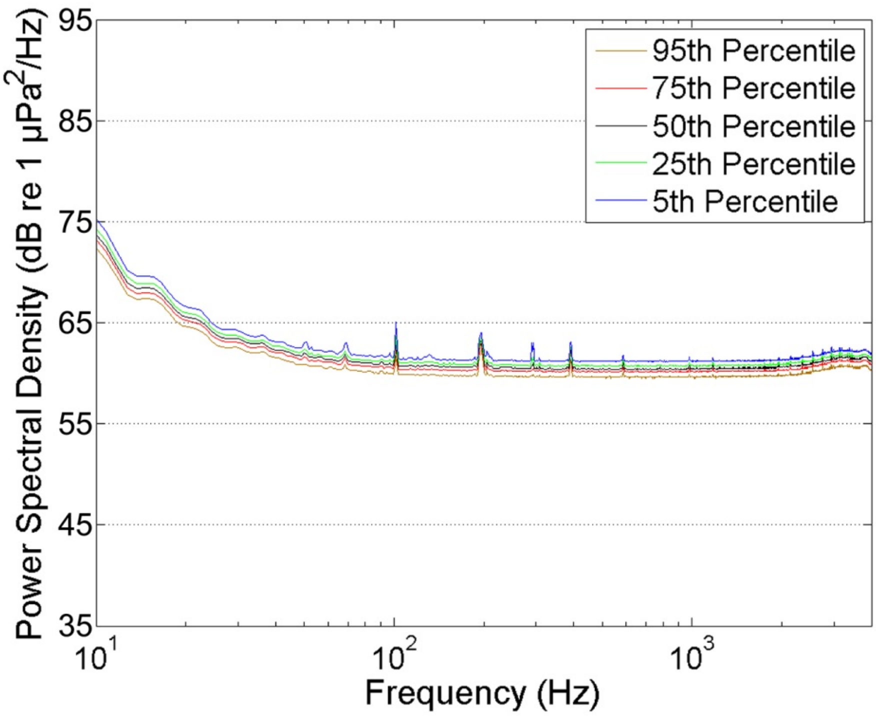

Figure E5. Self-noise of JASCO's 148-05.64000 logger (deployed at the BB3 station) with the same gain settings as during its deployment in Baffin Bay. Courtesy of JASCO.

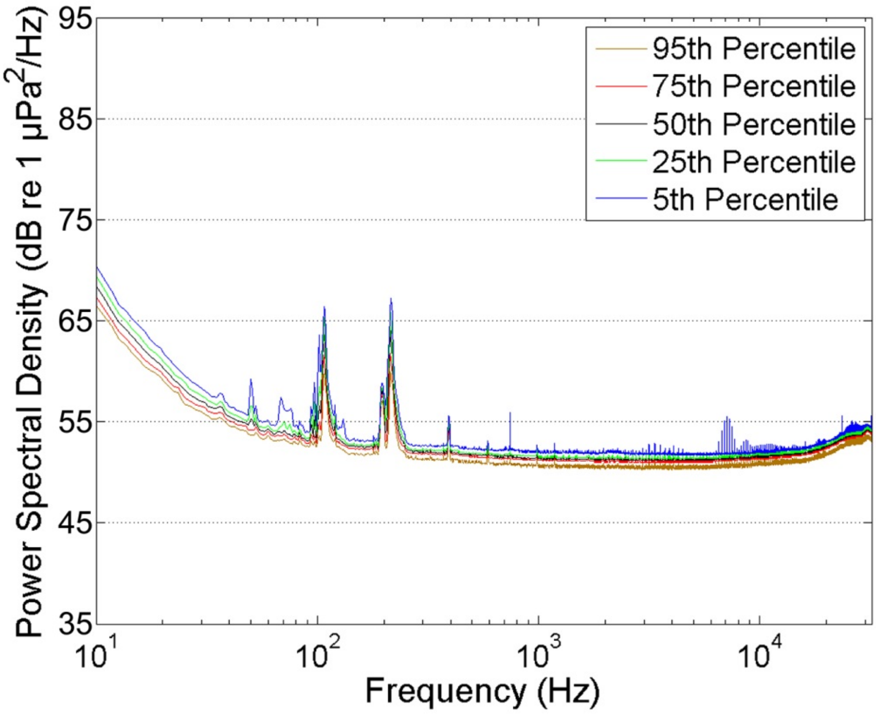

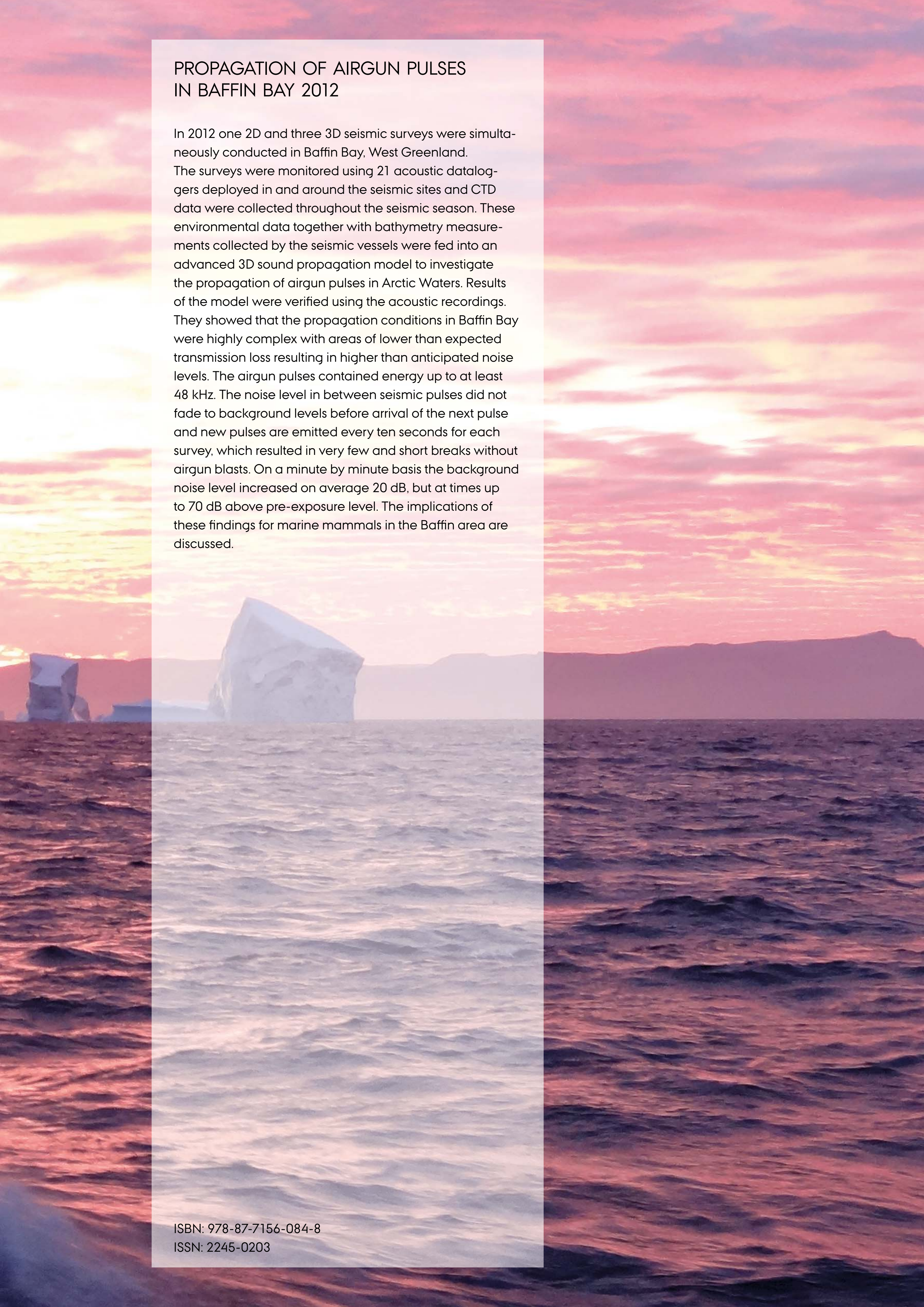

PROPAGATION OF AIRGUN PULSES IN BAFFIN BAY 2012

In 2012 one 2D and three 3D seismic surveys were simultaneously conducted in Baffin Bay, West Greenland. The surveys were monitored using 21 acoustic dataloggers deployed in and around the seismic sites and CTD data were collected throughout the seismic season. These environmental data together with bathymetry measurements collected by the seismic vessels were fed into an advanced 3D sound propagation model to investigate the propagation of airgun pulses in Arctic Waters. Results of the model were verified using the acoustic recordings. They showed that the propagation conditions in Baffin Bay were highly complex with areas of lower than expected transmission loss resulting in higher than anticipated noise levels. The airgun pulses contained energy up to at least 48 kHz. The noise level in between seismic pulses did not fade to background levels before arrival of the next pulse and new pulses are emitted every ten seconds for each survey, which resulted in very few and short breaks without airgun blasts. On a minute by minute basis the background noise level increased on average 20 dB, but at times up to 70 dB above pre-exposure level. The implications of these findings for marine mammals in the Baffin area are discussed.

ISBN: 978-87-7156-084-8
ISSN: 2245-0203